ENTROPY GENERATION DUE TO MICROPOLAR FLUID FLOW THROUGH CHANNELS AND PIPES

A

REVISED THESIS SUBMITTED TO

NATIONAL INSTITUTE OF TECHNOLOGY WARANGAL, INDIA

FOR THE AWARD OF THE DEGREE OF

DOCTOR OF PHILOSOPHY

IN

MATHEMATICS

BY

KETHIRI HIMABINDU

(Roll No. 701371)

UNDER THE SUPERVISION OF

Dr. D. SRINIVASACHARYA

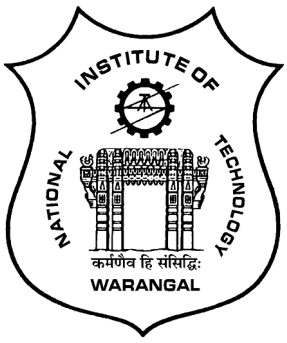

DEPARTMENT OF MATHEMATICS

NATIONAL INSTITUTE OF TECHNOLOGY

WARANGAL - 506004, INDIA

APRIL 2017

C E R T I F I C A T E

This is to certify that the thesis entitled " **ENTROPY GENERATION DUE TO MICROPOLAR FLUID FLOW THROUGH CHANNELS AND PIPES** " submitted to National Institute of Technology Warangal, for the award of the degree of ***Doctor of Philosophy***, is the bonafide research work done by **Mrs. KETHIRI HIMABINDU** under my supervision. The contents of this thesis have not been submitted elsewhere for the award of any degree.

Dr. D. Srinivasacharya
Associate Professor
Department of Mathematics
National Institute of Technology,
Warangal - 506004, T.S., INDIA

.

Dedicated to

My Family, My Supervisor

&

Sri Sai Baba

ACKNOWLEDGEMENTS

It is a rare privilege and boon that I could associate myself for pursuing my research work with Dr. D. Srinivasacharya, Associate Professor of Mathematics, National Institute of Technology Warangal, India. I sincerely record my gratitude for his invaluable guidance and constant encouragement throughout the preparation of this thesis and his involvement and meticulous supervision while my work was in progress. With his inimitable qualities as a good teacher, he chiseled my path towards perfection. Ever since I met him, he has been a perpetual source of inspiration, divine guidance, encouragement and enlightenment. He is responsible for making the period of my research work as an educative and enjoyable learning experience. He has been a great source of motivation and inspiration. The thesis would not have seen the light of the day without his unrelenting support and cooperation. I deem it a privilege to have worked under his amiable guidance. My vocabulary is inadequate to express my gratitude. I also thank to his wife Smt. D. Jaya for her hospitality and her patience during our elongated discussions.

I am greatly indebted to the dynamic personality, Prof. T. K. V. Iyengar for his affectionate support, encouragement and for sparing his valuable time in bringing a proper form for presentation of the results in the thesis. It is not an exaggeration to state that without his assistance and suggestions, this thesis would not have taken this form.

I am grateful to Prof. Debashis Dutta, Head of the Department, Prof. G. Radhakrishnamacharya and Prof. Y. N. Reddy, Senior Professors of the Department of Mathematics, for providing necessary help and support throughout the period of my research work.

I take this opportunity to thank the members of the Doctoral Scrutiny Committee, Prof. K. N. S. Kasi Viswanadham and Prof. J. V. Ramana Murthy, Department of Mathematics and Assoc. Prof. T. D. Gunneswar Rao, Department of Civil Engineering for their valuable suggestions, moral support and encouragement while my work was in progress.

I place on record my gratitude to all the Faculty members of the Department of Mathematics, for their constant encouragement. Also, I am grateful to Prof. D. S. Kesava Rao, Head, Department of Humanities and Social Sciences for his kind support.

I express my sincere thanks and gratitude to Prof. G. R. C. Reddy, Director I/c, National Institute of Technology, Warangal for awarding me Institute Fellowship (MHRD, GoI) to carry out my research work. I thank him for his kind support and encouragement at every stage of this endeavor.

I owe my special thanks to Dr. Ch. Ramreddy, who helped me in all aspects of my research work. My whole-hearted thanks to Dr. K. Kaladhar, Dr. M. Krishna Prasad, Dr. G. Swamy Reddy, Dr. M. Upendar, Dr. O. Surender, Dr. P. Vijay Kumar, G. Madhava Rao for their continuous support. I thank P. Jagadeeshwar, Md. Shafeeur Rahman, I. Srinath, G. Venkata Suman, T. Pradeepa, Ch. Venkata Rao, P. Naveen and my friends, who helped me during my Ph.D and all other Research colleagues in the Department for being cooperative and also for making my stay in the NIT campus fruitful and enjoyable every moment.

I am very much grateful to my parents K. Gopal Reddy and K. Sulochana, my in-laws L. Raghava Reddy and L. Sujatha, my sister K. Madhavi, my brother K. Madhuker Reddy and my sister in-law L. Sudhabindu whose encouragement gave me the determination to complete my work ahead of time. Their love and affection has been motivating force behind what I am today.

Last but not least, I would like to thank my better half Dr. L. Sudheer Reddy and my innocent daughter L. Sharvani for their prayers, patience, encouragement and understanding that were vital to complete this dissertation. Without their help and encouragement, I would not have been finished this thesis.

. Kethiri Himabindu

A B S T R A C T

The importance of entropy and entropy generation is noticeable in areas of immediate practical interest such as engineering and science. Entropy is used to establish criteria for the performance of engineering devices. Minimizing entropy generation is important to improving the efficiency of any system. The entropy generation analysis enables us to identify the factors that are the major cause of irreversible effects in the system. In order to preserve the quality of energy in a fluid flow process or at least to reduce the entropy generation, it is important to study the distribution of the entropy generation within the fluid volume. Further, the Newtonian fluids cannot precisely describe the characteristics of the fluid flow with suspended particles. This aspect is precisely taken care by micropolar fluids, which have been receiving much attention in the recent years. The physiological characteristics of most of the industrial fluids described by micropolar fluids. Hence, this thesis describes the entropy generation due to micropolar fluid flow through channels and pipes. The boundaries of the geometry are subject to (i)No slip for velocity and thermal/heat flux for temperature (ii)Slip for velocity and the convective boundary condition for temperature.

The thesis consists of EIGHT chapters. Chapter 1 provides an introduction to the concepts in laws of thermodynamics, entropy generation analysis, micropolar fluid and a review of the pertinent literature. Chapter 2 presents the numerical solution of entropy generation with micropolar fluid flow through an inclined channel. Chapter 3 investigates the entropy generation analysis for the micropolar fluid flow through a porous channel. Chapter 4 deals the numerical solution for entropy generation analysis of the MHD flow of micropolar fluid in a rectangular duct. Chapter 5 studies the entropy generation analysis of micropolar fluid flow through an inclined porous circular pipe. Chapter 6 presents the entropy generation analysis of micropolar fluid flow through concentric cylinders. Chapter 7 studies the numerical solution of entropy generation with micropolar fluid flow through porous concentric cylinders.

In all these chapters (except chapter 4), the governing equations are initially linearized by using the Quasilinearization method. The resulting linearized equations are solved by applying Chebyshev spectral collocation method. The governing partial differential equations of momentum, angular momentum, and energy in chapter - 4 are solved numerically using finite difference method. The effects of coupling number, Reynolds number, Brinkman number, slip parameter and Biot number on the velocity, microrotation, temperature, as well as entropy generation rate and Bejan number are presented through graphs. The last chapter (Chapter - 8) gives key findings of the thesis and scope of the work for further study.

NOMENCLATURE

a	radius of the pipe
A	constant pressure gradient
a_j	microinertia parameter
B	micropolar constant
Be	Bejan number
Bi	Biot number
B_0	magnetic flux density
Br	Brinkman number
C_p	specific heat at constant pressure
Ec	Eckert number
f'	dimensionless axial velocity
f	dimensionless transverse velocity
g	dimensionless microrotational component
Gr	Grashof number
g^*	acceleration due to gravity
h	channel width
Ha	Hartman number
K_f	thermal conductivity of the fluid
l	non-dimensional parameter
m^2	micropolar parameter
N	coupling number
N_h	entropy generation due to heat transfer
N_ϑ	entropy generation due to viscous dissipation
N_m	entropy generation due to magnetic effect
N_s	dimensionless entropy generation number
Pr	Prandtl number
r_1	radius of the inner cylinder
r_2	radius of the outer cylinder
R	suction or injection Reynolds number
Re	Reynolds number
T	dimensional temperature
T_p	dimensionless temperature difference
u	dimensional axial velocity
v	dimensional transverse velocity
U_0	characteristic velocity
V_0	injection velocity
V_1	suction velocity

Greek Symbols

α, β, γ	gyration viscosity coefficients
κ	vortex viscosity
ρ	density of the fluid.
θ	dimensionless temperature
μ	viscosity of the fluid
ϕ	inclined angle
ζ	slip coefficient
σ	dimensional microrotational component
σ_e	fluid electrical conductivity
Ω_1, Ω_2	angular velocities of the inner and outer cylinders

Superscripts

$'$	differentiation with respect to η.

Contents

[1]Case(a):Published in "**Alexandria Engineering Journal, 55 (2016) 973-982**", Case(b):Published in "**Energy, 91 (2015) 72-83**"

[2]Case(a):Communicated to "**Journal of Engineering Thermo Physics**", Case(b) Communicated to "**International Journal of Nonlinear Sciences and Numerical Simulation**"

[3]Case(a):Published in "**Procedia Engineering Journal, 127 (2015) 1150-1157**", Case(b) Communicated to "**Journal of Heat Transfer**"

[4]Case(a): Accepted in "**Advances and Applications in fluid Mechanics**", Case(b) Accepted in "**Sadhana**"

[5]Case(a): Communicated to "**Applied Thermal Engineering**", Case(b) Accepted in"**Ain Shams Engineering Journal**"

[6]Case(a): Communicated to "**Journal of Taiwan Institute of Chemical Engineers**", Case(b) Published in"**Energy, 111 (2016) 165-177**"

Chapter 1

Introduction

1.1 Introduction

Fluid flow through channels, pipes and annulus have received the considerable attention of the several investigators as it is encountered in many energy related applications. The channel configuration is relevant to solar energy collectors, transpiration cooling, gaseous diffusion technology, cooling of rocket, mechanized irrigation and filtration processes, thermal insulation engineering, etc. Further, flow in a pipe or induced by a relative rotating motion or axial movement between concentric cylinders is applicable to rotating electrical machines, swirl nozzles, rotating disks, standard commercial rheometers, journal bearings and other chemical and mechanical mixing equipment. Although a wide variety problems involving channel, circular pipe and concentric cylinder geometry were reported in the literature, these problems have been restricted, in thermodynamic point of view, to only the first law of thermodynamics analyses.

The improvement of thermal systems has gained a growing interest due to the relations with the problems of material processing, energy conversion and environmental effects. Ef-

ficient energy utilization during any fluid flow is one of the fundamental problems of the engineering processes to improve the system. One of the methods used for the prediction of performance of the engineering processes has been the second law analysis. Hence, the contemporary trend in the field of heat transfer and thermal design is to perform analysis of the second law of thermodynamics and its design-related concept of entropy generation and its minimization. This new trend is important and, at the same time, necessary to contribute to a viable engineering solution to the energy problems. Entropy generation analysis is gaining currency in engineering fields like heat exchangers, cooling of nuclear reactors, energy storage systems, cooling of electronic devices, pumps, turbine, and pipe networks, and so forth. A great surge of investigations on entropy generation aspects of fluid flow systems was carried out theoretically in idealized flow configurations having technological implications.

The thermodynamic systems and engineering devices involve various processes such as compression, expansion, cooling, heating, humidification etc. In all these processes, there is an exchange of mass, momentum and energy. Hence, a basic knowledge of the laws of thermodynamics, fluid mechanics and heat transfer that governs these processes is essential.

1.2 Laws of Thermodynamics

Thermodynamics is the study of energy, the conversion of energy between various forms and the ability of energy to do the work. It is concerned with heat and temperature and their relation to energy and work. The foundations of thermodynamics are the four laws of thermodynamics, which define the rules of temperature equivalence (zeroth law), energy conservation (first law), entropy tendencies (second law), and conditions for an absence of temperature (third law). These laws provide a sound basis for studying the relationships among the various forms of energy and their interactions.

1.2.1 First Law of Thermodynamics

The first law of thermodynamics, also known as the law of conservation of energy, states that the energy can be neither created nor destroyed during a process, but changes only forms. The first law of thermodynamics evaluates temperature distributions of fluids within the geometry and also heat transfer coefficients at the surrounding walls. However, it provides no information about the direction in which processes can spontaneously occur, that is, the reversibility aspect of thermodynamics processes. It gives no information about the inability of any thermodynamics processes to convert heat into mechanical work with full efficiency. An experimentally derived principle is required to characterize the availability of energy, which is precisely stated in the second law of thermodynamics.

1.2.2 Second Law of Thermodynamics

The first law is concerned with the quantity of energy and the transformation of energy from one form to another irrespective of its quality. Preserving the quality of energy is a major concern to engineers, and the second law provides the necessary means to determine the quality as well as the degree of degradation of energy during a process.

The second law of thermodynamics states that energy of all sorts, whether it be light, potential, chemical, kinetic, or whatever, tends to change itself spontaneously into a more dispersed, random, or less organized, form. It defines the fundamental physical quantity entropy as randomized energy state unavailable for direct conversion to work. It states that the entropy of the universe (i.e. system and the surroundings) increases in a spontaneous process and remains unchanged in an equilibrium process. The change in the entropy of the universe ($\triangle S_{\text{univ}}$) is sum of the entropy changes in the system ($\triangle S_{\text{sys}}$) and the surroundings ($\triangle S_{\text{surr}}$), which is expressed by the following mathematical equation:

$$\triangle S_{\text{univ}} = \triangle S_{\text{sys}} + \triangle S_{\text{surr}}$$

Then the second law of thermodynamics states that

$$\text{Spontaneous} \quad \text{process}: \quad \triangle S_{\text{univ}} = \triangle S_{\text{sys}} + \triangle S_{\text{surr}} > 0 \tag{1.1}$$

$$\text{Equilibrium} \quad \text{process}: \quad \triangle S_{\text{univ}} = \triangle S_{\text{sys}} + \triangle S_{\text{surr}} = 0 \tag{1.2}$$

$$\text{Nonspontaneous} \quad \text{process}: \quad \triangle S_{\text{univ}} = \triangle S_{\text{sys}} + \triangle S_{\text{surr}} < 0 \tag{1.3}$$

1.3 Entropy Generation Analysis

Entropy and entropy generation are fundamental quantities. They play essential role in understanding of many diverse phenomena ranging from cosmology to biology. A physical quantity termed entropy defined in the second law of thermodynamics is a measure of irreversibility of the systems. Entropy generation is not a property because it depends upon the process path. Generation of entropy destroys the available work of a system. Therefore, it makes good engineering sense to focus on the irreversibility of heat transfer and fluid flow processes to understand the function of the entropy generation mechanism. To optimize the performance of engineering systems containing devices in which simultaneous heat and mass exchange occur, their irreversibilities of individual devices must be minimized. Since the total irreversibility of a system is the sum of the component irreversibilities, this procedure improves the system performance. The factors that cause irreversibilities include friction, unrestrained expansion, mixing of two fluids, heat transfer across a finite temperature difference, electric resistance, inelastic deformation of solids, and chemical reactions.

The second law of thermodynamics can be combined with the principles of fluid mechanics and heat transfer to acquire knowledge about irreversibilities that influence the working efficiency of the system and processes. All the real processes related to thermal convection system are associated with thermal gradient and frictional effects and hence some amount of available energy is destroyed during the process due to irreversibilities. The optimization may therefore be carried out by minimizing the irreversibilities present in the system. This approach of thermodynamic optimization known as Entropy Generation Minimization(EGM) was first reported by Bejan [12]. Entropy generation minimization(EGM)is a method of

modeling and optimization. Since then the theories based on these foundations have rapidly developed. However, the entropy production resulting from temperature differences has remained untreated by classical thermodynamics, which motivates many researchers to analyze the fundamental and applied engineering problems based on the second law of thermodynamics. Bejan [15] presented the following expression for the volumetric entropy generation rate.

$$S_{gen} = \frac{K_f}{T_1^2}[\nabla T]^2 + \frac{1}{T_1}\Phi \tag{1.4}$$

where the first term on the right hand side of the above equation represents the entropy generation due to heat transfer and the second term represents the entropy generation due to viscous dissipation or friction.

It can be noted that second law analysis makes possible to compare many different interactions in a process or system and to identify the major sources of exergy distributions or losses. This enables us to exactly identify the region where the entropy generation rate is maximum in the entire fluid regime. This study facilitated through the entropy generation number introduced by Bejan. Consequently, the relative effects of heat transfer and fluid friction can be determined successfully by Bejan number.

1.4 Micropolar Fluid

Newtonian fluid is one for which the shear stress induced by flow is proportional to the rate of the strain (Newton's law of viscosity) and the constant of proportionality is the fluid's viscosity. Most of the common fluids used in our daily life, e.g., gasoline, honey, water and air are satisfactorily characterized as Newtonian fluids. There are numerous fluids such as multigrade engine oils, liquid soaps, paint, shampoo, toothpaste, peanut butter and mayonnaise, for which Newton's law of viscosity does not hold good. These fluids are termed as Non-Newtonian fluids. Further, examples include slurries and polymers in molten form. The rheological characteristics of the fluids can be described through the constitutive equations. In view of the diversity of non-Newtonian fluids, a single constitutive equation cannot

predict their rheological behavior. Therefore, several empirical and semi-empirical constitutive equations have been proposed in the literature. Micropolar fluid model, presented by Eringen [41], is one amongst them, which exhibit microinertial effects and support body couples and couple stresses. Shearing stress components are affected by the vorticity and microrotation in these fluids and are no longer symmetric. The important feature of these fluids is the microrotation.

The applications of the micropolar fluid model include the extrusion of polymer fluids and real fluids with suspensions, solidification of liquid crystals, cooling of a metallic plate in a bath, animal blood, porous media, turbulent shear flows, flow in capillaries, microchannels, colloidal and suspension solutions. In the micropolar fluid theory, rigid particles contained in a small fluid volume element are limited to rotation about the center of the volume element described by the micro-rotation vector. This local rotation of the particles is in addition to the usual rigid body motion of the entire volume element. Physically micropolar fluids may be described as the non-Newtonian fluids consisting of dumb-bell molecules or short rigid cylindrical elements.

The theory of micropolar fluids requires to append a transport equation representing the principle of conservation of local angular momentum to the usual transport equations for the conservation of mass and momentum with additional local constitutive parameters. Hence, this theory allows for two independent vectors, velocity vector $\overline{q}$ and microrotation vector $\overline{\sigma}$ associated with each fluid particle. The microrotation vector represents the rotation in an average sense of the rigid particles centered in a small volume element about the centroid of the element. The field equations of micropolar fluid dynamics [41, 20] are

Conservation of mass:

$$\frac{d\rho}{dt} + \rho(\bigtriangledown.\overline{q}) = 0 \tag{1.5}$$

Conservation of momentum:

$$\rho\frac{d\overline{q}}{dt} = \rho\overline{f} - \bigtriangledown p - (\mu+\kappa)\bigtriangledown\times\bigtriangledown\times\overline{q} + \kappa\bigtriangledown\times\overline{\sigma} + (\lambda+2\mu+\kappa)\bigtriangledown(\bigtriangledown.\overline{q}) \tag{1.6}$$

Conservation of angular momentum:

$$\rho j^{*}\frac{d\overline{\sigma}}{dt} = \rho\bar{l} + \kappa\bigtriangledown\times\overline{q} - 2\kappa\overline{\sigma} - \gamma\bigtriangledown\times\bigtriangledown\times\overline{\sigma} + (\alpha+\beta+\gamma)\bigtriangledown(\bigtriangledown.\overline{\sigma}) \tag{1.7}$$

Conservation of energy:

$$\rho\frac{dE}{dt} = -P(\bigtriangledown.\overline{q}) + \rho\Phi - \left(\bigtriangledown.\overline{h}\right) \tag{1.8}$$

where Φ is the viscous dissipation function of mechanical energy per unit mass and is given by

$$\rho\Phi = \lambda(\bigtriangledown.\overline{q})^{2} + 2\mu(D:D) + 4\kappa\left(\frac{1}{2}\bigtriangledown\times\overline{q} - \overline{\sigma}\right)^{2} + \alpha(\bigtriangledown.\overline{\sigma})^{2} + \gamma(\bigtriangledown\overline{\sigma}:\bigtriangledown.\overline{\sigma}) + \beta\left(\bigtriangledown\overline{\sigma}:(\bigtriangledown.\overline{\sigma})^{T}\right)$$

The scalar quantities ρ and j^{*} are density, micro-inertia and are assumed to be constants. The vectors $\overline{q}$, $\overline{\sigma}$, $\overline{f}$ and $\bar{l}$ are the velocity, microrotation, body force per unit mass and body couple per unit mass respectively. P is the fluid pressure at any point, D denotes deformation tensor i.e., $D = \frac{1}{2}\left(\bigtriangledown\overline{q}:(\bigtriangledown.\overline{q})^{T}\right)$, E is the specific internal energy, $\overline{h} = -K_{f}\bigtriangledown T$ is the heat flux and K_{f} is the thermal conductivity. The material constants (λ,μ,κ) are the viscosity coefficients and (α,β,γ) are the gyro-viscosity coefficients. These confirm the following inequalities,

$$\kappa\geq 0,\quad 2\mu+\kappa\geq 0,\quad 3\lambda+2\mu+\kappa\geq 0,\quad \gamma\geq 0,\quad 3\alpha+\beta+\gamma\geq 0,\quad \gamma\geq\mid\beta\mid \tag{1.9}$$

The stress tensor τ_{ij} in the theory of micropolar fluid is given by

$$\tau_{ij} = (-P+\lambda(\bigtriangledown.\overline{q}))\,\delta_{ij} + (2\mu+\kappa)\,d_{ij} + \kappa\epsilon_{ijm}(\omega_{m}-\sigma_{m})$$

where σ_{m} and ω_{m} are the components of microrotation vector and the vorticity vector respectively, d_{ij} are the components of rate of shear strain, δ_{ij} is the kronecker symbol and ϵ_{ijm} is the Levi-Civita

symbol.

In the special case where the fluid has constant physical properties, no external body forces exist and the flow is in steady state, the conservation equations can be greatly simplified. Additionally, in the case where $\kappa = 0$, $\alpha = \beta = \gamma = 0$ and with vanishing $\bar{l}$, the gyration vector disappears and angular momentum equation (1.7) vanishes identically and the equation (1.6) reduces to the classical Navier-Stokes equation. We also note that in the case of zero vortex viscosity ($\kappa = 0$) only, the velocity vector $\overline{q}$ and the microrotation vector $\overline{\sigma}$ are decoupled and the global motion is unaffected by the microrotations.

1.5 Magnetohydrodynamics

Magnetohydrodynamics (MHD) is the branch of continuum mechanics which deals with the motion of an electrically conducting fluid in the presence of a magnetic field. This subject has attracted numerous scientists and engineers for the last few decades because of its fascination and importance in various technological devices and in understanding the diverse cosmic phenomena. MHD describes the frontier area combining classical fluid mechanics and electrodynamics. MHD phenomena are outcome of mutual interaction between magnetic field and electrically conducting fluid flowing across it i.e., electric current induced in the fluid as a result of its motion modify the field, and at the same time their flow in the magnetic field produces a mechanical force called Lorentz force which modifies the motion.

The flow of electric currents in the magnetic field produces a mechanical force that brings a change in the fluid motion. Suppose that the fluid is incompressible, electrically conducting and is in the presence of an arbitrary magnetic field. The magnetic field, then interacts with the fluid by means of body force and body couple per unit mass. If gravitational effects are not present, then a regular magneto-fluid dynamics assumption is $\rho\overline{f} = \rho_e E + \overline{J} \times \overline{B}$, where ρ_e is the free charge density. Since, the electric force density $\rho_e E$ is smaller than $\overline{J} \times \overline{B}$, the electric force density can be neglected. Hence, the fluid dynamical aspects of MHD are handled by adding an electromagnetic force term to the momentum equation of the fluid. There are two key physical effects which occur when the fluid moves into the magnetic field: motion of a conducting liquid in an applied magnetic field will induce a magnetic field in the medium. The total field is the sum of the applied and induced

magnetic fields ($\overline{B} = \overline{B_0} + \bar{b}$, $\bar{b}$ is induced magnetic field). The relative strength of the induced field is characterized by the magnetic Reynolds number. The neglect of the induced magnetic field is a valid assumption when magnetic Reynolds number is small. The second key effect is dynamical. When currents are induced by a motion of a conducting fluid through a magnetic field, a force (Lorenz force or $\overline{J} \times \overline{B}$, where $\overline{J}$ is the current density and $\overline{B}$ is the magnetic field) will act on the fluid and alter its motion. Hence, fluid motion in a magnetic field induces

1.6 Boundary Conditions

The governing equations for the velocity, microrotation and temperature fields are partial differential equations. Which are applicable at every point in a fluid that is being modeled as a continuum. When they are integrated in any given situation, it can be expected to see arbitrary functions or constants appear in the solution. To evaluate these, an additional statement of velocity, microrotation, temperature fields and their gradients at the natural boundaries of the flow domain are needed. Such statements are known as boundary conditions. The different boundary conditions for the velocity (no-slip condition and slip condition), microrotation (hyperstick condition) and temperature (uniform temperature, heat flux and convective conditions) are given below.

No-slip Condition

In no-slip boundary condition, the fluid is in contact with a wall will have the same velocity as the velocity of the wall. Often, the walls are not moving, so as the fluid velocity is zero. In drag flows, the velocity of the wall is finite and the fluid velocity is equal to the wall velocity.

$$\overline{q}_{(\text{at the boundary})} = \overline{q}_{\text{wall}}$$

Slip Condition

Navier [82] proposed a general boundary condition that incorporates the possibility of fluid slip at a solid boundary. This condition states that the velocity at a solid surface is proportional to the

shear stress at the surface.

$$\overline{q}_{\text{wall}} = \zeta \, \overline{\tau}_{\text{wall}}$$

where ζ is the slip length or slip coefficient. The measure of the slip is called slip length. Factors that affect the slip length include weak wall fluid attraction, surface roughness and high shear stress. If $\zeta = 0$, then the general assumed no-slip boundary condition is obtained. The fluid slippage phenomenon at the solid boundaries appear in many applications such as in microchannels or nanochannels and in applications where a thin film of light oil is attached to the moving plates or when the surface is coated with special coatings such as thick monolayer of hydrophobic octadecyltrichlorosilane.

Hyper-stick Condition

In this thesis it has been taken the hyper-stick condition for microrotation. This condition states that the microrotation vector on the boundary is same as the angular velocity of the fluid on the boundary.

$$\sigma_{\text{wall}} = \frac{1}{2} \left(\nabla \times \overline{q}_{\text{wall}} \right)$$

A more general condition is taken as

$$\sigma_{\text{wall}} = n \ \left(\nabla \times \overline{q}_{\text{wall}} \right)$$

where $0 \leq n \leq 1$ (refer [62]). This value of n indicates the concentration of micropolarity or interaction of fluid particles with the boundary. The case $n = 0$ indicates $\sigma = 0$ at the boundary. It represents the flow of concentrated particles in which the micro elements closed to the wall surface are unable to rotate. This case is also known as strong concentration of micro elements. The case corresponding to $n = 0.5$ results in the vanishing of antisymmetric part of stress tensor and represents weak concentrations of microelements. The particle spin is equal to fluid vorticity at the boundary for the fine particle suspensions. The case corresponding to $n = 1$ represents a turbulent boundary layer flows.

Isothemral/Flux conditions

In most usual situations, heat transfer takes place in a fluid moving near a wall heated or cooled at a temperature different from that of the fluid. In this case, the boundary conditions are expressed at the fluid/solid interface. The most usual conditions consist of one of the following simplified assumptions:

1. The fluid/solid interface is at a uniform temperature : $T_{\text{fluid}} = T_{\text{solid}} = \text{constant}$
2. The heat flux is uniform on the interface : $q_w = -K_f\,(n.\nabla T)$.

Convective Boundary Conditions

Recently, a novel mechanism for the heating process has drawn the involvement of many researchers, namely, convective boundary condition (CBC), where the heat is supplied to the convecting fluid through a bounding surface with a finite heat capacity. Further, this results in the heat transfer rate through the surface being proportional to the local difference in temperature with the ambient conditions [74].

$$-K_f\,(n.\nabla T) = h(T_{\text{surface}} - T_\infty)$$

where h is the heat transfer coefficient, T_∞ is the ambient temperature.

1.7 Aim and Scope of the Thesis

The aim of the present thesis is to study the entropy generation analysis due to micropolar fluid flow through channels and pipes. In this thesis, two types of boundary conditions are considered. First type (or case) of boundary conditions are no-slip for velocity and iso thermal/iso flux for temperature and the second type are slip for velocity and convective boundary condition for temperature. Further, the hyperstick condition for microrotation is taken in both the cases. The governing non-linear equations are linearized using quasilinearization method and the resulting equations are solved using Chebyshev spectral collocation method. The influence of coupling number, Reynolds number, slip parameter, Biot number and Brinkman number on the velocity, microrotation, temperature, entropy generation and Bejan number are analyzed.

Quasilinearization Method

In this section we give a description of the quasilinearization method (QLM). The QLM was initially proposed by Bellman and Kalaba [16] to solve non-linear boundary layer problems. To develop the QLM we consider a system of m non-linear ordinary differential equations with m unknowns $z_i(\eta)(i = 1, 2, ...m)$ where η is the independent variable. The system can be written as a sum of its linear (L) and non-linear components (N) as

$$L\left[z_1(\eta), z_2(\eta), ...z_m(\eta)\right] + N\left[z_1(\eta), z_2(\eta), ...z_m(\eta)\right] = H(\eta) \tag{1.10}$$

Define vector Z_i to be the vector of the derivatives of the variable z_i with respect to the independent variable η, that is

$$Z_i = \left[z_i^{(0)}, z_i^{(1)}, ..., z_i^{(n_i)}\right] \tag{1.11}$$

where $z_i^{(0)} = z_i$ and $z_i^{(p)}$ is the p^{th} derivative of z_i with respect to η and $n_i(i = 1, 2, ...m)$ is the highest derivative order of the variable z_i appearing in the system of equations. In addition, we define L_i and N_i to be the linear and non-linear operators respectively, that operate on the Z_i for $i = 1, 2, ...m$. With these definitions equation (1.10) can be written as

$$L_i\left[Z_1, Z_2, ...Z_m\right] + N_i\left[Z_1, Z_2, ...Z_m\right] = \sum_{j=1}^{m}\sum_{p=0}^{n_i} \alpha_{ij}^{[p]} Z_j^{(p)} + N_i\left[Z_1, Z_2, ...Z_m\right] = H_i \tag{1.12}$$

where $\alpha_{ij}^{[p]}$ are the constant coefficient of $z_j^{(p)}$, the derivative of $z_j(j = 1, 2, ...m)$ that appears in the i_{th} equation for $i = 1, 2, ...m$.

Again, we assume that equation (1.10) is to be solved subject to separated two-point boundary conditions which are expressed as

$$\sum_{j=1}^{m}\sum_{p=0}^{n_j-1} \beta_{v,j}^{[p]} z_j^{(p)}(a) = K_{a,v}, \qquad v = 1, 2, ..., m_a \tag{1.13}$$

$$\sum_{j=1}^{m}\sum_{p=0}^{n_j-1} \gamma_{\sigma,j}^{[p]} z_j^{(p)}(b) = K_{a,\sigma}, \qquad \sigma = 1, 2, ..., m_b \tag{1.14}$$

where $\beta_{v,j}^{[p]}$, $\gamma_{\sigma,j}^{[p]}$ are the constant coefficients of $z_j^{(p)}$ in the boundary conditions and m_a, m_b are the total number of prescribed boundary conditions at $\eta = a$ and $\eta = b$ respectively.

Assume that the solution $z_i(\eta)$ of (1.12) at the $(r+1)^{th}$ iteration is $z_{i,r+1}$. If the solution at the previous iteration $z_{i,r}(\eta)$ is sufficiently close to $z_{i,r+1}$, the non-linear component N_i of equation (1.12) can be linearized using one term Taylor series for multiple variables so that equation (1.12) can be approximated as

$$L_i\left[Z_{1,r+1},.....Z_{m,r+1}\right]+N_i\left[...\right]=\sum_{j=1}^{m}\sum_{p=0}^{n_i}\left(Z_{j,r+1}^{(p)}-Z_{j,r}^{(p)}\right)\frac{\partial N_i}{\partial Z_j^{(p)}}\left[...\right]=H_i \tag{1.15}$$

where

$$\left[...\right]=\left[Z_{1,r},Z_{2,r},.....Z_{m,r}\right] \tag{1.16}$$

Equation (1.15) can be re-written as

$$L_i\left[Z_{1,r+1},.....Z_{m,r+1}\right]+\sum_{j=1}^{m}\sum_{p=0}^{n_i}Z_{j,r+1}^{(p)}\frac{\partial N_i}{\partial Z_j^{(p)}}\left[...\right]=H_i+\sum_{j=1}^{m}\sum_{p=0}^{n_i}Z_{j,r}^{(p)}\frac{\partial N_i}{\partial Z_j^{(p)}}\left[...\right]-N_i\left[...\right] \tag{1.17}$$

The above equation can then be solved using any numerical method. In this work we use the Chebyshev spectral collocation method and we call the resulting method, the spectral quasilinearization method ($SQLM$).

Chebyshev Spectral Collocation Method

The Chebyshev spectral collocation method [22, 36, 95] is based on the Chebyshev polynomials defined on the interval [-1, 1]. To solve the problems using this method, first transform the domain $[a,b]$ to the domain $[-1,1]$ by using the transformation

$$(b-a)\chi=2x-(a+b),\ \ -1\leq\chi\leq 1 \tag{1.18}$$

We discretize the domain [-1, 1] using the Gauss-Lobatto collocation points given by

$$\chi_j=\cos\frac{\pi j}{J},\quad j=0,1,2,.....,J \tag{1.19}$$

where J is the number of collocation points used. The function z_i is approximated at the collocation points as follows

$$z_i(\chi) = \sum_{k=0}^{J} z_i(\chi_k) T_k(\chi_j) \tag{1.20}$$

where T_k is the k^{th} Chebyshev polynomial defined by $T_k(\chi) = \cos[k\cos^{-1}\chi]$

The derivatives of the variables at the collocation points are represented as

$$\frac{d^r z_i}{dx^r} = \sum_{k=0}^{J} \left[\frac{2}{b-a}\mathbf{D}_{kj}\right]^r z_i(\chi_k), \tag{1.21}$$

where r is the order of differentiation and $\mathbf{D}$ being the Chebyshev spectral differentiation matrix whose entries are defined as

$$\left.\begin{array}{l} \mathbf{D}_{00} = \frac{2J^2+1}{6} \\ \mathbf{D}_{jk} = \frac{c_j}{c_k}\frac{(-1)^{j+k}}{\chi_j - \chi_k}, \;\; j \neq k; \;\; j,k = 0,1,2\cdots,J, \\ \mathbf{D}_{kk} = -\frac{\chi_k}{2(1-\chi_k{}^2)}, \;\; k = 1,2\cdots,J-1, \\ \mathbf{D}_{NN} = -\frac{2J^2+1}{6} \end{array}\right\} \tag{1.22}$$

Substituting equations (1.19) - (1.22) into the given equation leads to the following system of matrix equation

$$\mathbf{A}_{i-1}\mathbf{X}_i = \mathbf{R}_{i-1}, \tag{1.23}$$

in which A_{i-1} is a (J +1)×(J +1) square matrix while X_i and R_{i-1} are (J +1)× 1 column vectors. After incorporating the boundary conditions, the solution of the given equation is obtained as

$$\mathbf{X}_i = \mathbf{A}_{i-1}^{-1}\mathbf{R}_{i-1} \tag{1.24}$$

1.8 Literature Review

Entropy generation which is the measure of the destruction of available energy in a system that plays an important role in the design and development of engineering processes such as heat exchangers, pumps, turbine and pipe networks. The energy utilization during the convection in any fluid flow and the improvement in thermal system is one of the fundamental problems of the engineering

processes, this can be done by minimizing the entropy generation. Bejan [12] was the pioneer to work on entropy generation. Bejan [14, 15] investigated entropy generation minimization and showed the fundamental importance of entropy minimization for efficient engineering processes. Thereafter, many authors such as Baytas [11], Tasnim and Mahmud [91], Ganji *et al* [43], Esfahani and Shahabi [42], Tshehla *et al* [97, 96], Heidary *et al* [47], Chauhan and Kumar [23], Ramakrishna *et al* [86], etc., have studied the entropy generation and irreversibility profiles for different geometric configurations, flow situation and thermal boundary conditions.

Fluid flow and heat transfer in channels with simple geometry at different boundary conditions is one of the fundamental researches in engineering. Several researchers have discussed the entropy generation inside the channels under various flows. Tasnim *et al* [90] analyzed the first and second law characteristics of non-Darcy mixed convection flow in a porous channel in the presence of transverse magnetic field. They observed that the channel walls act as strong concentrator of irreversibility due to high velocity and temperature gradients. Entropy generation in a channel of two parallel plates with viscous dissipation was investigated by Mahmud and Fraser [70, 69]. Erbay [40] studied the entropy generation due to fluid flow through a channel where the bottom is moving. Havzali [46] investigated the entropy generation on a laminar, viscous, incompressible flow between two inclined, parallel, isothermal plates.

The study of fluids in porous channel has received adequate attention over the few centuries due to its wide applications in physical, biological and applied sciences. Consequently, investigation of entropy generation in porous channel due to the combined effects of wall suction/injection becomes essential. Chauhan and Kumar [23] studied entropy analysis in an annulus partly saturated with a porous medium due to third grade fluid flow. Entropy generation for couple stress fluid through a vertical channel filled with saturated porous medium was determined by Makinde [72]. Adesanya and Makinde [1, 2] examined the entropy generation in couple stress fluid flow through a porous channel with slip and convective heating. Mahdavi *et al* [65] discussed the fluid flow analysis and heat transfer in pipes partly occupied with porous medium and evaluated the entropy generation numerically.

The flow through the circular pipe and flow between two cylinders, where one or both of the cylinders rotate has many applications. Yilbas *et al* [101] studied the entropy analysis for non-Newtonian fluid flow in an annular Pipe. They found that the rate of entropy generation can be reduced by reducing both non-Newtonian parameter and Brinkman number. Bouzid *et al*

[19] investigated the entropy generation in a fully developed ice slurry pipe flow and found that the volumetric average entropy generation number increases as the mass fraction of ice or the dimensionless group parameter increases.

Fluid flow and heat transfer inside a cylindrical annular space through convection have many significant engineering applications. Mirzazadeh *et al* [75] have focused on the entropy generation induced by the flow of a non-linear viscoelastic fluid between concentric rotating cylinders. Their results showed that the entropy generation number increases with increase in Brinkman number. Atayilmaz [9] carried out both numerical and experimental analysis on natural convection of heat transfer from horizontal concentric cylinders. Considerable amount of research has been carried out to investigate the Newtonian and non-Newtonian fluid flow through concentric cylinders. Taylor [92] studied theoretically and experimentally the flow of viscous incompressible fluid between two concentric cylinders. Hessami *et al* [48] analyzed laminar mixed convection flow pattern and heat transfer of air inside a vertical cylindrical annular space. Borjini *et al* [18] studied the effect of radiation on unsteady numerical convection between two horizontal concentric and vertically eccentric cylinders.

The majority of entropy generation studies deal with convection processes in which the entropy generation is the result of fluid friction and heat transfers. Haddad *et al* [44] presented the entropy generation due to laminar forced convection in the entrance region of a concentric cylindrical annulus. It was found that the thermal entropy generation is relatively dominant over viscous entropy generation. Hooman and Ejlali [49] studied the entropy generation for forced convection in a circular tube filled by a saturated porous medium, with uniform wall temperature. Cimpean and Pop [28] studied the entropy generation for a mixed convection flow of a fluid saturated porous medium through an inclined channel with uniform heated walls. Several works have been carried out on entropy generation with natural convection (see, example [63, 64, 5, 25, 10]).

The flow and heat transfer in an electrically conducting fluid in the presence of a magnetic field has attracted several researchers in view of its applications in engineering, technology and science. Rashid and Mehr [87] studied the effects of the velocity slip and temperature jump conditions on the entropy generation in the MHD flow over a porous rotating disk. Numerical analysis of the entropy generation within a mixed convection magneto hydrodynamic (MHD) flow in a parallel-plate vertical channel was performed by Liu and Lo [61]. They observed that the minimum entropy generation number and the maximum Bejan number occur at centerline region of the channel under

asymmetric heating conditions.

The boundary condition of the fluid over a solid surface is the generally accepted no-slip condition. However, Navier [82] proposed a slip boundary condition where the slip velocity depends linearly on the shear stress. The fluid slippage phenomenon at the solid boundaries appear in many applications such as in microchannels or nanochannels and the polishing of artificial heart valves, internal cavities. Yari [100] studied the second-law analysis and entropy generation for heat transfer and fluid flow through microannulus by considering the viscous dissipation effect, slip velocity and temperature jump. Effects of velocity slip, temperature jump on entropy generation in a rectangular duct with forced convection is presented by Hooman [50].

Furthermore, heat transfer processes poses thermal boundary conditions, heat flux boundary conditions and convective boundary conditions. Consequently, investigation of entropy generation due to the effects of Navier slip and different temperature conditions becomes essential. Eegunjobi and Makinde [38, 39] presented the effect of slip and convection heating on entropy generation in a channel. Ibanez [52] considered the problem of entropy generation with slip and convective boundary conditions. Iman [53] investigated the importance of thermal boundary conditions of the heated/cooled walls in the development of flow, heat transfer, and observed the characteristics of entropy generation in a porous enclosure.

The flows of non-Newtonian fluids are very important because of their industrial and technological applications. In many chemical and processing industries, the products such as polymer, foods, and plastics exhibit non-Newtonian behavior. Adequate research has been done on entropy generation due to various non-Newtonian fluid flows through different geometries. Langeroudi and Aghanajafi [59] applied power-law, Bingham and Casson fluid flow models in a circular pipe to evaluate entropy generation. Mahian *et al* [66, 67, 68] determined the influence MHD flow on the entropy generation of nanofluid flow through a vertical annulus. Entropy generation due to nanofluid flow through a channel with convective cooling/heating was investigated by [24, 76, 30]. The entropy generation and heat transfer characteristics of the fully developed flows of power law fluids in a micro channel was discussed in [33, 4] .

Micropolar fluid theory is one of the non-Newtonian fluids introduced by Eringen [41] has distinct features, such as microscopic effects arising from the local structure, micro motion of fluid elements, presence of couple stresses, body couples and non-symmetric stress tensor. Weng *et al* [98]

applied the micropolar fluid to study the stability problem of flow between two concentric rotating cylinders. Nadeem *et al* [80] studied the peristaltic flow of a micropolar fluid with heat transfer in an annulus. Imtiaz and Mahfouz [54] investigated numerically the conjugate heat transfer in an annulus between two concentric cylinders. Devi *et al* [35] studied the mixed convection micro polar flow through a porous medium in a cylindrical annulus using finite element analysis.

Heat transfer enhancement in a rectangular duct is of great interest and importance in many industrial applications like heat exchangers, cooling devices and gas turbines because of higher heat transfer rates increase the efficiency of a system and reduce thermal load. Narusawa [81] investigated the mixed convection and entropy generation numerically in three dimensional rectangular duct with heating at the bottom. Oztop [83] studied the entropy generation in a semicircular duct with constant heat flux. Ko and Ting [57] analyzed the entropy generation in a curved rectangular duct caused by forced convection with external heating. Haji-Sheikh [45] considered the fully developed forced convection in a duct of rectangular cross section. Jarungthammachote [55] studied the entropy generation for laminar fluid flow through a hexagonal duct. Yang *et al* [99] investigated heat transfer and entropy generation in the entrance region of a three dimensional vertical rectangular duct. They noticed that increase in Reynolds number increases the entropy generation rate due to heat transfer and fluid friction in the channel.

1.9 Outline of the Thesis

The present thesis aims at presenting entropy generation analysis for micropolar fluid flow through channels and pipes. A quantitative analysis has been performed based on numerical computations in order to know the effects of certain physical parameters on entropy generation and Bejan number through graphs. This thesis consists of EIGHT chapters.

Chapter - 1 is introductory in nature and motivates the investigations carried out in the thesis. The basic terminology is introduced and a survey of pertinent literature is presented to exhibit the importance of the problems considered. The basic equations governing the micropolar fluid flow and heat transfer are given.

In chapter-2, the entropy generation for steady incompressible micropolar fluid flow through an inclined channel for two types of boundary conditions is investigated. In the first case, the lower

plate of the channel is kept at constant temperature and upper plate is subjected to uniform heat flux. Slip and convective boundary conditions are prescribed in the second case. The governing equations are simplified for velocity, microrotation and temperature profiles, which are used to compute entropy generation and Bejan number. The obtained numerical results are compared and are found to be in good agreement with previously published results dealing with special cases.

Chapter-3 analyzes the entropy generation due to micropolar fluid flow through a porous channel under different boundary conditions. In the previous chapter one dimensional channel flow is considered, whereas in this chapter the two dimensional flow through the channel is considered. The governing non-linear partial differential equations are transformed to ordinary differential equations by using similarity transformations. The entropy generation number is computed numerically by utilizing the velocity, microrotation and temperature.

Chapter-4 deals with the problem of entropy generation due to heat transfer, fluid friction and magnetic field. The steady, incompressible micropolar fluid flow in a rectangular duct has been considered associated with different boundary conditions. An external uniform magnetic field is applied, which is directed arbitrarily in a plane perpendicular to the flow direction. The governing partial differential equations of momentum, angular momentum and energy are solved numerically using finite difference method. The obtained velocity, microrotation and temperature distributions are then used to evaluate the entropy generation and Bejan number.

Chapter-5 describes the second law analysis of micropolar fluid flow and heat transfer inside an inclined porous circular pipe for different boundary conditions. The cylindrical polar coordinate system (r, φ, z) with z-axis along the direction of the fluid flow is considered. The non-linear governing equations are transformed using similarity transformations and then solved numerically. The velocity, microrotation, temperature, entropy generation number and Bejan number are calculated and discussed quantitatively for various values of the embedded parameters.

Chapter-6 presents the analysis of entropy generation in micropolar fluid flow between concentric cylinders. The non-linear model problem is tackled numerically. The velocity, microrotation and temperature profiles are obtained and used to compute entropy generation and Bejan number. The entropy generation number and Bejan number are presented graphically and discussed quantitatively for various values of the fixed parameters. The numerical results are compared and are found to be in good agreement with previously published results as special cases of the present

investigation.

The objective of Chapter-7 is to analyze the entropy generation of micropolar fluid flow through porous concentric cylinders. A relative rotational motion is present between inner and outer cylinders, thus inducing the flow. The injection fluid flow rate at one wall is assumed to be same as the suction flow rate at the other wall. A uniform magnetic field is applied along the radial direction. The flow phenomenon has been characterized by the non-dimensional parameters like coupling number, cross flow Reynolds number and Brinkman number. The numerical data for velocity, microrotation and temperature fields are used to evaluate entropy generation and Bejan number.

The Spectral quasilinearization method is employed to solve the problems in Chapters (2, 3, 5, 6 and 7). In all these chapters, the governing equations are initially linearized by using the quasilinearization method. In this method, the iteration scheme is obtained by linearizing the non-linear component of a differential equation using the Taylor series expansion. The resulting linearized equations are solved by applying Chebyshev spectral collocation method. In all the chapters the effects of various physical parameters on the velocity, microrotation, temperature, as well as entropy generation rate and Bejan number are presented through graphs

In Chapter - 8, the main conclusions of the earlier chapters are recorded and the directions in which further investigations may be carried out are indicated.

A list of references is given at the end of the thesis. The references are arranged in an alphabetical order.

Considerable part of the work in the thesis is published/accepted for publication in journals. The remaining part is communicated for publications. The details are presented below.

List of Papers Published

1. "Entropy generation in a micropolar fluid flow through an inclined channel", *Alexandria Engineering Journal*, Vol. 55 (2016), pp.973–982.

2. "Entropy generation in a micropolar fluid flow through an inclined channel with slip and convective boundary conditions", *Energy*, Vol. 91 (2015), pp.72–83.

3. "Effect of magnetic field on entropy generation due to micropolar fluid flow in a rectangular duct", *Procedia Engineering*, Vol. 127 (2015), pp.1150–1157.

4. "Entropy generation in porous annulus due to micropolar fluid flow with slip and convective boundary conditions", *Energy*, Vol. 111 (2016), pp.165–177.

List of Papers Accepted

1. "An analysis of entropy generation in a micropolar fluid flow through an inclined porous circular pipe" *Advances and Applications in fluid Mechanics.*

2. "Entropy generation of micropolar fluid flow in an inclined porous pipe with convective boundary conditions", *Sadhana.*

3. "Entropy generation due to micropolar fluid flow between concentric cylinders with slip and convective boundary conditions", *Ain Shams Engineering Journal*,
DOI NO:10.1016/j.asej.2015.10.016.

List of Papers Communicated

1. "Entropy generation in a micropolar fluid flow through a porous channel", *Journal of Engineering Thermo Physics.*

2. "Effect of slip and convective boundary conditions on entropy generation in a porous channel due to micropolar fluid flow", *International Journal of Numerical methods for Heat and Fluid Flow.*

3. "Analysis of Entropy generation due to micropolar fluid flow in a rectangular duct subjected to slip and convective boundary conditions", *Journal of Heat Transfer.*

4. "Entropy generation due to micropolar fluid flow between concentric cylinders", *Applied Thermal Engineering.*

5. "Analysis of entropy generation between porous concentric cylinders due to micropolar fluid flow", *Journal of Taiwan Institute of Chemical Engineers.*

Chapter 2

Entropy Generation in a Micropolar Fluid Flow Through an Inclined Channel [1]

2.1 Introduction

The study of fluid flow and heat transfer has a wide range of thermal engineering applications such as thermal insulation engineering, water movement in geothermal reservoirs, heat pipes, etc. At the same time the optimal design criteria for thermal systems by minimizing their entropy generation have been recently a topic of great interest. Moreover, the performance of thermal devices is always affected by irreversible losses that lead to an increase of entropy and reduces the thermal efficiency. Therefore, in the energy optimization problems and in the design of many traditional heat removal engineering devices, it is necessary to minimize the entropy generation due to heat transfer and fluid friction. Starting from the pioneering work of Bejan [14], several investigations [12, 71, 27, 26, 33] have been carried on entropy generation under various flow configurations. Havzali [46] investigated the effect of entropy generation on a laminar, viscous, incompressible fluid flow between two inclined, parallel, isothermal plates. Kamisli and Oztop [56] examined the entropy

[1] Case(a):Published in "**Alexandria Engineering Journal, 55 (2016) 973-982**", Case(b):Published in "**Energy, 91 (2015) 72-83**"

generation in two immiscible incompressible fluid flows under the influence of pressure difference in thin slit of constant wall heat fluxes. Komurgoz *et al* [58] investigated the magnetic effect on heat-fluid and entropy generation interactions in an inclined channel consisting of two regions: one filled with clear fluid and the second with a porous medium.

The present chapter concentrates on investigating the characteristics of micropolar fluid flow and entropy generation in an inclined channel. Two types(cases) of boundary conditions are considered for the velocity and temperature on the plates of the inclined channel. In the first type(case a), the plates of the channel are subjected to no-slip and isoflux/isothermal boundary conditions. In the second type (case b), the plates of the channel are subject to slip and convective boundary conditions. The effect of pertinent parameters on velocity, microrotation, temperature, entropy generation and Bejan number are discussed through graphs.

2.2 Mathematical Formulation

Consider a steady, laminar, incompressible, fully developed, micropolar fluid flow bounded by two infinite inclined parallel plates separated by a distance $2h$. Assume that the channel is porous and inclined at an angle ϕ. Let the plates are of infinite length in x and z-directions i.e. -$\infty < x < \infty$ and -$\infty < z < \infty$. We consider the fluid to be flowing between the two plates under the influence of a constant pressure gradient $\frac{\partial p}{\partial x}$ in the x-direction, and a uniform suction or injection from below and above with a constant velocity v_0 where $v_0 < 0$ is the velocity of suction and $v_0 > 0$ is the velocity of injection. Hence, the flow is along x and y- directions and can be taken as $(u(y), v, 0)$. Therefore, the continuity equation takes the form $\frac{\partial v}{\partial y} = 0$ which on integration gives $v = constant$. This constant is equal to the suction velocity v_0. In particular, the velocity of the fluid is given as $\overline{q}(y) = u(y)i + v_0 j$.

With these assumptions and Boussinesq approximations, the governing equations are

$$\frac{\partial v}{\partial y} = 0 \tag{2.1}$$

$$(\mu + \kappa)\frac{d^2u}{dy^2} - \rho v\frac{du}{dy} + \kappa\frac{d\sigma}{dy} + \rho g^*\beta(T - T_1)\sin(\phi) - \frac{\partial p}{\partial x} = 0 \tag{2.2}$$

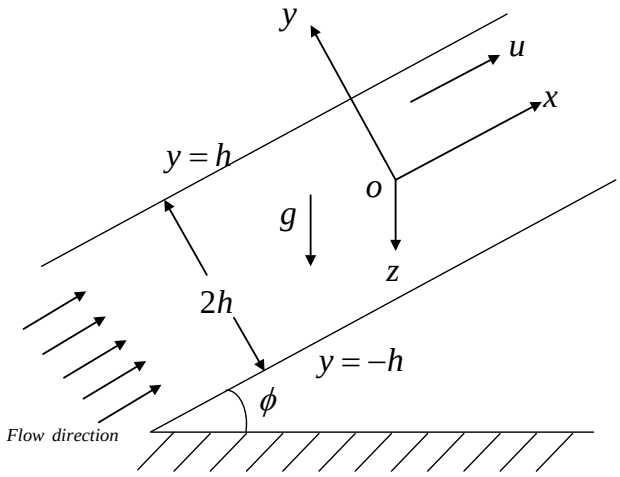

Figure 2.1: Physical model and coordinate system.

$$\gamma\frac{d^2\sigma}{dy^2} - \rho j^* v\frac{d\sigma}{dy} - 2\kappa\sigma - \kappa\frac{du}{dy} = 0 \tag{2.3}$$

$$K_f\frac{d^2T}{dy^2} - \rho C_p v\frac{dT}{dy} + (\mu+\kappa)\left(\frac{du}{dy}\right)^2 + 2\kappa\left(\sigma^2 + \sigma\frac{du}{dy}\right) + \gamma\left(\frac{d\sigma}{dy}\right)^2 = 0 \tag{2.4}$$

where u is the velocity component in x-direction, σ is the microrotation, ρ and j^* are the fluid density and gyration parameter, μ, κ and γ are the material constants (viscosity coefficients), g^* is the acceleration due to gravity, p is pressure, β is the coefficient of thermal expansion and K_f is the thermal conductivity of the fluid.

2.2.1 Case(a): No-slip and Isothermal/Isoflux Boundary Conditions

In this case, no-slip and hyper-stick conditions are considered for the velocity and microrotation respectively on both plates of the channel. Further, the upper plate of the channel is subject to uniform heat flux q (isoflux) while the lower plate of the channel is kept at uniform temperature T_1 (isothermal). These boundary conditions are given by

$$\begin{aligned} u = 0, \quad \sigma = 0, \quad \frac{dT}{dy} = \frac{q}{K_f}, \quad \text{at} \quad y = h \\ u = 0, \quad \sigma = 0, \quad T = T_1, \quad \text{at} \quad y = -h \end{aligned} \tag{2.5}$$

Introducing the following non-dimensional variables

$$\eta = \frac{y}{h}, \quad u = U_0 f(\eta), \quad \sigma = \frac{U_0}{h} g(\eta), \quad \theta(\eta) = \frac{T - T_1}{\frac{qh}{K_f}} \tag{2.6}$$

in Eqs.(2.2) - (2.4), to get the following coupled non-linear system of differential equations:

$$\frac{1}{1-N} f'' - Rf' + \frac{N}{1-N} g' + \frac{Gr}{Re} \sin(\phi)\theta = A \tag{2.7}$$

$$\frac{2-N}{m^2} g'' - a_j R \left(\frac{1-N}{N} \right) g' - 2g - f' = 0 \tag{2.8}$$

$$\theta'' - R\, Pr \theta' + \frac{Br}{1-N} \left[f'^2 + 2N(g^2 + gf') + \frac{N(2-N)}{m^2} g'^2 \right] = 0 \tag{2.9}$$

where U_0 is the characteristic velocity, $Pr = \frac{\mu C_p}{K_f}$(Prandtl number), $Re = \frac{\rho U_0 h}{\mu}$(Reynolds number), $R = \frac{\rho v_0 h}{\mu}$(suction/injuction Reynolds number), $N = \frac{\kappa}{\kappa+\mu}$(coupling number), $Gr = \frac{\rho^2 g \beta q h^4}{\mu^2 K_f}$(Grashof number), $A = \frac{h^2}{\mu U 0} \frac{\partial p}{\partial x}$(constant pressure gradient), $m^2 = \frac{h^2 \kappa (2\mu+\kappa)}{\gamma(\mu+\kappa)}$(micropolar parameter), $a_j = \frac{j^*}{h^2}$(micro-inertia parameter), $Br = \frac{\mu U_0^2}{hq}$(Brinkman number).

The corresponding dimensionless boundary conditions are

$$\begin{aligned} f = 0, \quad g = 0, \quad \theta' = 1, \quad \text{at} \quad \eta = 1 \\ f = 0, \quad g = 0, \quad \theta = 0, \quad \text{at} \quad \eta = -1 \end{aligned} \tag{2.10}$$

Method of Solution

The system of Eqs. (2.7) to (2.9) along with the boundary conditions (2.10) are solved using the Spectral quasilinearization method(SQLM) [77, 78, 79]. Initially Quasilinearization technique is applied to linearize the system of equations (2.7) to (2.9) and then Chebyshev spectral collocation method is implemented to solve the linearized equations.

Let f_r, g_r and θ_r be an approximate current solution and f_{r+1}, g_{r+1} and θ_{r+1} be an improved solution of the system of equations (2.7) to (2.9). By taking the Taylors series expansion of non-linear terms in (2.7) to (2.9) around the current solution and neglecting the second and higher

order derivative terms, to get the following linearized equations

$$\frac{1}{1-N}f''_{r+1} - Rf'_{r+1} + \frac{N}{1-N}g'_{r+1} + \frac{Gr}{Re}\sin(\phi)\theta_{r+1} = A \tag{2.11}$$

$$\frac{2-N}{m^2}g''_{r+1} - a_j R\left(\frac{1-N}{N}\right)g'_{r+1} - 2g_{r+1} - f'_{r+1} = 0 \tag{2.12}$$

$$\theta''_{r+1} - RPr\theta'_{r+1} + a_{1,r}f'_{r+1} + a_{2,r}g'_{r+1} + a_{3,r}g_{r+1} = a_{4,r} \tag{2.13}$$

where the coefficients $a_{s,r}, s = 1, 2, 3, 4$ are known functions calculated from previous iterations and are obtained as

$$a_{1,r} = \frac{2Br}{1-N}\left(f'_r + Ng_r\right), \quad a_{2,r} = \frac{2Br}{1-N}\frac{N(2-N)}{m^2}g'_r, \quad a_{3,r} = \frac{2BrN}{1-N}\left(f'_r + 2g_r\right),$$
$$a_{4,r} = \frac{Br}{1-N}\left[f'^2_r + 2N(g^2_r + g_r f'_r) + \frac{N(2-N)}{m^2}g'^2_r\right]$$

The above linearized equations (2.11) - (2.13) are solved using the Chebyshev spectral collocation method [21]. The approximations are done by using the Chebyshev interpolating polynomials for the unknown functions. Further, they are collocated at the Gauss-Lobatto points represented as

$$\xi_j = \cos\frac{\pi j}{J}, \quad j = 0, 1, 2, ..., J \tag{2.14}$$

where J is the number of collocation points used.

The functions f_{r+1}, g_{r+1} and θ_{r+1} are approximated at the collocation points by

$$f_{r+1}(\xi_j) = \sum_{k=0}^{J} f_{r+1}(\xi_k)T_k(\xi_j), \quad g_{r+1}(\xi_j) = \sum_{k=0}^{J} g_{r+1}(\xi_k)T_k(\xi_j),$$
$$\theta_{r+1}(\xi_j) = \sum_{k=0}^{J} \theta_{r+1}(\xi_k)T_k(\xi_j), \quad j = 0, 1, 2, ..., J \tag{2.15}$$

where T_k is the k^{th} Chebyshev polynomial defined by $T_k(\xi) = \cos(k\cos^{-1}\xi)$.

The derivatives of the variables at the collocation points are represented as

$$\frac{d^a f_{r+1}}{d\eta^a} = \sum_{k=0}^{J} \mathbf{D}_{jk}^a f_{r+1}(\xi_k), \quad \frac{d^a g_{r+1}}{d\eta^a} = \sum_{k=0}^{J} \mathbf{D}_{jk}^a g_{r+1}(\xi_k),$$
$$\frac{d^a \theta_{r+1}}{d\eta^a} = \sum_{k=0}^{J} \mathbf{D}_{jk}^a \theta_{r+1}(\xi_k), j = 0, 1, 2, ..., J \tag{2.16}$$

where "a" is the order of differentiation and $\mathbf{D}$ being the Chebyshev spectral differentiation matrix. Substituting Eqs. (2.15) - (2.16) into Eqs. (2.11) - (2.13) leads to the matrix equation

$$\mathbf{A}_r \mathbf{X}_{r+1} = \mathbf{B}_r, \tag{2.17}$$

Here $\mathbf{A}_r$ is a $(3J+3) \times (3J+3)$ square matrix and $\mathbf{X}_{r+1}$ and $\mathbf{B}_r$ are $(3J+3) \times 1$ column vectors defined by

$$\mathbf{A}_r = \begin{bmatrix} A_{11} & A_{12} & A_{13} \\ A_{21} & A_{22} & A_{23} \\ A_{31} & A_{32} & A_{33} \end{bmatrix}, \quad \mathbf{X}_{r+1} = \begin{bmatrix} \mathbf{F}_{r+1} \\ \mathbf{G}_{r+1} \\ \Theta_{r+1} \end{bmatrix}, \quad \mathbf{B}_r = \begin{bmatrix} \mathbf{r}_{1,r} \\ \mathbf{r}_{2,r} \\ \mathbf{r}_{3,r} \end{bmatrix} \tag{2.18}$$

where

$$\left.\begin{aligned} &\mathbf{F}_{r+1} = [f_{r+1}(\xi_0), f_{r+1}(\xi_1), ..., f_{r+1}(\xi_{J-1}), f_{r+1}(\xi_J)]^T, \\ &\mathbf{G}_{r+1} = [g_{r+1}(\xi_0), g_{r+1}(\xi_1), ..., g_{r+1}(\xi_{J-1}), g_{r+1}(\xi_J)]^T, \\ &\Theta_{r+1} = [\theta_{r+1}(\xi_0), \theta_{r+1}(\xi_1), ..., \theta_{r+1}(\xi_{J-1}), \theta_{r+1}(\xi_J)]^T, \\ &A_{11} = \tfrac{1}{1-N}\mathbf{D^2} - R\mathbf{D}, \quad A_{12} = (\tfrac{N}{1-N})\mathbf{D}, \quad A_{13} = \tfrac{Gr}{Re}\sin\phi\mathbf{I}, \quad \mathbf{r}_{1,r} = A, \\ &A_{21} = -\mathbf{D}, \quad A_{22} = \tfrac{2-N}{m^2}\mathbf{D^2} - a_j R(\tfrac{1-N}{N})\mathbf{D} - 2\mathbf{I}, \quad A_{23} = \mathbf{0}, \quad \mathbf{r}_{2,r} = \mathbf{0}, \\ &A_{31} = a_{1,r}\mathbf{D}, \quad A_{32} = a_{2,r}\mathbf{D} + a_{3,r}\mathbf{I}, \quad A_{33} = \mathbf{D^2} - RPr\mathbf{D}, \quad \mathbf{r}_{3,r} = a_{4,r}. \end{aligned}\right\} \tag{2.19}$$

Here $\mathbf{I}$, $\mathbf{0}$ represents $(J+1) \times (J+1)$ identity matrix, zero matrix respectively.

The corresponding boundary conditions

$$f_{r+1}(\xi_0) = 0, \quad g_{r+1}(\xi_0) = 0, \quad \sum_{k=0}^{J} \mathbf{D}_{0k}\theta_{r+1}(\xi_k) = 1$$
$$f_{r+1}(\xi_J) = 0, \quad g_{r+1}(\xi_J) = 0, \quad \theta_{r+1}(\xi_J) = 0 \tag{2.20}$$

Incorporate the boundary conditions (2.20) in the matrix system (2.17), the solution is obtained as

$$\mathbf{X}_{r+1} = \mathbf{A}_r^{-1}\mathbf{B}_r \tag{2.21}$$

The initial approximations f_0, g_0 and θ_0 are chosen such that they satisfy the boundary conditions (2.20) i.e.

$$f_0(\eta) = 0, \quad g_0(\eta) = 0, \quad \theta_0(\eta) = \frac{1}{2}\left(\eta^2 - 1\right) \tag{2.22}$$

Entropy Generation

The second law of thermodynamics is an important tool to understand the irreversible effects due to flow and heat transfer. Thermodynamic irreversibility is closely related to entropy production. A convection process involving channel flow of micropolar fluids is inherently irreversible due to the exchange of energy and momentum within the fluid and at solid boundaries. For the present study the volumetric rate of entropy generation from Eq. (1.4) is given by

$$S_G = \frac{K_f}{T_1^2}\left(\frac{dT}{dy}\right)^2 + \left[\frac{\mu+\kappa}{T_1}\left(\frac{du}{dy}\right)^2 + \frac{2\kappa}{T_1}\left(\sigma^2 + \sigma\frac{du}{dy}\right) + \frac{\gamma}{T_1}\left(\frac{d\sigma}{dy}\right)^2\right] \tag{2.23}$$

where the first term on the right hand side of the above equation represents the entropy generation due to heat transfer while the second term gives the entropy generation due to micropolar fluid friction. According to Bejan [15], the dimensionless entropy generation number N_s is the ratio of the volumetric entropy generation rate to the characteristic entropy generation rate. The dimensionless entropy generation number is given by

$$N_s = \overbrace{\theta'^2}^{N_h} + \underbrace{\frac{Br}{1-N}L\left[f'^2 + 2N(g^2 + gf') + \frac{N(2-N)}{m^2}g'^2\right]}_{N_v} \tag{2.24}$$

where the characteristic entropy generation rate is $\frac{q^2}{K_f T_1^2}$ and $L = \frac{K_f T_1}{hq}$ is the dimensionless value and it is a controlling parameter that depends on the heat flux, temperature of the fluid, length of the channel and the thermal conductivity. In order to have an idea whether fluid friction or heat transfer entropy generation dominates, an alternate parameter Be (Bejan number) was introduced by Paoletti [85], which is the ratio of entropy generation due to heat transfer to the overall entropy

generation.

$$Be = \frac{N_h}{N_h + N_v} \tag{2.25}$$

The Bejan number varies from 0 to 1. Subsequently, $Be = 0$ reveals that the irreversibility due to viscous dissipation dominates, whereas $Be = 1$ indicates that the irreversibility due to heat transfer is dominant. It is obvious that the $Be = 0.5$ is the case in which the irreversibility due to heat transfer is equal to viscous dissipation in the entropy production.

Results and Discussion

To check the accuracy of the numerical scheme, the velocity and microrotation(for hydrodynamic case) are compared with analytical solution given by Ariman and Cakmak [6] in the absence of R and ϕ. The comparison is found to be in good agreement as shown in Table. 2.1.

The dimensionless velocity, microrotation, temperature, entropy generation and Bejan number are shown graphically through the Figs. 2.2 to 2.6. To study the effect of different parameters on the above mentioned quantities, the parameters $a_j = 0.001$, $A = -1$, $m = 2$, $Gr = 1$, $L = 0.1$ and $R = 1$ are taken as constants.

The effect of coupling number on velocity, microrotation, temperature, entropy generation and Bejan number of the micropolar fluid flow through an inclined channel is plotted in Fig. 2.2. The coupling of linear and rotational motion arising from the micromotion of the fluid molecules is characterized by coupling number. Hence, coupling between the Newtonian and rotational viscosities is represented by N. The microstructure effect is significant as $N \to 1$, and for a smaller value of N the substructure individuality is limited. The fluid is non polar as its micropolarity is lost as $\kappa \to 0$ i.e. $N \to 0$. Thus, for viscous fluid $N \to 0$.

From Fig. 2.2(a) it is observed that as the coupling number increases, velocity decreases. As $N \to 1$ fluid particles rotate about themselves with high angular velocities, thus, the fluid velocity decreases. It is observed from Fig. 2.2(b) that the component of microrotation increases near the lower plate and decreases near the upper plate with an increase of coupling number. In Figs. 2.2(c) and 2.2(d), it can be noticed that the temperature and entropy generation decrease with an increase in the value of coupling number. As the velocity is decreasing, the dissipation energy

decreases, leading to decrease in temperature, thus the consequently entropy generation decreases. It is clear from Fig. 2.2(e) that the Bejan number increases with an increase in the value of N. From this figure, it is also observed that the heat transfer irreversibility dominates around the centerline region of the channel, and the fluid friction dominates at the lower plate of the channel.

Figs. 2.3(a) to 2.3(e) describe the effect of angle of inclination ϕ on velocity, microrotation, temperature, entropy generation and Bejan number. It is noticed from Fig. 2.3(a) that the velocity increases with the angle of inclination due to increase in forces acting upon the fluid flow. It is clear from Fig.2.3(b) that the microrotation component decreases near the lower plate and increases near the upper plate with an increase in the value of angle of inclination thus, showing a reverse rotation near the two boundaries. It is observed from Figs. 2.3(c) and 2.3(d) that the temperature and entropy generation are increasing with the increase in the value of angle of inclination. It is noticed that the entropy-generation rate is less at the lower plate of the channel and increases quite rapidly to its maximum value at the upper plate of the channel for all the parameter variations. It can be seen from Fig. 2.3(e) that as the angle of inclination ϕ has no effect on the Bejan number at the center of the channel, but Be decreases at the upper plate and increases at the lower plate with increase in ϕ.

From Figs. 2.4(a) - 2.4(d), it is observed that as Reynolds number increases the velocity, microrotation(numerically), temperature and entropy generation are decreasing. Fig. 2.4(e) shows the effect of Reynolds number on Bejan number. The Bejan number at the lower plate decreases whereas, it increases, at the upper plate leading to the increasing influence of fluid friction irreversibility at the lower plate and heat transfer irreversibility at the upper plate.

The influence of Prandtl number on velocity, microrotation, temperature, entropy generation and Bejan number of the micropolar fluid flow through an inclined channel is displayed in Fig. 2.5. It is observed from Fig. 2.5(a) that the velocity decreases with increase in Prandtl number. It is shown in the Fig. 2.5(b) that the microrotation component increases near the lower plate and decreases near the upper plate with an increase in the value of Prandtl number. Fig. 2.5(c) represents the effect of Prandtl number on temperature. It is observed that the increase in Prandtl number causes a decrease in temperature. Entropy generation decreases with increase in the Prandtl number shown in Fig. 2.5(d). Fig. 2.5(e) shows that the Bejan number decreases as Prandtl number increases.

The effect of Brinkman number on velocity, microrotation, temperature, entropy generation and Bejan number is displayed in Fig. 2.6. Fig. 2.6(a) depicts that the non-dimensional velocity increases with an increase in the Brinkman number. It is seen from Fig. 2.6(b) that the microrotation component decrease near the lower plate and increase near the upper plate with increasing Brinkman number showing a reverse rotation near the two boundaries. However, the magnitude of the microrotation is increasing near the plates. The reason is that the microrotation field in this region is dominated by a small number of particles spins that are generated by collisions with the boundary. It is observed from Figs. 2.6(c) and 2.6(d) that the temperature and entropy generation increases with an increase in the value of Brinkman number. Brinkman number is related to heat conduction from a channel wall to a flowing fluid. The effect of viscous forces on entropy generation is significant in the region close to the channel walls. From Fig. 2.6(e) it is interesting to note that increasing values of Br results an increase in the dominant effect of fluid-friction irreversibility near the upper plate and decrease in the dominant effect of fluid friction irreversibility near the lower plate.

Table 2.1: Comparison of velocity and microrotation by the present method and analytical solution given by Ariman and Cakmak [6] for $N = 0.1$, $m = 1$ and $A = -1$.

	Velocity $f(\eta)$		Microrotation $g(\eta)$	
η	Ariman and Cakmak [6]	Present	Ariman and Cakmak [6]	Present
-1	0	0	0	0
-0.8090	0.1557	0.1557	-0.0204	-0.0204
-0.6129	0.2817	0.2817	-0.0275	-0.0275
-0.4258	0.3696	0.3696	-0.0248	-0.0248
-0.2181	0.4302	0.4302	-0.0147	-0.0147
0	0.4518	0.4518	0	0
0.2181	0.4302	0.4302	0.0147	0.0147
0.4258	0.3696	0.3696	0.0248	0.0248
0.6129	0.2817	0.2817	0.0275	0.0275
0.8090	0.1557	0.1557	0.0204	0.0204
1	0	0	0	0

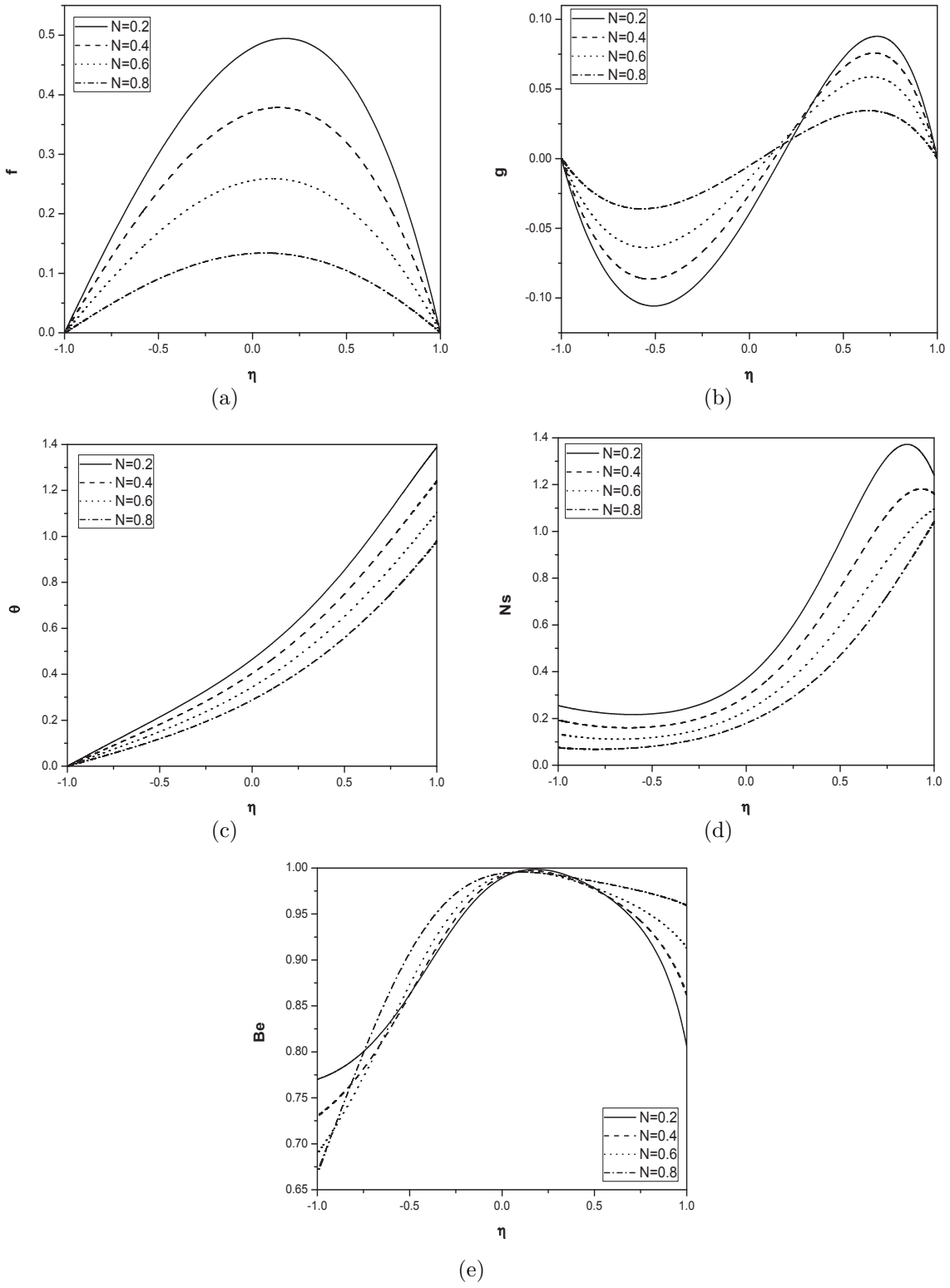

Figure 2.2: Effect of coupling number on (a)velocity, (b)microrotation, (c)temperature, (d)entropy generation and (e)Bejan number for $Pr = 1$, $Re = 1$, $Br = 1$ and $\phi = \frac{\pi}{6}$.

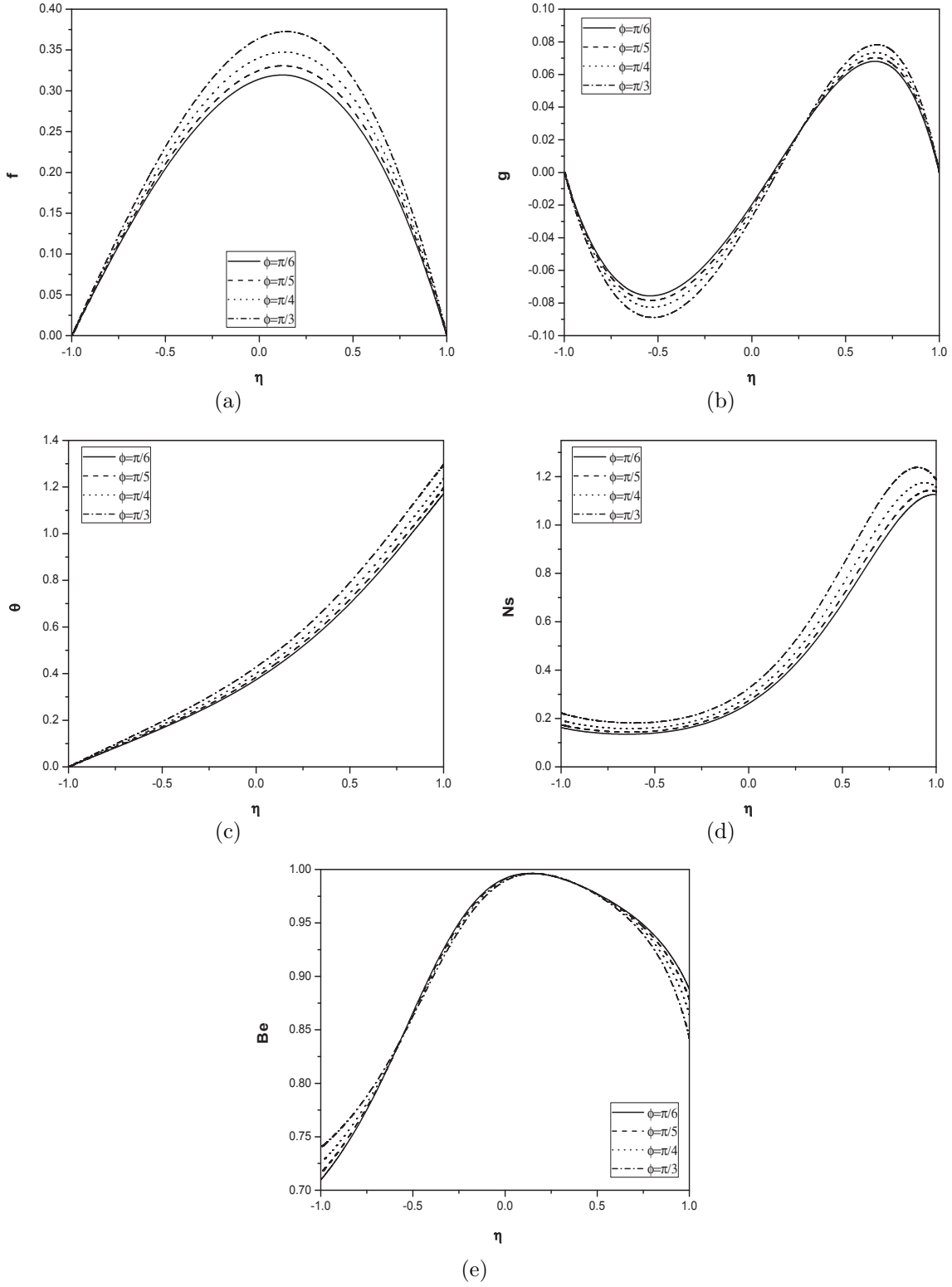

Figure 2.3: Effect of angle of inclination on (a)velocity, (b)microrotation, (c)temperature, (d)entropy generation and (e)Bejan number for $N = 0.5$, $Pr = 1$, $Re = 1$ and $Br = 1$.

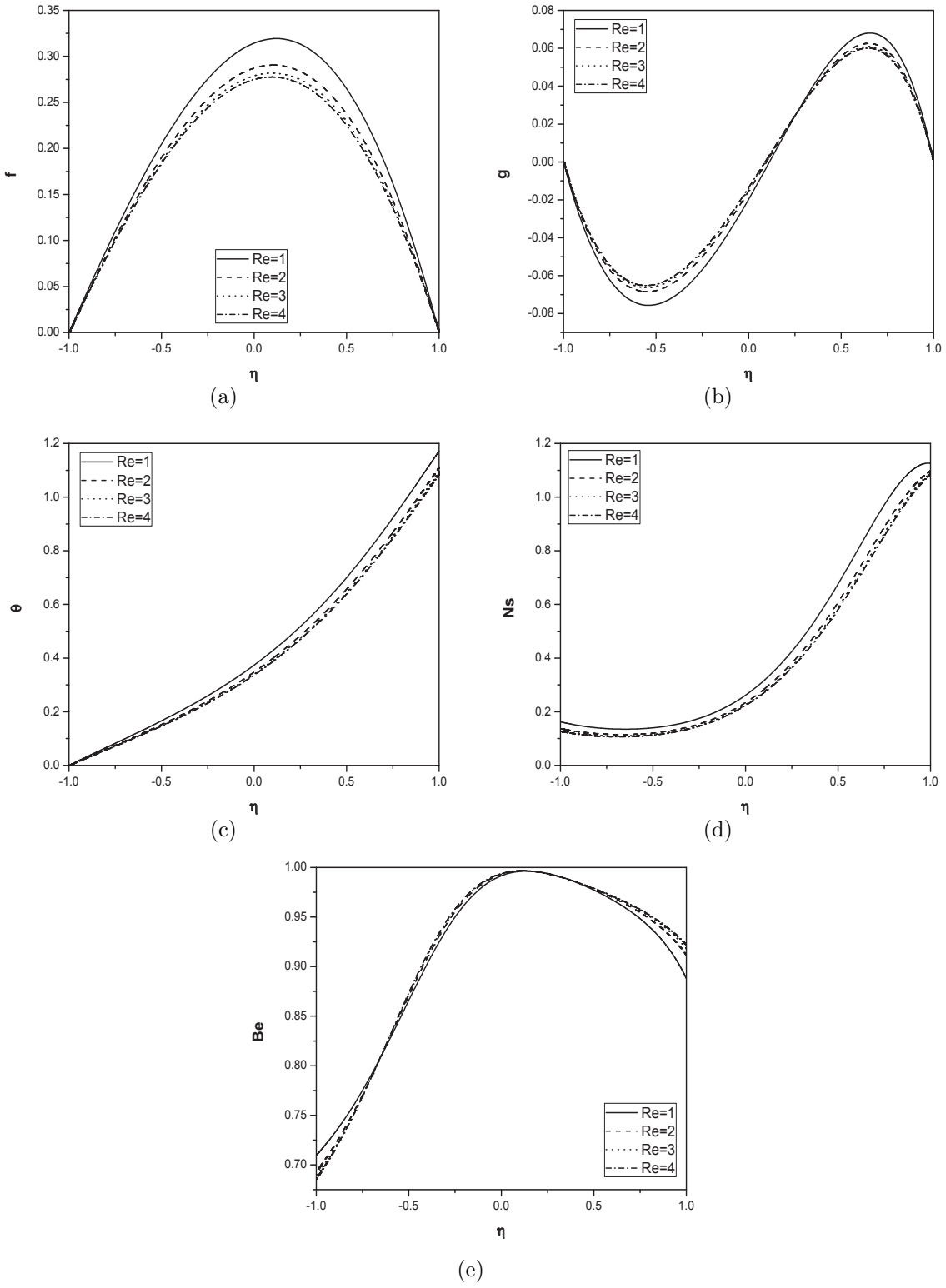

Figure 2.4: Effect of Reynolds number on (a)velocity, (b)microrotation, (c)temperature, (d)entropy generation and (e)Bejan number for $N = 0.5$, $Pr = 1$, $Br = 1$ and $\phi = \frac{\pi}{6}$.

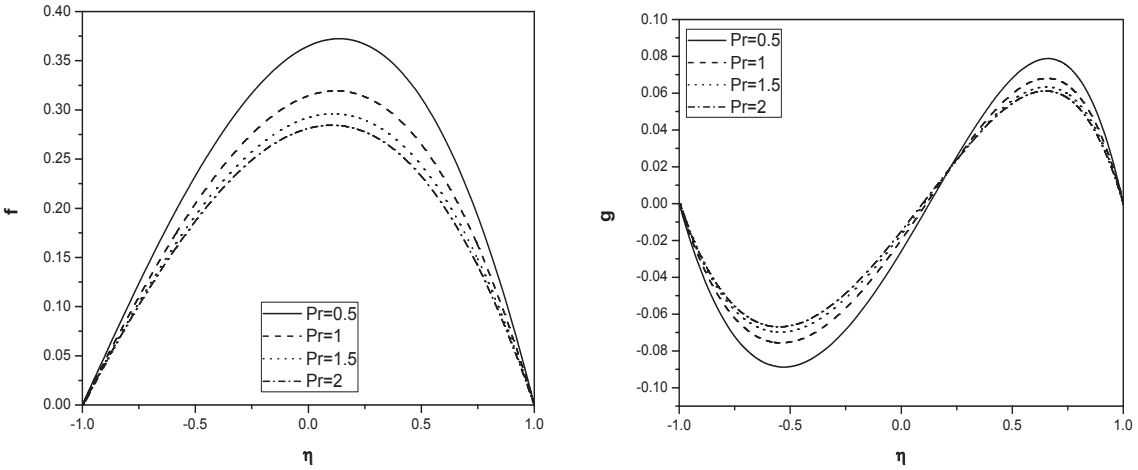

(a)

(b)

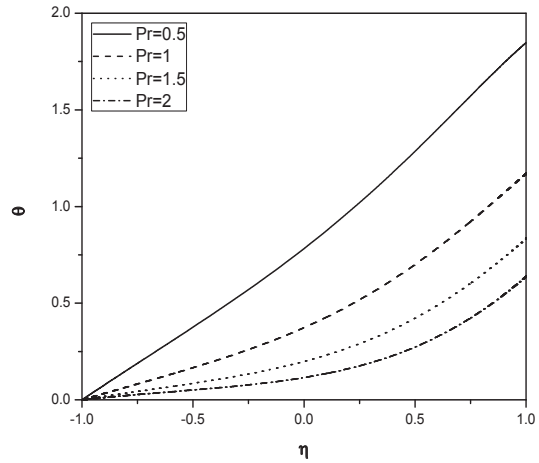

(c)

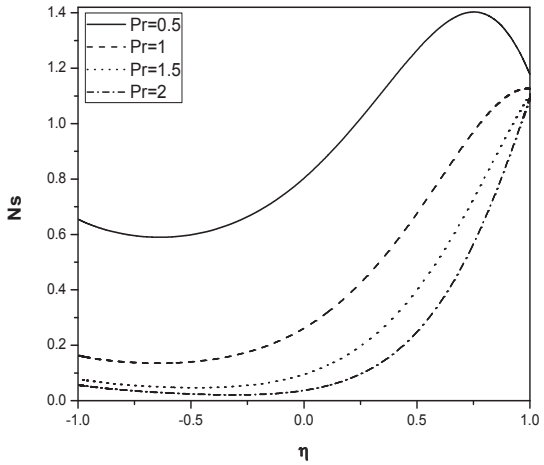

(d)

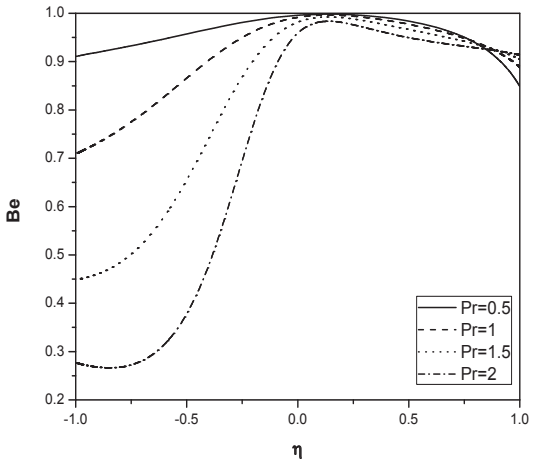

(e)

Figure 2.5: Effect of Prandtl number on (a)velocity, (b)microrotation, (c)temperature, (d)entropy generation and (e)Bejan number for $N = 0.5$, $Re = 1$, $Br = 1$ and $\phi = \frac{\pi}{6}$.

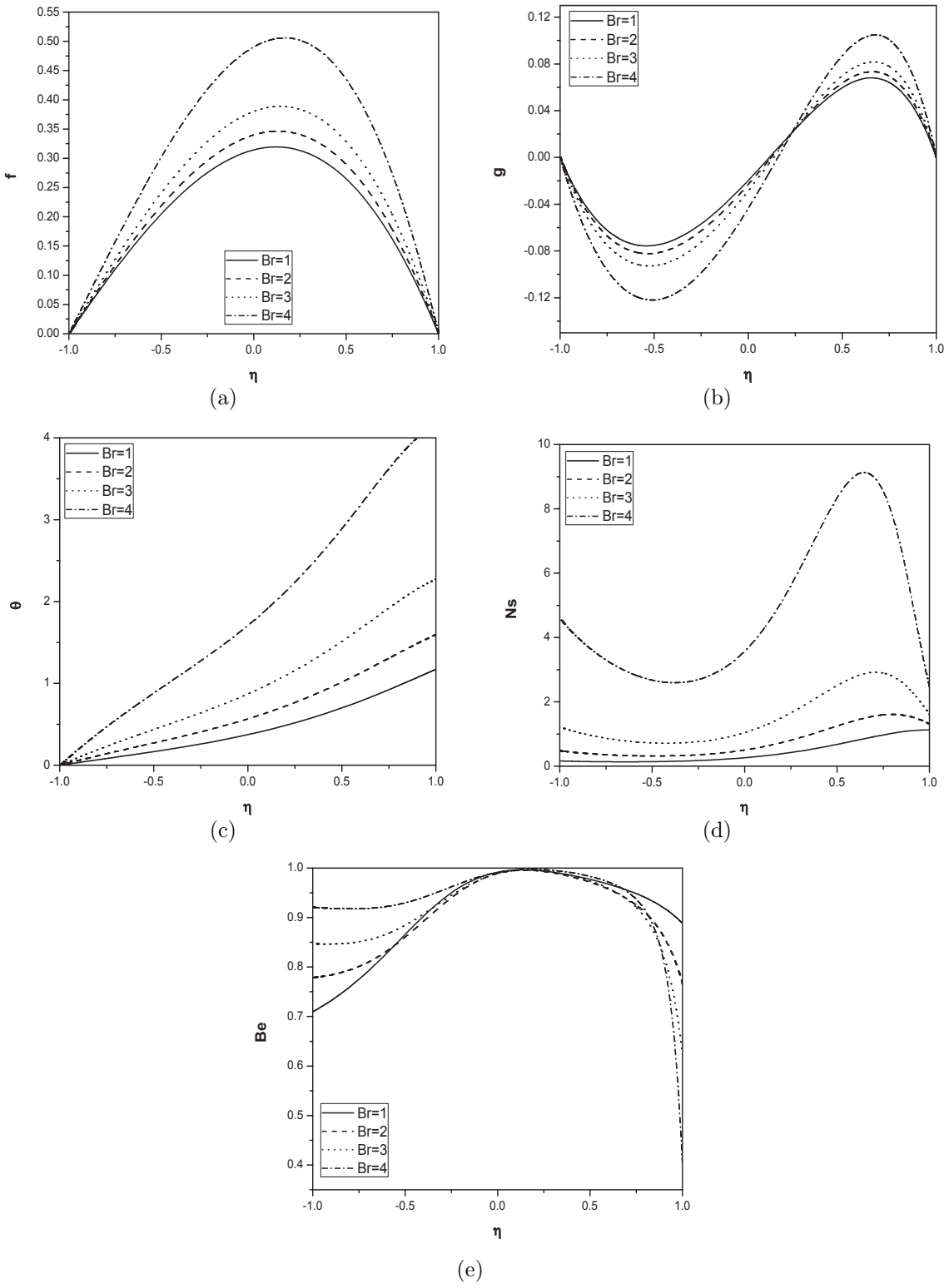

Figure 2.6: Effect of Brinkman number on (a)velocity, (b)microrotation, (c)temperature, (d)entropy generation and (e)Bejan number for $N = 0.5$, $Pr = 1$, $Re = 1$ and $\phi = \frac{\pi}{6}$.

2.2.2 Case(b): Slip and Convective Boundary Conditions

Assume that the fluid slips at the lower, upper plates of the channel and the microelements close to the channel plates are unable to rotate. Let the lower plate is heated by convection from a hot fluid with temperature T_2 which provides a heat transfer coefficient h_1 while the upper plate losses heat to the ambient with a heat transfer coefficient h_2. Thus, the boundary conditions are

$$\begin{aligned} u &= -\zeta' \left[(\mu + \kappa) \frac{du}{dy} + \kappa\sigma \right], \quad \sigma = 0, \quad K_f \frac{dT}{dy} + h_1(T - T_1) = 0, \quad \text{at} \quad y = h \\ u &= \zeta' \left[(\mu + \kappa) \frac{du}{dy} + \kappa\sigma \right], \quad \sigma = 0, \quad K_f \frac{dT}{dy} - h_2(T - T_2) = 0, \quad \text{at} \quad y = -h \end{aligned} \tag{2.26}$$

where ζ' is the slip length of the upper and lower plates of the channel.

Introducing the following non-dimensional variables

$$\eta = \frac{y}{h}, \quad u = U_0 f(\eta), \quad \sigma = \frac{U_0}{h} g(\eta), \quad \theta(\eta) = \frac{T - T_1}{T_2 - T_1}, \quad \overline{\zeta} = \frac{\zeta'}{h} \tag{2.27}$$

in Eqs. (2.2) - (2.4), to obtain the non-linear system of differential equations (2.7) - (2.9) that are mentioned in case(a).

The corresponding boundary conditions are:

$$\begin{aligned} f &= -\frac{\zeta}{1 - N} f', \quad g = 0, \quad \theta' + Bi_1 \theta = 0, \quad \text{at} \quad \eta = 1 \\ f &= \frac{\zeta}{1 - N} f', \quad g = 0, \quad \theta' - Bi_2 \theta = -Bi_2, \quad \text{at} \quad \eta = -1 \end{aligned} \tag{2.28}$$

where $\zeta = \overline{\zeta}\mu$ is the slip parameter, $Bi_k = \frac{hh_k}{K_f}$ is the Biot number for each plate. Subindexes $k = 1, 2$ refer to the lower and upper plates, respectively. In this thesis, it is assumed that the Biot number at the two boundaries is numerically same in every chapter.

Method of Solution

Proceeding as in Case (a), to obtain the following matrix equation

$$\mathbf{A}_r \mathbf{X}_{r+1} = \mathbf{B}_r \tag{2.29}$$

where $\mathbf{A}_r$ is a $(3J+3)\times(3J+3)$ square matrix and $\mathbf{X}_{r+1}$ and $\mathbf{B}_r$ are $(3J+3)\times 1$ column vectors defined in (2.18).

The corresponding boundary conditions are

$$\begin{aligned} f_{r+1}(\xi_0) = -\frac{\zeta}{1-N}\sum_{k=0}^{J}\mathbf{D}_{0k}f_{r+1}(\xi_k),\ g_{r+1}(\xi_0)=0,\ \sum_{k=0}^{J}\mathbf{D}_{0k}\theta_{r+1}(\xi_k)+Bi\theta_{r+1}(\xi_0)=0 \\ f_{r+1}(\xi_J) = \frac{\zeta}{1-N}\sum_{k=0}^{J}\mathbf{D}_{Jk}f_{r+1}(\xi_k),\ g_{r+1}(\xi_J)=0,\ \sum_{k=0}^{J}\mathbf{D}_{Jk}\theta_{r+1}(\xi_k)-Bi\theta_{r+1}(\xi_J)=-Bi \end{aligned} \tag{2.30}$$

Incorporate the boundary conditions (2.30) in the matrix system (2.29), the solution is obtained as

$$\mathbf{X}_{r+1} = \mathbf{A}_r^{-1}\mathbf{B}_r \tag{2.31}$$

The initial approximations f_0, g_0 and θ_0 are chosen to be functions that satisfy the boundary conditions (2.30) i.e..

$$f_0(\eta)=0,\quad g_0(\eta)=0,\quad \theta_0(\eta)=\frac{1}{2}\left(1-\frac{Bi}{1+Bi}\eta\right) \tag{2.32}$$

Entropy Generation

The Eq. (2.23) mentioned in case(a) is the entropy generation for the micropolar fluid flow through an inclined channel. The dimensionless entropy generation in this case is given by

$$N_s = \frac{S_G}{S_{GC}} = \theta'^2 + \frac{Br}{T_p(1-N)}\left[f'^2 + 2N(g^2+gf') + \frac{N(2-N)}{m^2}g'^2\right] \tag{2.33}$$

where $T_p = \frac{T_2-T_1}{T_1}$ is the dimensionless temperature difference, $S_{GC} = \dfrac{K_f(T_2-T_1)^2}{h^2T_1^2}$ is the characteristic entropy generation rate. In order to have an idea whether the entropy generation due to viscous dissipation dominates over the irreversibility due to heat transfer or vice versa, an alternate parameter Bejan number is introduced in equation (2.25).

Results and Discussion

To study the effects of pertinent parameters, computations were carried out by taking $a_j = 0.001$, $A = -1$, $m = 2$, $Gr = 2$, $R = 1$ and $Pr = 1$.

The effect of coupling number on velocity, microrotation, temperature, entropy generation and Bejan number is displayed in Fig. 2.7. It is observed from the Fig. 2.7(a) that the velocity decreases with increase in coupling number N. The peak velocity decreases with the increase of N. It is seen from Fig. 2.7(b) that the microrotation component increases near the lower plate and decreases near the upper plate with an increase in the value of coupling number N. The shear stress at the two plates tends to rotate the fluid in opposite directions because of which the microrotation has opposite signs near the two plates. It is observed from Figs. 2.7(c) and 2.7(d) that the temperature and entropy generation decreases with an increase in the value of coupling number. It is observed from Fig. 2.7(e) that the two crossovers in the Bejan number profile with an increase in the value of N. The crossovers due to the consequence of the microstructure of the particles as N varies from 0 to 1. The microstructure effect is significant as $N \to 1$, and for a smaller value of N the substructure individuality is limited. Further, the region near the plates is dominated by a small number of particles spins that are generated by collisions with the boundary.

Fig. 2.8 presents the effect of angle of inclination ϕ on velocity, microrotation, temperature, entropy generation and Bejan number. It is noticed from Fig. 2.8(a) that the velocity increases with an increase in the value of angle of inclination. It is shown from Fig. 2.8(b) that the microrotation component decreases near the lower plate and increases near the upper plate with an increase in the value of angle of inclination. It is observed from Figs. 2.8(c) and 2.8(d) that the temperature and entropy generation increases with an increase in the value of angle of inclination. It is observed from Fig. 2.8(e) that the Bejan number decreases with an increase in the value of ϕ.

The variation of slip parameter on velocity, microrotation, temperature, entropy generation and Bejan number is displayed in Fig. 2.9. It is observed that the increase in slip parameter increases the velocity and decreases the microrotation as shown in Figs. 2.9(a) and 2.9(b). It is clear from Figs. 2.9(c) and 2.9(d) that there is no effect of slip parameter on temperature and entropy generation. Eventhough the temperature is related to convection, in this case the convection is not influenced by the slip prameter and thus, the temperature is not influenced by slip parameter. Hence, entropy is also not influenced by the slip parameter. The effect of slip parameter on Bejan number is shown

in Fig. 2.9(e). It is observed that the slip parameter does not influence the Bejan number from the lower plate to the center of the channel, but it increases near the upper plate.

Fig. 2.10 shows the influence of Reynolds number on velocity, microrotation, temperature, entropy generation and Bejan number. From Figs. 2.10(a) - 2.10(d), it is observed that as the Reynolds number increases, decrease in nature of velocity, microrotation(numerically), temperature and entropy generation is seen. Also, it is observed from Ns profile that the entropy generation number is high in magnitude near the upper plate due to the presence of high temperature and velocity gradients. Fig. 2.10(e) shows that as the Reynolds number increases, Bejan number also increases. This implies that in the entire flow region as Re increases, the relative increase of dissipation of energy dominates the fluid friction.

The effect of Brinkman number on velocity, microrotation, temperature, entropy generation and Bejan number is displayed in Fig. 2.11. Fig. 2.11(a) depicts that the non-dimensional velocity increases with an increase in the value of Brinkman number. It is seen from Fig. 2.11(b) that the microrotation component decreases near the lower plate and increases near the upper plate with an increase in the value of Brinkman number. It is observed from Figs. 2.11(c) and 2.11(d) that the temperature and entropy generation increases with an increase in the value of Brinkman number. The Brinkman number Br is an indicative of the rate at which energy is dissipated by the viscous forces within the fluid. Thus, the entropy generation becomes significant in the region close to the channel walls and negligible at the center of the channel. An increase in Brinkman number, increases the fluid temperature (Fig. 2.11(c)) as well as the temperature gradient within the channel. Consequently, as shown in Fig. 2.11(e), the dominance of fluid friction irreversibility over heat transfer irreversibility decreases with increase in Br.

The Biot number Bi is the ratio of internal thermal resistance of a solid to the boundary layer thermal resistance. When $Bi = 0$ the plate is totally insulated, the internal thermal resistance of the plate is extremely high therefore no convective heat transfer takes place to the cold fluid on the upper part of the plate. Fig. 2.12(a) depicts that the non-dimensional velocity decreases with an increase in the value of Biot number. It is seen from Fig. 2.12(b) that the microrotation component increases near the lower plate and decreases near the upper plate with an increase in the value of Biot number. It is observed from Fig. 2.12(c) that the temperature decreases with an increase in the value of Biot number. It is noticed from Fig. 2.12(d) that the entropy generation Ns decreases slightly with an increase in the Biot number. As Bi increases, the Bejan number

increases as depicted in Fig. 2.12(e).

2.3 Conclusions

In this chapter, the problem of entropy generation due to micropolar fluid flow through an inclined channel with (a)No-slip and isoflux/isothermal boundary conditions and (b)Slip and convective boundary conditions are presented. From the analysis, the following are the observations in both the cases (a) and (b).

The presence of microstructure N, decreases the velocity, temperature, entropy generation and increases the Bejan number. Velocity, temperature and entropy generation increases with increase in angle of inclination. The Less effect of angle of inclination is observed in Bejan number in Case (a) whereas in Case (b) Bejan number decreases with an increase in the value of angle of inclination. Higher values of Re lead to lower values of velocity, temperature and entropy generation. Minimum entropy generation at the lower plate and maximum entropy generation at the upper plate is observed for the variation of all parameters in Case (a). Almost zero entropy generation at the center of the channel is observed in Case (b) due to low velocity and temperature gradients. On the other hand, slip velocity has no effect on the entropy generation and Bejan number. An increase in the Biot number leads to decrease the entropy generation near the lower plate and increase the Bejan number in the entire flow region. From the Bejan number profiles it is observed that the heat transfer irreversibility dominates the flow process within the channel centerline region and fluid friction irreversibility dominates at the channel plates.

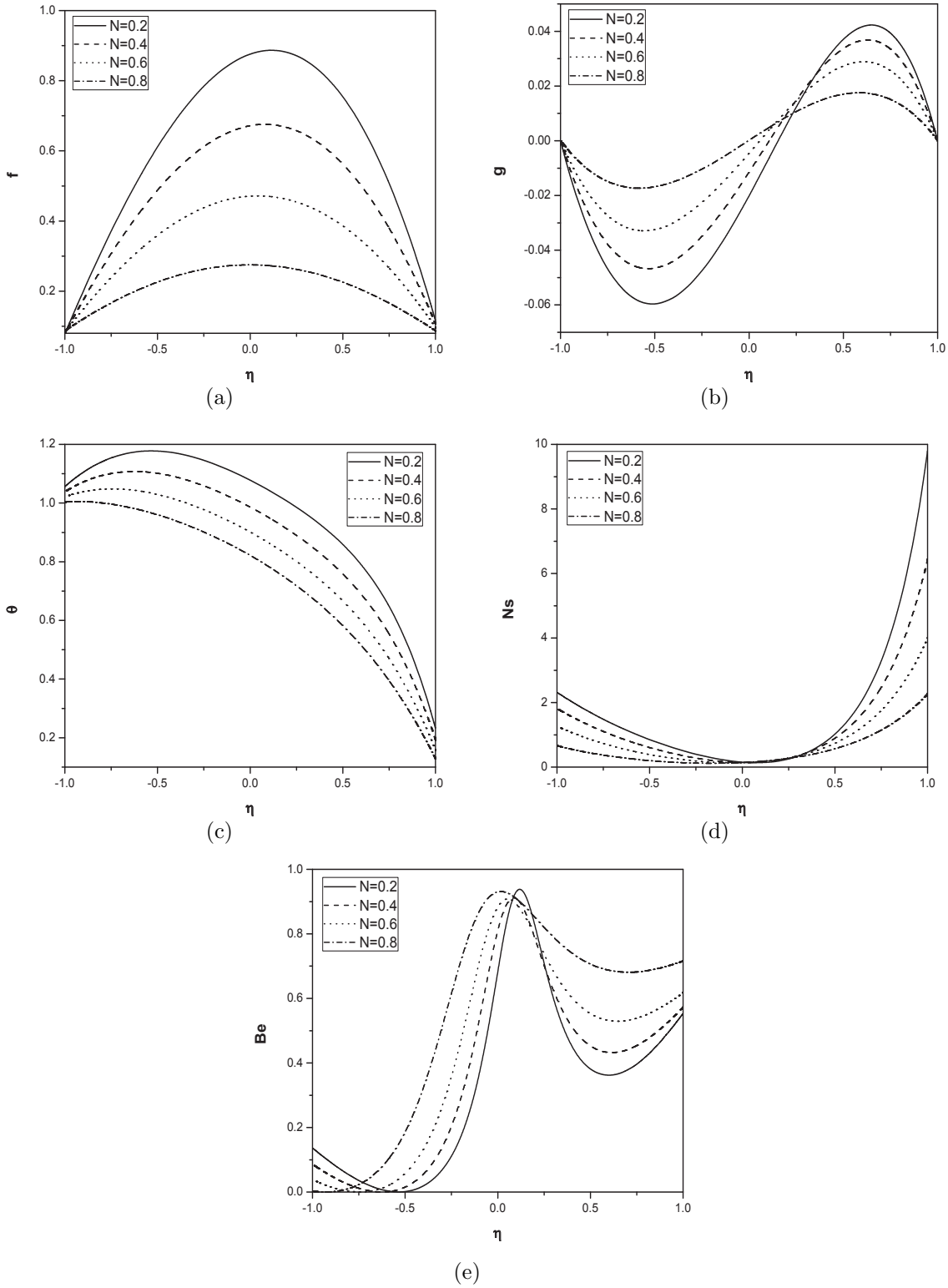

Figure 2.7: Effect of coupling number on (a)velocity, (b)microrotation, (c)temperature, (d)entropy generation and (e)Bejan number for $Re = 1$, $Bi = 10$, $Br = 1$, $\phi = \frac{\pi}{6}$ and $\zeta = 0.05$.

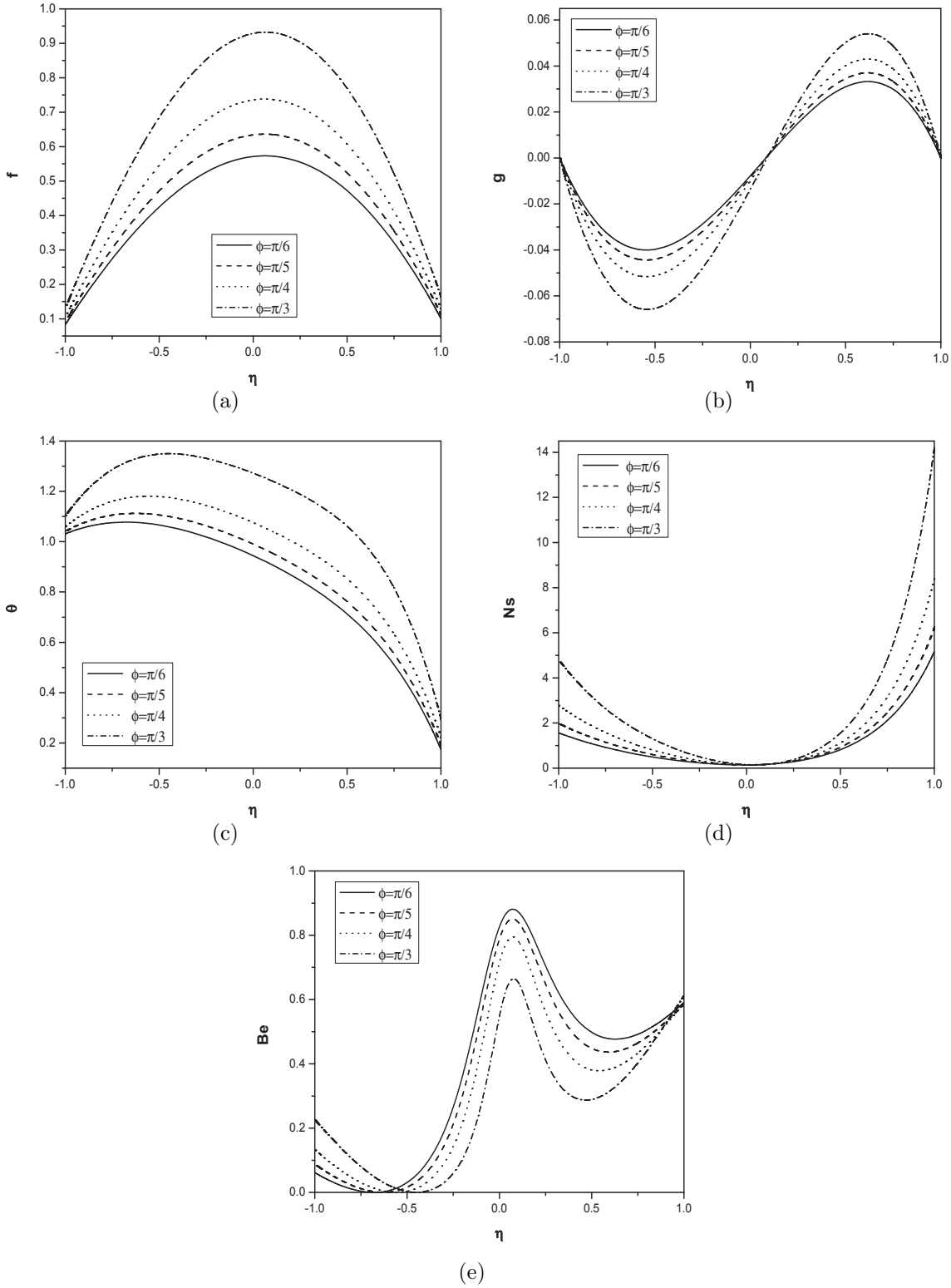

Figure 2.8: Effect of angle of inclination on (a)velocity, (b)microrotation, (c)temperature, (d)entropy generation and (e)Bejan number for $N = 0.5$, $Re = 1$, $Bi = 10$, $Br = 1$ and $\zeta = 0.05$.

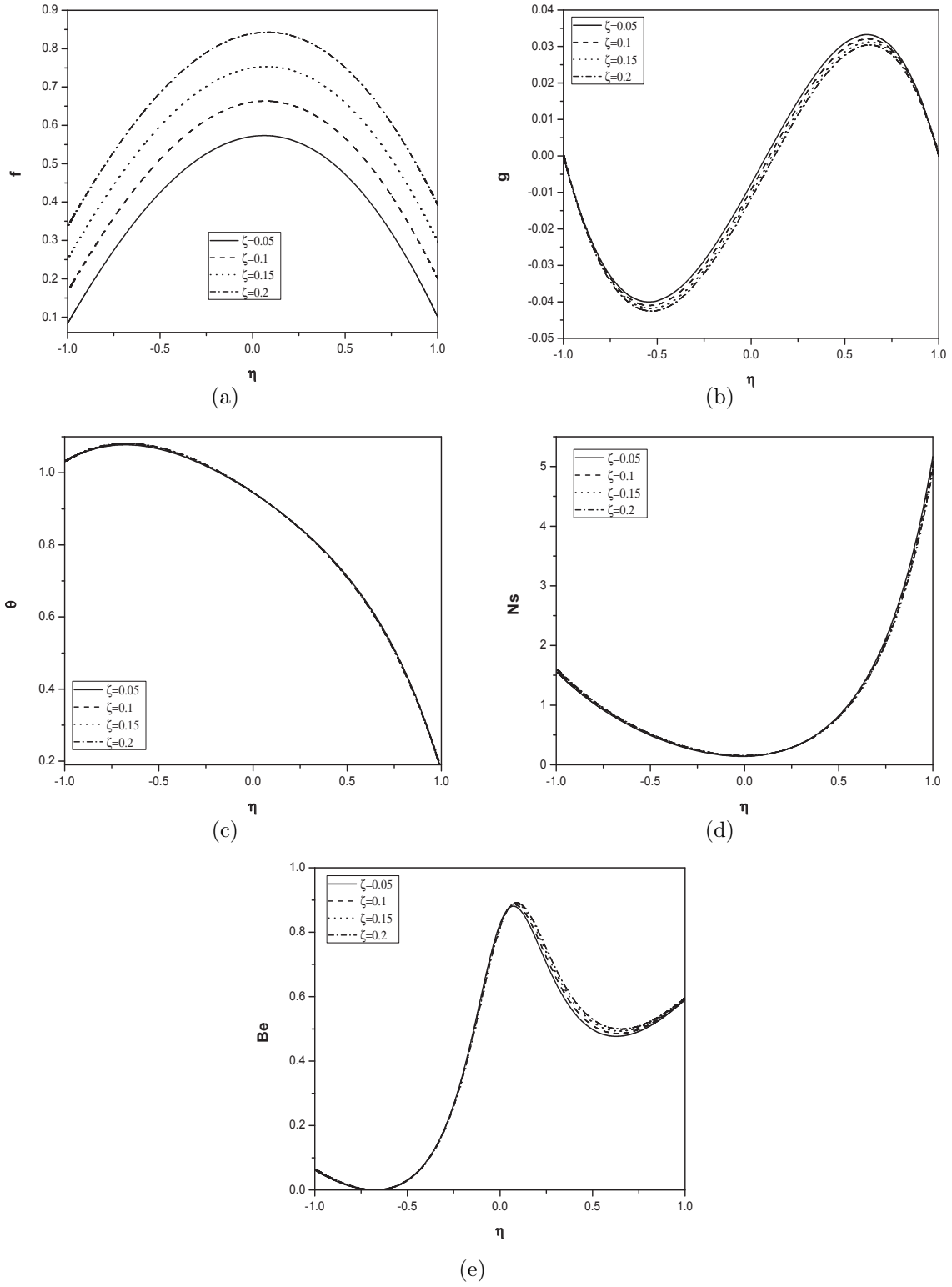

Figure 2.9: Effect of slip parameter on (a)velocity, (b)microrotation, (c)temperature, (d)entropy generation and (e)Bejan number for $N = 0.5$, $Re = 1$, $Bi = 10$, $Br = 1$ and $\phi = \frac{\pi}{6}$.

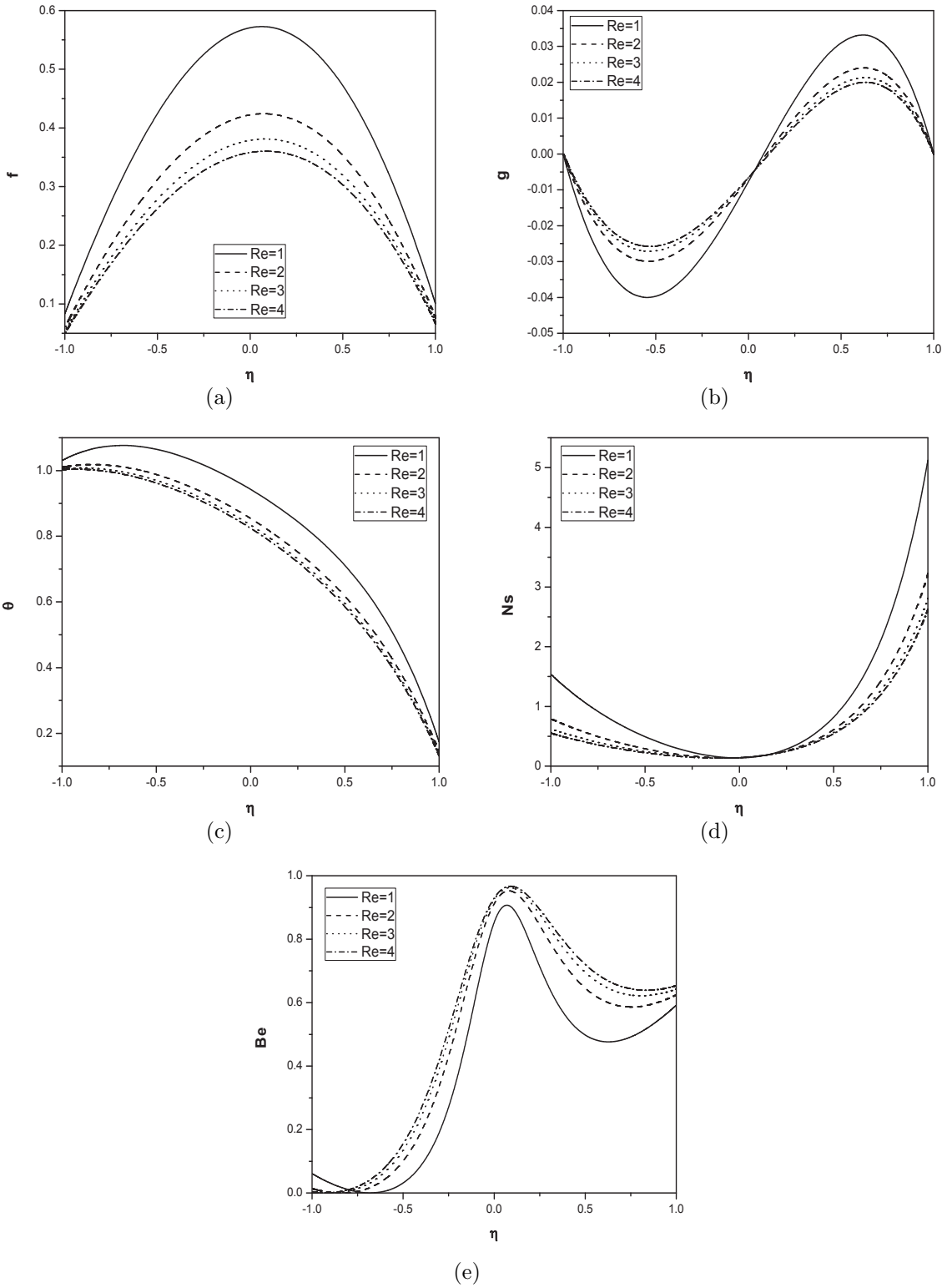

Figure 2.10: Effect of Reynolds number on (a)velocity, (b)microrotation, (c)temperature, (d)entropy generation and (e)Bejan number for $N = 0.5$, $Bi = 10$, $Br = 1$, $\phi = \frac{\pi}{6}$ and $\zeta = 0.05$.

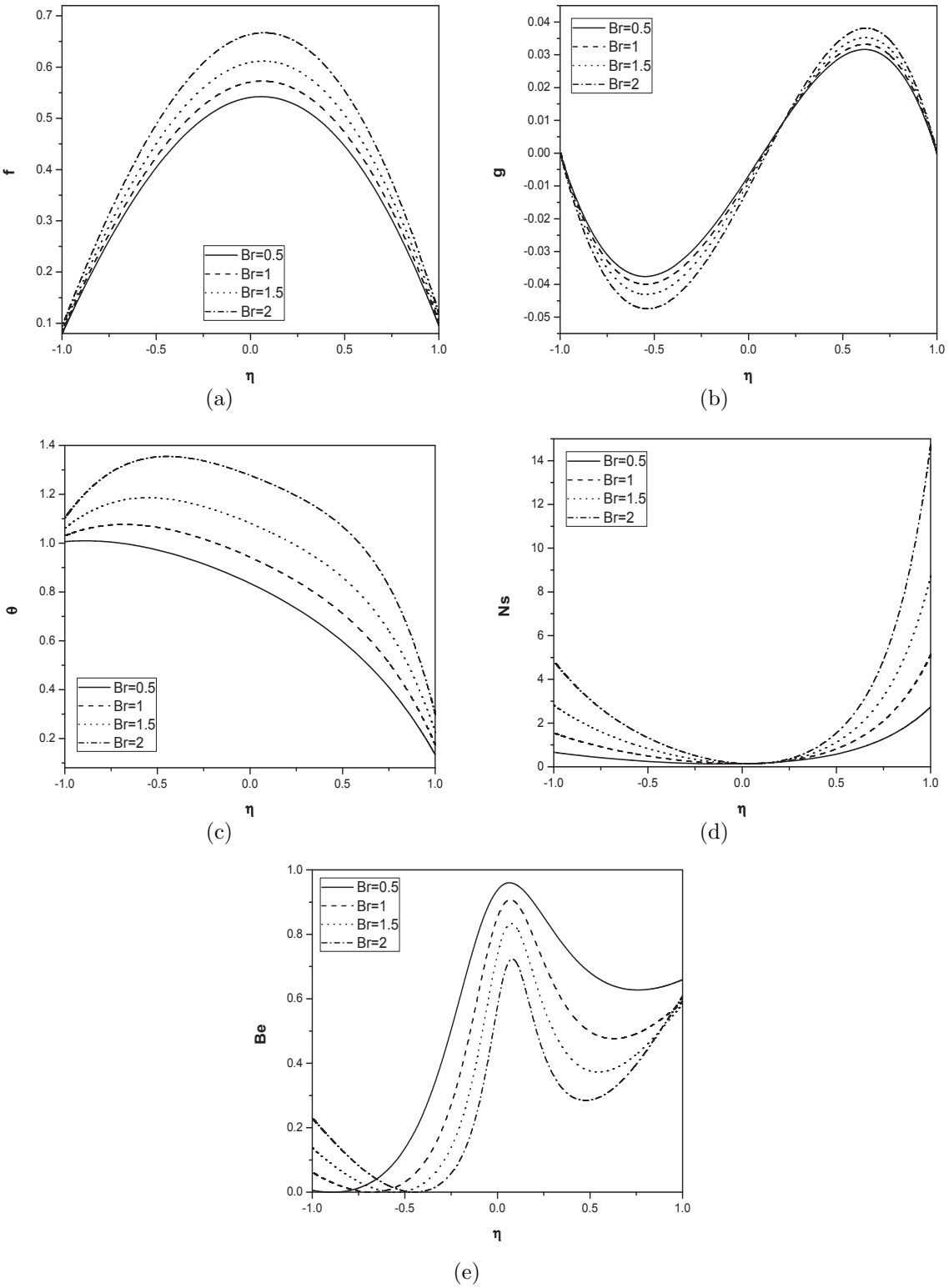

Figure 2.11: Effect of Brinkman number on (a)velocity, (b)microrotation, (c)temperature, (d)entropy generation and (e)Bejan number for $N = 0.5$, $Re = 1$, $Bi = 10$, $\phi = \frac{\pi}{6}$ and $\zeta = 0.05$.

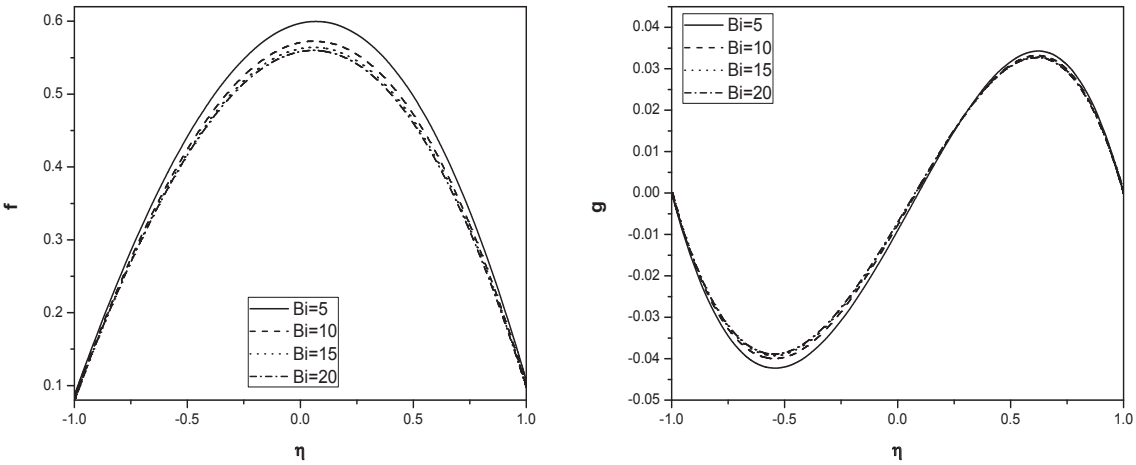

(a)

(b)

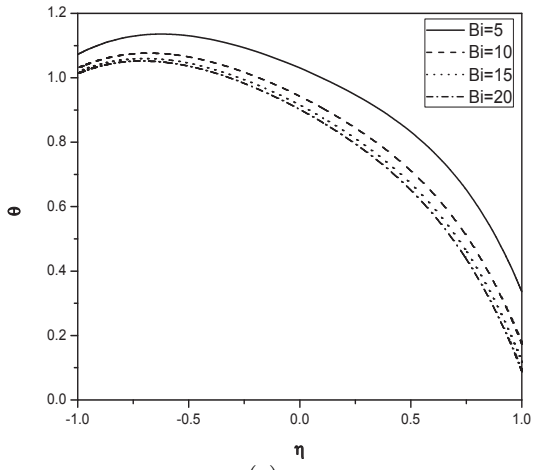

(c)

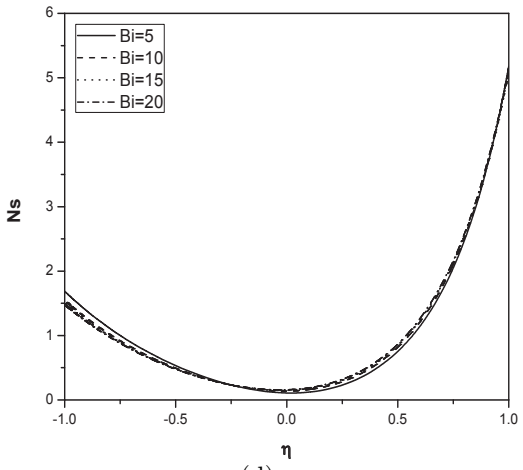

(d)

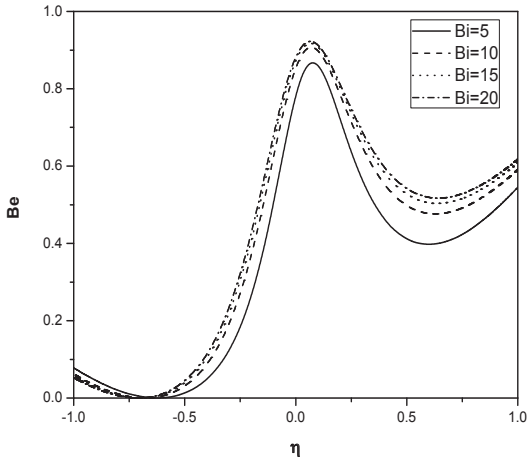

(e)

Figure 2.12: Effect of Biot number on (a)velocity, (b)microrotation, (c)temperature, (d)entropy generation and (e)Bejan number for $N = 0.5$, $Re = 1$, $Br = 1$, $\phi = \frac{\pi}{6}$ and $\zeta = 0.05$.

Chapter 3

Second Law Analysis of Micropolar Fluid Flow Through a Porous Channel [1]

3.1 Introduction

The study of fluid flow between two porous boundaries has gained tremendous attention by researchers as the theory has wide applications such as transpiration cooling, lubrication of porous bearings, petroleum technology, ground water hydrology, seepage of water in river beds, purification and filtration processes and so forth.

The industrial system efficiency calculations are more appropriate in using the second law of thermodynamics rather than the first law, because the first law of thermodynamics does not refer to the irreversibility minimization present in the physical process. In most of the thermal systems, thermal efficiency can be defined as the ratio of actual efficiency of thermal system to reversible thermal efficiency, in which the applied conditions are same. The fluid flow and heat transfer processes are intrinsically irreversible, which leads to increase entropy generation and useful energy destruction. Hooman *et al* [51] investigated the forced convective heat transfer in a porous channel

[1] Case(a):Communicated to "**Journal of Engineering Thermo Physics**", Case(b) Communicated to "**International Journal of Nonlinear Sciences and Numerical Simulation**"

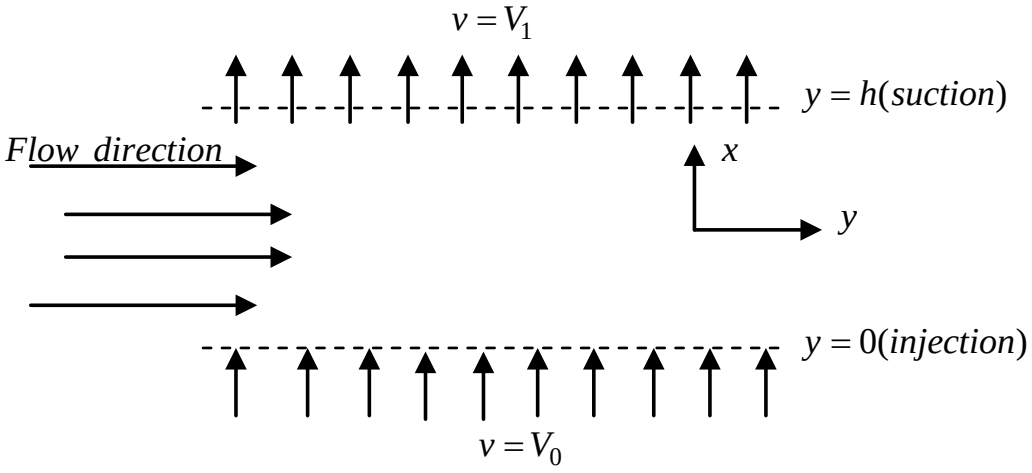

Figure 3.1: Physical model and coordinate system.

with isothermal or isoflux walls. The effect of suction/injection, magnetic field and Navier slip on entropy generation in a porous channel with constant pressure gradient has been studied by Das and Jana [31]. Torabi *et al* [94] presented the analysis of heat transfer and entropy generation in a channel partially filled with porous medium.

In the previous chapter, the entropy generation in an inclined channel due to micropolar fluid flow is considered. In this chapter, analysis of entropy generation is undertaken for micropolar fluid flow through a two-dimensional porous channel. For this, two types (cases) of boundary conditions for the velocity and temperature of the plates of the porous channel are chosen as mentioned in the previous chapter. Specifically, the investigations focus on the effect of different parameters on the components of velocity, microrotation, temperature, entropy generation and Bejan number.

3.2 Mathematical Formulation

Consider a steady, laminar, incompressible, micropolar fluid flow through the horizontal porous parallel plates separated by a distance h as shown in Fig. 3.1. Let V_0 be the injection velocity of the lower plate and V_1 be the suction velocity of the upper plate. Without loss of generality, it is assumed that $|V_1| \geq |V_0|$. Assume that the fluid flows along x-direction and the flow variables are independent of z co-ordinate. Thus, the velocity and microrotation vectors are taken as $\overline{q} = u(x,y)\widehat{i} + v(x,y)\widehat{j}$ and $\overline{\omega} = \sigma(x,y)\widehat{k}$ respectively. Under these assumptions, the governing equations

[93] of an incompressible micropolar fluid in the absence of body force and body couple are given by

$$\frac{\partial u}{\partial x}+\frac{\partial v}{\partial y}=0 \tag{3.1}$$

$$\rho\left[u\frac{\partial u}{\partial x}+v\frac{\partial u}{\partial y}\right]=-\frac{\partial p}{\partial x}+\kappa\frac{\partial \sigma}{\partial y}+(\mu+\kappa)\left(\frac{\partial^2 u}{\partial x^2}+\frac{\partial^2 u}{\partial y^2}\right) \tag{3.2}$$

$$\rho\left[u\frac{\partial v}{\partial x}+v\frac{\partial v}{\partial y}\right]=-\frac{\partial p}{\partial y}-\kappa\frac{\partial \sigma}{\partial x}+(\mu+\kappa)\left(\frac{\partial^2 v}{\partial x^2}+\frac{\partial^2 v}{\partial y^2}\right) \tag{3.3}$$

$$\rho j^*\left[u\frac{\partial \sigma}{\partial x}+v\frac{\partial \sigma}{\partial y}\right]=\kappa\left(\frac{\partial v}{\partial x}-\frac{\partial u}{\partial y}\right)-2\kappa\sigma+\gamma\left(\frac{\partial^2 \sigma}{\partial x^2}+\frac{\partial^2 \sigma}{\partial y^2}\right) \tag{3.4}$$

$$\begin{aligned}\rho C_p\left[u\frac{\partial T}{\partial x}+v\frac{\partial T}{\partial y}\right]&=K_f\left(\frac{\partial^2 T}{\partial x^2}+\frac{\partial^2 T}{\partial y^2}\right)+(2\mu+\kappa)\left\{\left(\frac{\partial u}{\partial x}\right)^2+\left(\frac{\partial v}{\partial y}\right)^2\right.\\&\left.+\frac{1}{2}\left(\frac{\partial u}{\partial y}+\frac{\partial v}{\partial x}\right)^2\right\}+\frac{\kappa}{2}\left[\left(\frac{\partial v}{\partial x}-\frac{\partial u}{\partial y}\right)-2\sigma\right]^2+\gamma\left[\left(\frac{\partial \sigma}{\partial x}\right)^2+\left(\frac{\partial \sigma}{\partial y}\right)^2\right]\end{aligned} \tag{3.5}$$

Apply the following similarity transformation proposed by [93, 7] to convert the governing partial differential equations to ordinary differential equations.

$$u(x,\eta)=\left(\frac{U_0}{a}-\frac{V_1 x}{h}\right)f'(\eta),\quad v(x,\eta)=V_1 f(\eta),\quad \sigma(x,\eta)=\frac{1}{h}\left(\frac{U_0}{a}-\frac{V_1 x}{h}\right)g(\eta) \tag{3.6}$$

where $\eta=\dfrac{y}{h}$, $a=1-\dfrac{V_0}{V_1}$.

Substituting (3.6) in Eqs. (3.2), (3.3) and (3.4), to get the following non-dimensional equations

$$Re(-f'f''+ff''')=\frac{N}{1-N}g''+\frac{1}{1-N}f^{iv} \tag{3.7}$$

$$Re\,a_j(fg'-f'g)=\frac{-2N}{1-N}g-\frac{N}{1-N}f''+\frac{N(2-N)}{m^2(1-N)}g'' \tag{3.8}$$

where $Re=\dfrac{\rho V_1 h}{\mu}$ is the suction Reynolds number.

Eq.(3.5) together with (3.6), propose the formation of temperature can be taken as

$$T(x,\eta) = T_1 + \frac{\mu V_1}{\varrho h C_p}\left[\theta_1 + \left(\frac{U_0}{aV_1} - \frac{x}{h}\right)^2 \theta_2\right] \tag{3.9}$$

Substituting Eq. (3.9) in Eq. (3.5), equating the coefficients of $\left(\frac{U_0}{a} - \frac{V_1 x}{h}\right)^2$ and the terms without $\left(\frac{U_0}{a} - \frac{V_1 x}{h}\right)$ on both sides of the equation thus, obtained

$$\theta_1'' + 2\theta_2 + PrRe\left[\frac{2(2-N)}{(1-N)} f'^2 + \frac{N(2-N)}{m^2(1-N)} g^2 - f\theta_1'\right] = 0 \tag{3.10}$$

$$\theta_2'' + PrRe\left[\frac{2-N}{2(1-N)} f''^2 + \frac{N}{2(1-N)}(f''+2g)^2 + \frac{N(2-N)}{m^2(1-N)} g'^2 - (f\theta_2' - 2f'\theta_2)\right] = 0 \tag{3.11}$$

The dimensionless form of temperature can be written as

$$\theta = \frac{T - T_1}{T_2 - T_1} = Ec\left(\theta_1 + \widehat{x}^2 \theta_2\right) \tag{3.12}$$

where $Ec = \dfrac{\mu V_1}{\rho(T_2 - T_1) h c_p}$ is the Eckert number and $\widehat{x} = \left(\dfrac{U_0}{a} - \dfrac{V_1 x}{h}\right)$ is the dimensionless axial variable.

3.2.1 Case(a): No-slip and Isothermal Boundary Conditions

Assume that the no-slip condition for velocity and hyper-stick condition for microrotation on lower and upper plates of the channel. Let the channel plates are maintained at uniform temperatures T_1 and T_2 respectively. These boundary conditions are given by

$$\begin{aligned} &u(x,\eta) = 0, \quad v(x,\eta) = V_0, \quad \sigma(x,\eta) = 0, \quad T(x,\eta) = T_1 \quad \text{at} \quad \eta = 0 \\ &u(x,\eta) = 0, \quad v(x,\eta) = V_1, \quad \sigma(x,\eta) = 0, \quad T(x,\eta) = T_2 \quad \text{at} \quad \eta = 1 \end{aligned} \tag{3.13}$$

The boundary conditions in terms of f, g, θ_1 and θ_2 become

$$\begin{aligned} f(0) = 1 - a, \quad f'(0) = 0, \quad g(0) = 0, \quad \theta_1(0) = 0, \quad \theta_2(0) = 0 \\ f(1) = 1, \quad f'(1) = 0, \quad g(1) = 0, \theta_1(1) = \frac{1}{Ec}, \quad \theta_2(1) = 0 \end{aligned} \tag{3.14}$$

The Quasilinearization method is used to convert the non-linear differential equations (3.7), (3.8), (3.10), (3.11) to a system of linear differential equations. The resultant system is solved using the Chebyshev spectral collocation method, as described in detail in chapter-2. The physical region $[0, 1]$ is transformed into the region $[-1, 1]$ using the mapping

$$\eta = \frac{\xi + 1}{2}, \quad -1 \leq \xi \leq 1 \tag{3.15}$$

Proceeding as in chapter-2 and incorporate the boundary conditions (3.14) in the matrix system $\mathbf{A}_r \mathbf{X}_{r+1} = \mathbf{B}_r$, the solution is obtained as

$$\mathbf{X}_{r+1} = \mathbf{A}_r^{-1} \mathbf{B}_r \tag{3.16}$$

Entropy Generation

The micropolar fluid flow through a porous channel is naturally irreversible. The non-equilibrium condition arises due to the exchange of energy and momentum within the micropolar fluid and at the solid boundaries, that leads to continuous entropy generation in the porous channel.

For the present study, the volumetric rate of entropy generation is given by

$$\begin{aligned} S_G = \frac{K_f}{T_1^2}\left[\left(\frac{\partial T}{\partial x}\right)^2 + \frac{1}{h^2}\left(\frac{\partial T}{\partial \eta}\right)^2\right] + \frac{2\mu + \kappa}{T_1}\left[\left(\frac{\partial u}{\partial x}\right)^2 + \frac{1}{h^2}\left(\frac{\partial v}{\partial \eta}\right)^2 + \frac{1}{2}\left(\frac{1}{h}\frac{\partial u}{\partial \eta} + \frac{\partial v}{\partial x}\right)^2\right] \\ + \frac{\kappa}{2T_1}\left[\left(\frac{\partial v}{\partial x} - \frac{1}{h}\frac{\partial u}{\partial \eta}\right) - 2\sigma\right]^2 + \frac{\gamma}{T_1}\left[\left(\frac{\partial \sigma}{\partial x}\right)^2 + \frac{1}{h^2}\left(\frac{\partial \sigma}{\partial \eta}\right)^2\right] \end{aligned} \tag{3.17}$$

The dimensionless entropy generation number is given by

$$\begin{aligned} N_s = \overbrace{Ec^2\left[4\theta_2^2 + \left(\theta_1' + \widehat{x}^2\theta_2'\right)^2\right]}^{N_h} \\ \underbrace{+ \frac{Br}{T_p(1-N)}\left[(2-N)\left(2f'^2 + \frac{\widehat{x}^2}{2}f''^2\right) + \frac{N\widehat{x}^2}{2}(f'' + 2g)^2 + \frac{N(2-N)}{m^2}(g^2 + \widehat{x}^2 g'^2)\right]}_{N_v} \end{aligned} \tag{3.18}$$

The Eq. (3.18) is useful for producing the entropy generation profiles, but it fails to give an idea about the relative importance of friction and heat transfer effects. Therefore, an alternative

parameter Bejan number (Be) is introduced. It is defined as the ratio of entropy generation due to heat transfer to the overall entropy generation given below.

$$Be = \frac{N_h}{N_h + N_v} \tag{3.19}$$

Results and Discussion

The numerical expressions for velocity, microrotation and temperature are given in Eqs. (3.7), (3.8) and (3.12) respectively. These values are used to evaluate the entropy generation number and Bejan number. The results are presented in the form of graphs for $Pr = 1$, $T_p = 0.5$, $m = 2$ and $a_j = 0.001$.

Fig. 3.2 displays the effect of coupling number N on the dimensionless axial velocity, transverse velocity, microrotation, temperature, entropy generation and Bejan number. It is observed from Fig. 3.2(a) that the axial velocity increases near the lower plate and decreases near the upper plate with an increase in coupling number. It is seen from Fig. 3.2(b) that an increase in coupling number increases the transverse velocity. The microrotation component decreases near the lower plate and increases near the upper plate with an increase in the value of coupling number as shown in Fig. 3.2(c). Fig. 3.2(d) shows the temperature distribution θ against η, for several values of coupling number. It is observed that the temperature increases with an increase in the value of coupling number. Increase in coupling number N tends to enhance the entropy generation near the lower plate and reduces the entropy generation near the upper plate as shown in Fig. 3.2(e). It is observed from Fig. 3.2(f) that as N increases, the Bejan number decreases. This is attributed to increase in the dominance of fluid friction irreversibility with an increase in N.

The effect of suction Reynolds number Re on the dimensionless axial velocity, transverse velocity, microrotation, temperature, entropy generation and Bejan number is plotted in Fig. 3.3. It is observed from Fig. 3.3(a) that increase in suction Reynolds number(Re) leads to decrease the axial fluid velocity at the lower plate and increase the axial fluid velocity at the upper plate. Since the suction velocity of the upper plate is greater than the injection velocity of the lower plate and thus the axial velocity profile becomes asymmetric with respect to the middle of the channel and it is pushed towards the upper plate. Fig. 3.3(b) shows that the radial velocity decreases with increase

in suction Reynolds number. It can be noticed from Fig. 3.3(c) that the microrotation component decreases with an increase in suction Reynolds number except near the lower plate, where microrotation slightly increases. An increase in the value of suction Reynolds number reduces the temperature, as shown in Fig. 3.3(d). Entropy generation number decreases near the lower plate $\eta = 0$ and increases near the upper plate $\eta = 1$ with an increase in suction Reynolds number Re as displayed in Fig. 3.3(e). It is observed from Fig. 3.3(f) that the Bejan number Be decreases near the plate $\eta = 0$ and increases near the plate $\eta = 1$ with an increase in Re.

It is observed from Fig. 3.4(a) that the axial velocity increases as the suction injection ratio increases (i.e., a increases) and the velocity is maximum at the center of the channel for all values of a. Fig. 3.4(b) shows that the transverse velocity decreases with the increase of a. A general trend is observed from Fig. 3.4(c) that the microrotation changes its concavity in the center of the channel. In the lower half, the profiles are concave downward whereas in the upper half they are upward. The magnitude of the maximum microrotation increases with the increase of the suction injection ratio. Fig. 3.4(d) depicts the temperature profile with the variation of a. An increase in the value of a leads to increase the temperature at both injection and suction plates. It is observed from Fig. 3.4(e) that as a increases, the entropy generation increases at the lower plate and decreases at the upper plate. It is noticed from Fig. 3.4(f) that the Bejan number (Be) decreases with an increase in the value of a.

Figs. 3.5(a) and 3.5(b) describe the effect of $\widehat{x}$ on entropy generation and Bejan number. It is clear from Fig. 3.5(a) that the entropy generation increases at the lower plate and there is no significant effect at the upper plate with increase in $\widehat{x}$. Fig. 3.5(b) shows that as $\widehat{x}$ increases, Bejan number decreases near the lower and upper plates. Hence, irreversibility due to fluid friction dominates the flow process at the lower and upper plates.

Fig. 3.6 illustrates the effect of Eckert number (Ec) on temperature, entropy generation and Bejan number. Fig. 3.6(a) shows the effect of Eckert number on the temperature profile. The higher values of Eckert number signifies the higher heat levels, which are formed by friction. Thus temperature increases with an increase in the value of Eckert number. It is observed from Fig. 3.6(b) that as Ec increases, the entropy generation increases near the lower plate and decreases near the upper plate. Fig. 3.6(c) shows that as Ec increases, Bejan number increases near the lower plate and decreases near the upper plate. Hence, irreversibility due to heat transfer dominates the flow process at the lower plate and irreversibility due to fluid friction dominates at the upper plate.

The effect of the Brinkman number on entropy generation and Bejan number is plotted in Fig. 3.7. It is noticed from Fig. 3.7(a) that as Br increases, the entropy generation number increases. In the energy equation the coefficient of viscous dissipation is the Brinkman number. As the Brinkman number increases the fluid temperature increases consecutively, the viscous dissipation also increases. In the channel considered as the temperature of the fluid increases, the gradient of temperature increases and consequently, the entropy generation number increases. It is also observed that the entropy generation number is less at lower plate of the channel and increases rapidly to its maximum values at the upper plate of the channel for variation of all parameters. Fig. 3.7(b) shows that the Bejan number decreases with an increase in the value of Brinkman number.

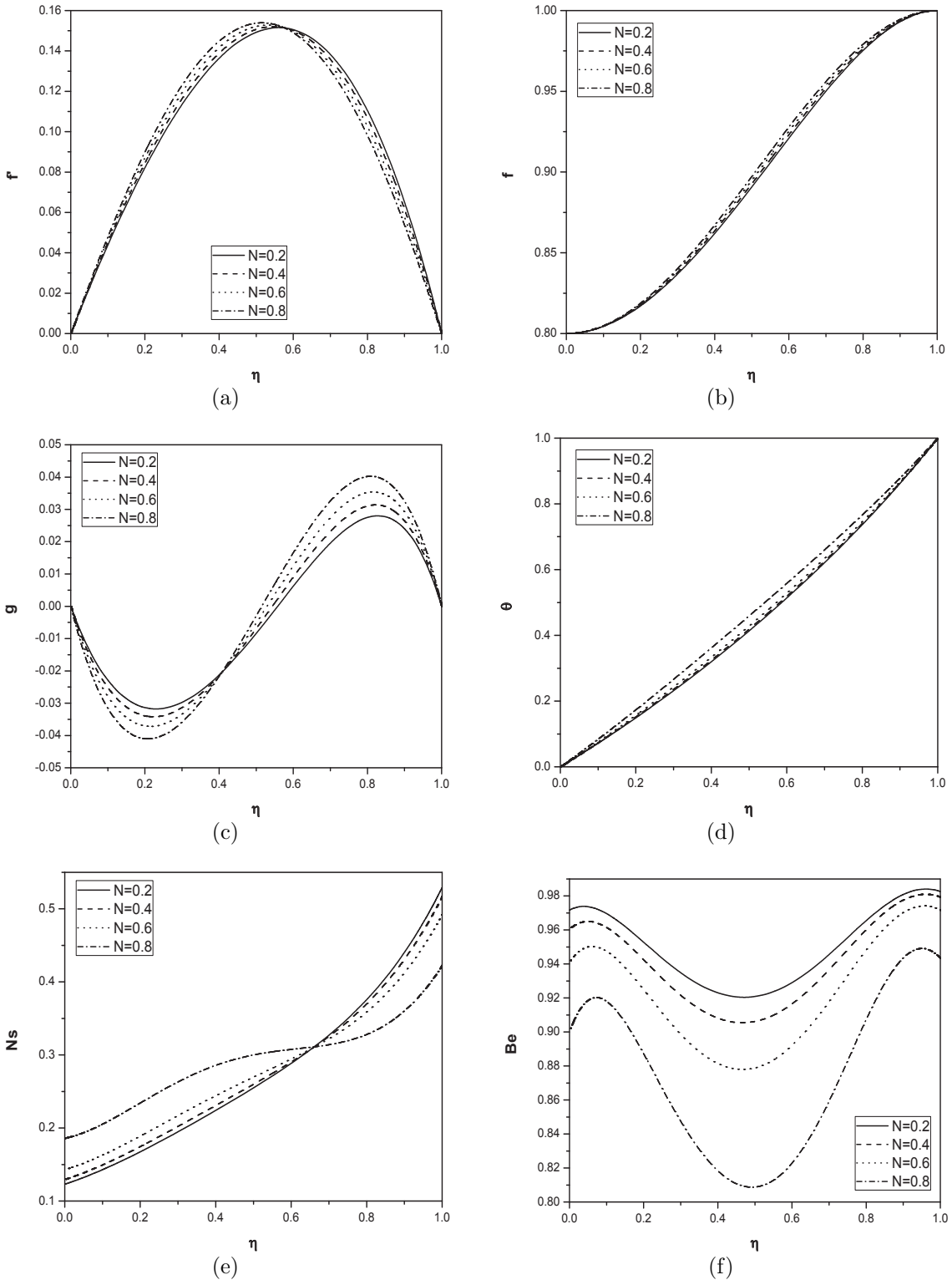

Figure 3.2: Effect of coupling number on (a)axial velocity, (b)transverse velocity, (c)microrotation, (d)temperature, (e)entropy generation and (f)Bejan number for $Ec = 1$, $Br = 0.1$, $Re = 1$, $a = 0.2$ and $\widehat{x} = 0.5$.

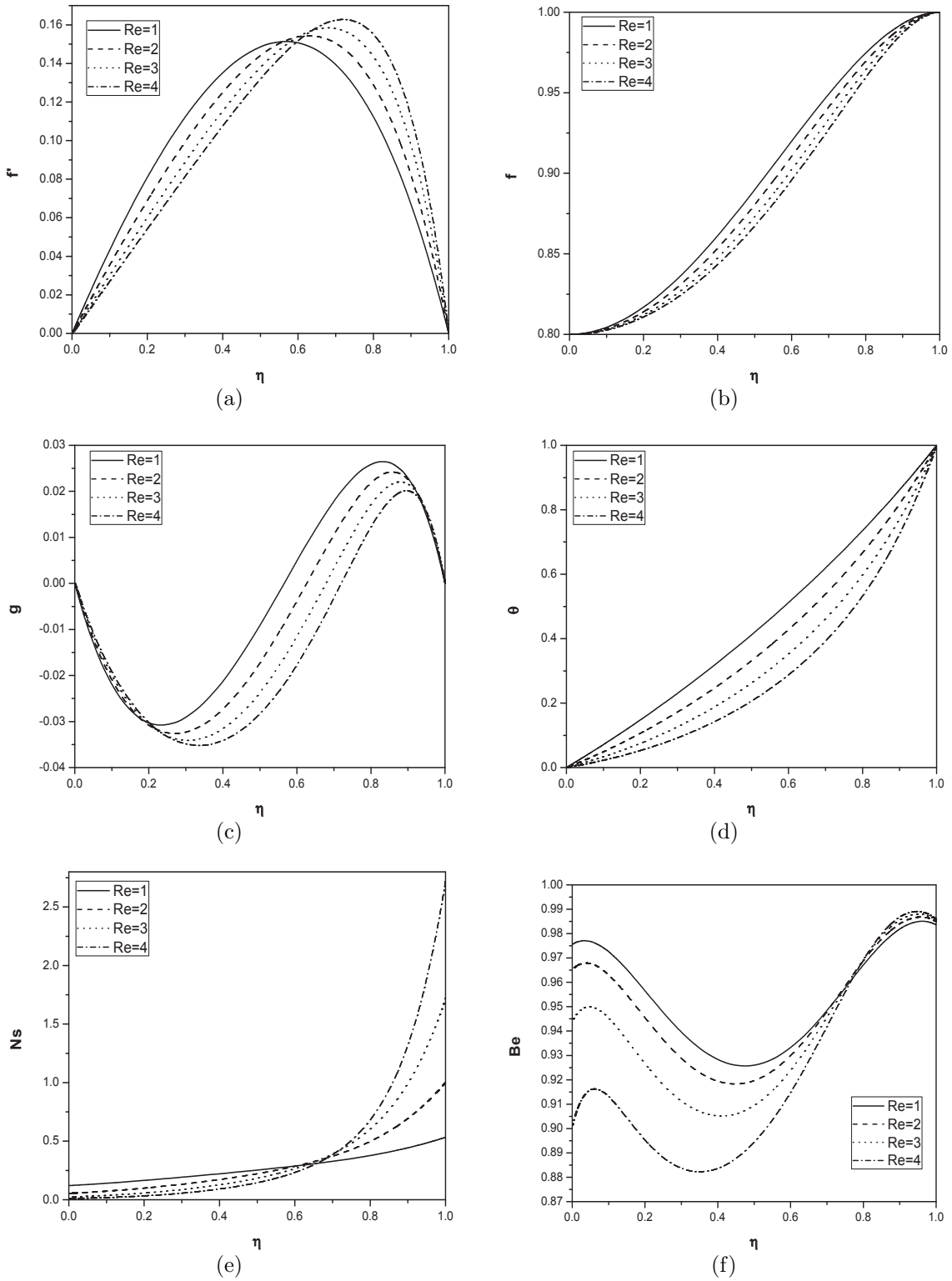

Figure 3.3: Effect of suction Reynolds number on (a)axial velocity, (b)transverse velocity, (c)microrotation, (d)temperature, (e)entropy generation and (f)Bejan number for $Ec = 1$, $Br = 0.1$, $N = 0.5$, $a = 0.2$ and $\widehat{x} = 0.5$.

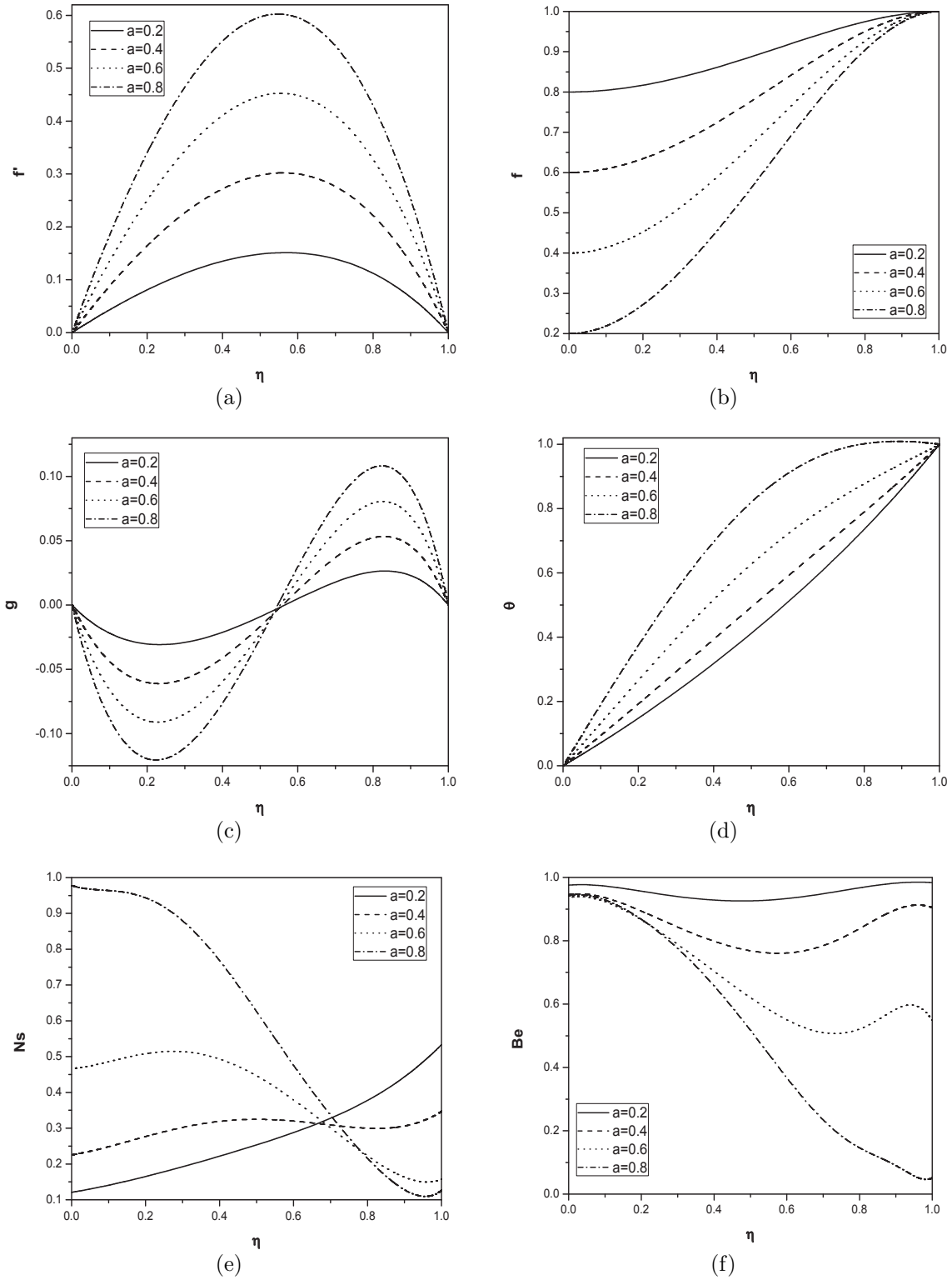

Figure 3.4: Effect of a on (a)axial velocity, (b)transverse velocity, (c)microrotation, (d)temperature, (e)entropy generation and (f)Bejan numberfor $Ec = 1$, $Br = 0.1$, $Re = 1$, $N = 0.5$ and $\widehat{x} = 0.5$.

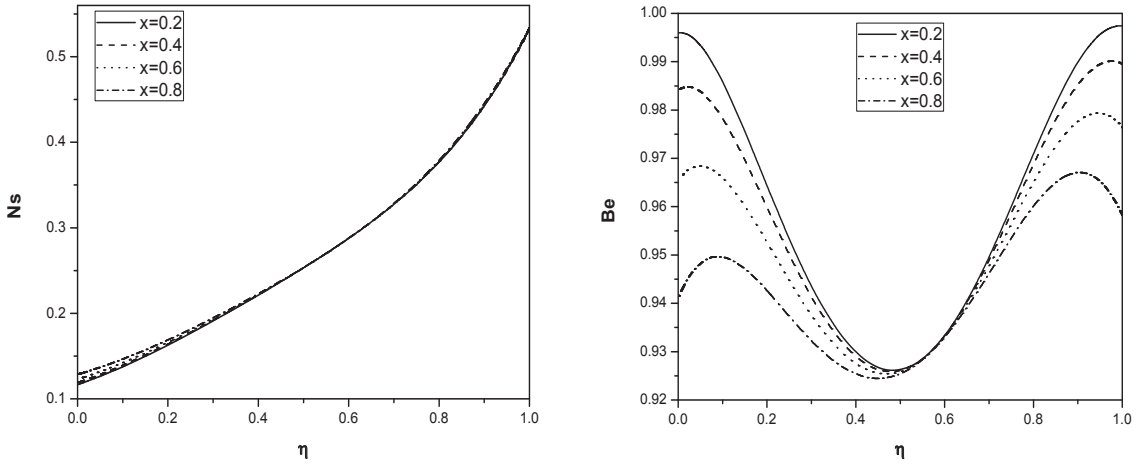

(a) (b)

Figure 3.5: Effect of $\widehat{x}$ on (a)entropy generation and (b)Bejan number for $Ec = 1$, $Br = 0.1$, $Re = 1$, $a = 0.2$ and $N = 0.5$.

3.2.2 Case(b): Slip and Convective Boundary Conditions

Assume that the fluid adjacent to the channel plates has finite tangential velocity, it slips along the boundary and the microelements close to the channel plates are unable to rotate. Further, the fluid is convectively heated at the lower plate while at the upper plate convective heat loss can take place. Hence, the boundary conditions are

$$\begin{aligned} u(x,\eta) = \frac{\zeta'}{h}\frac{\partial u}{\partial \eta}, \quad v(x,\eta) = V_0, \quad \sigma(x,\eta) = 0, \quad \frac{K_f}{h}\frac{\partial T}{\partial \eta} - h_1(T - T_1) = 0 \quad \text{at} \quad \eta = 0 \\ u(x,\eta) = -\frac{\zeta'}{h}\frac{\partial u}{\partial \eta}, \quad v(x,\eta) = V_1, \quad \sigma(x,\eta) = 0, \quad \frac{K_f}{h}\frac{\partial T}{\partial \eta} + h_2(T - T_2) = 0 \quad \text{at} \quad \eta = 1 \end{aligned} \tag{3.20}$$

The boundary conditions (3.20) in terms of f, g, θ_1 and θ_2 are:

$$\begin{aligned} f(0) = 1 - a,\ f'(0) - \zeta f''(0) = 0,\ g(0) = 0,\ \theta_1'(0) - Bi_1\theta_1(0) = 0,\ \theta_2'(0) - Bi_1\theta_2(0) = 0 \\ f(1) = 1,\ f'(1) + \zeta f''(1) = 0,\ g(1) = 0,\ \theta_1'(1) + Bi_2\theta_1(1) = \frac{Bi_2}{Ec},\ \theta_2'(1) + Bi_2\theta_2(1) = 0 \end{aligned} \tag{3.21}$$

where $\zeta = \frac{\zeta'}{h}$ is the slip parameter and consider $Bi_1 = Bi_2 = Bi$.

Proceeding as in Case(a), the solution is obtained from the following matrix equation

$$\mathbf{X}_{r+1} = \mathbf{A}_r^{-1}\mathbf{B}_r \tag{3.22}$$

The entropy generation and Bejan number have been calculated for the slip and convective boundary conditions(Eq. (3.21)) from equations (3.18) and (3.19).

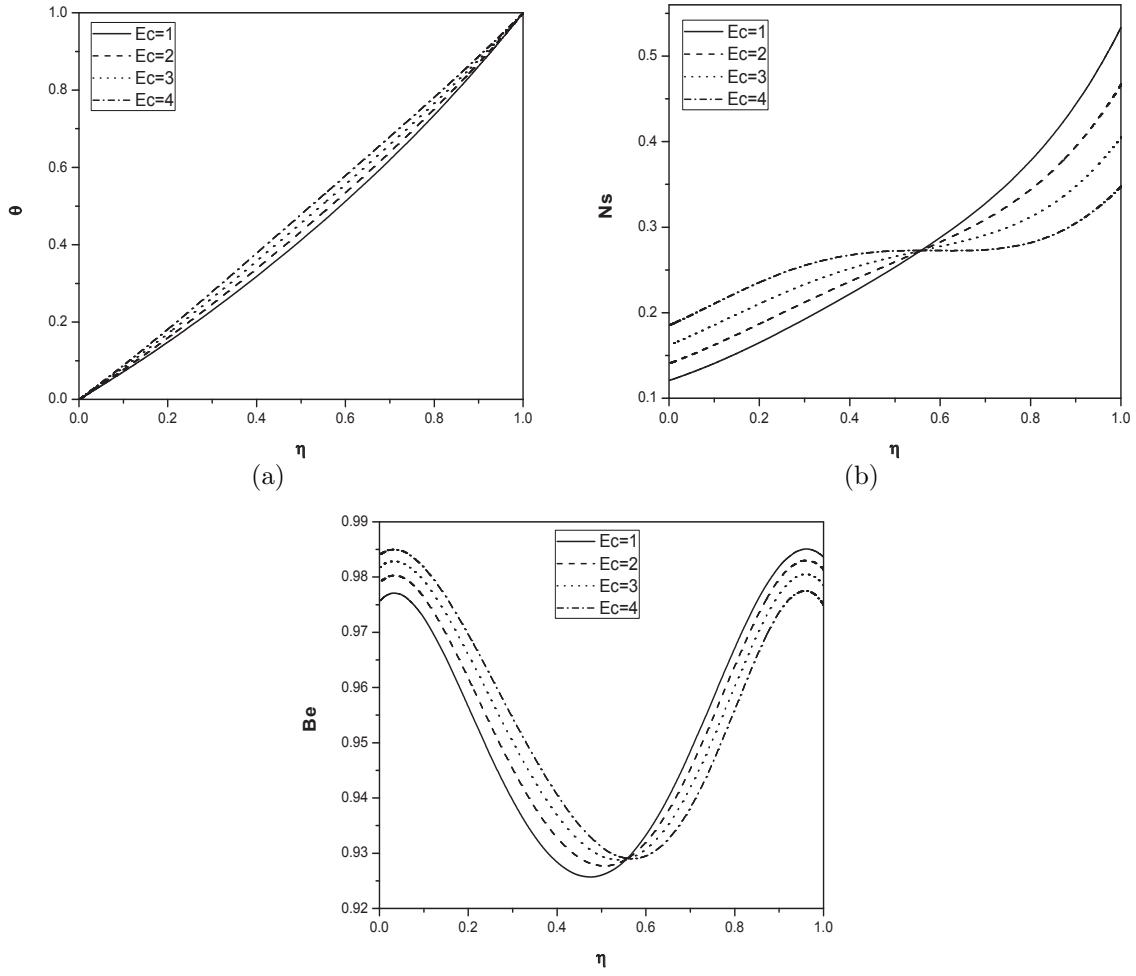

Figure 3.6: Effect of Eckert number on (a)temperature, (b)entropy generation and (c)Bejan number for $N = 0.5$, $Br = 0.1$, $Re = 1$, $a = 0.2$ and $\widehat{x} = 0.5$.

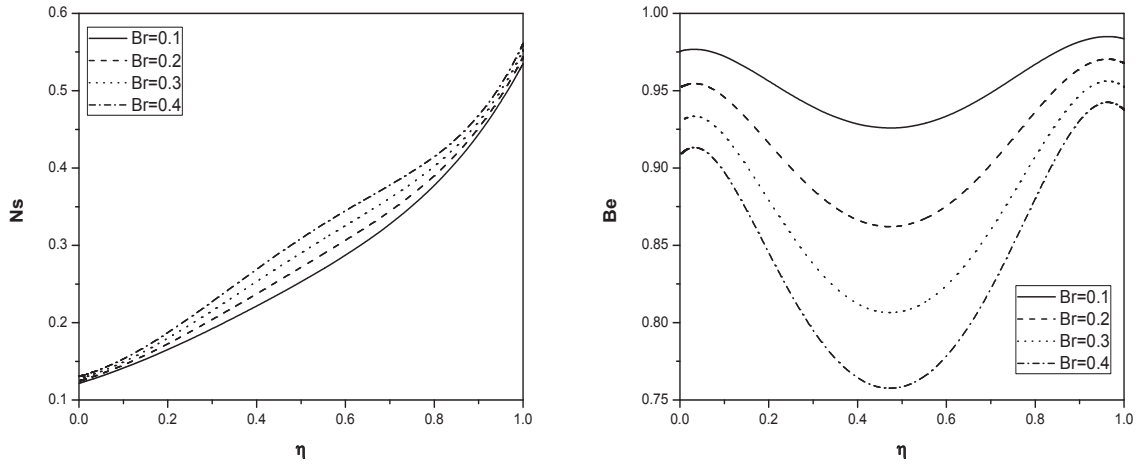

(a) (b)

Figure 3.7: Effect of Brinkman number on (a)entropy generation and (b)Bejan number for $Ec = 1$, $N = 0.5$, $Re = 1$, $a = 0.2$ and $\widehat{x} = 0.5$.

Results and Discussion

Extensive calculations have been performed to obtain the entropy generation and the Bejan number for different values of the parameters N, Re, ζ, Ec, Bi and Br. The following parameters are taken as constant in the overall study: $Pr = 1$, $T_p = 0.5$, $m = 2$, $a = 2$, $\widehat{x} = 0.5$ and $a_j = 0.001$.

Fig. 3.8, displays the effects of coupling number N on the dimensionless axial velocity, transverse velocity, microrotation, temperature, entropy generation and Bejan number. It is observed from Fig. 3.8(a) that the axial velocity increases near the lower plate and decreases near the upper plate with an increase in coupling number. It is noticed from Fig. 3.8(b) that as N increases, the transverse velocity increases. Fig. 3.8(c) depicts that the microrotation component decreases near the lower plate and increases near the upper plate with an increase in the value of N. Fig. 3.8(d) shows the temperature distribution θ against η, for several values of coupling number. It is observed that the temperature increases with increase in N. Fig. 3.8(e) reveals that the entropy generation number Ns increases with the increase of the coupling number N. It is observed from Fig. 3.8(f) that as N increases, the Bejan number decreases.

Fig. 3.9, represents the effect of suction Reynolds number Re on the dimensionless axial velocity, transverse velocity, microrotation, temperature, entropy generation and Bejan number. Fig. 3.9(a) shows the effect of an increase in the suction Reynolds number on the axial velocity of the fluid flow. The result shows that an increase in the suction parameter breaks the symmetric nature of

the flow due to continuous increase in the injection flow at the lower plate which is sucked off at the upper plate. Due to a break in symmetry, the fluid flow is observed to be skewed towards the upper plate with suction. Fig. 3.9(b) shows that the radial velocity is not effected with an increase in the value of Re. From the Fig. 3.9(c) it is observed that with an increase in suction Reynolds number, the microrotation component decreases and this decrease is significant in the middle of the channel and negligible near the upper plate, whereas the trend is reversed with negligible difference near the lower plate. No change in the temperature with an increase in the value of suction Reynolds number is observed from Fig. 3.9(d). Fig. 3.9(e) illustrates that an increase in the suction Reynolds number decreases the entropy generation at the lower plate due to injection and convective heating, whereas Ns increases near the upper plate due to convective cooling. It is observed from Fig. 3.9(f) that the Bejan number Be decreases with an increase in Re.

Fig. 3.10, displays the effect of ζ on governing parameters, entropy generation and Bejan number. Fig. 3.10(a) shows that the axial velocity increases near the lower and upper plates, whereas it decreases in the middle of the channel as the slip parameter increases. Fig. 3.10(b) depicts that the transverse velocity increases slightly near the lower plate with the increase of ζ. A general trend is observed from Fig. 3.10(c) that the microrotation changes its concavity in the center of the channel. Fig. 3.10(d), depicts the temperature profile with the variation of ζ. An increase in the value of ζ, leads to decrease the temperature at both injection and suction plates. It is observed from Fig. 3.10(e) that as ζ increases, entropy generation increases at the lower and upper plates and decreases at the center line region of the channel. It is noticed from Fig. 3.10(f) that the Bejan number (Be) decreases near the lower plate and then increases with an increase in the value of ζ.

Fig. 3.11(a) shows the effect of convective heating parameter(Bi) on the fluid temperature. It is observed that the fluid temperature falls at the lower plate of the channel as the fluid exchange heat with the plate and opposite phenomena is experienced at the other plate. The influence of the Biot number on entropy generation and Bejan number is shown in Figs. 3.11(b) and 3.11(c). It is noticed that the increase in the Biot number enhances the entropy generation and Bejan number.

Fig. 3.12, illustrates the effect of Eckert number (Ec) on temperature, Entropy generation and Bejan number. As observed from the previous case that the temperature increases with increase in Eckert number as indicated in Fig. 3.12(a). It is observed from Fig. 3.12(b) that as Ec increases, the entropy generation increases near the lower plate and decreases near the upper plate. Fig.

3.12(c) shows that as Ec increases, Bejan number increases near the lower plate and decreases near the upper plate.

The effect of the Brinkman number on entropy generation and Bejan number is plotted in Fig. 3.13. It is noticed from Fig. 3.13(a) that as Br increases, the entropy generation number increases. It is observed that the entropy generation number is less at lower plate of the channel and increases rapidly to its maximum value around the center of the channel and gradually decreases at the upper plate of the channel for variation in all parameters. From Fig. 3.13(b) an increase in the Brinkman number reduces the heat transfer in the channel so, the Bejan number also decreases.

3.3 Conclusions

In this Chapter, the entropy generation in a micropolar fluid flow through a horizontal porous channel is analyzed subject to (a)No-slip and isothermal boundary conditions and (b)Slip and convective boundary conditions. From the analysis, the following are the observations in both the cases (a) and (b).

An increase in the microrotation parameter N, increases the temperature and decreases the Bejan number. An increase in the suction parameter(i.e. suction Reynolds number) breaks the symmetric nature of the flow due to continuous increase in the injection flow at the lower plate which is sucked off at the upper plate. Due to a break in symmetry, the fluid flow is observed to be skewed towards the upper plate with suction. Entropy generation decreases near the lower plate and increases near the upper plate with an increase in the suction Reynolds number. High Eckert numbers imply high heat levels are produced by friction resulting in increased temperatures on the system. It is observed that as Ec increases, the entropy generation and Bejan number increases near the lower plate and decreases near the upper plate. As Brinkman number increases the entropy generation increases and Bejan number decreases. Further, it is observed in Case (b) that as increase in slip parameter enhances the velocity at the lower and upper plates, and reduction in the velocity at the center of the channel. The similar trend is observed for entropy generation. It is found that, the entropy generation increases with an increase in the Biot number.

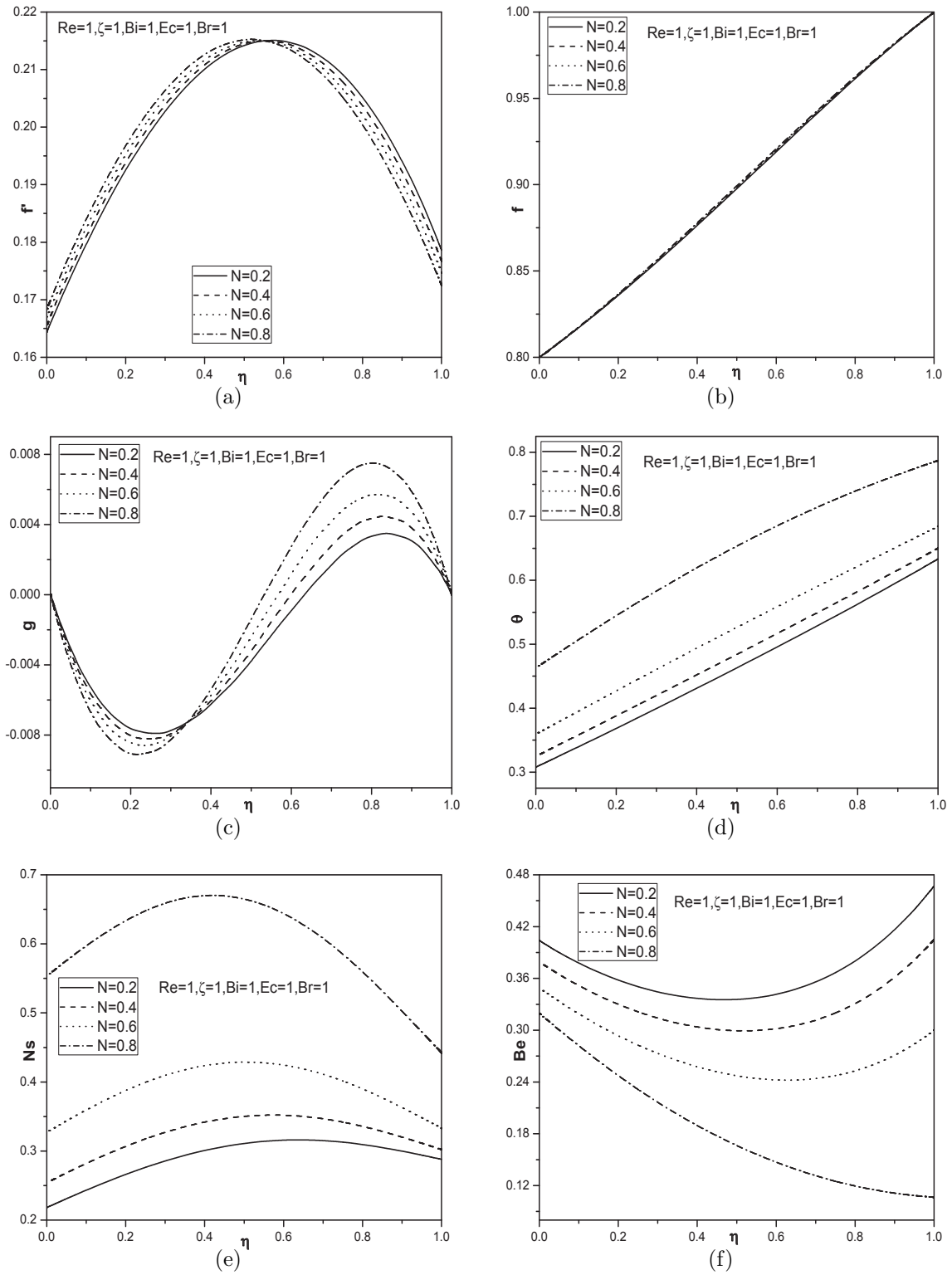

Figure 3.8: Effect of coupling number on (a)axial velocity, (b)transverse velocity, (c)microrotation, (d)temperature, (e)entropy generation and (f)Bejan number.

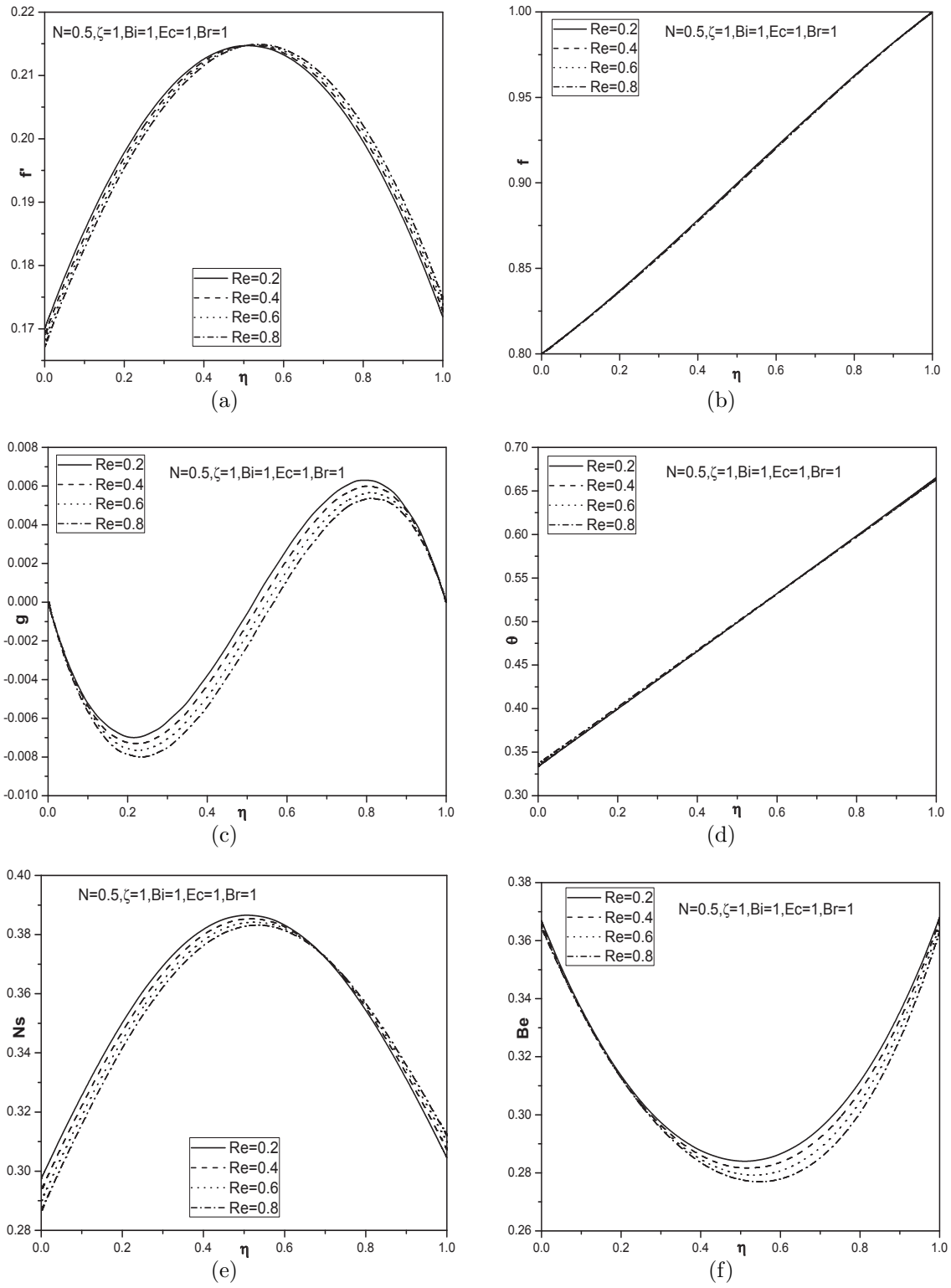

Figure 3.9: Effect of suction Reynolds number on (a)axial velocity, (b)transverse velocity, (c)microrotation, (d)temperature (e)entropy generation and (f)Bejan number.

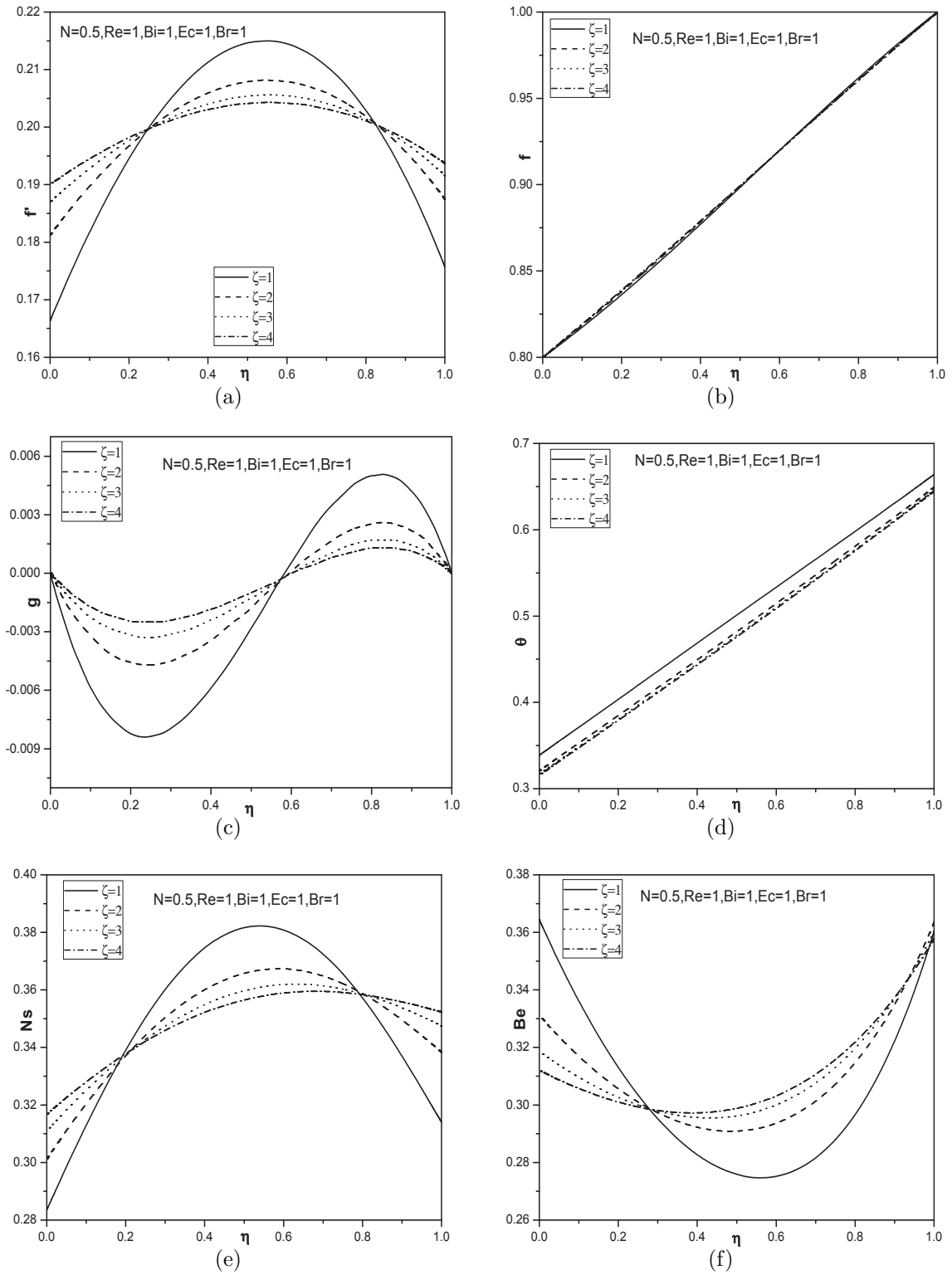

Figure 3.10: Effect of slip parameter on (a)axial velocity, (b)transverse velocity, (c)microrotation, (d)temperature, (e)entropy generation and (f)Bejan number.

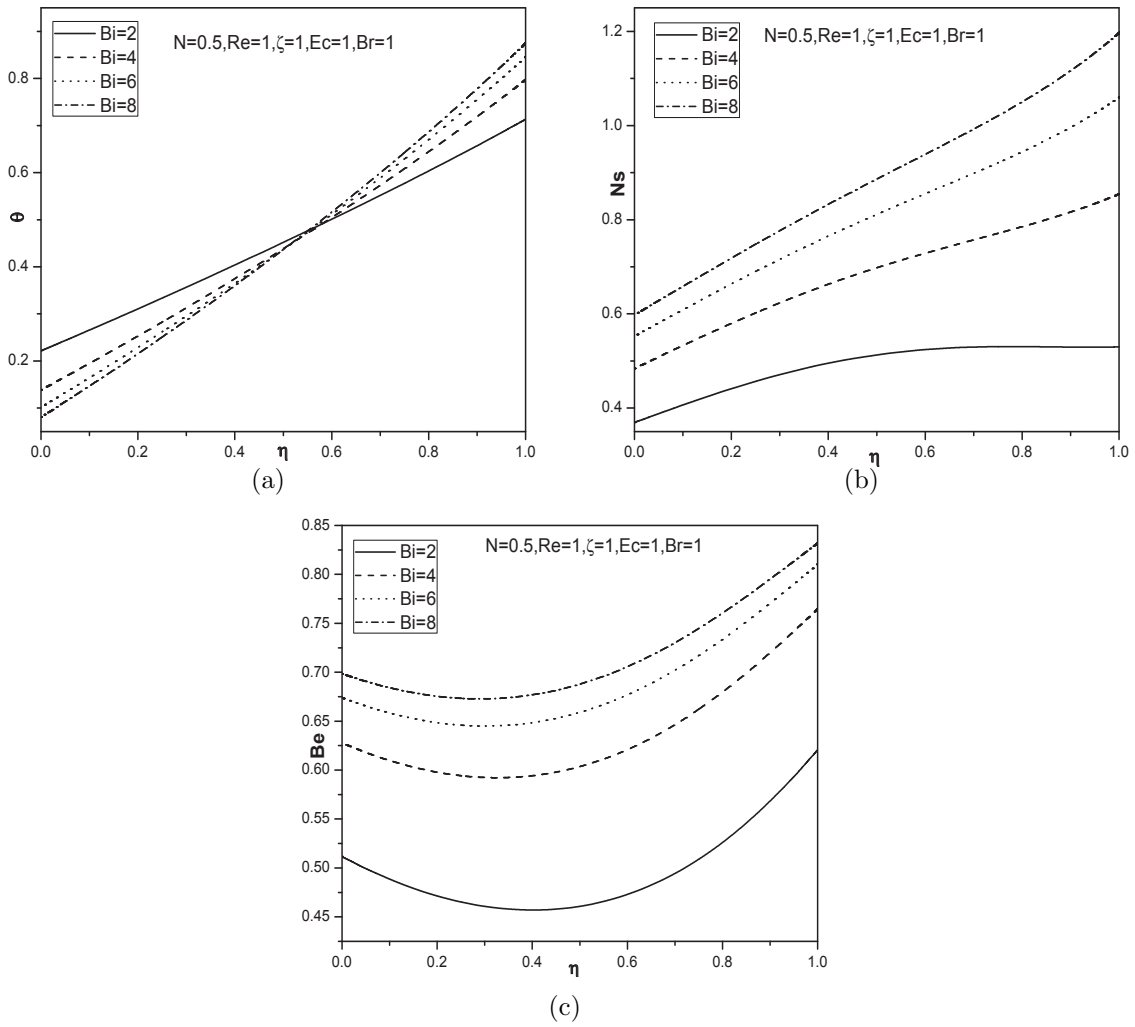

Figure 3.11: Effect of Biot number on (a)temperature, (b)entropy generation and (c)Bejan number.

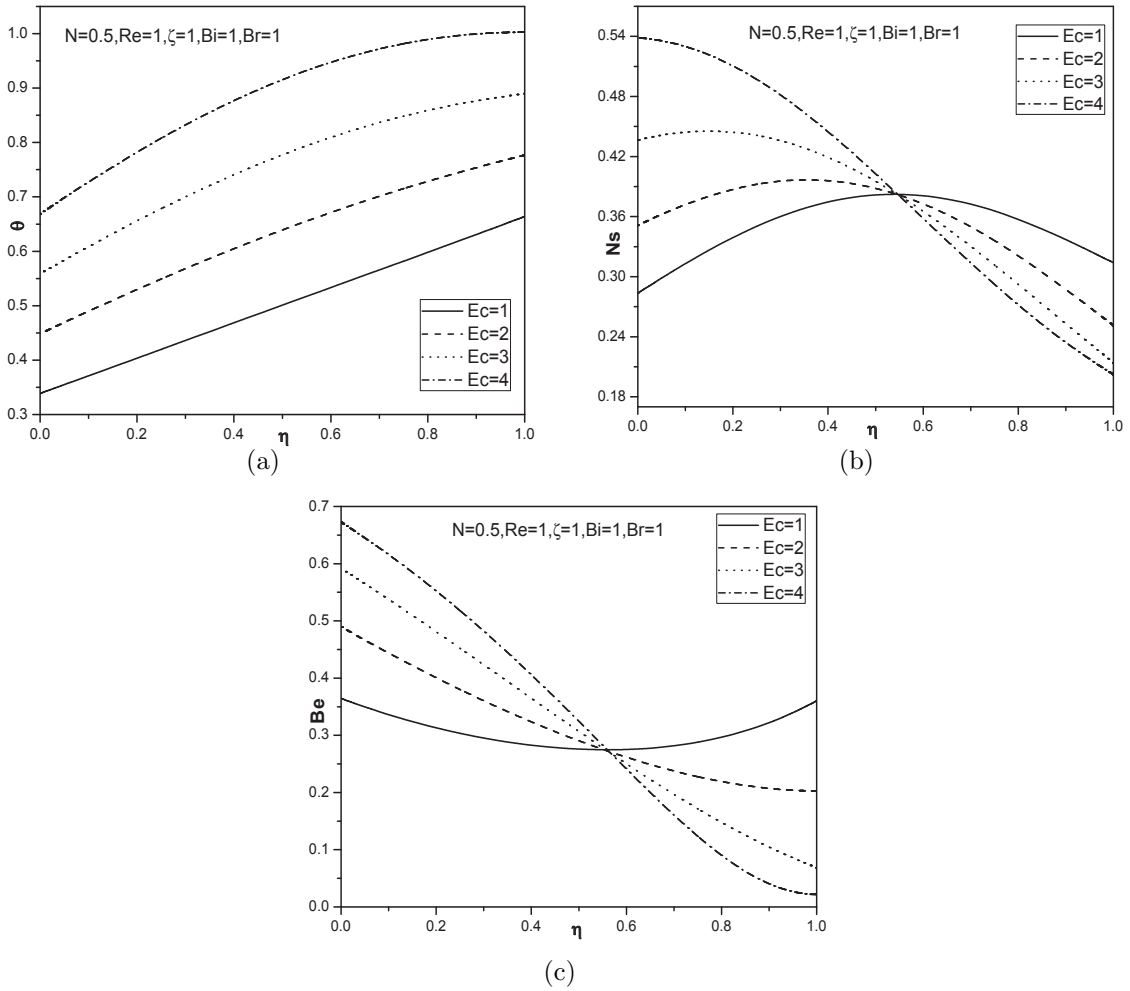

Figure 3.12: Effect of Eckert number on (a)temperature, (b)entropy generation and (c)Bejan number.

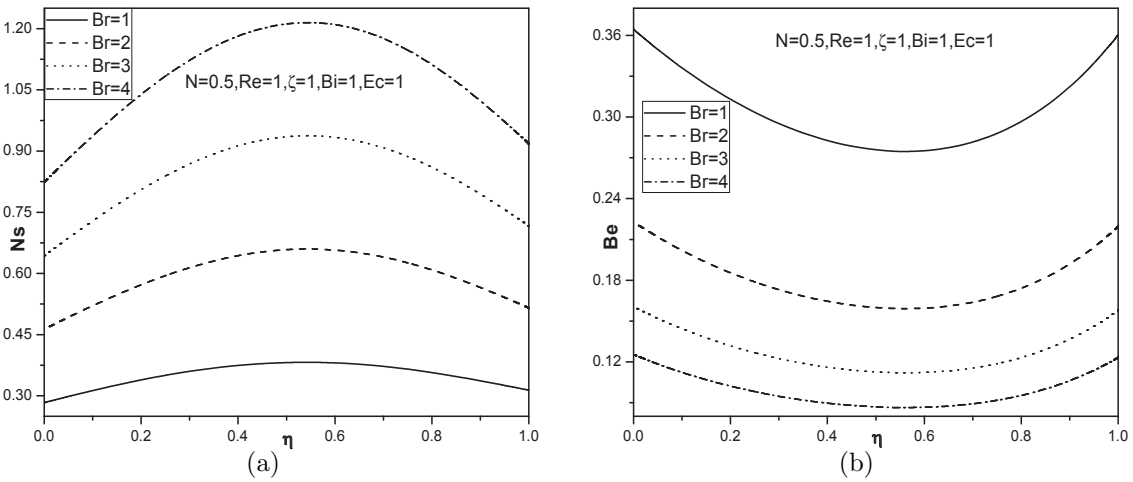

Figure 3.13: Effect of Brinkman number on (a)entropy generation and (b)Bejan number.

Chapter 4

Effect of Magnetic Field on Entropy Generation due to Micropolar Fluid Flow in a Rectangular Duct [1]

4.1 Introduction

The present trend in the field of heat transfer and thermal design is to conduct second law (of thermodynamics) analysis, including, design related concept of entropy generation and its minimization. Entropy generation is a measure of irreversibilities associated to the real process. Entropy generation is present in all heat transfer processes. The Magnetic effect, viscous effect, heat transfer down temperature gradient etc., are responsible for the generation of entropy. The entropy generation is encountered in many energy related applications such as geothermal energy systems, cooling of modern electronic systems and solar power collectors.

The heat transfer behavior of laminar flow through non-circular ducts is an area of special interest as it has got wide applications in compact heat exchangers. Sahin [88] described the entropy generation analysis for viscous flow through a duct with constant temperature. Hooman *et al* [49] analyzed heat transfer and optimization of entropy generation in porous saturated ducts

[1] Case(a):Published in "**Procedia Engineering Journal, 127 (2015) 1150-1157**", Case(b) Communicated to "**Journal of Heat Transfer**"

of rectangular cross section. Oztop *et al* [84] studied the entropy generation through rectangular shaped ducts with semicircular ends. Leong and Ong [60] discussed the characteristics of entropy generation in various shapes of cross section ducts with constant heat flux. An electrically conducting fluid in a duct with the effect of the magnetic field has special technical significance because of its frequent occurrence in many industrial applications such as cooling of nuclear reactors, MHD marine propulsion, electronic packages, microelectronic devices, etc. The aim of this chapter is to investigate the effect of magnetic field on entropy generation with micropolar fluid flow in a rectangular duct. The governing equations are simplified and solved using finite difference method. The effects of coupling number, Hartman number and Brinkman number on entropy generation and Bejan number are presented through graphs.

4.2 Mathematical Formulation

Consider a steady, laminar, incompressible flow of an electrically conducting micropolar fluid through a rectangular duct of uniform cross-section(shown in Fig. 4.1). The flow is generated due to constant pressure gradient along the axis of the duct(z-axis). An external uniform magnetic field is applied in a plane normal to the z-axis, which has a constant magnetic flux density B_0 that is assumed constant by taking the magnetic Reynolds number much smaller than the fluid Reynolds number. The flow variables are invariant in the flow direction (z-direction), except the pressure gradient $\frac{\partial p}{\partial z}$, which is a constant. The velocity and microrotation vectors of the fluid are $\overline{q} = w(x,y)\widehat{k}$ and $\overline{\sigma} = \sigma_1(x,y)\widehat{i} + \sigma_2(x,y)\widehat{j}$ respectively. Under these assumptions the governing equations for the MHD flow of micropolar fluid in the absence of both body force and body couple are

$$-\frac{\partial p}{\partial z} + \kappa\left(\frac{\partial \sigma_2}{\partial x} - \frac{\partial \sigma_1}{\partial y}\right) + (\mu+\kappa)\left(\frac{\partial^2 w}{\partial x^2} + \frac{\partial^2 w}{\partial y^2}\right) - \sigma B_0^2 w = 0 \tag{4.1}$$

$$-2\kappa\sigma_1 + \kappa\frac{\partial w}{\partial y} - \gamma\frac{\partial}{\partial y}\left[\frac{\partial \sigma_2}{\partial x} - \frac{\partial \sigma_1}{\partial y}\right] + (\alpha+\beta+\gamma)\frac{\partial}{\partial x}\left[\frac{\partial \sigma_1}{\partial x} + \frac{\partial \sigma_2}{\partial y}\right] = 0 \tag{4.2}$$

$$-2\kappa\sigma_2 - \kappa\frac{\partial w}{\partial x} + \gamma\frac{\partial}{\partial x}\left[\frac{\partial \sigma_2}{\partial x} - \frac{\partial \sigma_1}{\partial y}\right] + (\alpha+\beta+\gamma)\frac{\partial}{\partial y}\left[\frac{\partial \sigma_1}{\partial x} + \frac{\partial \sigma_2}{\partial y}\right] = 0 \tag{4.3}$$

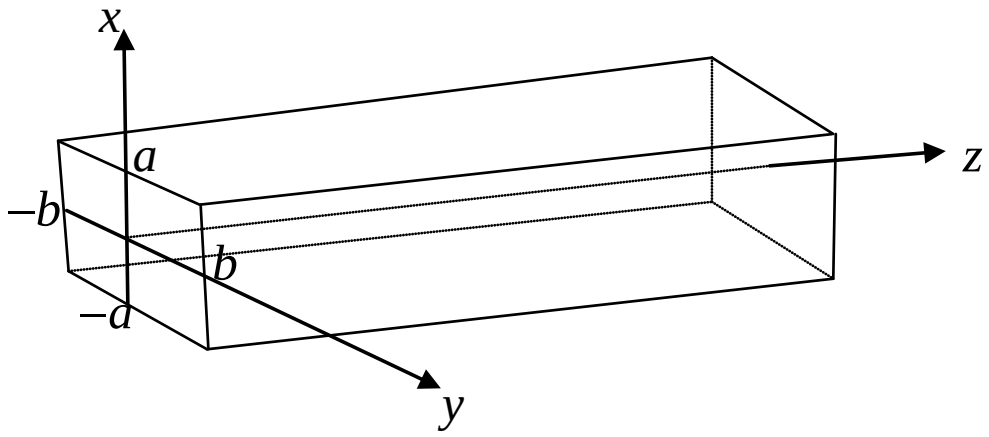

Figure 4.1: Schematic diagram of the problem

$$K_f\left[\frac{\partial^2 T}{\partial x^2}+\frac{\partial^2 T}{\partial y^2}\right]+(2\mu+\kappa)\left[\left(\frac{\partial w}{\partial x}\right)^2+\left(\frac{\partial w}{\partial y}\right)^2\right]+2\kappa\left[\sigma_1^2+\sigma_2^2-\sigma_1\frac{\partial w}{\partial y}+\sigma_2\frac{\partial w}{\partial x}\right]$$
$$+\alpha\left(\frac{\partial \sigma_1}{\partial x}+\frac{\partial \sigma_2}{\partial y}\right)^2+\gamma\left[\left(\frac{\partial \sigma_1}{\partial x}\right)^2+\left(\frac{\partial \sigma_2}{\partial x}\right)^2+\left(\frac{\partial \sigma_1}{\partial y}\right)^2+\left(\frac{\partial \sigma_2}{\partial y}\right)^2\right] \tag{4.4}$$
$$+\beta\left[\left(\frac{\partial \sigma_1}{\partial x}\right)^2+2\frac{\partial \sigma_1}{\partial y}\frac{\partial \sigma_2}{\partial x}+\left(\frac{\partial \sigma_2}{\partial y}\right)^2\right]=0$$

Introducing the following non-dimensional variables

$$x=a\widetilde{x},\quad y=a\widetilde{y},\quad w=U_0\widetilde{w},\quad \sigma_1=\frac{U_0}{a}\widetilde{\sigma_1},\quad \sigma_2=\frac{U_0}{a}\widetilde{\sigma_2},\quad \frac{T-T_1}{T_2-T_1}=\theta,\quad \frac{\partial p}{\partial z}=\frac{\rho U_0^2}{a}p_0 \tag{4.5}$$

Substituting (4.5) into the Eqs. (4.1) to (4.4) and dropping tildes, to obtain

$$-Re\ p_0+\frac{N}{1-N}\left(\frac{\partial \sigma_2}{\partial x}-\frac{\partial \sigma_1}{\partial y}\right)+\frac{1}{1-N}\left(\frac{\partial^2 w}{\partial x^2}+\frac{\partial^2 w}{\partial y^2}\right)-Ha^2 w=0 \tag{4.6}$$

$$-\sigma_1+\frac{1}{2}\frac{\partial w}{\partial y}-\frac{1}{2}\frac{2-N}{m^2}\frac{\partial}{\partial y}\left[\frac{\partial \sigma_2}{\partial x}-\frac{\partial \sigma_1}{\partial y}\right]+\frac{1}{l^2}\frac{\partial}{\partial x}\left[\frac{\partial \sigma_1}{\partial x}+\frac{\partial \sigma_2}{\partial y}\right]=0 \tag{4.7}$$

$$-\sigma_2-\frac{1}{2}\frac{\partial w}{\partial x}+\frac{1}{2}\frac{2-N}{m^2}\frac{\partial}{\partial x}\left[\frac{\partial \sigma_2}{\partial x}-\frac{\partial \sigma_1}{\partial y}\right]+\frac{1}{l^2}\frac{\partial}{\partial y}\left[\frac{\partial \sigma_1}{\partial x}+\frac{\partial \sigma_2}{\partial y}\right]=0 \tag{4.8}$$

$$\frac{\partial^2\theta}{\partial x^2}+\frac{\partial^2\theta}{\partial y^2}+Br\left\{\left(\frac{1}{1-N}\right)\left(\left(\frac{\partial w}{\partial x}\right)^2+\left(\frac{\partial w}{\partial y}\right)^2\right)+\frac{2N}{1-N}\left[\sigma_1^2+\sigma_2^2-\sigma_1\frac{\partial w}{\partial y}+\sigma_2\frac{\partial w}{\partial x}\right]\right.$$
$$+A\left[\frac{\partial\sigma_1}{\partial x}+\frac{\partial\sigma_2}{\partial y}\right]^2+\frac{N(2-N)}{m^2(1-N)}\left[\left(\frac{\partial\sigma_1}{\partial x}\right)^2+\left(\frac{\partial\sigma_2}{\partial x}\right)^2+\left(\frac{\partial\sigma_1}{\partial y}\right)^2+\left(\frac{\partial\sigma_2}{\partial y}\right)^2\right]$$
$$\left.B\left[\left(\frac{\partial\sigma_1}{\partial x}\right)^2+2\frac{\partial\sigma_1}{\partial y}\frac{\partial\sigma_2}{\partial x}+\left(\frac{\partial\sigma_2}{\partial y}\right)^2\right]\right\}=0 \tag{4.9}$$

where $l^2=\dfrac{2a^2\kappa}{\alpha+\beta+\gamma}$ is non-dimensional parameter, $Ha=B_0a\sqrt{\dfrac{\sigma}{\mu}}$ is Hartman number, $Br=\dfrac{\mu U_0^2}{K_f(T_2-T_1)}$ is the Brinkman number, and $A=\dfrac{\alpha}{\mu a^2}$, $B=\dfrac{\beta}{\mu a^2}$ are micropolar parameters. Here in this chapter also, two types (cases) of boundary conditions are considered for the velocity and temperature on the walls of the rectangular duct.

4.2.1 Case(a): No-slip and Isothermal Boundary Conditions

Assume that the fluid particles closest to the rectangular duct stick to it, neither rotating nor translating. Moreover, the duct is maintained at a uniform temperature. Hence, the boundary conditions are

$$\begin{aligned} w=0 \quad \text{at} \quad x=\pm1 \quad \text{and} \quad y=\pm y_0 \quad \text{where} \quad y_0=\frac{b}{a} \\ \sigma_1=\sigma_2=0 \quad \text{at} \quad x=\pm1 \quad \text{and} \quad y=\pm y_0 \\ \theta=0 \quad \text{at} \quad x=\pm1 \quad \text{and} \quad y=\pm y_0 \end{aligned} \tag{4.10}$$

Method of Solution

The governing equations given by Eqs. (4.6) - (4.9) along with the boundary conditions Eq. (4.10) are solved numerically using finite difference method. The derivatives are replaced by the central difference approximations to get the algebraic system of equations and these equations are solved using Gauss-Seidel iteration method. A numerical experiment was conducted with various meshes in the rectangular region and axial step lengths in x and y-directions to check the independence of the mesh resolution of the numerical results. There are three mesh distributions tested in the

analysis. They are 21×21, 41×41 and 81×81 respectively. It is found that the deviations in the velocity, microrotation and temperature components calculated with 41×41 and 81×81 are always less than 10^{-3}. Therefore the computations with mesh distribution of 41×41 are considered to be sufficiently accurate to describe the flow in this study. The obtained velocity, microrotation and temperature distributions are then used to evaluate the entropy generation and Bejan number.

Entropy Generation

Non-equilibrium conditions arise due to the exchange of energy and momentum within the fluid and at the walls of the duct. This causes a continuous entropy generation. The mechanisms of entropy generation are heat transfer, fluid friction and magnetic effect. The volumetric rate of entropy generation for incompressible micropolar fluid is given as

$$S_G = \frac{K_f}{T_1^2}[\nabla T]^2 + \frac{1}{T_1}\Phi + \frac{1}{T_1}\left[(J - Q\overline{q}).(E + \overline{q} \times \overline{B})\right] \tag{4.11}$$

For the present study, the dimensionless entropy generation number is given by

$$\begin{aligned} N_s = {} & \left(\frac{\partial\theta}{\partial x}\right)^2 + \left(\frac{\partial\theta}{\partial y}\right)^2 + \frac{Br}{T_p}\left\{\frac{1}{1-N}\left(\left(\frac{\partial w}{\partial x}\right)^2 + \left(\frac{\partial w}{\partial y}\right)^2\right)\right. \\ & + \frac{2N}{1-N}\left[\sigma_1^2 + \sigma_2^2 - \sigma_1\frac{\partial w}{\partial y} + \sigma_2\frac{\partial w}{\partial x}\right] + A\left[\frac{\partial\sigma_1}{\partial x} + \frac{\partial\sigma_2}{\partial y}\right]^2 \\ & \left. + \frac{N(2-N)}{m^2(1-N)}\left[\left(\frac{\partial\sigma_1}{\partial x}\right)^2 + \left(\frac{\partial\sigma_2}{\partial x}\right)^2 + \left(\frac{\partial\sigma_1}{\partial y}\right)^2 + \left(\frac{\partial\sigma_2}{\partial y}\right)^2\right] + B\left[\left(\frac{\partial\sigma_1}{\partial x}\right)^2 + 2\frac{\partial\sigma_1}{\partial y}\frac{\partial\sigma_2}{\partial x} + \left(\frac{\partial\sigma_2}{\partial y}\right)^2\right]\right\} \\ & + \frac{BrHa^2}{T_p}w^2 \end{aligned} \tag{4.12}$$

The Eq. (4.12) can be expressed alternatively as follows

$$N_s = N_h + N_v + N_m \tag{4.13}$$

Alternatively, the dominant effect of either heat transfer irreversibility or fluid friction irreversibility can be investigated using the Bejan number (Be) defined mathematically as follows

$$Be = \frac{N_h}{N_s} \tag{4.14}$$

Results and Discussion

The magnetohydrodynamic flow and heat transfer in a micropolar fluid flow through a rectangular duct has been solved numerically using finite difference method. Numerical expressions of velocity, microrotation and temperature have been used to compute entropy generation and Bejan number. These quantities are evaluated numerically by dividing the rectangular region into a grid of mesh points (x_i, y_j). The effects of various parameters like coupling number(N), magnetic parameter (Ha) and Brinkman number (Br) on entropy generation and Bejan number are described graphically for $y_0 = 1, Ha = 2, m = 1, l = 0.5, N = 0.25, Re = 1, p_0 = 1, T_p = 1, Br = 1, A = 1$ and $B = 0.1$.

In order to validate the accuracy of the method, the results of velocity have been compared with the analytical solution of [29] for Newtonian fluids in the absence of N and Ha as a special case by taking $Re = 1$ and $p_0 = 1$. The comparison in this case is found to be in good agreement, as shown in Table. 4.1.

Table 4.1: Comparison analysis for the velocity calculated by the present method and that of analytical solution [29] of Newtonian fluids for $N = 0$, $Ha = 0$, $Re = 1$ and $p_0 = 1$.

x	y	Analytical solution	Present solution
-1	-1	0	0
-0.75	-0.75	0.07292	0.07274
-0.5	-0.5	0.18141	0.18104
-0.25	-0.25	0.26454	0.26401
0	0	0.29512	0.29454
0.25	0.25	0.26454	0.26401
0.5	0.5	0.18141	0.18104
0.75	0.75	0.07292	0.07274
1	1	0	0

Fig. 4.2 shows the 3 - dimensional profiles of entropy generation and Bejan number. It is

clear from Fig. 4.2(a) that the maximum magnitude of the entropy generation is observed at the boundaries of the rectangular duct and minimum at the center of the duct due to their suppressing effect on the flow and thermal fields. Furthermore, a similar phenomenon also occurs in $2-D$ figures. Fig. 4.2(b) shows the Bejan number profile in the rectangular duct. Contribution of either thermal or viscous irreversibility on entropy generation is characterized by the dimensionless number called Bejan number (Be). The Bejan number at the boundary of the duct is higher than than the center region of the duct. It is observed that the fluid friction irreversibility dominates at the center of the duct than the periphery of the duct.

The effect of coupling number on entropy generation is shown in Figs. 4.3(a) and 4.3(b) in x and y-directions. It is observed that the entropy generation decreases with an increase in the value of N in x and y-directions.The peak value of entropy generation is noticed at the boundaries of the rectangular duct. It is seen from Figs. 4.3(c) and 4.3(d) that the Bejan number initially increases and then decreases with an increase in the value of N in both x and y-directions. It is noticed that the fluid friction irreversibility dominates around the center of the duct.

Fig. 4.4 presents the effect of Hartman number on entropy generation and Bejan number in x and y-directions. It is observed from Figs. 4.4(a) and 4.4(b) that the entropy generation near the boundaries of the duct is higher than the center of the duct, due to high temperature and velocity gradients. With the increase in Hartman number the entropy generation rises at the center of the duct, as in this region the velocities are maximum and hence the contribution of MHD flow is maximized on the entropy generation. Likewise near the boundaries of the duct the entropy generation is less when Ha is more, because increasing the magnetic field results in a decrease in the irreversibility caused by fluid friction. Figs. 4.4(c) and 4.4(d) show that the decrease in Bejan number with increase in Hartman number.

Fig. 4.5, analyses the effect of Brinkman number on entropy generation and Bejan number in x and y-directions. Figs. 4.5(a) and 4.5(b) show that the entropy generation increases with an increase in the value of Br in the entire rectangular duct. The entropy generation number is high in magnitude at the boundaries of the duct due to the presence of high temperature and velocity gradients. Ns profiles are similar in shape and almost parallel to one another for any parameter, but they do vary in magnitude. The Bejan number indicates whether the entropy generation is dominated by the heat transfer or fluid friction. It is observed from Figs. 4.5(c) and 4.5(d) that the Bejan number increases with increase in Brinkman number due to decrease in viscous dissipation

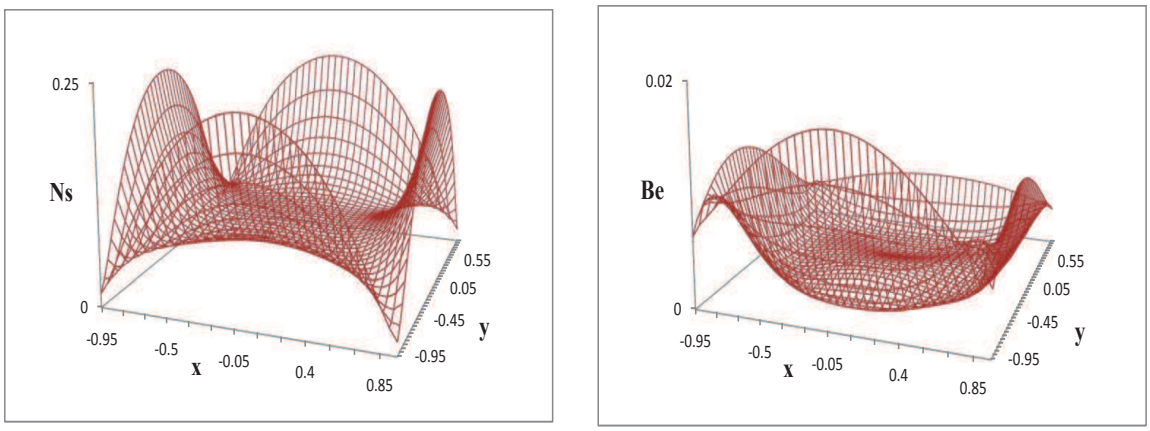

(a) (b)

Figure 4.2: 3-Dimensional profiles of entropy generation and Bejan nuber.

irreversibility.

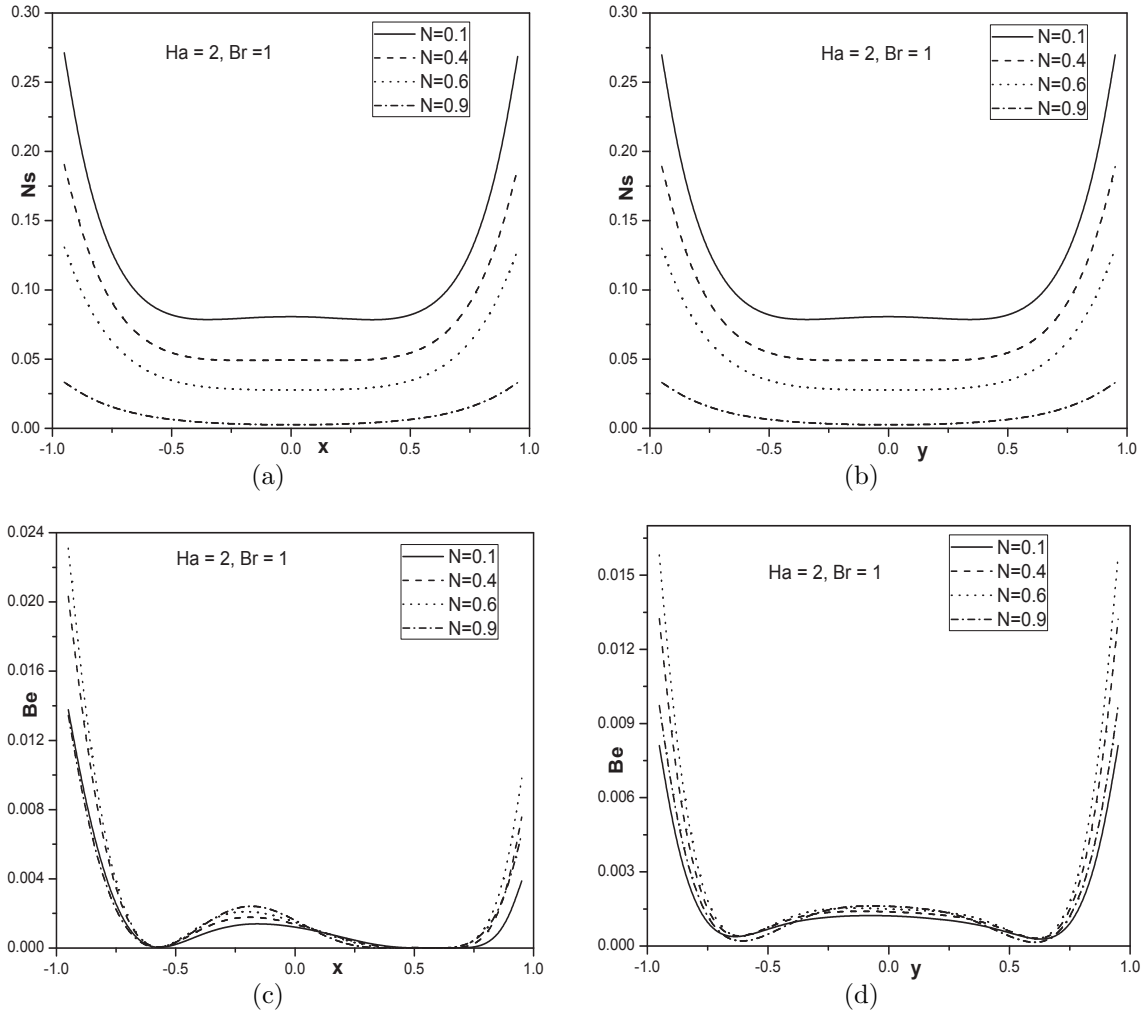

Figure 4.3: Effect of coupling number on entropy generation and Bejan number.

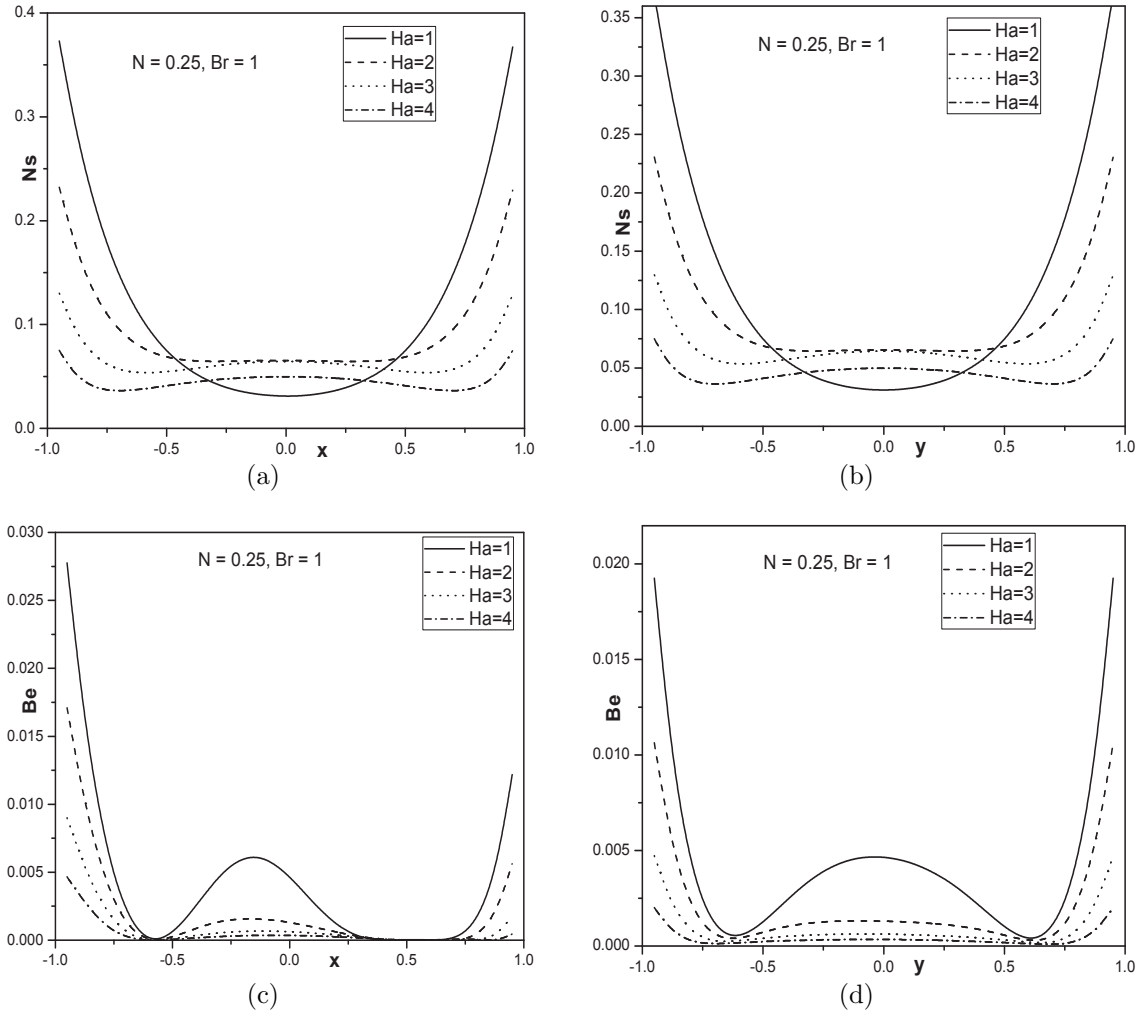

Figure 4.4: Effect of Hartman number on entropy generation and Bejan number.

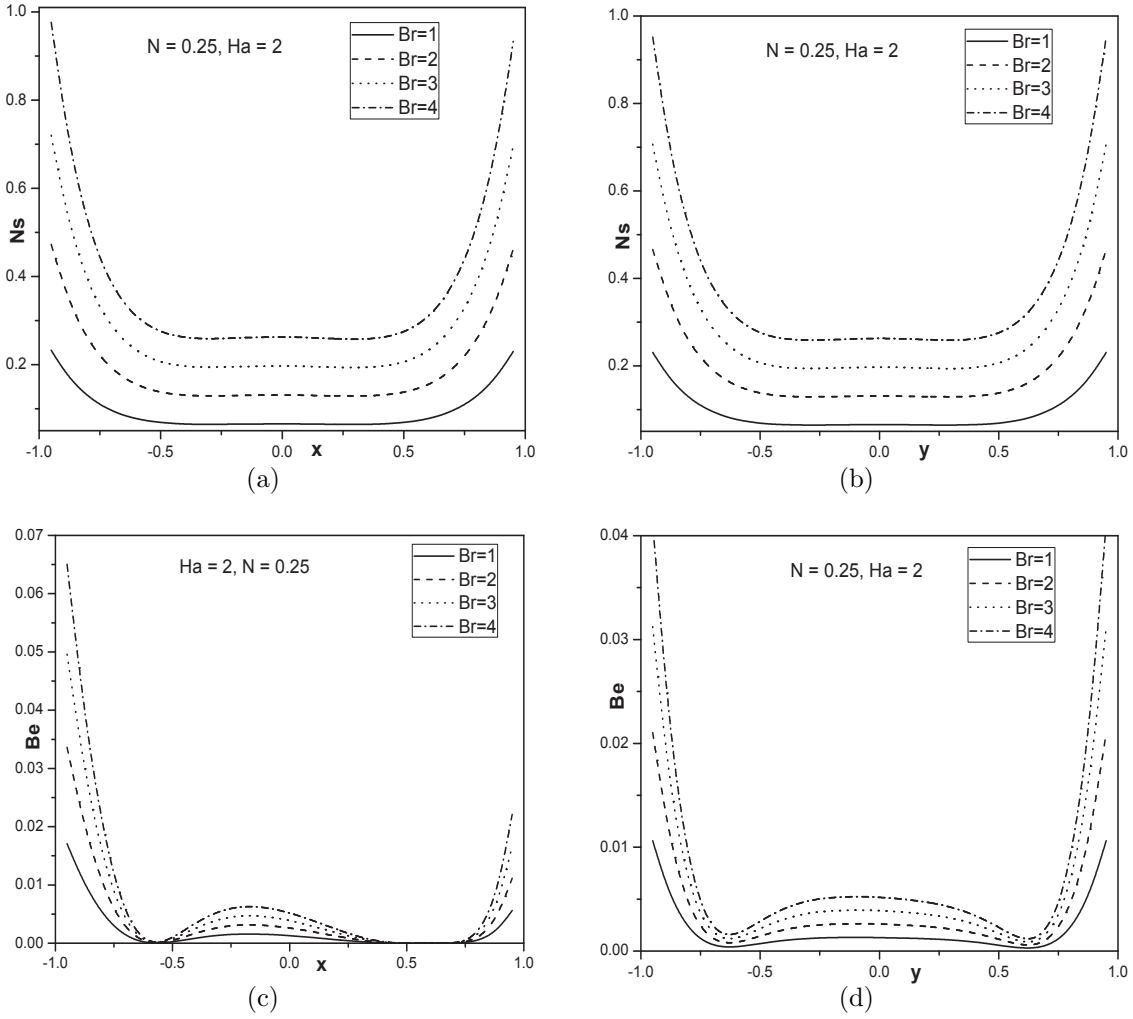

Figure 4.5: Effect of Brinkman number on entropy generation and Bejan number.

4.2.2 Case(b): Slip and Convective Boundary Conditions

Assume that the no-slip boundary condition is considered at the top and bottom walls of the duct while the slip condition is taken at the side walls of the duct. Let the bottom wall of the duct is convectively heated, whereas the convective heat loss can take place at the top wall and the side walls of the duct are maintained at uniform temperature T_1. Further, it is assumed that the microrotation is zero at all sides of the duct.

$$\begin{gathered} w=0, \quad \sigma_1=0, \quad \sigma_2=0, \quad \text{at} \quad x=\pm a \\ K_f\frac{dT}{dx}-h(T-T_2)=0, \ \text{at} \ x=-a, \quad K_f\frac{dT}{dx}+h(T-T_1)=0, \ \text{at} \ x=a, \\ w=\zeta_1'\frac{dw}{dy}, \quad \text{at} \quad y=-b, \quad w=-\zeta_1'\frac{dw}{dy}, \quad \text{at} \quad y=b, \\ \sigma_1=0, \quad \sigma_2=0, \quad T=T_1 \quad \text{at} \quad y=\pm b \end{gathered} \tag{4.15}$$

The non-dimensional boundary conditions are

$$\begin{gathered} w=0, \quad \sigma_1=0, \quad \sigma_2=0 \quad \text{at} \quad x=\pm 1 \\ \frac{d\theta}{dx}-Bi(\theta-1)=0 \ \text{at} \quad x=-1, \quad \frac{d\theta}{dx}+Bi\,\theta=0 \ \text{at} \ x=1 \\ w=\zeta\frac{dw}{dy} \quad \text{at} \quad y=-y_0, \quad w=-\zeta\frac{dw}{dy} \quad \text{at} \quad y=y_0 \\ \sigma_1=0, \quad \sigma_2=0, \quad \theta=0 \quad \text{at} \quad y=\pm y_0 \end{gathered} \tag{4.16}$$

where $\zeta=\frac{\zeta'}{a}$ and $y_0=\frac{b}{a}$.

The entropy generation and Bejan number have been calculated for the slip and convective boundary conditions (4.16) from Eqs. (4.12) and (4.14).

Results and Discussion

The problem of magnetohydrodynamic flow and heat transfer in a micropolar fluid flow through a rectangular duct subject to slip and convective boundary conditions has been solved numerically using finite difference method by taking the values of the parameters $y_0=1, Ha=2, m=1, l=0.5, N=0.25, Re=1, p_0=1, T_p=1, Br=1, A=1, B=0.1, \zeta=0.1$ and $Bi=1$ are constant as mentioned in case(a).

Fig. 4.6, shows the 3-Dimensional profiles of entropy generation and Bejan number. Fig. 4.6(a) shows that the maximum value of the entropy generation is at the wall of the rectangular duct where the convective boundary condition is applied. Moreover, the entropy generation rate decreases in both the directions due to the suppressing effect on the flow and thermal fields. Fig. 4.6(b) shows the profile of Bejan number in the rectangular duct. It is observed that the heat transfer irreversibility dominates at the bottom wall of the duct and fluid friction irreversibility dominates at the top wall of the duct.

The effect of coupling number on entropy generation is shown in Fig. 4.7 in x and y-directions. It is observed from Fig. 4.7(a) that there is no significant effect of coupling number on entropy generation in the x-direction. Fig. 4.7(b) states that the entropy generation decreases with an increase in the value of coupling number in y-direction. The Bejan number increases with increase of N along x-direction as shown in Fig. 4.7(c). It is noticed that the heat transfer irreversibility dominates near lower plate and fluid friction irreversibility dominates near the upper plate. It is seen from Fig. 4.7(d) that the Bejan number increases with an increase in the value of N in y-direction.

Fig. 4.8, presents the effect of magnetic parameter on entropy generation and Bejan number in x and y-directions. It is observed from Figs. 4.8(a) and 4.8(b) that the entropy generation decreases with an increase in the value of Hartman number, which indicates that the presence of magnetic field reduces the entropy generation. Figs. 4.8(c) and 4.8(d), show that the Bejan number increases with an increase in the value of Hartman number in both the directions.

Fig. 4.9, shows the effect of Reynolds number Re on entropy generation and Bejan number in x and y-directions. From Figs. 4.9(a) and 4.9(b) it is observed that the entropy generation increases more rapidly in y-direction than in x-direction. This is due to the fact that the fluid is more viscous in y-direction. From Figs. 4.9(c) and 4.9(d), it is clear that as the Reynolds number increases, Bejan number decreases.

The effect of slip parameter ζ on entropy generation and Bejan number is shown in Fig. 4.10 along x and y-directions. It is observed from Fig. 4.10(a) that the slip parameter does not show a significant effect on entropy generation. Fig. 4.10(b) shows that the entropy generation decreases near the side walls of the duct with increase in ζ. From Fig. 4.10(c) it is seen that the Bejan number is high at the lower plate due to domination of heat transfer irreversibility on entropy generation.

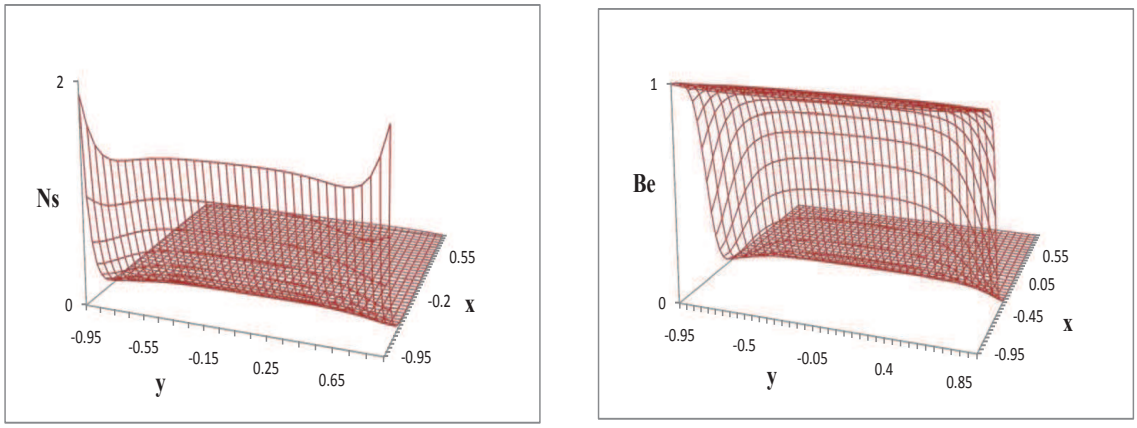

(a) (b)

Figure 4.6: 3-Dimensional profiles of entropy generation and Bejan number.

Fig. 4.10(d) illustrates that the Bejan number slightly increases near the side walls of the duct in y-direction with an increase in the value of ζ.

Figs. 4.11(a) and 4.11(b) illustrate that increase in the entropy generation rate with an increase in the value of Bi in x and y-directions due to convection on lower and upper plates. It is noticed from Figs. 4.11(c) and 4.11(d) that the Bejan number increases with increasing values of Bi due to the dominant effect of heat transfer irreversibility. Hence the convective thermal boundary conditions enhance the dominant effects of heat transfer irreversibility on the flow system.

The effect of Brinkman number on the entropy generation and Bejan number in x and y-directions are shown in Fig. 4.12. The Brinkman number Br is indicative of the rate at which energy is dissipated by the viscous forces within the fluid. Due to the effect of these viscous and magnetic forces, the entropy generation becomes significant in the rectangular duct. Ns profiles remain similar but they vary in magnitude for variation of all parameters. With the increase in the value of Br, the entropy generation increases, but the Bejan number decreases as shown in Fig. 4.12.

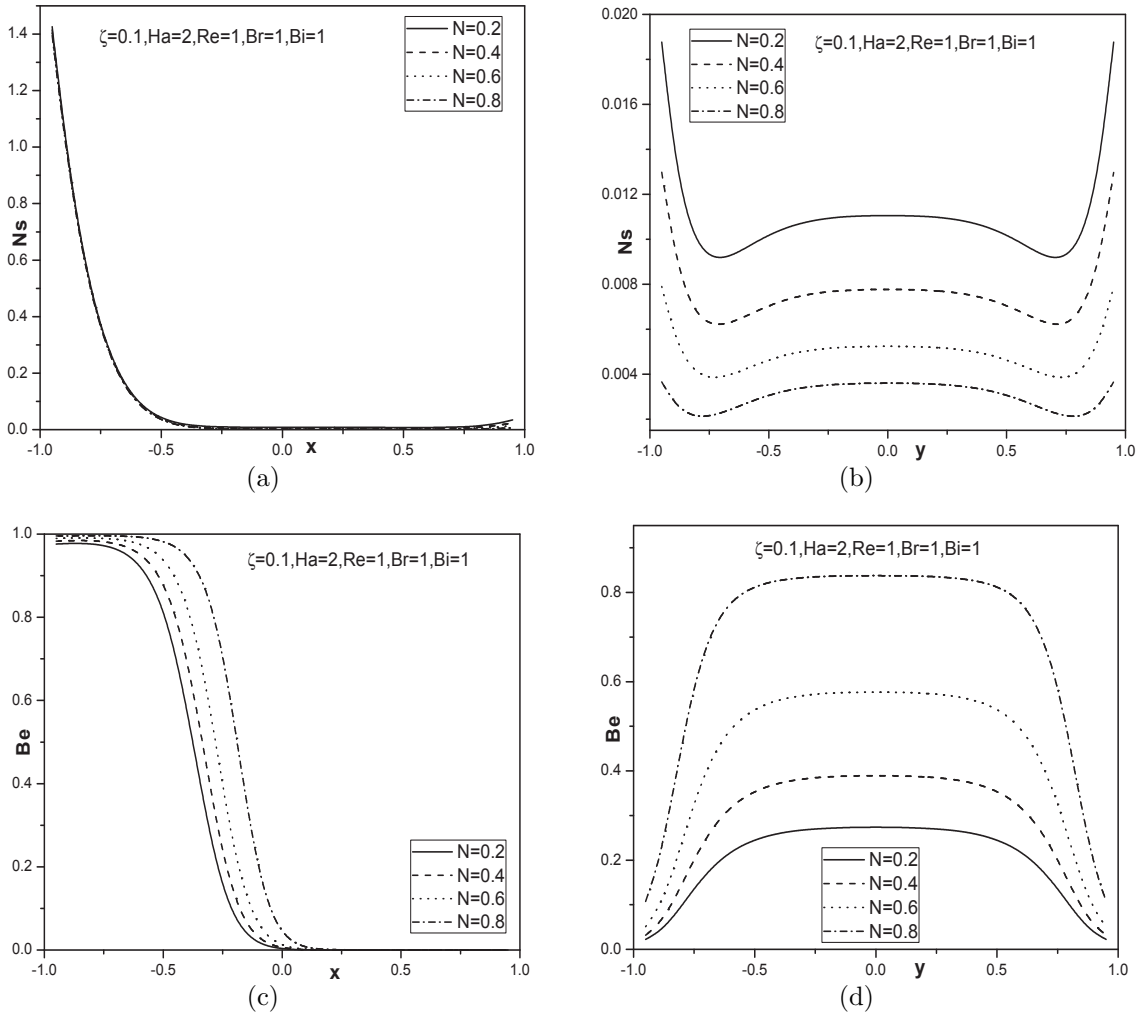

Figure 4.7: Effect of coupling number on entropy generation and Bejan number.

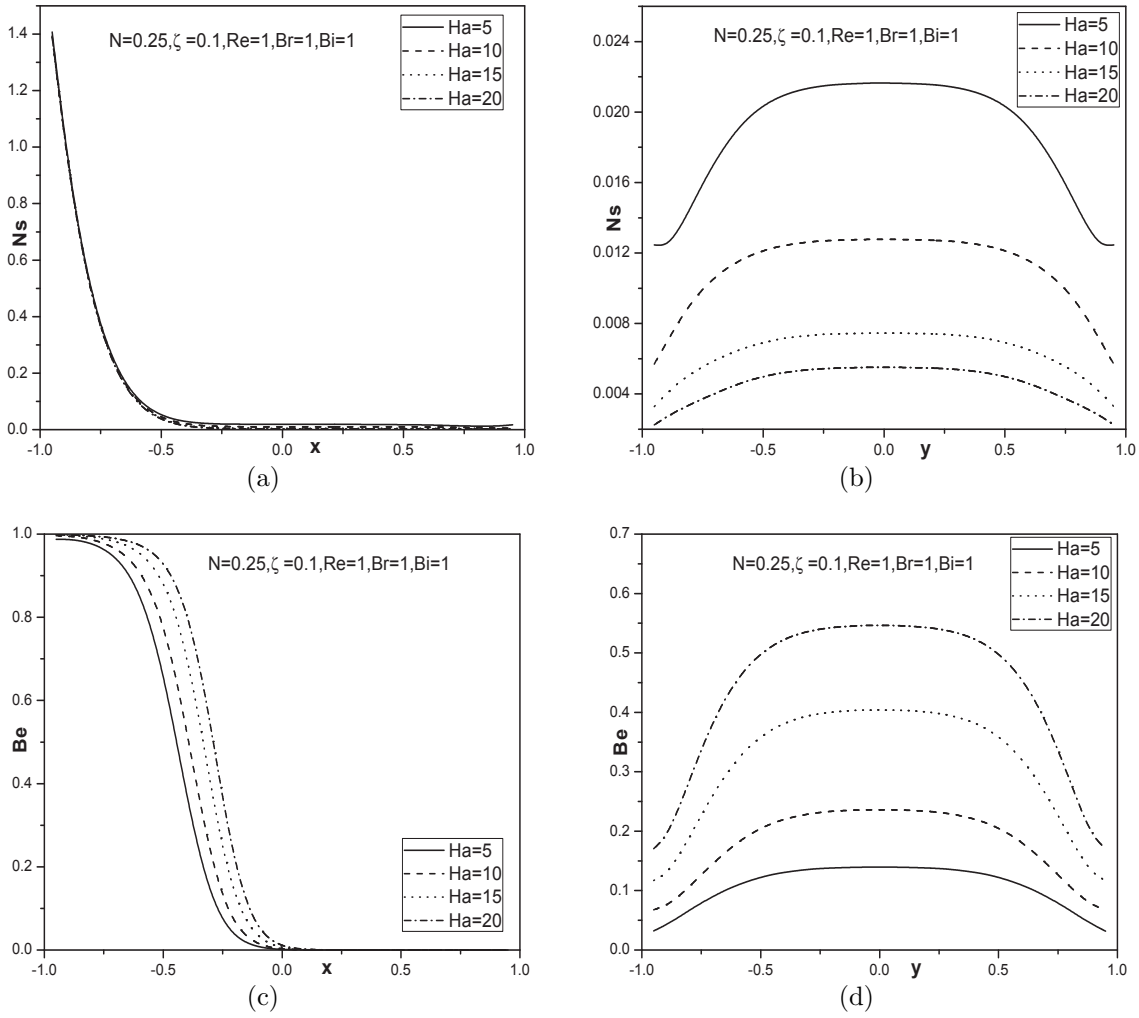

Figure 4.8: Effect of Hartman number on entropy generation and Bejan number.

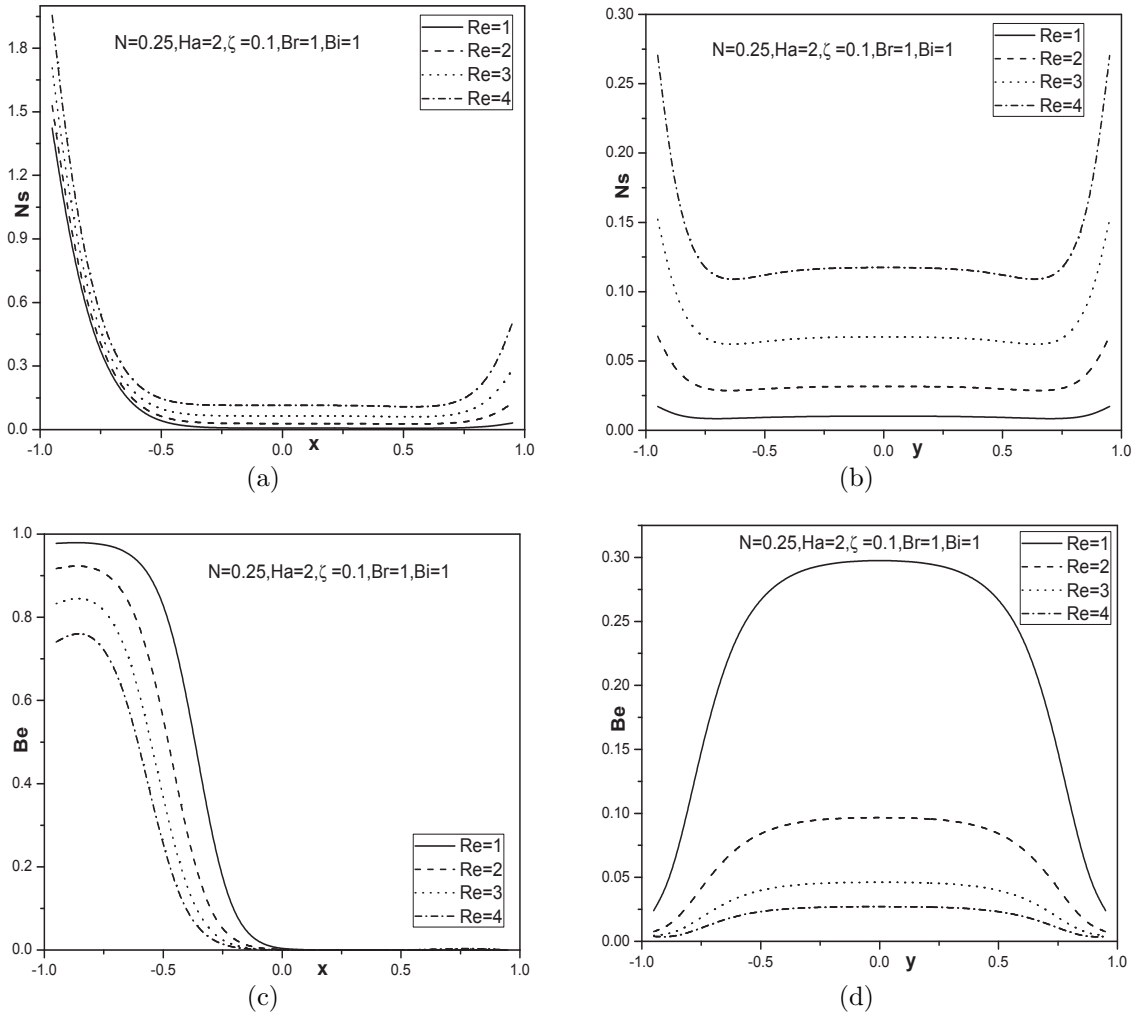

Figure 4.9: Effect of Reynolds number on entropy generation and Bejan number.

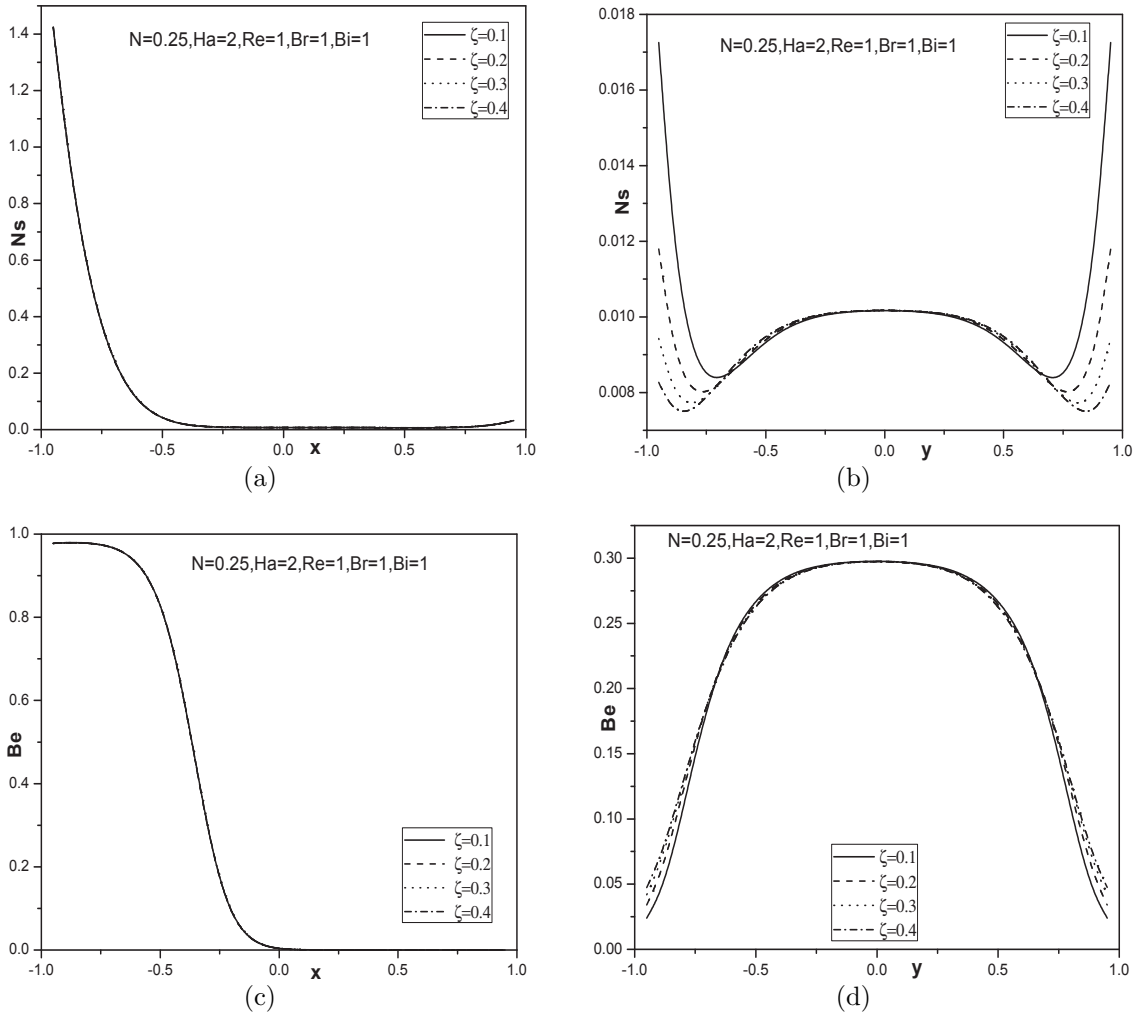

Figure 4.10: Effect of slip parameter on entropy generation and Bejan number.

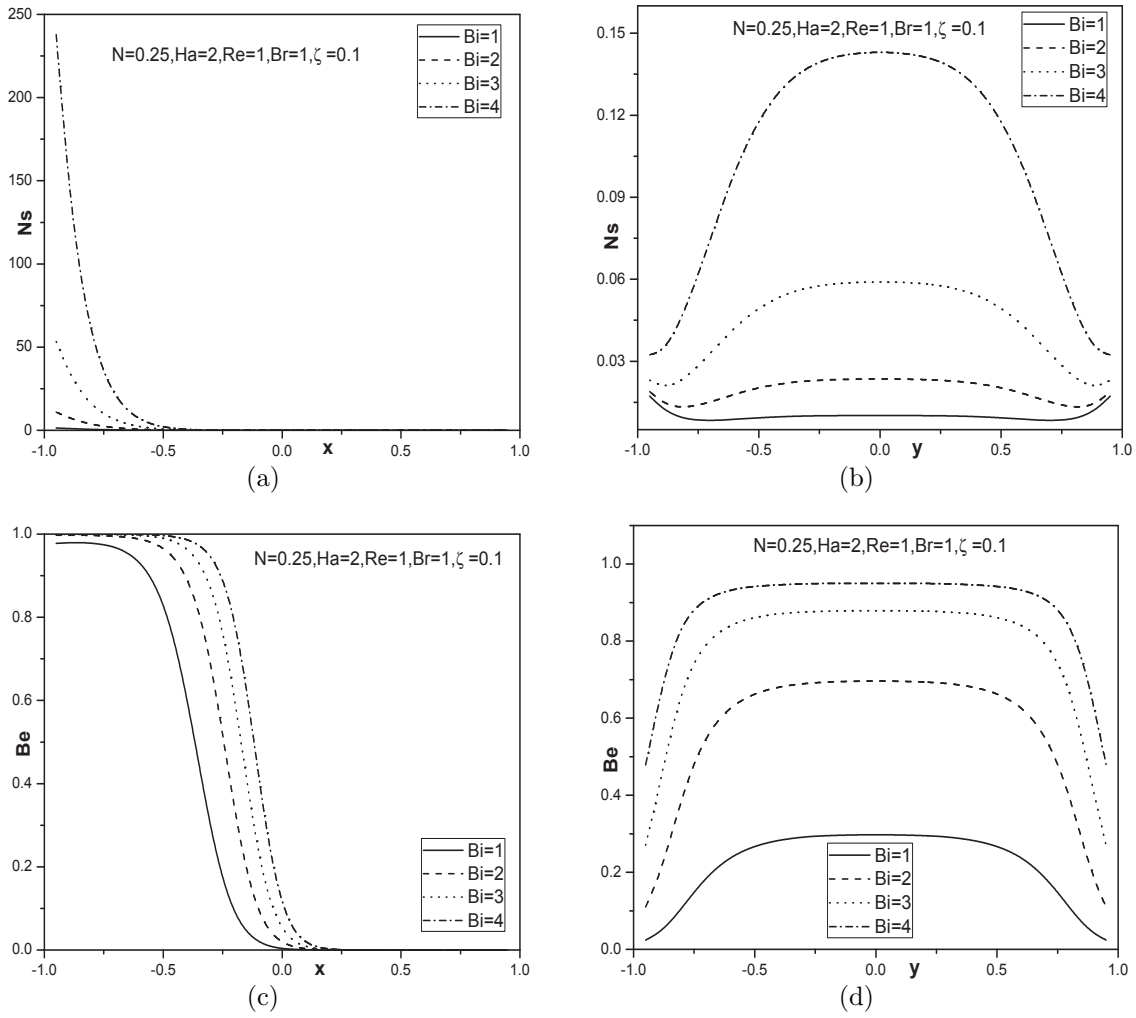

Figure 4.11: Effect of Biot number on entropy generation and Bejan number.

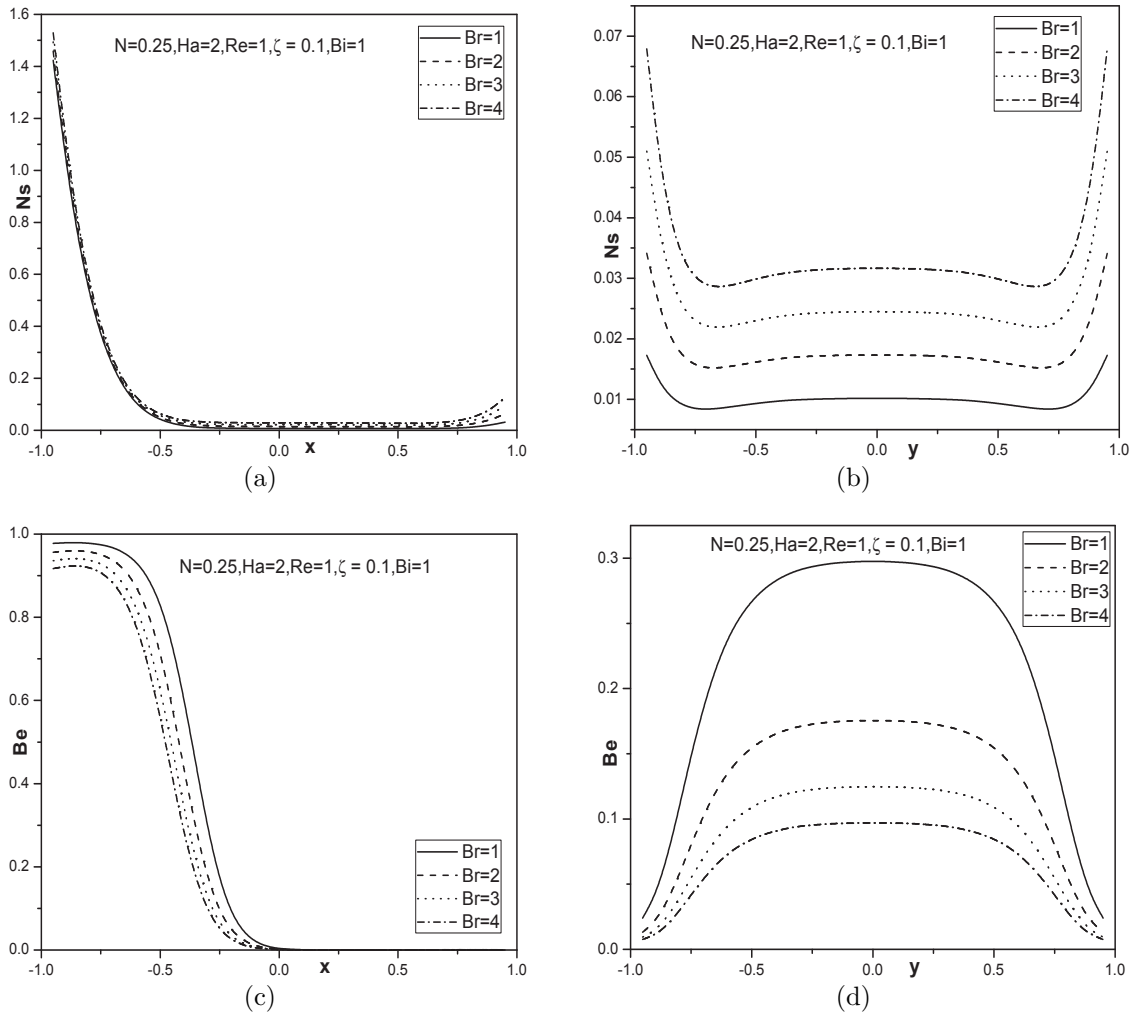

Figure 4.12: Effect of Brinkman number on entropy generation and Bejan number.

4.3 Conclusions

In this chapter, the problem of entropy generation due to steady, laminar, incompressible, micropolar fluid flow through a rectangular duct with magnetic field effect is investigated. This problem is solved for two types of boundary conditions. Case (a)No-slip and isothermal boundary conditions and Case (b)Slip and convective boundary conditions. From the analysis, the following are the observations in both the cases (a) and (b).

It is observed that the entropy generation number of viscous fluid is more than the corresponding values in micropolar fluid case. This may be due to the fact that in viscous fluids, microrotations are absent and hence available energy is not being used. As micropolarity increases, entropy generation decreases and Bejan number increases. Thus, these fluids can be used as good lubricants. In Case (a) it is noticed that with increase in Hartman number the entropy generation rises at the center of the duct, as in this region the velocities are maximum and hence the contribution of MHD flow is maximized on the entropy generation. In Case (b) Hartman number has no influence on entropy generation. As Brinkman number increases, entropy generation increases in both the cases. The domination of heat transfer irreversibility on entropy generation is observed at the center of the rectangular duct from the Bejan number profiles in y-direction in Case (b).

Chapter 5

Analysis of Entropy Generation in a Micropolar Fluid Flow Through an Inclined Porous Circular Pipe [1]

5.1 Introduction

The cornerstone in the field of heat transfer and thermal design is the second law of thermodynamics and its design is related to the concept of entropy generation minimization. Entropy generation destroys the available energy of a system and as a result imposes considerable extra costs to any thermal system. In order to improve the efficiency in all types of thermal systems, it is important to minimize the entropy generation and thus optimizing the energy resources. The concept of entropy generation minimization is developed by Bejan [13, 14, 15] which is based on the second law of thermodynamics.

The flow through pipes or ducts is commonly used in heating and cooling applications and fluid distribution networks. In fluid flow systems, thermodynamic irreversibility can be quantified through entropy analysis. In order to preserve the quality of energy in a fluid flow process or at least to reduce the entropy generation, it is important to study the distribution of the entropy

[1] Case(a): Accepted in "**Advances and Applications in fluid Mechanics**", Case(b) Accepted in "**Sadhana**"

generation within the fluid volume. Al-Zaharnah [3] investigated the entropy generation in the pipe flow by considering different pipe wall temperatures. Mansour and Sahin [17] studied the entropy generation in a circular pipe as a two-dimensional flow with uniform wall heat flux boundary condition and observed that the viscosity variation with temperature is important for determining the entropy generation especially when highly viscous fluids are used as working fluids.

The objective of the present chapter is to investigate the entropy generation rate of micropolar fluid flow in an inclined porous circular pipe. Two types (cases) of boundary conditions are considered for the velocity and temperature as in earlier chapters.

5.2 Mathematical Formulation

Consider a steady, axisymmetric, fully developed, laminar, incompressible, micropolar fluid flow through an inclined porous circular pipe is driven by a constant pressure gradient(see Fig. 5.1). Choose the cylindrical polar coordinate system (r, φ, z) with z - axis is in the direction of fluid flow. As the flow is fully developed and the pipe is of infinite length, the flow depends only on r. Let w, v, u be the velocity components. We apply uniform suction or injection with velocity w_o on the wall $r = a$ of the pipe., Here $w_0 < 0$ is the velocity of the suction and $w_0 > 0$ is the velocity of the injection. The motion being rotationally symmetric, suction or injection to be uniform, and assuming that the pipe is long enough, all the physical quantities will be independent of φ and z, and v will be zero. The corresponding equation of continuity is $\frac{\partial}{\partial r}(rw) = 0$, which on integration gives $w = w_0$ a constant. The equations that govern the fluid flow in the absence of both body force (force per unit volume) and body couple (moment per unit volume) are:

$$\frac{\partial}{\partial r}(rw) = 0 \tag{5.1}$$

$$-\frac{\partial p}{\partial z} + \frac{\kappa}{r}\left[\sigma + r\frac{d\sigma}{dr}\right] + (\mu + \kappa)\left[\frac{d^2u}{dr^2} + \frac{1}{r}\frac{du}{dr}\right] + \rho g^* \beta (T - T_1)\sin\phi = \rho w \frac{du}{dr} \tag{5.2}$$

$$-2\kappa\sigma - \kappa\frac{du}{dr} + \gamma\left[\frac{d^2\sigma}{dr^2} + \frac{1}{r}\frac{d\sigma}{dr} - \frac{\sigma}{r^2}\right] = \rho j^* w \frac{d\sigma}{dr} \tag{5.3}$$

$$K_f\left[\frac{d^2T}{dr^2} + \frac{1}{r}\frac{dT}{dr}\right] + (\mu + \frac{\kappa}{2})\left(\frac{du}{dr}\right)^2 - 2\beta\frac{\sigma}{r}\frac{d\sigma}{dr} + \frac{\kappa}{2}\left[\frac{du}{dr} + 2\sigma\right]^2 + \gamma\left[\left(\frac{d\sigma}{dr}\right)^2 + \frac{\sigma^2}{r^2}\right] = \rho C_p w \frac{dT}{dr} \tag{5.4}$$

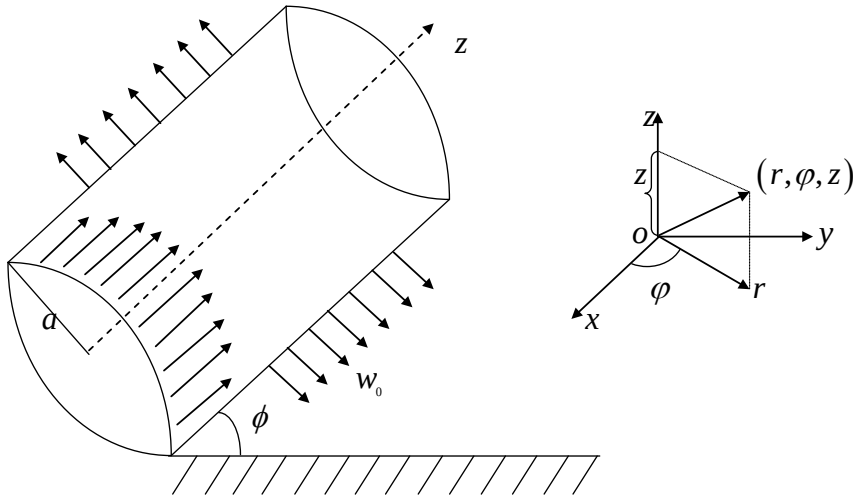

Figure 5.1: Physical model and coordinate system.

where $u(r)$ is the component of velocity in the flow direction, σ is the microrotation component, T is the temperature of the fluid and β is the coefficient of thermal expansion.

5.2.1 Case(a): No-slip and Isothermal Boundary Conditions

Assume that the fluid velocity on the pipe wall is same as the velocity of the pipe wall(no-slip velocity). The fluid particles are neither rotating nor translating at the pipe wall(hyper-stick) and the pipe is maintained at a uniform temperature (T_2). The mathematical expressions of these conditions are given by

$$\begin{aligned} \frac{du}{dr} = 0, \quad \sigma = 0, \quad \frac{dT}{dr} = 0, \quad \text{at} \quad r = 0 \\ u = 0, \quad \sigma = 0, \quad T = T_2, \quad \text{at} \quad r = a \end{aligned} \tag{5.5}$$

Introducing the following non-dimensional variables

$$r = a\eta, \quad u = u_0 f(\eta), \quad \sigma = \frac{u_0}{a} g(\eta), \quad \theta(\eta) = \frac{T - T_1}{T_2 - T_1} \tag{5.6}$$

in Eqs. (5.2) - (5.4), to get the following non-linear system of differential equations:

$$\frac{1}{1-N}\left(f'' + \frac{1}{\eta} f'\right) + \frac{N}{1-N}\left(g' + \frac{1}{\eta} g\right) + g_s \sin(\phi)\theta - A = R\, f' \tag{5.7}$$

$$\frac{N(2-N)}{m^2(1-N)}\left(g''+\frac{1}{\eta}g'-\frac{1}{\eta^2}g\right)-\frac{2N}{1-N}g-\frac{N}{1-N}f'=R\,a_j g' \tag{5.8}$$

$$\theta''+\frac{1}{\eta}\theta'+Br\left[\frac{2-N}{2(1-N)}f'^2+\frac{1}{2}\frac{N}{1-N}\left(f'+2g\right)^2-\frac{2B}{\eta}gg'+\frac{N(2-N)}{m^2(1-N)}\left(g'^2+\frac{1}{\eta^2}g^2\right)\right]=Pr\,R\theta' \tag{5.9}$$

where $R=\frac{\rho w_0 a}{\mu}$(suction Reynolds number), $A=\frac{a^2}{\mu u_0}\frac{\partial p}{\partial Z}$(constant pressure gradient) and $B=\frac{\beta}{\mu a^2}$(material constant).

The corresponding boundary conditions are:

$$\begin{aligned} f'(\eta)=0, \quad g(\eta)=0, \quad \theta'(\eta)=0, \quad \text{at} \quad \eta=0 \\ f(\eta)=0, \quad g(\eta)=0, \quad \theta(\eta)=1, \quad \text{at} \quad \eta=1 \end{aligned} \tag{5.10}$$

The Quasilinearization method is used to convert the non-linear boundary value problems (5.7) - (5.9) to a system of linear differential equations. The resultant equations are solved using the Chebyshev spectral collocation method, which is described in detail in chapter-2. The physical region $[0,1]$ is transformed into the region [-1, 1] using the mapping

$$\eta=\frac{\xi+1}{2} \qquad -1\le\xi\le 1 \tag{5.11}$$

Proceeding as in chapter-2 and incorporate the boundary conditions (5.10) in the matrix system $\mathbf{A}_r\mathbf{X}_{r+1}=\mathbf{B}_r$, the solution is obtained as

$$\mathbf{X}_{r+1}=\mathbf{A}_r^{-1}\mathbf{B}_r \tag{5.12}$$

Entropy Generation

In the fluid flow, irreversibility arises due to the heat transfer and the viscous effects of the fluid. The entropy generation rate can be expressed as the sum of contributions due to viscous effects and thermal effects, and thus it depends functionally on the local values of velocity and temperature in the domain of interest. For the present study, the volumetric rate of entropy generation reduces to

$$S_G=\frac{K_f}{T_1^2}\left(\frac{dT}{dr}\right)^2+\frac{\mu+\frac{\kappa}{2}}{T_1}\left(\frac{du}{dr}\right)^2+\frac{\kappa}{2T_1}\left[2\sigma+\frac{du}{dr}\right]^2-\frac{2\beta}{T_1}\frac{\sigma}{r}\frac{d\sigma}{dr}+\frac{\gamma}{T_1}\left[\left(\frac{d\sigma}{dr}\right)^2+\frac{\sigma^2}{r^2}\right]$$

The dimensionless entropy generation number is given by

$$N_s = \theta'^2 + \frac{Br}{T_p(1-N)}\left[\frac{2-N}{2}f'^2 + \frac{N}{2}(f'+2g)^2 - \frac{2B(1-N)}{\eta}gg' + \frac{N(2-N)}{m^2}\left(g'^2 + \frac{1}{\eta^2}g^2\right)\right] \tag{5.13}$$

The dimensionless entropy generation number gives a good idea about the rate of total entropy generation. However, it does not convey which of the two entropy generation mechanisms, namely, heat transfer and fluid friction, dominates. To resolve this, Paoletti *et al* [85], defined a dimensionless number, called Bejan number, defined as

$$Be = \frac{\text{Entropy generation due to heat transfer}}{\text{Total entropy generation}} \tag{5.14}$$

Results and Discussion

Figs. 5.2 - 5.5 show the variation of velocity, microrotation, temperature, entropy generation and Bejan number with η for different values of coupling number (N), angle of inclination (ϕ), suction Reynolds number (R) and Brinkman number (Br) for $m = 2$, $Pr = 1$, $a_j = 0.001$, $g_s = 0.5$ $A = -2$, $B = 0.1$ and $T_p = 1$.

In order to validate the accuracy of the present method, the results of velocity and microrotation are compared with the analytical solution given by Eringen [41] in the absence of g_s, R, ϕ as a special case by taking $N = 0.5$, $m = 2$ and $A = -2$. The comparison in this case is found to be in good agreement, as shown in Table. 5.1.

The effect of coupling number on velocity, microrotation, temperature, entropy generation and Bejan number of the micropolar fluid flow through an inclined porous pipe is plotted in Fig. 5.2. It is observed from Figs. 5.2(a) - 5.2(e) that the velocity, microrotation, temperature, entropy generation and Bejan number decrease with an increase in the value of N. As $N \to 0$ equations (5.7) and (5.8) reduce to the corresponding equation for viscous fluid. Hence, it is observed that the velocity of the micropolar fluid is less than the viscous fluid. Furthermore, for fixed N, the microrotation increases and then decreases as radial distance from the axis increases. Since, it is assumed that the microrotation is zero at the centre of the pipe and also at the wall of the pipe. This implies that the fluid particles cannot rotate near the boundary and also at the centre of the pipe. The microrotation field in this region is dominated by a small number of particles spins that

are generated by collisions with the boundary. The particles moves to the middle from the wall and also from the centre of the pipe to rotate and hence the microrotation becomes maximum.

The effect of angle of inclination (ϕ) of the circular pipe on the velocity, microrotation, temperature, entropy generation and Bejan number is shown in Fig. 5.3. Fig. 5.3(a) shows that the velocity increases with increase in angle of inclination ϕ, due to increase in forces acting upon the fluid flow. It is observed that the microrotation increases with increase in angle of inclination as shown in Fig. 5.3(b). It is clear from Figs. 5.3(c) to 5.3(e) that the temperature, entropy generation and Bejan number increase as increase in ϕ. Moreover, the peak value of temperature is observed at the center of the channel. The maximum entropy generation is noticed at the pipe wall due to high velocity and temperature gradients.

The behavior of flow quantities in response to increase in suction Reynolds number is similar to that with respect to angle of inclination as shown in Fig. 5.4. The fluid velocity, microrotation and temperature increase with increase in R as shown in Figs. 5.4(a) - 5.4(c). It is observed from the Fig. 5.4(d) that the entropy generation is maximum at the pipe wall where velocity and temperature gradients are highest and minimum at the channel center line where zero velocity and temperature gradients are recorded. The same trend is observed for the Bejan number profile as interpreted in Fig. 5.4(e).

The effect of Brinkman number on velocity, microrotation and temperature fields are shown in Figs. 5.5(a) to 5.5(c). It is clear that the velocity, microrotation and temperature increase as Brinkman number increases. The analogous importance between viscous dissipation and fluid conduction is determined by the Brinkman number. As Br increases more heat is generated by the viscous dissipation effect in the fluid. This results in increasing temperature profile with increase in Br. It is observed from Fig. 5.5(d) that the contribution of Brinkman number is nil on the entropy generation at the center of the pipe since the velocity and temperature gradients are zero. It can be seen from Fig. 5.5(e) that the Bejan number increases with an increase in the value of Br. It is observed that the heat transfer irreversibility dominates at the pipe wall and fluid friction irreversibility dominates at the center of the pipe.

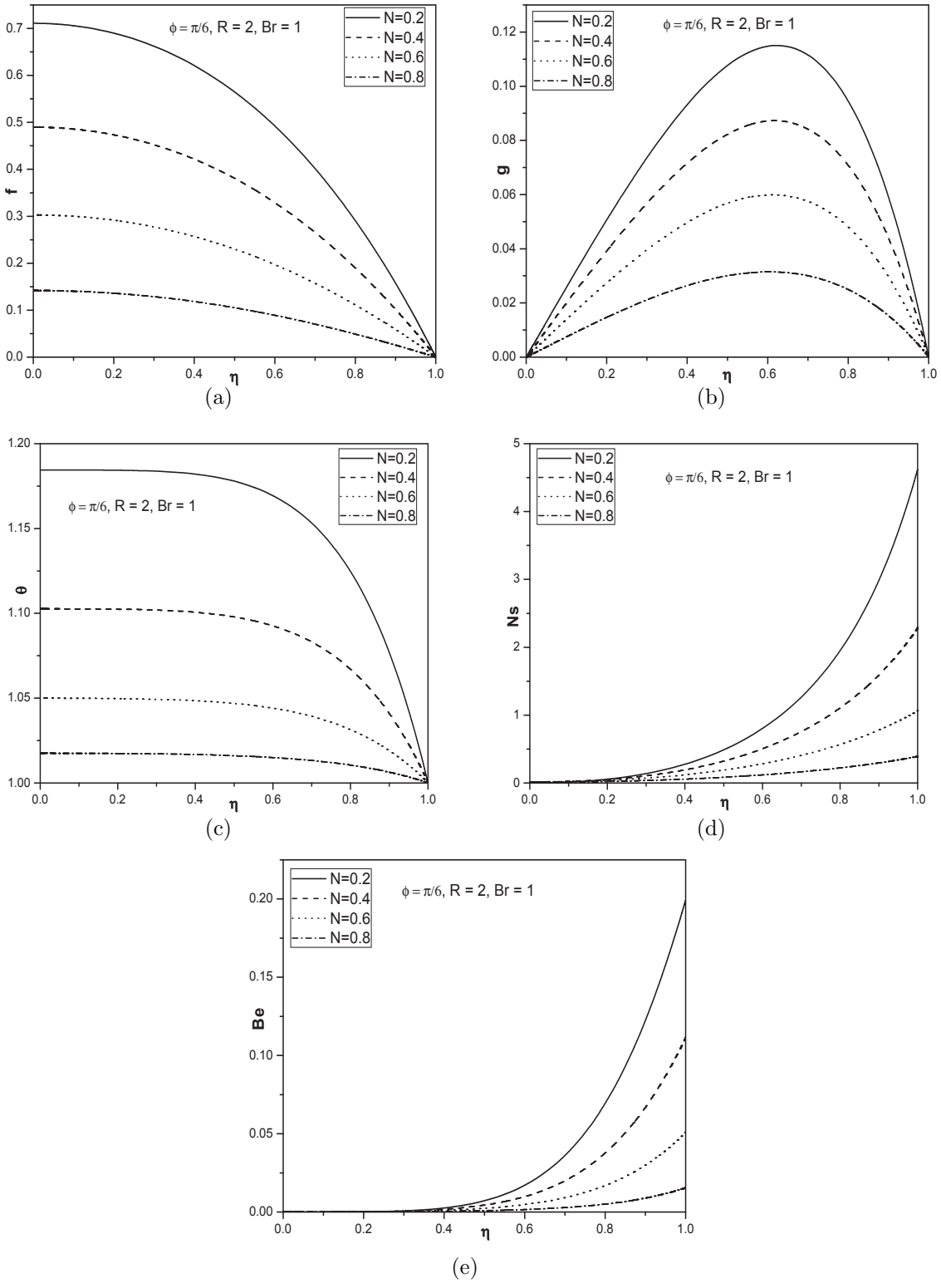

Figure 5.2: Effect of coupling number on (a)velocity, (b)microrotation (c)temperature (d)entropy generation and (e)Bejan number.

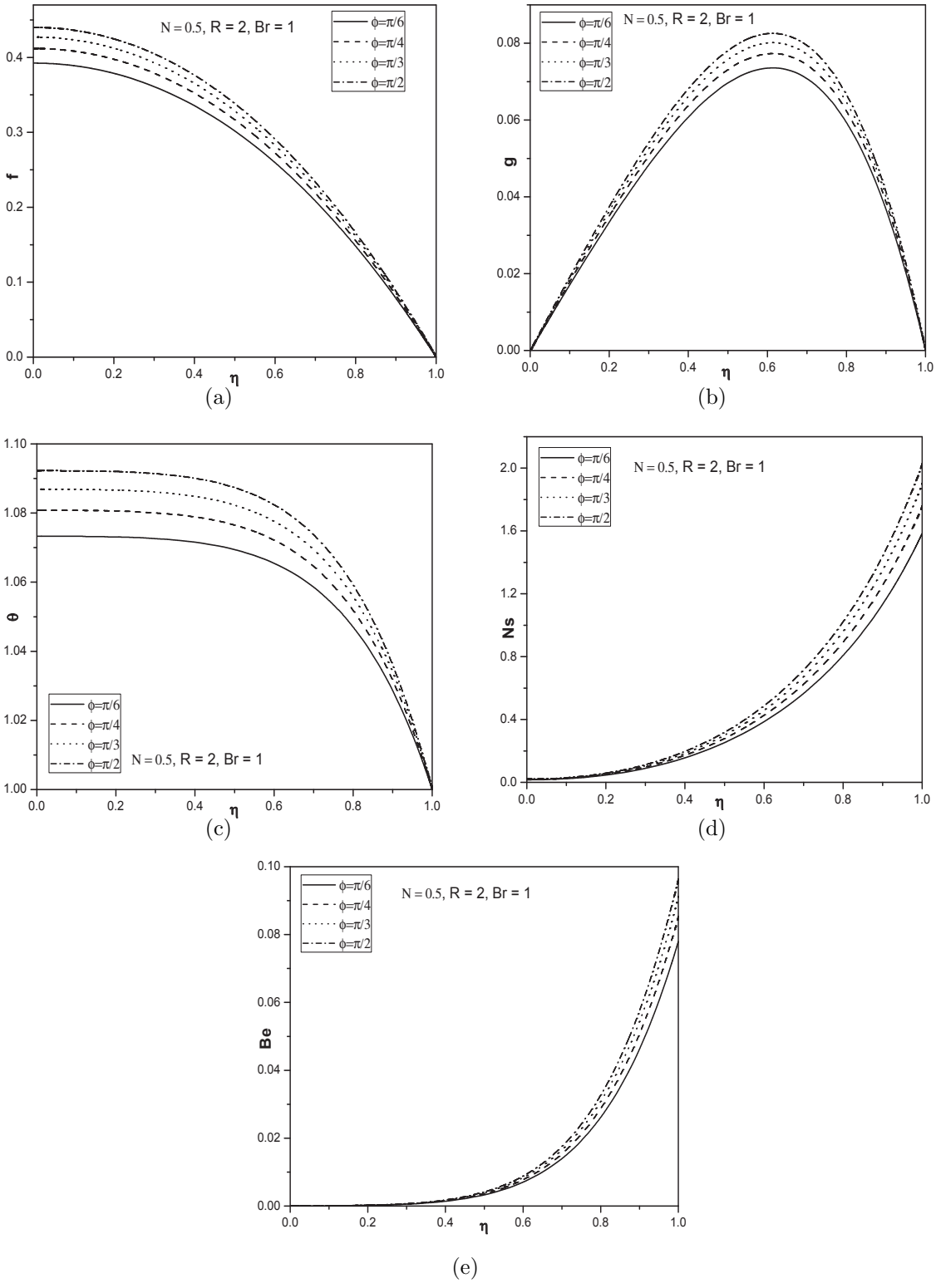

Figure 5.3: Effect of angle of inclination on (a)velocity, (b)microrotation, (c)temperature, (d)entropy generation and (e)Bejan number.

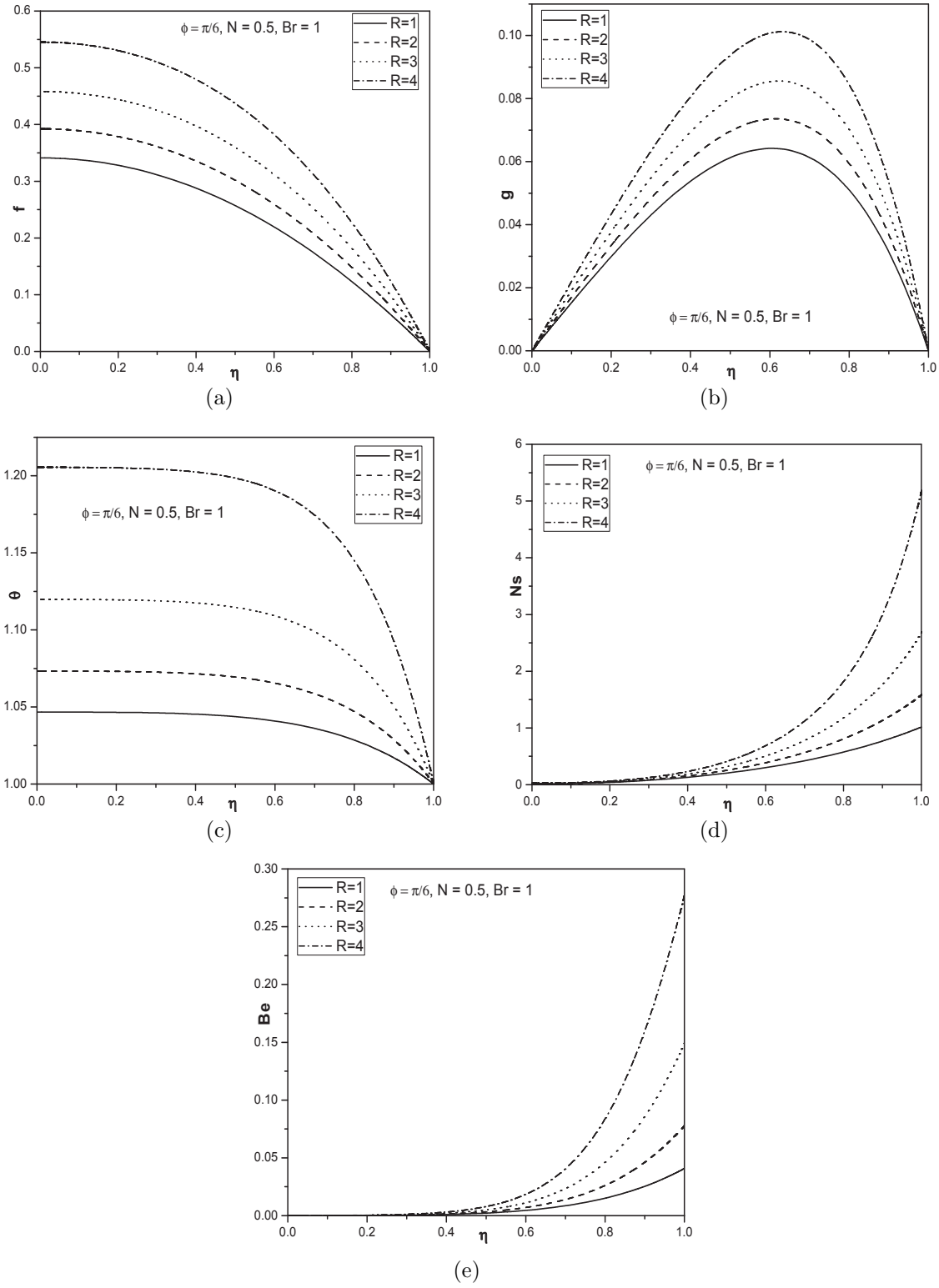

Figure 5.4: Effect of suction Reynolds number on (a)velocity, (b)microrotation, (c)temperature, (d)entropy generation and (e)Bejan number.

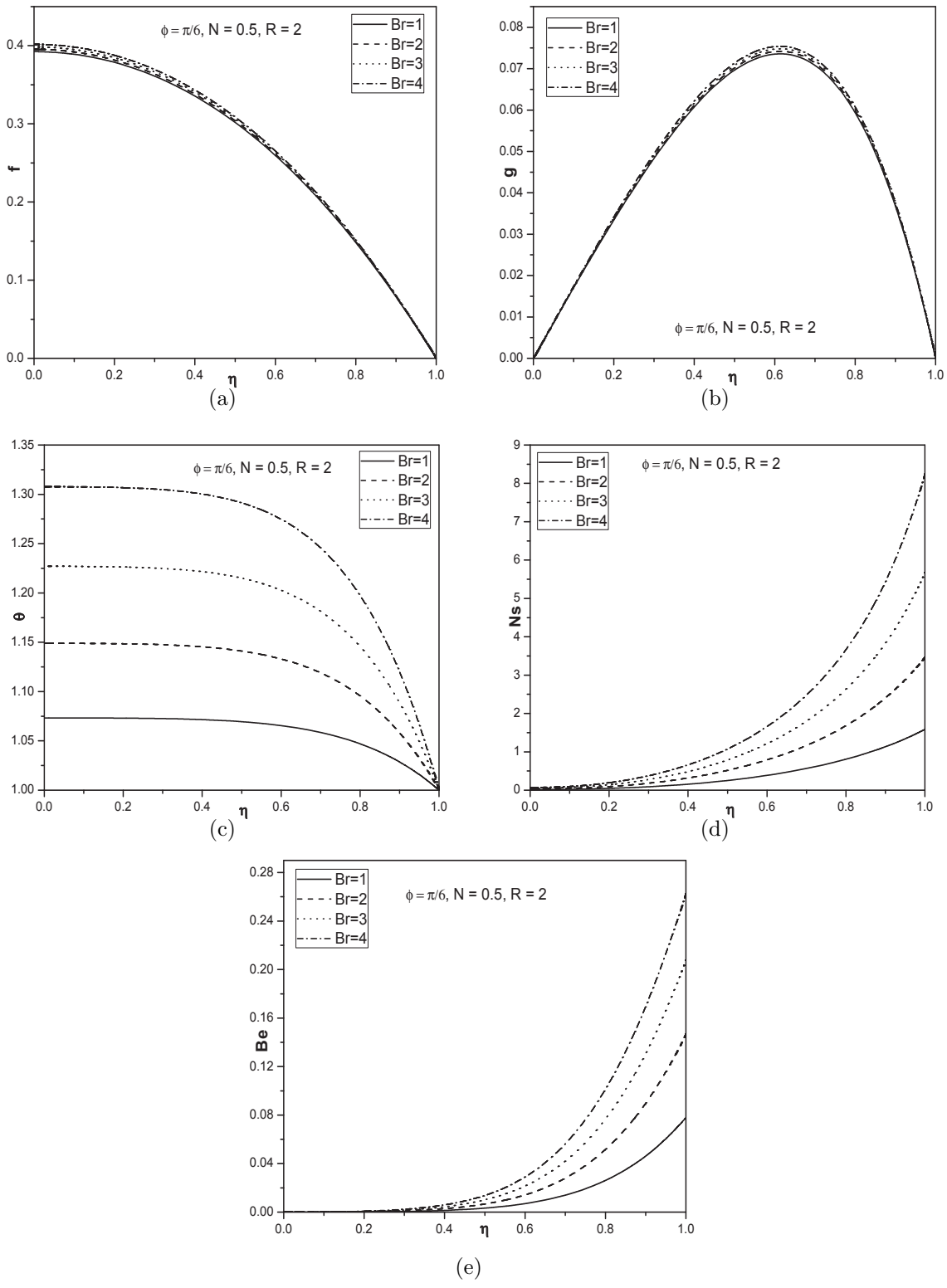

Figure 5.5: Effect of Brinkman number on (a)velocity, (b)microrotation, (c)temperature, (d)entropy generation and (e)Bejan number.

Table 5.1: Comparison of SQLM solutions for the velocity and microrotation with that of analytical solution given by Eringen [41] for $gs = 0$, $R = 0$ and $\phi = 0$.

	Velocity $f(\eta)$		Microrotation $g(\eta)$	
η	Analytical solution[41]	Present	Analytical solution[41]	Present
1	0	0	0	0
0.9755	0.01213	0.012128	0.00675	0.006758
0.9045	0.04605	0.046052	0.02309	0.023092
0.7939	0.09479	0.094809	0.04001	0.040029
0.6545	0.14845	0.148466	0.04944	0.049459
0.5	0.19688	0.196902	0.04821	0.048232
0.3455	0.23292	0.232950	0.03835	0.038355
0.2061	0.25435	0.254385	0.02458	0.024587
0.0955	0.26370	0.263735	0.01173	0.011728
0.0245	0.26609	0.266128	0.003032	0.003027
1	0.26626	0.266296	0	0

5.2.2 Case(b): Slip and Convective Boundary Conditions

Assume that the surface of the pipe is convectively heated with hot fluid T_2, which provides a heat transfer coefficient h. The slip velocity and zero microrotation are considered at the pipe wall. Thus, the boundary conditions are given by

$$\begin{aligned} \frac{du}{dr} = 0,\ \sigma = 0,\ \frac{dT}{dr} = 0,\ \text{at } r = 0 \\ u = -\zeta_1 \frac{du}{dr},\ \sigma = 0,\ -K_f \frac{dT}{dr} = h(T - T_1),\ \text{at } r = a \end{aligned} \tag{5.15}$$

The dimensionless boundary conditions are:

$$\begin{aligned} f'(\eta) = 0, \quad g(\eta) = 0, \quad \theta'(\eta) = 0, \quad \text{at} \quad \eta = 0 \\ \zeta f'(\eta) + f(\eta) = 0, \quad g(\eta) = 0, \quad \theta'(\eta) + Bi\theta(\eta) = 0, \quad \text{at} \quad \eta = 1 \end{aligned} \tag{5.16}$$

where $\zeta = \frac{\zeta_1}{a}$ is the slip parameter and $Bi = \frac{ah}{K_f}$ is the Biot number. Proceeding as in Case (a), the solution is obtained from the following matrix equation

$$\mathbf{X}_{r+1} = \mathbf{A}_r^{-1}\mathbf{B}_r \tag{5.17}$$

The entropy generation and Bejan number have been calculated for the slip and convective boundary conditions from equations (5.13) and (5.14).

Results and Discussion

For the numerical validation of the results, physically meaningful values have been chosen for the parameters $Pr = 1$, $g_s = 0.5$, $m = 2$, $A = -2$, $B = 0.1$ and $T_p = 1$ in the problem.

Fig. 5.6, presents the effect of coupling number (N) on non-dimensional velocity, microrotation, temperature, entropy generation and Bejan number. It is observed from Figs. 5.6(a) - 5.6(e) that the velocity, microrotation, temperature, entropy generation and Bejan number decrease with an increase in the value of coupling number (N).

The influence of the angle of inclination on velocity, microrotation, temperature, entropy generation and Bejan number is shown in Fig. 5.7. It is observed that the fluid velocity increases with increase in angle of inclination ϕ as displayed in Fig. 5.7(a). It is observed from Fig. 5.7(b) that the microrotation increases at the center of the channel as the angle of inclination increases. It is clear from Figs. 5.7(c) to 5.7(e) that the temperature, entropy generation and Bejan number increase as ϕ increases.

The variation of suction Reynolds number on velocity, microrotation, temperature, entropy generation and Bejan number are presented in Fig. 5.8. Increase in the suction Reynolds number causes an increase in all the governing parameters. It is noticed that the heat transfer irreversibility dominates at the pipe wall and fluid friction irreversibility dominates at the axis of the pipe as shown in Fig. 5.8(e) with an increase in suction Reynolds number.

It is observed from Figs. 5.9(a) and 5.9(b) that the velocity and microrotation decrease with increase in Biot number. As the Biot number increases, the circular pipe thermal resistance enhances significantly, and the velocity decreases. Fig. 5.9(c) reveals that the temperature decreases as Biot number increases. Since the Biot number depends on heat transfer coefficient h, which leads to decrease in temperature. Decrease in entropy generation is observed with an increase in Biot number Bi as shown in Fig. 5.9(d). This is due to the fact that both velocity and temperature gradients within the pipe decreases as Bi increases. Fig. 5.9(e) shows that the Bejan number decreases as Biot number increases. This implies an increase in the dominant effect of fluid friction irreversibility.

Increase in Brinkman number, increases the velocity, microrotation and temperature fields as shown in Figs. 5.10(a) to 5.10(c). Brinkman number is the term act as a strong heat source in the

energy equation thus, increase in Brinkman number significantly increases the fluid temperature and hence increase the fluid velocity and microrotation. It is observed from Fig. 5.10(d) that the entropy generation increases as Brinkman number increases. The zero value of the entropy generation along the pipe centerline can be attributed to the axialsymmetric nature of the pipe flow with zero velocity and temperature gradients along the centerline. It is noticed from Fig. 5.10(e) that the Bejan number increases with an increase in the value of Br.

5.3 Conclusions

In this chapter, the problem of entropy generation due to micropolar fluid flow through an inclined porous pipe is studied with (a)No-slip and isothermal boundary conditions and (b)Slip and convective boundary conditions. From the analysis, the following are the observations in both the cases (a) and (b).

The presence of microstructure N decreases the velocity, temperature, entropy generation and Bejan number in both cases. As there is an increase in angle of inclination, the entropy generation and Bejan number increases in Case(a). In Case(b) entropy generation and Bejan number does not increase significantly with the angle of inclination. It is observed that the fluid friction irreversibility dominates around the center of the pipe and heat transfer irreversibility dominates at the pipe wall in both cases from the Bejan number graphs for variation of all parameters. Increase in suction Reynolds number, increases the entropy generation and Bejan number. In Case(b) slight decrease in entropy generation and Bejan number are observed with increase in Biot number. All the Bejan number profiles show a minimum value at the center of the pipe and maximum value at the pipe wall since the velocity and temperature gradients are zero at the center of the pipe.

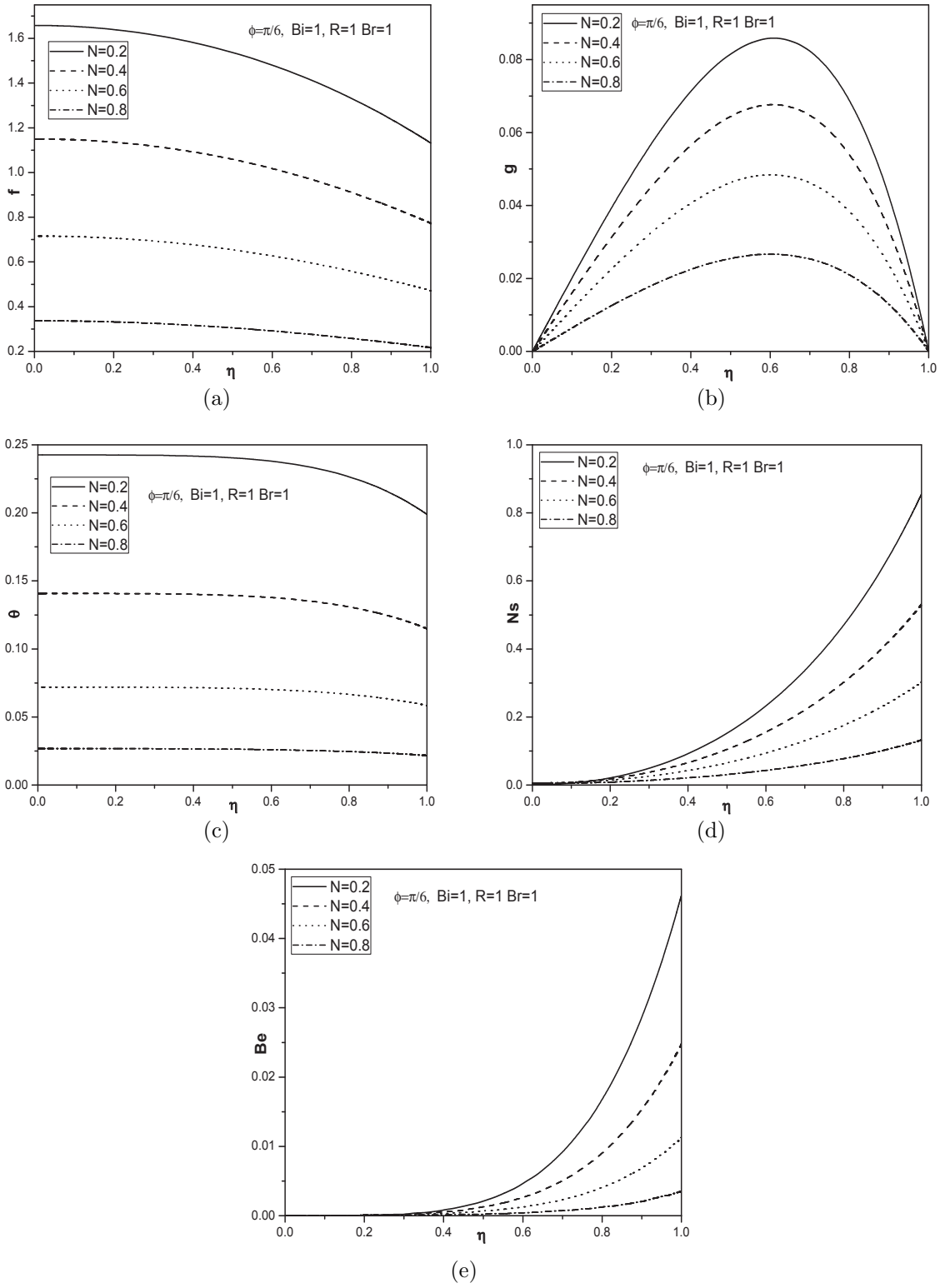

Figure 5.6: Effect of coupling number on (a)velocity, (b)microrotation, (c)temperature, (d)entropy generation and (e)Bejan number.

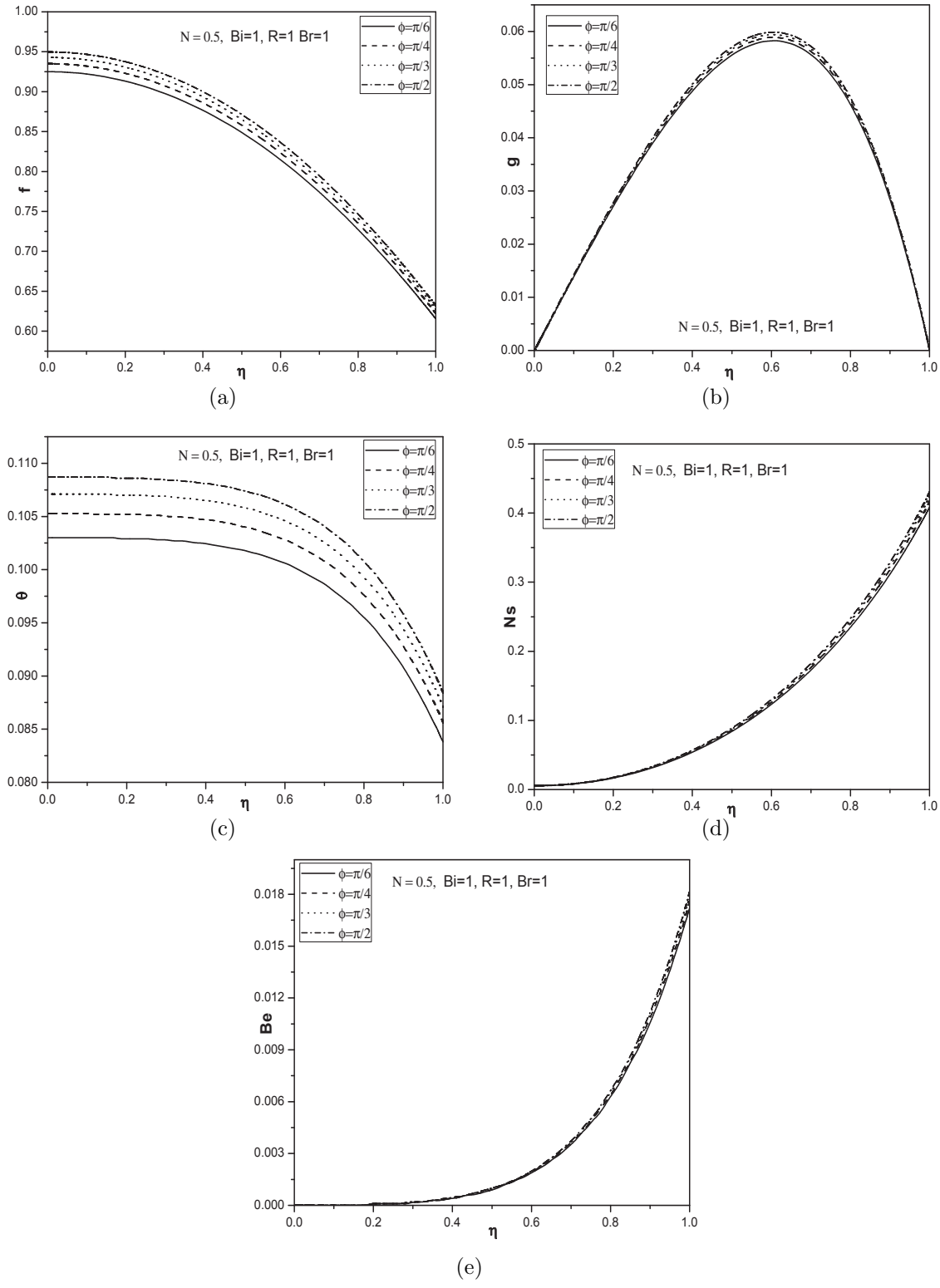

Figure 5.7: Effect of angle of inclination on (a)velocity, (b)microrotation, (c)temperature, (d)entropy generation and (e)Bejan number.

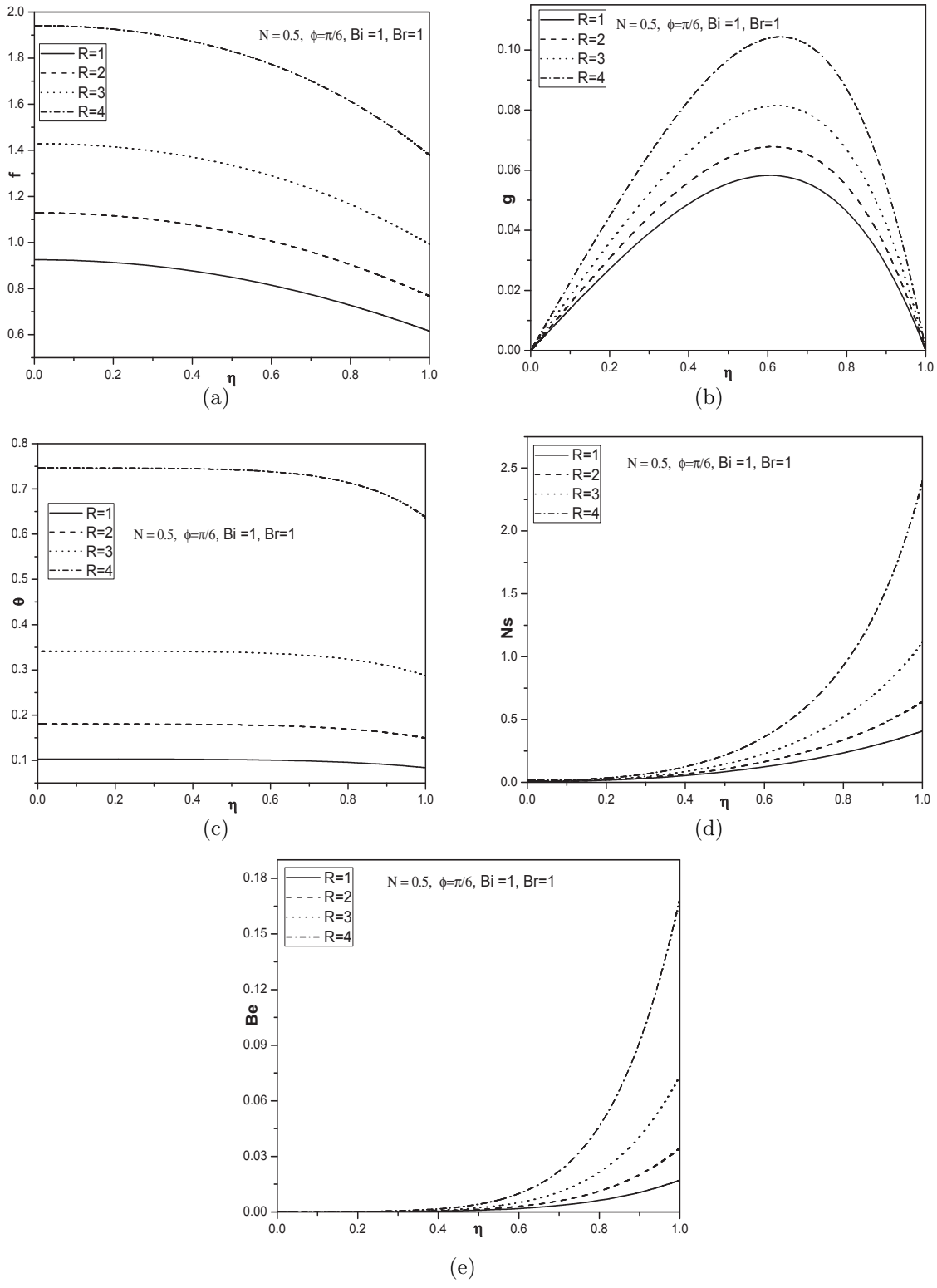

Figure 5.8: Effect of suction Reynolds number on (a)velocity, (b)microrotation, (c)temperature, (d)entropy generation and (e)Bejan number.

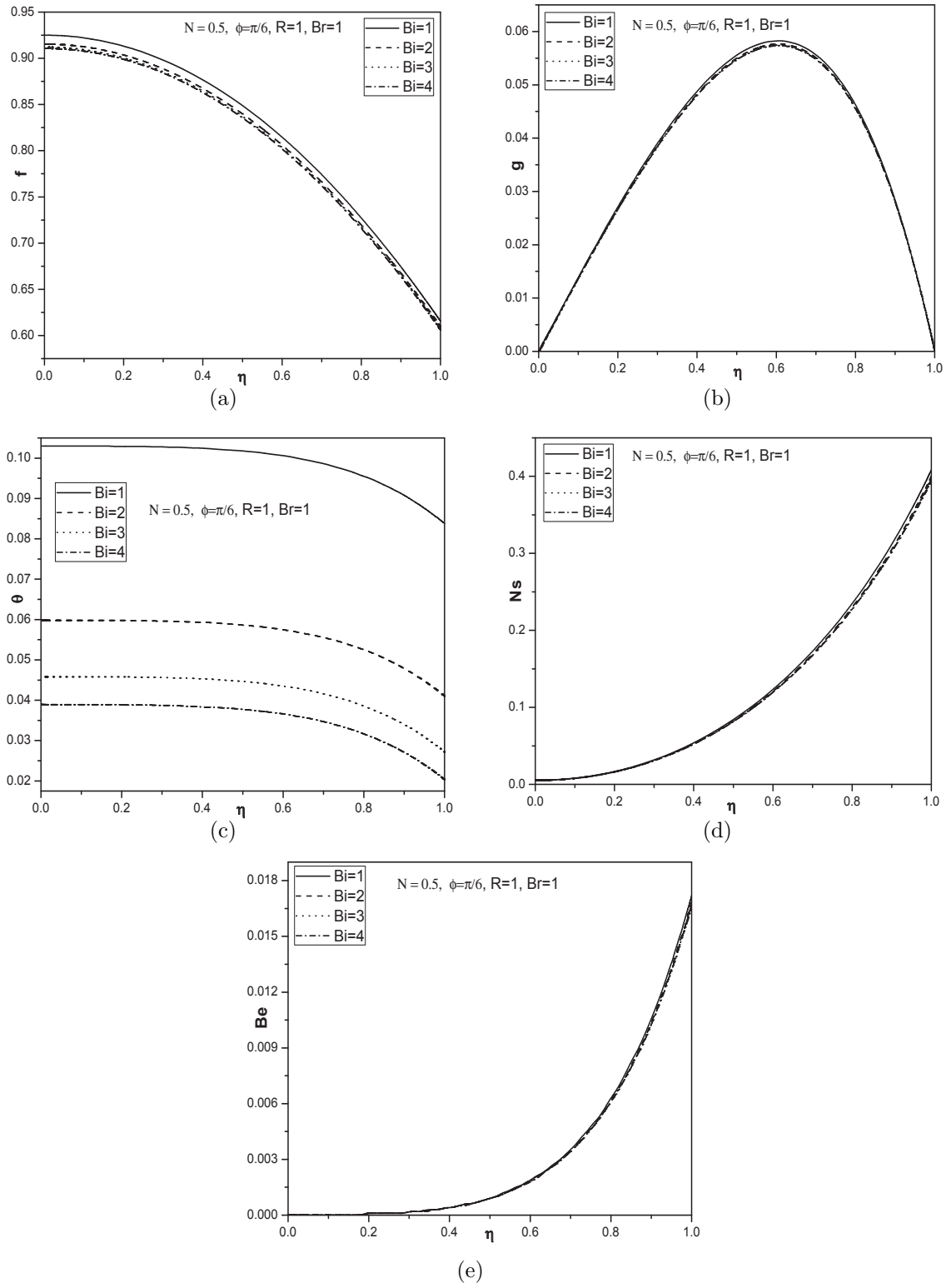

Figure 5.9: Effect of Biot number on (a)velocity, (b)microrotation, (c)temperature, (d)entropy generation and (e)Bejan number.

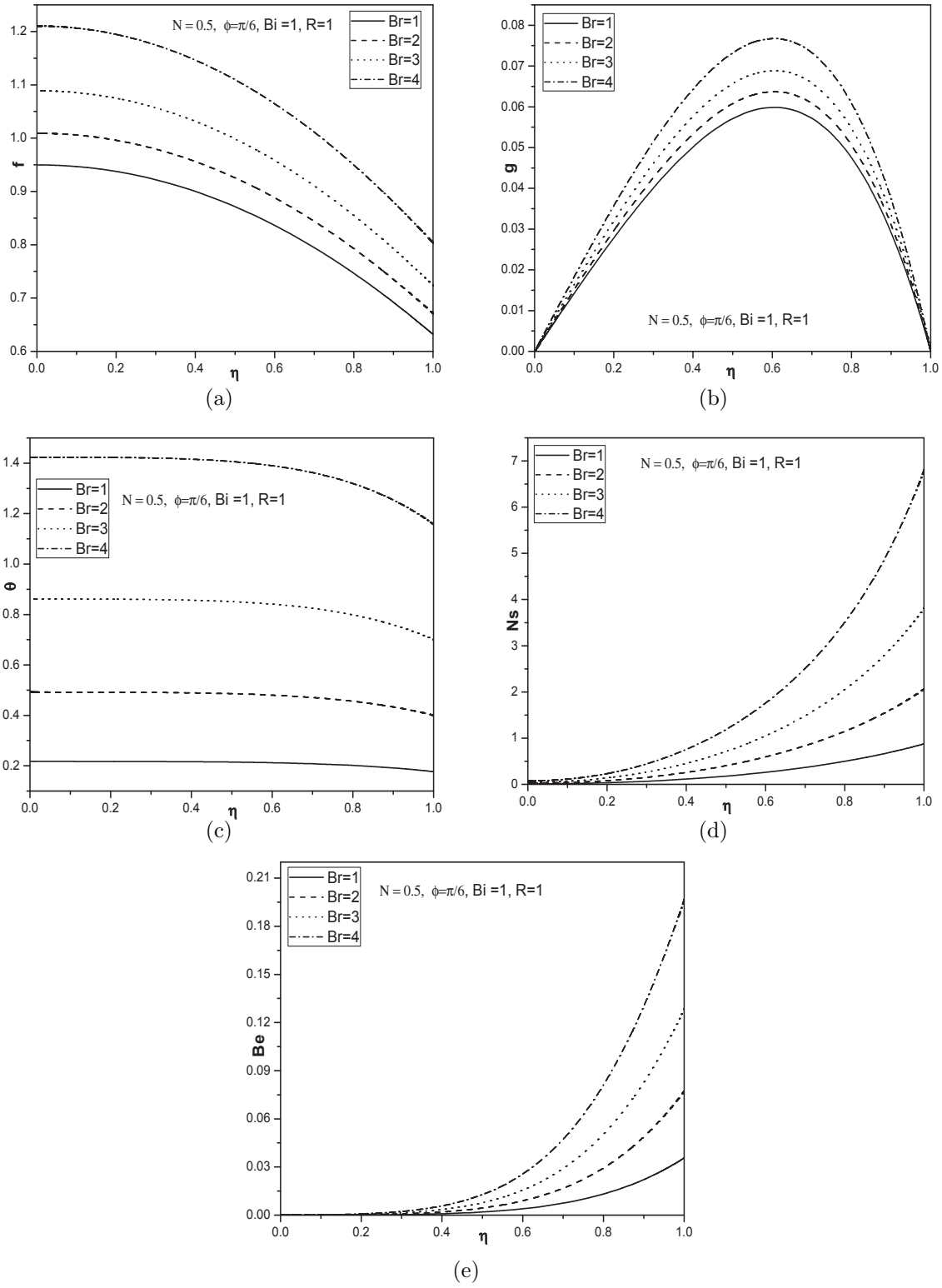

Figure 5.10: Effect of Brinkman number on (a)velocity, (b)microrotation, (c)temperature, (d)entropy generation and (e)Bejan number.

Chapter 6

Entropy Generation due to Micropolar Fluid Flow between Concentric Cylinders [1]

6.1 Introduction

The study of fluid flow between two cylinders, where one or both of the cylinders rotate has many applications such as swirl nozzles, rotating electrical machines, commercial viscometers, journal bearings and chemical and mechanical mixing devices. In practical situations, many factors affect the flow and heat transfer through annular space. Considerable research studies [92, 18, 34] were carried out to investigate the Newtonian and non-Newtonian fluid flow through concentric cylinders.

The entropy generation plays an important role in the design and development of thermal machines such as power plants, heat engines, refrigerators, turbine, and pipe networks. Entropy generation in these systems is an important issue because it gives information about local and global losses of energy due to heat transfer and fluid friction irreversibility. Thus, the energy saving can be obtained by reducing these losses. As irreversibility destroys the system energy, its minimization has been considered as the optimal design criteria for thermal systems to utilize its maximum

[1] Case(a): Communicated to "**Applied Thermal Engineering**", Case(b) Accepted in"**Ain Shams Engineering Journal**"

available energy. Hence, the efficient utilization of energy can be achieved by entropy generation minimization. Chen *et al* [25] analyzed the natural convection and entropy generation in a vertically concentric annular space. Eegunjobi and Makinde [37] investigated the entropy generation rate in transient Couette flow of variable viscosity fluid between two concentric pipes where inner pipe is moving and outer pipe is fixed. Chinyoka *et al* [26] analyzed the presence of irreversibility inside a porous vertical pipe and also investigated the entropy generation. Das *et al* [32] analyzed the entropy generation in a Couette flow caused due to the movement of the upper channel wall with suction/injection in a rotating frame of reference.

The study of entropy generation of micropolar fluid through concentric cylindrical annulus associated with or without slip and convective boundary conditions has been discussed in this chapter. The governing equations in cylindrical coordinates are simplified and numerically solved using the spectral quasilinearization method to obtain the entropy generation and Bejan number in the annulus.

6.2 Mathematical Formulation

Consider a steady, laminar, incompressible, micropolar fluid in an annulus between infinite vertical concentric circular cylinders of radii a and b ($a < b$). Choose the cylindrical polar coordinate system (r, φ, z) with z-axis as the common axis for both cylinders. The inner cylinder is at rest and the outer cylinder is rotating with constant angular velocity Ω(shown in Fig. 6.1). The flow is generated due to rotation of the outer cylinder. Since the flow is fully developed and the cylinders are of infinite length, the flow depends only on r . Further, it is assumed that, except density all the fluid properties are constant in the buoyancy term of the balance of momentum equation. With the above assumptions and Boussinesq approximations with energy, the equations governing the steady flow of an incompressible micropolar fluid are

$$\frac{\partial u}{\partial \varphi} = 0 \tag{6.1}$$

$$\frac{\partial p}{\partial r} = \frac{\rho u^2}{r} \tag{6.2}$$

$$-\kappa \frac{\partial \sigma}{\partial r} + (\mu + \kappa)\left(\frac{1}{r}\frac{\partial u}{\partial r} - \frac{u}{r^2} + \frac{\partial^2 u}{\partial r^2}\right) + \rho g^* \beta_T (T - T_1) = 0 \tag{6.3}$$

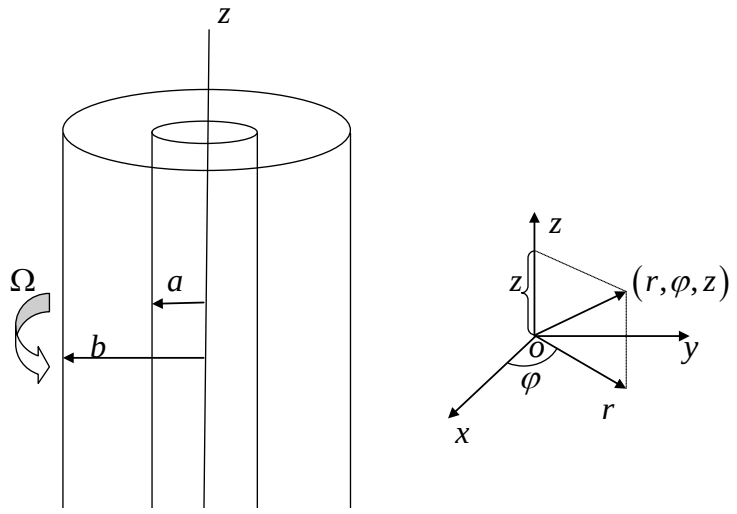

Figure 6.1: Physical model and coordinate system.

$$-2\kappa\sigma + \kappa\left(\frac{\partial u}{\partial r} + \frac{u}{r}\right) + \gamma\left(\frac{1}{r}\frac{\partial \sigma}{\partial r} + \frac{\partial^2 \sigma}{\partial r^2}\right) = 0 \tag{6.4}$$

$$K_f\left(\frac{1}{r}\frac{\partial T}{\partial r} + \frac{\partial^2 T}{\partial r^2}\right) + 2\kappa\left(\frac{1}{2r}\frac{\partial (ru)}{\partial r} - \sigma\right)^2 + (\mu + \kappa)\left(\frac{\partial u}{\partial r} - \frac{u}{r}\right)^2 + \gamma\left(\frac{\partial \sigma}{\partial r}\right)^2 = 0 \tag{6.5}$$

where u is velocity in φ direction, σ is microrotaion, T is the temperature of the fluid.

6.2.1 Case(a): No-slip and Isothermal Boundary Conditions

In this case, it is assumed that the inner cylinder is at rest and the outer cylinder is rotating with constant angular velocity Ω. Moreover, the inner and outer cylinders are maintained at uniform temperatures T_1 and T_2 respectively. Hence, the boundary conditions are

$$\begin{aligned} u = 0, \quad \sigma = 0, \quad T = T_1, \quad \text{at} \quad r = a \\ u = b\Omega, \quad \sigma = \frac{1}{2r}\frac{\partial}{\partial r}(ru), \quad T = T_2, \quad \text{at} \quad r = b \end{aligned} \tag{6.6}$$

Introducing the following non-dimensional variables

$$r = b\sqrt{\eta}, \quad u = \frac{\Omega}{\sqrt{\eta}} f(\eta), \quad \sigma = \frac{\Omega}{b} g(\eta), \quad T - T_1 = (T_2 - T_1)\theta(\eta) \tag{6.7}$$

in Eqs. (6.3) to (6.5), to get the following non-linear system of differential equations:

$$-\frac{2N}{1-N}\eta g' + \frac{4\eta}{1-N}f'' + \sqrt{\eta}\frac{Gr}{Re}\theta = 0 \tag{6.8}$$

$$-g + f' + \frac{2(2-N)}{m^2}(g' + \eta g'') = 0 \tag{6.9}$$

$$(\eta^3\theta'' + \eta^2\theta') + \frac{Br}{1-N}\left[\frac{N}{2}\eta^2(f'-g)^2 + (f-\eta f')^2 + \frac{N(2-N)}{m^2}\eta^3 g'^2\right] = 0 \tag{6.10}$$

The corresponding boundary conditions in dimensionless form are:

$$\begin{aligned} f(\eta_0) = 0, \quad g(\eta_0) = 0, \quad \theta(\eta_0) = 0, \quad \text{where} \quad \eta_0 = \left(\frac{a}{b}\right)^2, \\ f(1) = b, \quad g(1) = \left[\frac{df}{d\eta}\right]_{\eta=1}, \quad \theta(1) = 1 \end{aligned} \tag{6.11}$$

The Quasilinearization method is used to convert the non-linear boundary value problems (6.8)-(6.10) to a system of linear differential equations. The resultant equations are solved using the Chebyshev spectral collocation method, which is described in detail in chapter-2. Proceeding as in chapter-2, the solution is obtained as

$$\mathbf{X}_{r+1} = \mathbf{A}_r^{-1}\mathbf{B}_r \tag{6.12}$$

Entropy Generation

In fluid flow, irreversibility arises due to heat transfer and viscous frictional effects in the fluid. The entropy generation rate can be expressed as the sum of contributions due to viscous and thermal effects and depends functionally on local velocities and temperatures in the domain of interest. When both temperature and velocity fields are known, the volumetric entropy generation rate S_G at a point in a system is given in equation (1.4).

For the present study, the volumetric rate of entropy generation reduces to

$$S_G = \frac{K_f}{T_1^2}\left(\frac{\partial T}{\partial r}\right)^2 + \frac{\mu+\kappa}{T_1}\left[r\frac{\partial}{\partial r}\left(\frac{u}{r}\right)\right]^2 + \frac{2\kappa}{T_1}\left[\frac{1}{2r}\frac{\partial}{\partial r}(ru) - \sigma\right]^2 + \frac{\gamma}{T_1}\left(\frac{\partial \sigma}{\partial r}\right)^2 \tag{6.13}$$

The dimensionless entropy generation number is given by

$$N_s = \overbrace{4\eta\left(\frac{d\theta}{d\eta}\right)^2}^{N_h} + \underbrace{\frac{4Br}{T_p}\left[\frac{1}{1-N}\left(f'-\frac{f}{\eta}\right)^2 + \frac{N}{2(1-N)}\left(\frac{df}{d\eta}-g\right)^2 + \frac{N\eta}{1-N}\left(\frac{2-N}{m^2}\right)\left(\frac{dg}{d\eta}\right)^2\right]}_{(N_v)} \tag{6.14}$$

To evaluate the irreversibility distribution, the parameter Be(Bejan number), which is the ratio of entropy generation due to heat transfer to the overall entropy generation is defined as follows

$$Be = \frac{N_h}{N_h + N_v} \tag{6.15}$$

Results and Discussion

The case of Newtonian fluid flow between concentric cylinders of Sinha and Chaudhary [89] can be obtained by taking $N = 0, Gr = 0, m = 0$. Thus, in order to assess the accuracy of SQLM method, the results of the present problem, in the absence of N, Gr, m have been compared with the analytical solution of Sinha and Chaudhary [89] for Newtonian fluids. The comparison was found to be in good agreement, as shown in Table. 6.1.

In order to investigate the effect of the parameters coupling number (N), Brinkman number (Br), Reynolds number (Re) on the velocity(f), microrotation(g), temperature(θ), entropy generation number(Ns) and Bejan number(Be), the parameters are fixed as $m = 2$, $T_p = 1$, and $Gr = 1$.

Fig. 6.2, displays the effect of coupling number N on the dimensionless velocity, microrotation, temperature, entropy generation and Bejan number. It is observed from Fig. 6.2(a) that the velocity decreases, as N increases. The velocity in case of micropolar fluid is less compared to that of the viscous fluid case. But the values of microrotation profile enhances with an increase in coupling number as shown in Fig. 6.2(b). From Fig. 6.2(c), it is seen that the temperature increases with an increase in the value of coupling number. Entropy generation enhances with an increase in coupling number as shown in Fig. 6.2(d). It can be seen from Fig. 6.2(e) that the Bejan number decreases as N increases.

The variation of the non-dimensional velocity, microrotation, temperature, entropy generation and Bejan number profiles with η for different values of Brinkman number is illustrated in Fig. 6.3. It is observed from Fig. 6.3(a) that velocity slightly increases as Br increases. From Fig. 6.3(b), it is seen that as Br increases, the microrotation increases at the outer cylinder and there is no change at the inner cylinder. Fig. 6.3(c) illustrates the effect of Br on the temperature profile. It is also noticed that as Br increases, the temperature profile increases. According to the definition, Br is the ratio of the viscous heat generation of external heating. Thus higher values of Br, the lesser will be the conduction of heat produced by viscous dissipation and hence the larger is the temperature. The entropy generation profile for different values of Br is described in Fig. 6.3(d). It is observed that as Br increases, the entropy generation increases at both cylinders. The parameter Br determines the relative importance of viscous effects and has a significant effect on entropy generation. For all parameters, the inner cylinder acts as a strong concentrator of irreversibility. Entropy generation number is high in magnitude near the inner cylinder due to the high temperature and velocity gradients. It is observed from Fig. 6.3(e) that the Be decreases with η and tends to 0 and then increases. Further, it is noticed that as the Brinkman number increases the Bejan number Be decreases.

Fig. 6.4, illustrates the effect of Reynolds number (Re) on the dimensionless velocity, microrotation, temperature, entropy generation and Bejan number. Fig. 6.4(a) shows the velocity profile with increase in Re. As Re increases, the flow velocity decreases. Fig. 6.4(b) depicts that increase in Re, increases the microrotation. From Fig. 6.4(c), it is clear that the increase in the value of Reynolds number slightly increases the temperature near the outer cylinder. The effect of Reynolds number Re on entropy generation is presented in Fig. 6.4(d). As the value of Re increases, the entropy generation decreases near the inner cylinder and increases near the outer cylinder. As the Reynolds number increases, the Bejan number increases at the inner cylinder with the dominant effect of heat transfer irreversibility and decreases at the outer cylinder with increasing effect of fluid friction irreversibility as demonstrated in Fig. 6.4(e).

6.2.2 Case(b): Slip and Convective Boundary Conditions

In this case, it is assumed that the fluid adjacent to the cylinders has finite tangential velocity, it slips along the boundary. The inner cylinder is heated by convection from a hot fluid with

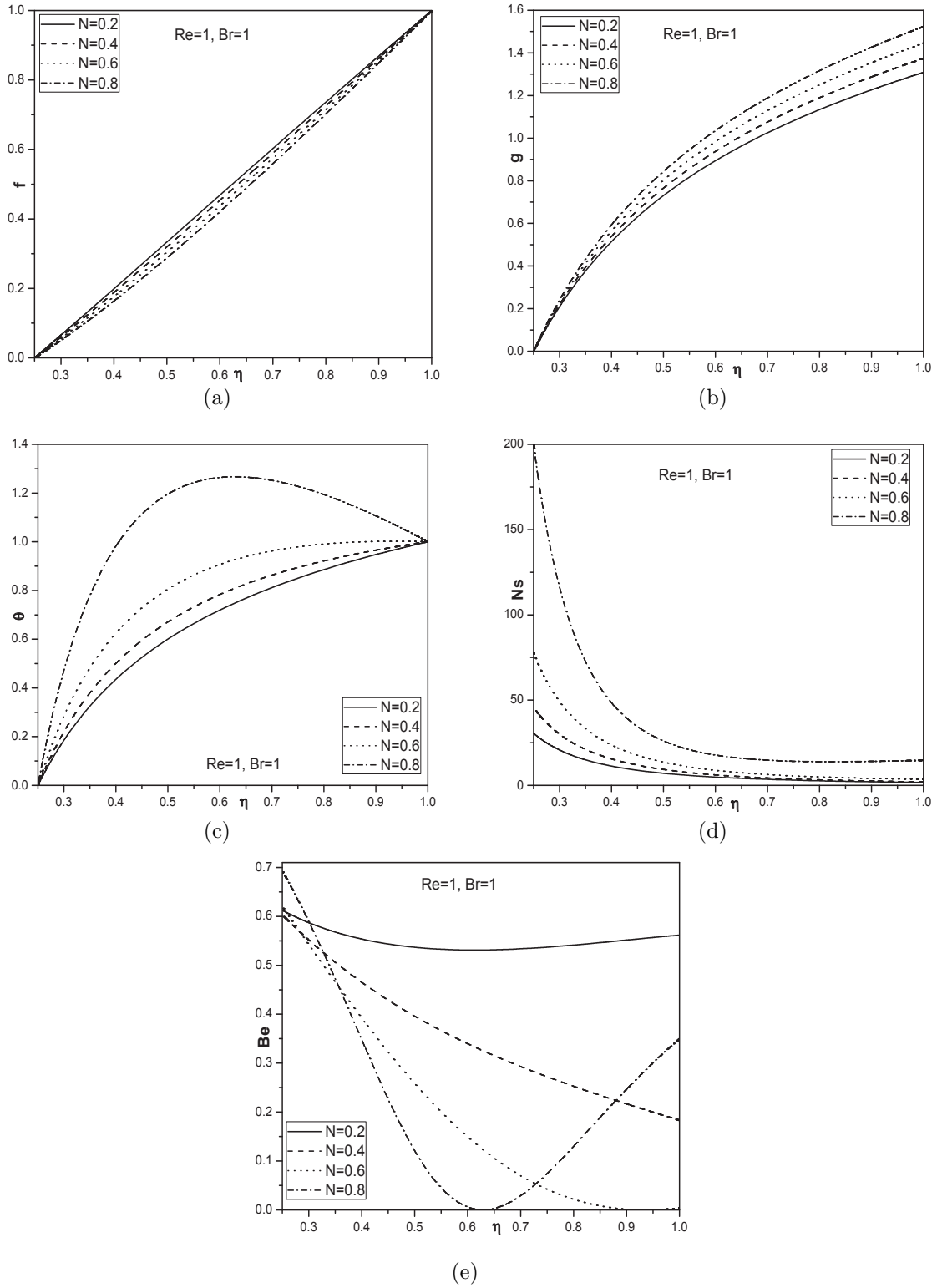

Figure 6.2: Effect of coupling number on (a)velocity, (b)microrotation, (c)temperature, (d)entropy generation and (e)Bejan number.

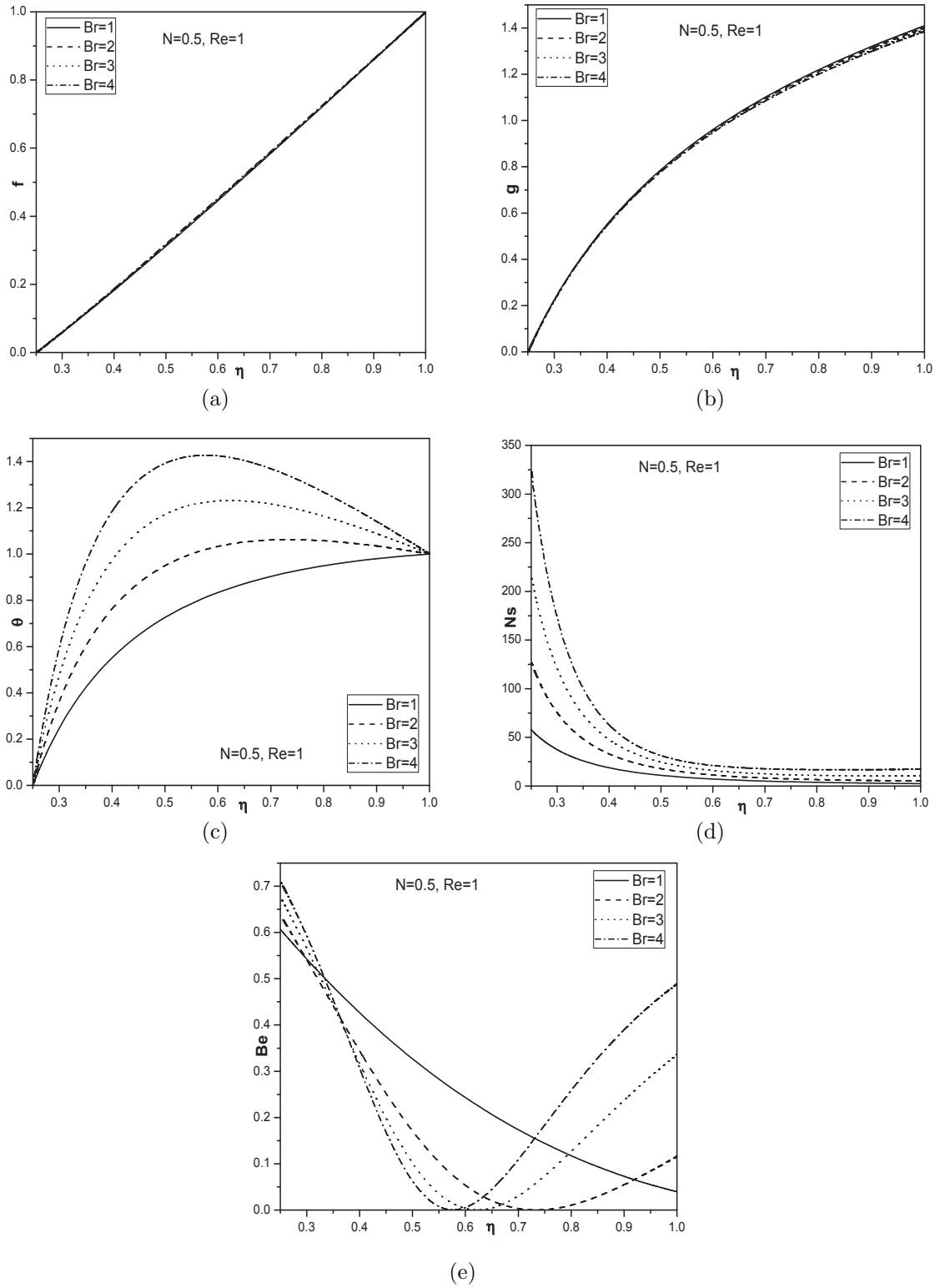

Figure 6.3: Effect of Brinkman number on (a)velocity, (b)microrotation, (c)temperature, (d)entropy generation and (e)Bejan number.

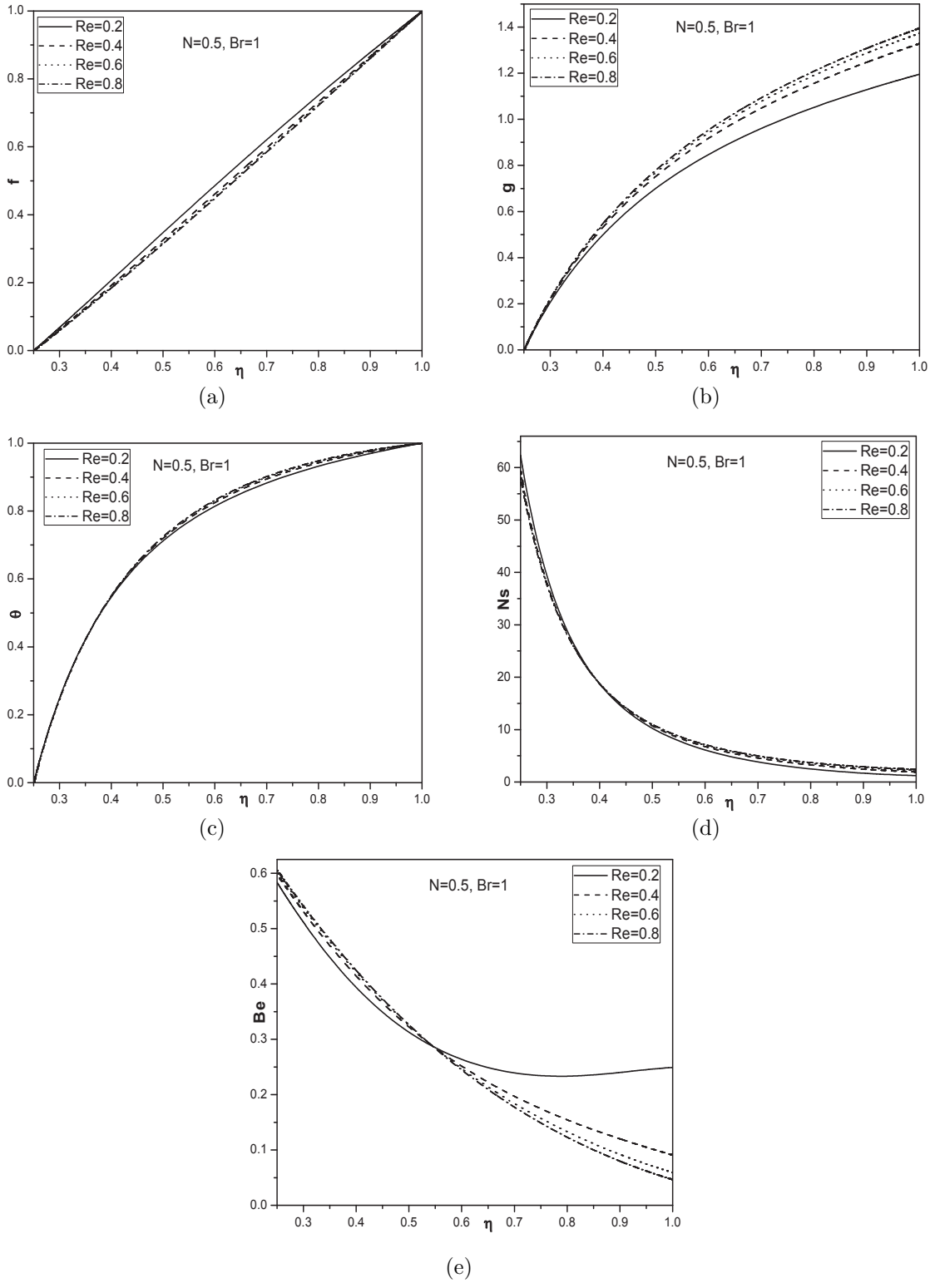

Figure 6.4: Effect of Reynolds number on (a)velocity, (b)microrotation, (c)temperature, (d)entropy generation and (e)Bejan number.

Table 6.1: Comparison analysis for the velocity calculated by the present method and that of analytical solution [89] for $N = 0$.

η	Analytical solution	Present solution
1	1	1
0.9816	0.97546	0.975528
0.9284	0.90453	0.904509
0.8454	0.79386	0.793893
0.7409	0.65453	0.654509
0.625	0.5	0.5
0.5091	0.34546	0.345492
0.4046	0.20613	0.206107
0.3216	0.09546	0.095492
0.2684	0.02453	0.024472
0.25	0	0

temperature T_1 which provides a heat transfer coefficient h_1 while, the upper cylinder losses heat to the ambient with a heat transfer coefficient h_2. Thus, the boundary conditions are

$$\begin{aligned} u = \zeta' \left[\frac{\partial u}{\partial r} - \frac{u}{r}\right], \quad \sigma = 0, \quad K_f \frac{\partial T}{\partial r} - h_1(T - T_1) = 0, \quad \text{at} \quad r = a \\ u = b\Omega - \zeta' \left[\frac{\partial u}{\partial r} - \frac{u}{r}\right], \quad \sigma = \frac{1}{2r}\frac{\partial}{\partial r}(ru), \quad K_f \frac{\partial T}{\partial r} + h_2(T - T_2) = 0, \quad \text{at} \quad r = b \end{aligned} \tag{6.16}$$

where ζ' slip length of the inner and outer cylinders.

The corresponding boundary conditions in dimensionless form are:

$$\begin{aligned} -2\zeta\eta_0 f'(\eta_0) + (\sqrt{\eta_0} + 2\zeta) f(\eta_0) = 0,\ g(\eta_0) = 0,\ Bi_1\theta(\eta_0) = 2\sqrt{\eta_0}\theta'(\eta_0),\ \text{where}\, \eta_0 = (\frac{a}{b})^2 \\ 2\zeta f'(1) + (1 - 2\zeta) f(1) = b,\ g(1) = \left[\frac{df}{d\eta}\right]_{\eta=1},\ Bi_2(1 - \theta(1)) = 2\theta'(1) \end{aligned} \tag{6.17}$$

where $\zeta = \frac{\zeta'}{b}$ is the slip parameter. In general Biot number is assumed to be same for the two cylinders. ($Bi_1 = Bi_2 = Bi$) Proceeding as in Case (a), the solution is obtained from the following matrix equation

$$\mathbf{X}_{r+1} = \mathbf{A}_r^{-1}\mathbf{B}_r \tag{6.18}$$

The entropy generation and Bejan number have been calculated for the slip and convective boundary conditions from equations (6.14) and (6.15).

Results and Discussion

The effects of N, Br, ζ and Bi on velocity, microrotation, temperature, entropy generation and Bejan number have been studied. The computations were carried out by taking $m = 2, gs = 1$, $T_p = 1$, $a = 0.5$, $b = 1$.

Fig. 6.5, presents the effect of coupling number (N) on nondimensional velocity, microrotation, temperature, entropy generation and Bejan number. Fig. 6.5(a) shows that the velocity decreases as N increases. Fig. 6.5(b) depicts that, the microrotation component decreases with an increase in the value of N. Fig. 6.5(c) reveals that as N increases temperature increases. In Fig. 6.5(d) it is observed that the entropy generation increases as coupling number increases. Fig. 6.5(e) reveals that the Bejan number Be decreases near the inner cylinder and increases near the outer cylinder with an increase in the coupling number N.

Fig. 6.6(a) shows that the velocity increases with an increase in the value of Br. Fig. 6.6(b) shows that the microrotation increases as Br increases. It is noticed from Figs. 6.6(c) and 6.6(d) that the temperature and entropy generation increase as Br increases. For all parameters, the inner cylinder acts as a strong concentrator of irreversibility. Entropy generation number is high in magnitude near the inner cylinder due to the presence of high temperature and velocity gradients. Ns then falls exponentially along the radial direction, approaching an asymptote near the outer cylinder. Entropy generation profiles are similar in shape and almost parallel to one another for all the parameter variations, but they vary in magnitudes. It is noticed from Fig. 6.6(e) that as Br increases, the Bejan number decreases at the inner cylinder which indicates that the fluid friction contribution to entropy generation increases. It is also observed that the Bejan number increases near the outer cylinder due to the high heat transfer contribution.

Figs. 6.7(a) to 6.7(d) illustrate the effect of slip parameter on the velocity, microrotation, temperature and entropy generation. It is observed that the slip parameter (ζ) has a significant influence on all the parameters. As slip parameter increases, the velocity, microrotation, temperature, and entropy generation decrease. The existence of slip condition in velocity increases convection by rotating the outer cylinder leading to influence the temperature consequently, affects the entropy generation. It is noticed from Fig. 6.7(e) that the effect of ζ has not significant on the Bejan number near the inner cylinder, but at the outer cylinder the Bejan number decreases as ζ increases.

Fig. 6.8, shows the velocity, microrotation, temperature, entropy generation and Bejan number profiles for different values of the Biot number. Physically, Biot number is expressed as the convection at the surface of the body to the conduction within the surface of the body. It is assumed the convective heat transfer coefficients $(h1, h2)$ are same at the inner and outer cylinders i.e. $Bi_1 = Bi_2 = Bi$. It is observed from Fig. 6.8(a) that an increase in the Biot number decreases the velocity profile of the fluid in an annular space. It is due to the fact that Biot number reduces the heat transfer rate in the cylinder walls. Fig. 6.8(b) shows that the microrotation decreases as Bi increases. It is noticed from Fig. 6.8(c) that the temperature decreases with a rise in Biot number due to a convective cooling at the cylinders. Fig. 6.8(d) reveals that the entropy generation increases as Bi increases. The effect of Biot number Bi on Be is shown in Fig. 6.8(e). As Biot number increases, Bejan number also increases.

6.3 Conclusions

In this chapter, the entropy generation in a steady flow of an incompressible micropolar fluid between concentric cylinders is analyzed. This problem of entropy generation is solved for two cases, i.e. Case (a)No-slip and isothermal boundary conditions and Case (b)slip and convective boundary conditions. The following are the observations from the analysis of both the cases.

Flow in the annular space is induced by the rotation of the outer cylinder. The results reveal that the entropy generation is higher near the inner cylinder in both the cases due to velocity and temperature gradients. Entropy generation profiles show an asymptotic behavior towards the outer cylinder. The fluid friction irreversibility dominates around the center of the annulus while the influence of heat transfer irreversibility can be observed near the cylinders. The influence of microrotation and the Brinkman number increases the entropy generation irrespective of the boundary conditions. The presence of slip in the fluid particles at the rotating outer cylinder increases the domination of fluid friction irreversibility. Thus, the Bejan number decreases near the outer cylinder as observed in the case (b). An increase in the Biot number causes the convective cooling at the inner and outer cylinders, leading to an increase in the Bejan number.

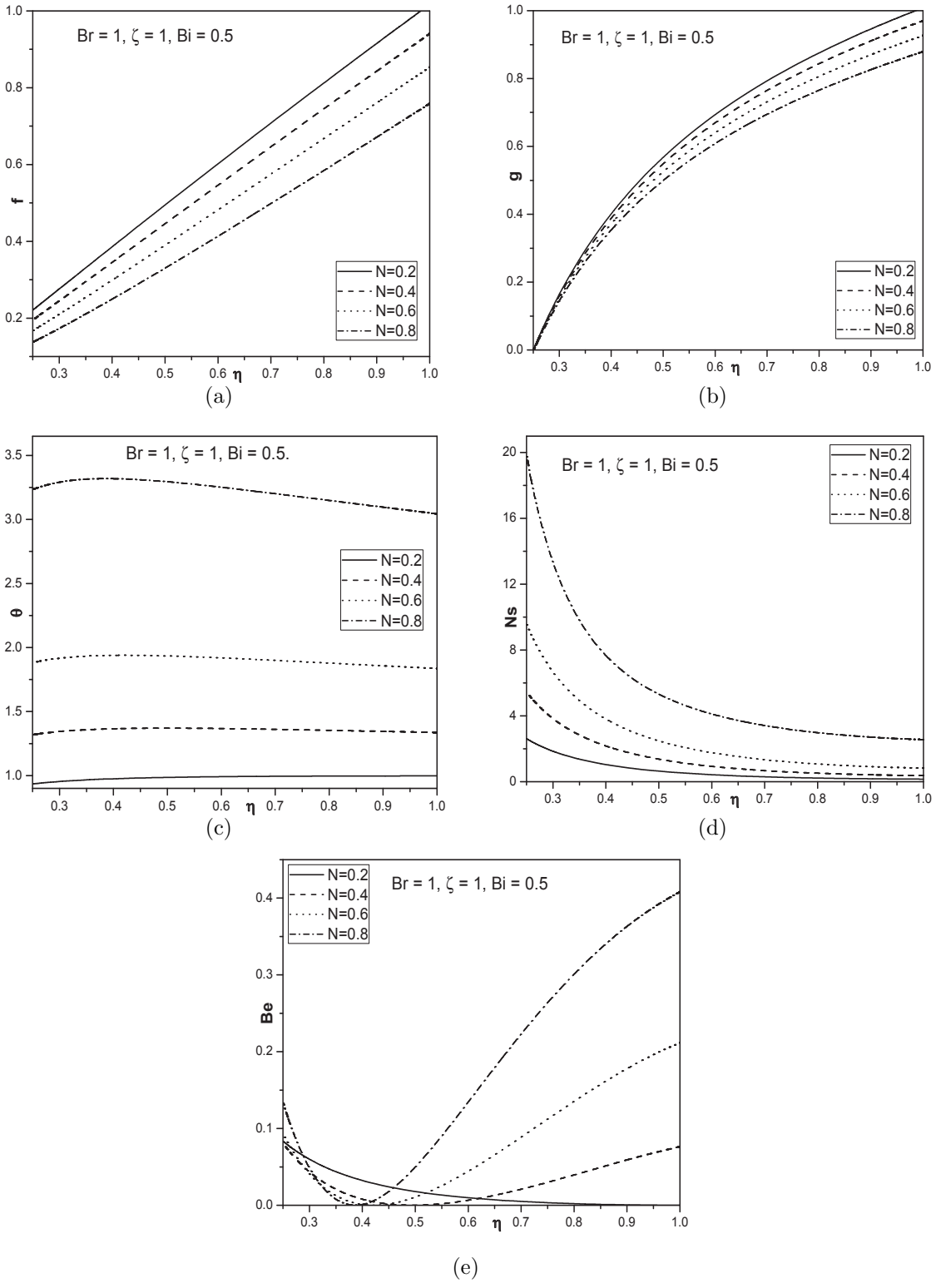

Figure 6.5: Effect of coupling number on (a)velocity, (b)microrotation, (c)temperature, (d)entropy generation and (e)Bejan number.

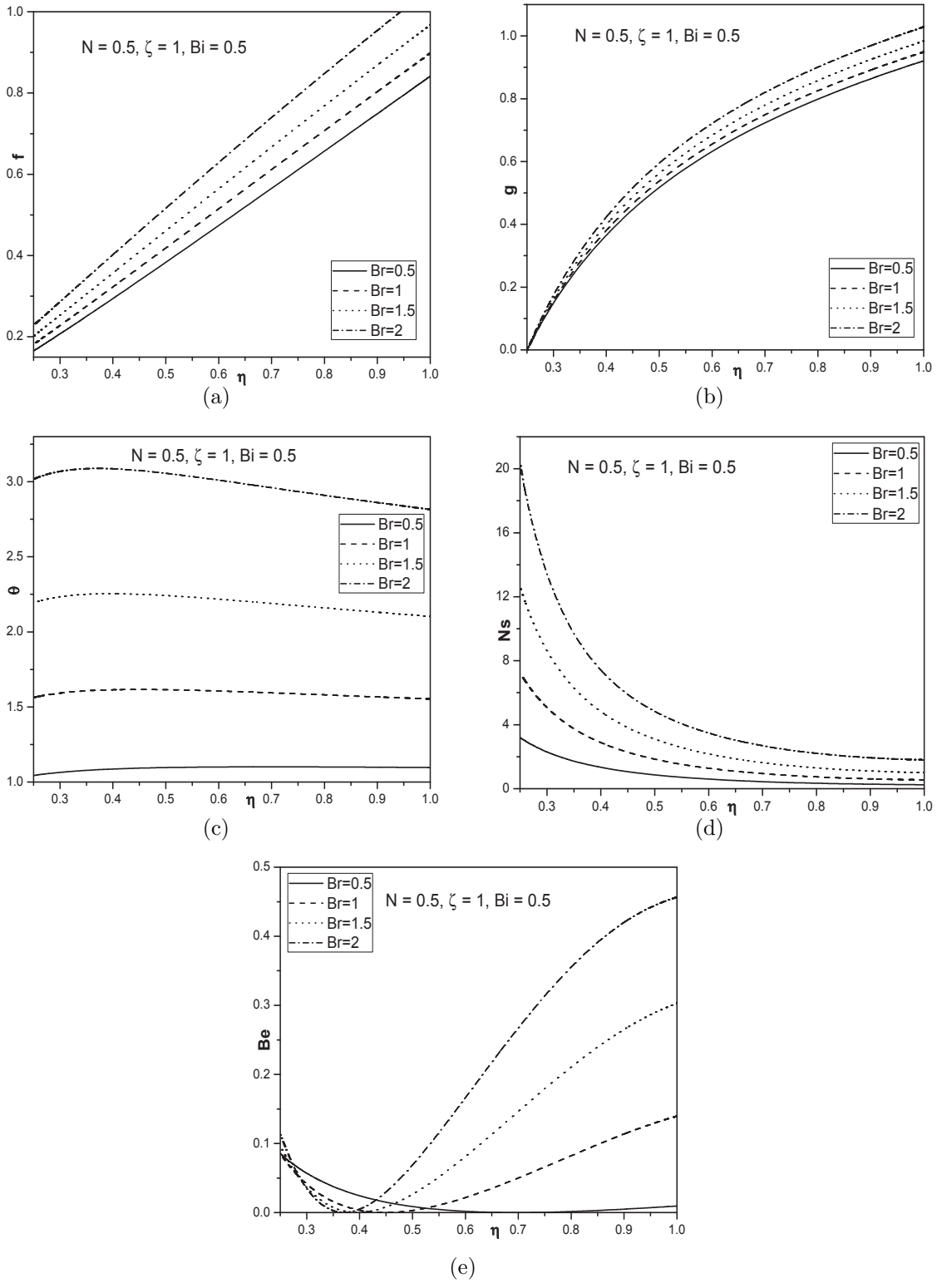

Figure 6.6: Effect of Brinkman number on (a)velocity, (b)microrotation, (c)temperature, (d)entropy generation and (e)Bejan number.

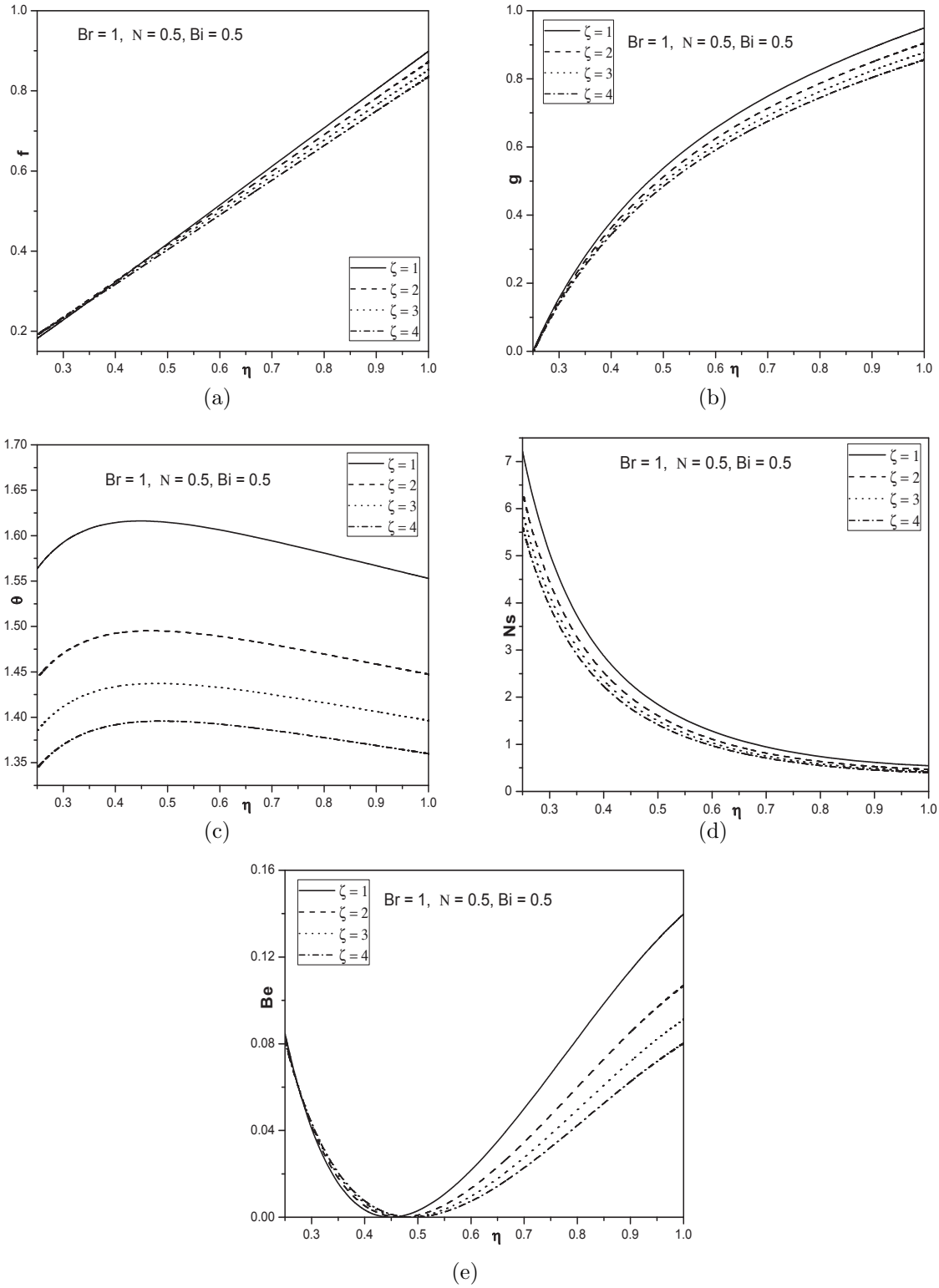

Figure 6.7: Effect of slip parameter on (a)velocity, (b)microrotation, (c)temperature, (d)entropy generation and (e)Bejan number.

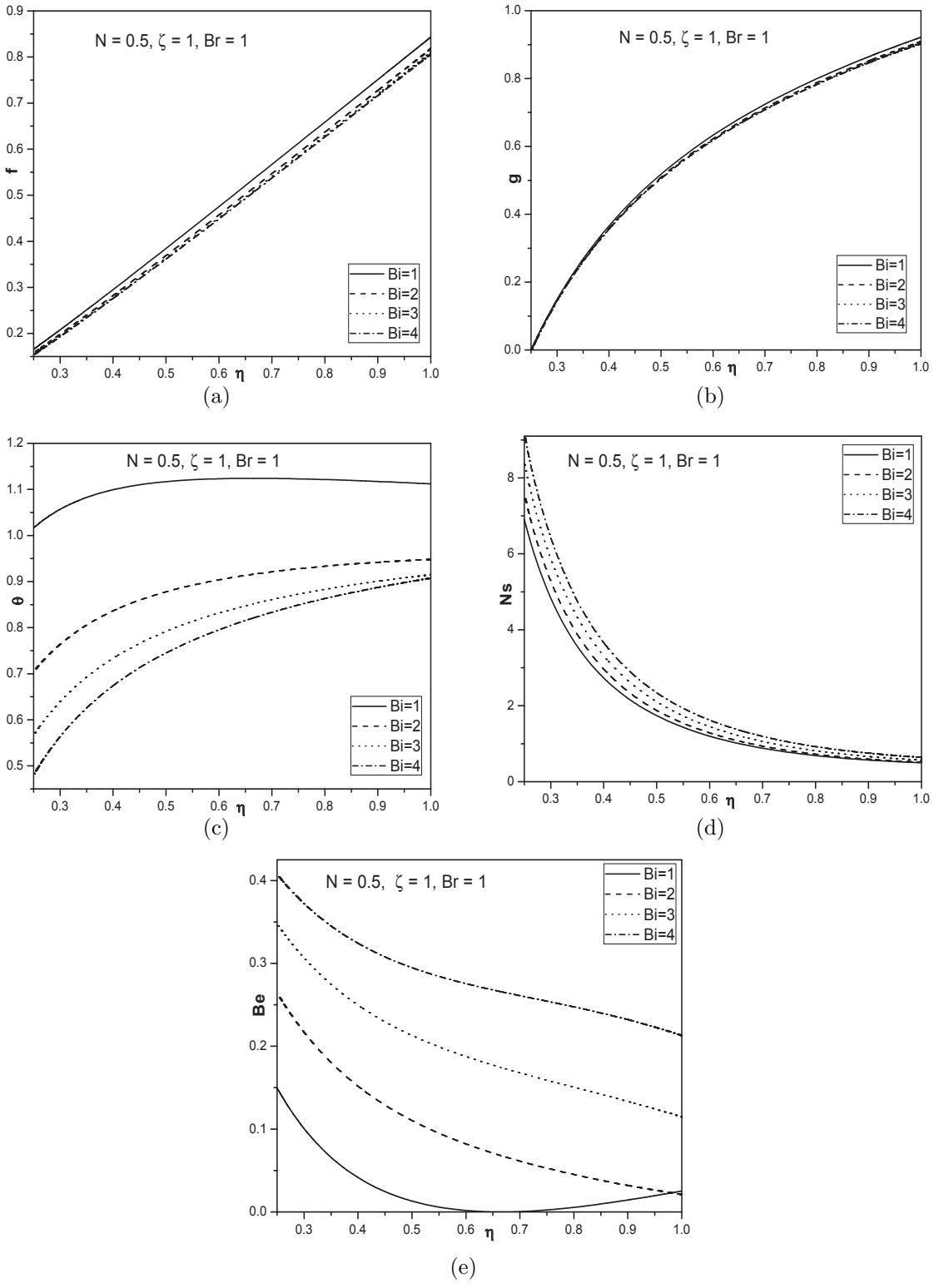

Figure 6.8: Effect of Biot number on (a)velocity, (b)microrotation, (c)temperature, (d)entropy generation and (e)Bejan number.

Chapter 7

Analysis of Entropy Generation between Porous Concentric Cylinders due to Micropolar Fluid Flow [1]

7.1 Introduction

In the present decade, the entropy generation analysis has been the topic of great interest in view of its applications in many fields such as electronics cooling, heat exchangers, porous media, turbo machinery and combustion. The optimization of thermal systems has been received a unique attention. Thermal systems have been analyzed and optimized using the second law of thermodynamics. The second law of thermodynamics states that the Exergy(available energy) is always destroyed partially or totally and the destroyed amount of energy is proportional to the entropy generation.

Even though there are various sources for entropy generation in engineering systems the main sources are heat transfer, viscous dissipation, electrical conduction and chemical reaction. Bejan [12, 13] investigated the different factors behind the entropy generation in applied thermal engineering, where the destruction of available work of a system occurs during the generation of entropy. Assad and Oztop [8] presented the effect of internal heat generation on entropy generation between two

[1] Case(a): Communicated to "**Journal of Taiwan Institute of Chemical Engineers**", Case(b) Published in "**Energy, 111 (2016) 165-177**"

rotating cylinders. Mazgar *et al* [73] presented entropy generation due to the interaction between thermal radiation and mixed convection in a semi-transparent and non-gray gas, bounded by two vertical coaxial cylinders.

In the previous chapter, the entropy generation analysis of micropolar fluid flow between concentric cylinders was studied. In this chapter, the problem of entropy generation is undertaken for the micropolar fluid flow through porous concentric cylinders with magneto hydrodynamic effect. Specifically, the investigations focus on the effect of different parameters on the components of velocity, microrotation, temperature, entropy generation and Bejan number.

7.2 Mathematical Formulation

Consider the electrically conducting micropolar fluid flow between two horizontal porous coaxial rotating cylinders(see Fig. 7.1). The following assumptions are made to formulate the present problem.

1. The flow is steady, laminar, incompressible and axisymmetric.
2. The fluid motion is due to the rotation of the cylinders.
3. The rate of flow through the walls is uniformly equal for both cylinders such that the rate of injection is equal to the rate of suction.
4. The radii and angular velocities of the inner and outer cylinders are r_1, Ω_1 and r_2, Ω_2 $(r_1 < r_2)$, respectively.
5. A constant magnetic field of strength B_0 is imposed transversely in the r-direction. The magnetic Reynolds number is very small, so that induced magnetic field can be neglected in comparison to the applied magnetic field.

With the above assumptions the equations governing the micropolar fluid flow [41, 20] are

$$\frac{\partial u}{\partial r} + \frac{u}{r} = 0 \tag{7.1}$$

$$\rho \left[u\frac{\partial u}{\partial r} - \frac{v^2}{r} \right] = -\frac{\partial p}{\partial r} \tag{7.2}$$

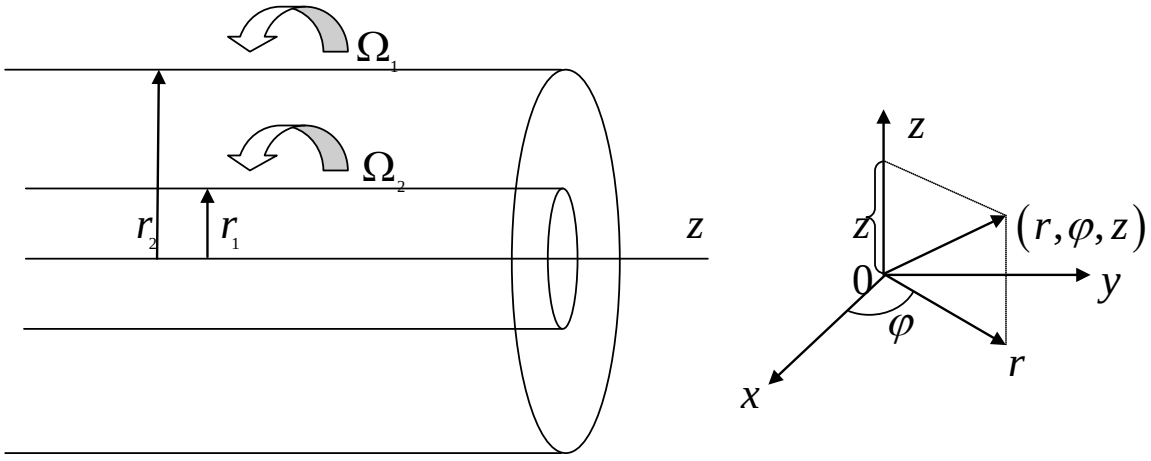

Figure 7.1: Schematic diagram of the problem

$$\rho\left[u\frac{\partial v}{\partial r}+\frac{uv}{r}\right]=(\mu+\kappa)\left[\frac{\partial^2 v}{\partial r^2}+\frac{1}{r}\frac{\partial v}{\partial r}-\frac{v}{r^2}\right]-\kappa\frac{\partial \sigma}{\partial r}-\sigma_e B_0^2 v \tag{7.3}$$

$$\frac{\partial p}{\partial z}=0 \tag{7.4}$$

$$\rho j^* u\frac{\partial \sigma}{\partial r}=\kappa\left[\frac{\partial v}{\partial r}+\frac{v}{r}\right]-2\kappa\sigma+\gamma\left[\frac{\partial^2 \sigma}{\partial r^2}+\frac{1}{r}\frac{\partial \sigma}{\partial r}\right] \tag{7.5}$$

$$\rho C_p u\frac{\partial T}{\partial r}=K_f\left[\frac{\partial^2 T}{\partial r^2}+\frac{1}{r}\frac{\partial T}{\partial r}\right]+(2\mu+\kappa)\left[2\frac{u^2}{r^2}+\frac{1}{2}\left(\frac{\partial v}{\partial r}-\frac{v}{r}\right)^2\right]+2\kappa\left[\frac{1}{2}\left(\frac{\partial v}{\partial r}+\frac{v}{r}\right)-\sigma\right]^2+\gamma\left(\frac{\partial \sigma}{\partial r}\right)^2 \tag{7.6}$$

Eq. (7.4) states that the condition of uniform pressure distribution along the axis of the cylinders. Simplifying Eqs. (7.1) and (7.2) to get

$$\rho\left(\frac{u^2+v^2}{r}\right)=\frac{\partial p}{\partial r} \tag{7.7}$$

Eq. (7.7) gives the Bernoulli's type pressure variation in the radial direction, which will not be discussed further in the present investigation. Integration of Eq. (7.1) gives

$$ru(r)=\text{constant} \tag{7.8}$$

consider u_1,u_2 are the radial velocities of the inner and outer cylinders

$$u_2 r_2=u_1 r_1 \tag{7.9}$$

Simplifying Eqs. (7.8) and (7.9) give

$$ur=u_2 r_2=u_1 r_1 \tag{7.10}$$

Substitute (7.10) in (7.3), to get

$$\frac{R}{r}\left[\frac{dv}{dr}+\frac{v}{r}\right]=\frac{1}{1-N}\left[\frac{d^2v}{dr^2}+\frac{1}{r}\frac{dv}{dr}-\frac{v}{r^2}\right]-\frac{N}{1-N}\frac{d\sigma}{dr}-\frac{\sigma_e B_0^2}{\mu}v \tag{7.11}$$

Introducing the following dimensionless quantities

$$\eta=\frac{r}{r_1},\quad f=\frac{vr_1}{\nu},\quad g=\frac{\sigma r_1^2}{\nu},\quad \theta=\frac{T-T_1}{T_2-T_1} \tag{7.12}$$

in equations (7.11), (7.5) and (7.6) to get the following non-linear system of differential equations

$$\frac{1}{1-N}f''+\left(\frac{1}{1-N}-R\right)\frac{1}{\eta}f'-\left(\frac{1}{1-N}+R+\eta^2Ha^2\right)\frac{f}{\eta^2}-\frac{N}{1-N}g'=0 \tag{7.13}$$

$$\frac{N(2-N)}{m^2(1-N)}g''+\left[\frac{N(2-N)}{m^2(1-N)}-R\,a_j\right]\frac{g'}{\eta}-\frac{2N}{1-N}g+\frac{N}{1-N}\left(f'+\frac{f}{\eta}\right)=0 \tag{7.14}$$

$$\begin{aligned}\theta''+\frac{(1-RPr)}{\eta}\theta'+\frac{Br}{1-N}\Bigg\{(2-N)\left[\frac{2}{\eta^4}+\frac{1}{2R^2}\left(f'-\frac{f}{\eta}\right)^2\right]+\frac{2N}{R^2}\left[\frac{1}{2}\left(f'+\frac{f}{\eta}\right)-g\right]^2\\ +\frac{N(2-N)}{m^2R^2}g'^2\Bigg\}=0\end{aligned} \tag{7.15}$$

where $R=\frac{u_1r_1}{\nu}$ is the cross flow Reynolds number, $Ha=B_0r_1\sqrt{\frac{\sigma_e}{\mu}}$ is the Hartman number.

In this chapter, the analysis was done for fluid subjected to two types of boundary conditions, given in the previous chapter.

7.2.1 Case(a): No-slip and Isothermal Boundary Conditions

In this case, it is assumed that the two cylinders are rotating with angular velocities Ω_1 and Ω_2. Also the inner and outer cylinders are maintained at uniform temperatures T_1 and T_2 respectively. Thus, the boundary conditions are

$$\begin{aligned}v=r_1\Omega_1,\quad \sigma=\frac{1}{2r}\frac{\partial}{\partial r}(rv),\quad T=T_1,\quad \text{at}\quad r=r_1\\ v=r_2\Omega_2,\quad \sigma=\frac{1}{2r}\frac{\partial}{\partial r}(rv),\quad T=T_2,\quad \text{at}\quad r=r_2\end{aligned} \tag{7.16}$$

The corresponding boundary conditions in dimensionless form are:

$$\begin{aligned}f=P_1,\quad g=\frac{1}{2}\left(f'+\frac{f}{\eta}\right),\quad \theta=0,\quad \text{at}\quad \eta=1\\ f=P_2,\quad g=\frac{1}{2}\left(f'+\frac{f}{\eta}\right),\quad \theta=1,\quad \text{at}\quad \eta=\frac{r_2}{r_1}\end{aligned} \tag{7.17}$$

where $P_1 = \frac{r_1^2\Omega_1}{\nu}$ and $P_2 = \frac{r_1 r_2 \Omega_2}{\nu}$ are constants. Consider $r_1 = 0.5$ and $r_2 = 1$. The Quasilinearization method is used to convert the non-linear boundary value problems (7.13) - (7.15) to the system of linear differential equations. The resultant equations are solved using the Chebyshev spectral collocation method, which is described in detail in chapter-2. Proceeding as in chapter-2, the solution is obtained from the following matrix equation.

$$\mathbf{X}_{r+1} = \mathbf{A}_r^{-1}\mathbf{B}_r \tag{7.18}$$

Entropy Generation

Once the velocity, microrotation, and temperature fields have been obtained, the entropy generation distribution can be determined in a flow channel. This function, which characterizes the irreversible behavior of the system, will be used to optimize(minimize) the entropy generation rate by evaluating parameters as well as fluid properties. For the present study, the volumetric rate of entropy generation reduces to

$$S_G = \frac{K_f}{T_1^2}\left(\frac{\partial T}{\partial r}\right)^2 + \frac{2\mu+\kappa}{T_1}\left[\frac{2u^2}{r^2} + \frac{1}{2}\left(\frac{\partial v}{\partial r} - \frac{v}{r}\right)^2\right] + \frac{2\kappa}{T_1}\left[\frac{1}{2}\left(\frac{\partial v}{\partial r} + \frac{v}{r}\right) - \sigma\right]^2 + \frac{\gamma}{T_1}\left(\frac{\partial \sigma}{\partial r}\right)^2 + \frac{\sigma_e B_0^2}{T_1}v^2$$

The dimensionless entropy generation number is given by

$$N_s = \overbrace{\theta'^2}^{N_h} + \underbrace{\frac{Br}{T_p R^2(1-N)}\left\{(2-N)\left[\frac{2R^2}{\eta^4} + \frac{1}{2}\left(f' - \frac{f}{\eta}\right)^2\right] + 2N\left[\frac{1}{2}\left(f' + \frac{f}{\eta}\right) - g\right]^2 + \frac{N(2-N)}{m^2}g'^2\right\}}_{N_v}$$

$$+ \overbrace{\frac{Br}{T_p}\frac{Ha^2}{R^2}f^2}^{N_m} \tag{7.19}$$

The convective heat transfer processes are analyzed by the second law of thermodynamics namely entropy generation due to the irreversibility of the processes. In convective heat transfer, both fluid friction and heat transfer make contributions to the rate of entropy generation. Entropy generation number (Ns) is useful for generating entropy generation profiles, but it fails to give any

idea about the relative importance of friction and heat transfer effects. Therefore, an alternative parameter Bejan number (Be) is introduced for this purpose, which is the ratio of entropy generation due to heat transfer to the overall entropy generation.

$$Be = \frac{N_h}{N_h + N_v + N_m} \tag{7.20}$$

Results and Discussion

The micropolar fluid flow through a horizontal porous concentric cylindrical annulus is studied in this chapter. Entropy generation in the flow field due to heat transfer, fluid friction and magnetic field is formulated. The influence of various parameters on velocity, microrotation, temperature, entropy generation and Bejan number are examined. To study the effects of N, Ha, R and Br, computations were carried out by taking $r_1 = 0.5$, $r_2 = 1$, $P_1 = 0.5$, $P_2 = 1$, $m = 2$, $Pr = 1$, $a_j = 0.001$ and $T_p = 1$.

Fig. 7.2, presents the effect of coupling number (N) on non-dimensional velocity, microrotation, temperature, entropy generation and Bejan number. Fig. 7.2(a) shows that the velocity increases as N increases. Fig. 7.2(b) depicts that the microrotation component increases at the inner cylinder and decreases at the outer cylinder with an increase in the value of N. Fig. 7.2(c) reveals that as N increases temperature increases. In Fig. 7.2(d) it is observed that the entropy generation increases as coupling number increases. Fig. 7.2(e) reveals that the Bejan number Be decreases with an increase in the value of coupling number and Be increases in the region very close to the inner cylinder.

The variation of Hartman number on velocity, microrotation, temperature, entropy generation and Bejan number is displayed in Fig. 7.3. It is observed from Fig. 7.3(a) that the velocity decreases as Hartman number Ha increases. As the imposing magnetic field is normal to the flow direction, the resistive force, and the fluid movement reduces. Fig. 7.3(b) depicts that, the microrotation component decreases near the inner cylinder and increases near the outer cylinder with an increase in the value of Ha, thus showing a reverse rotation near the two boundaries. From Fig. 7.3(c), it is observed that the temperature increases as Hartman number increases. As seen from Fig. 7.3(d) an increase in the Hartmann number leads to increase in the entropy generation number near the

walls of the cylinders whereas the less contribution of Ns in the middle of the two cylinders due to the small temperature gradient in this region. The distribution of the Bejan number Be in Fig. 7.3(e) explains that the viscous dissipation contribution (N_v), which decreases near the walls with an increase in the magnetic parameter (Ha). From Eq. (7.19) it is noticed that there is no effect of magnetic field on the temperature field and so N_h remains constant. Thus, from the Bejan number definition (see Eq. (7.20)), with a decrease of N_v, Bejan number will increase.

Fig. 7.4, presents the influence of cross flow Reynolds number on velocity, microrotation, temperature, entropy generation and Bejan number. It is observed from Fig. 7.4(a) that the velocity decreases with the increase of cross flow Reynolds number. It is seen from Fig. 7.4(b) that the microrotation component decreases near the inner cylinder and increases near the outer cylinder with an increase in the value of a cross flow Reynolds number. Fig. 7.4(c) shows that as R increases, temperature decreases. It is noticed from Figs. 7.4(d) and 7.4(e) that the entropy generation and Bejan number decreases near the inner cylinder and increases near the outer cylinder as R increases.

The variation of temperature, entropy generation and Bejan number with Brinkman number is displayed in Fig. 7.5. The parameter Br determines a relative importance of viscous effects and has a significant effect on entropy generation. Fig. 7.5(a) shows an increase in temperature with Brinkman number. It is observed from Fig. 7.5(b) that the entropy generation increases with an increase in the value of Brinkman number. Due to the higher gradient of temperature, velocity, the entropy generation number is high in magnitude near the inner cylinder. The effect of Brinkman number on Bejan number is shown in Fig. 7.5(c). As it can be seen from the figure that the Bejan number decreases with increase in Br, except at the boundaries.

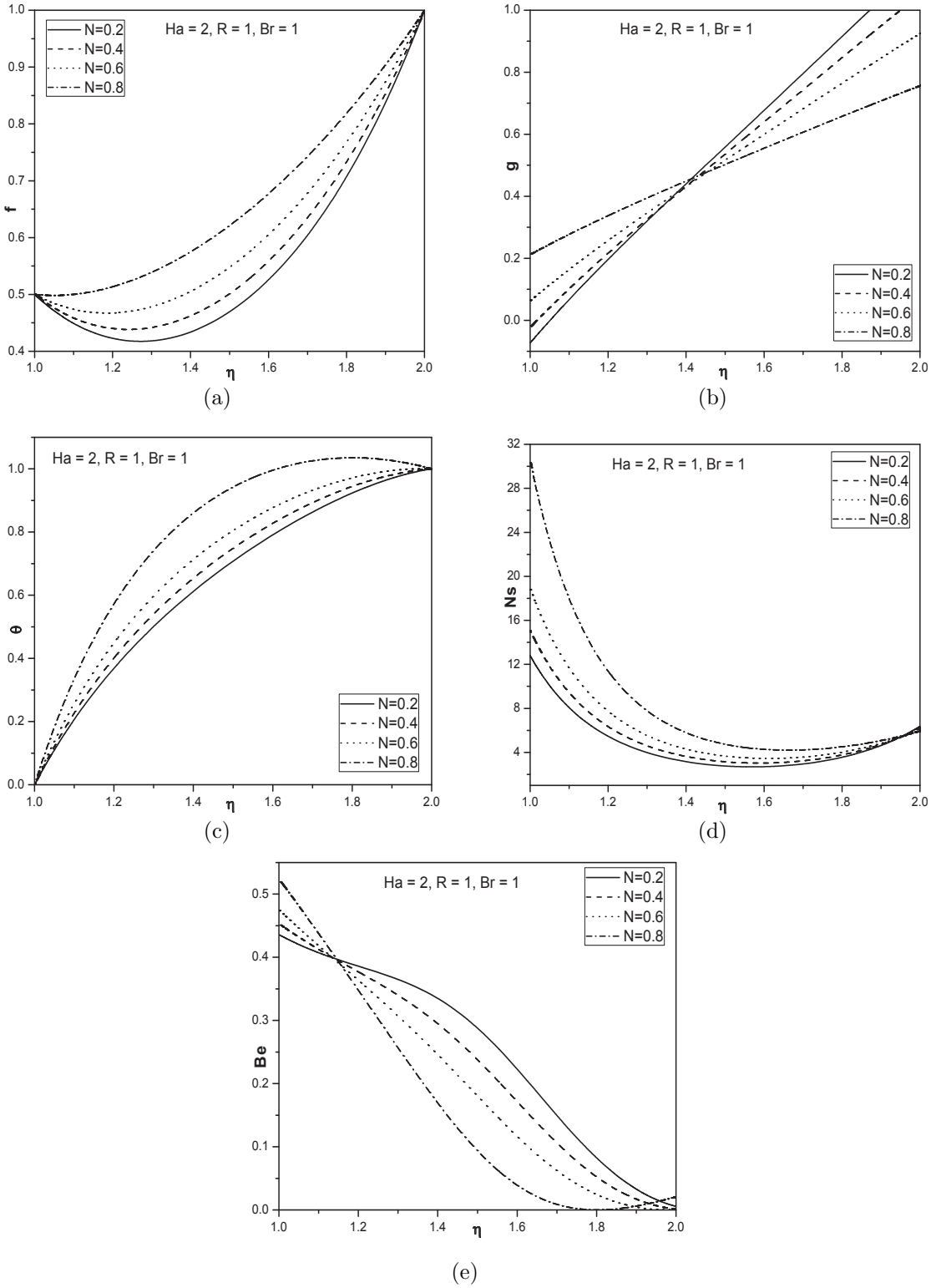

Figure 7.2: Effect of coupling number on (a)velocity, (b)microrotation, (c)temperature, (d)entropy generation and (e)Bejan number.

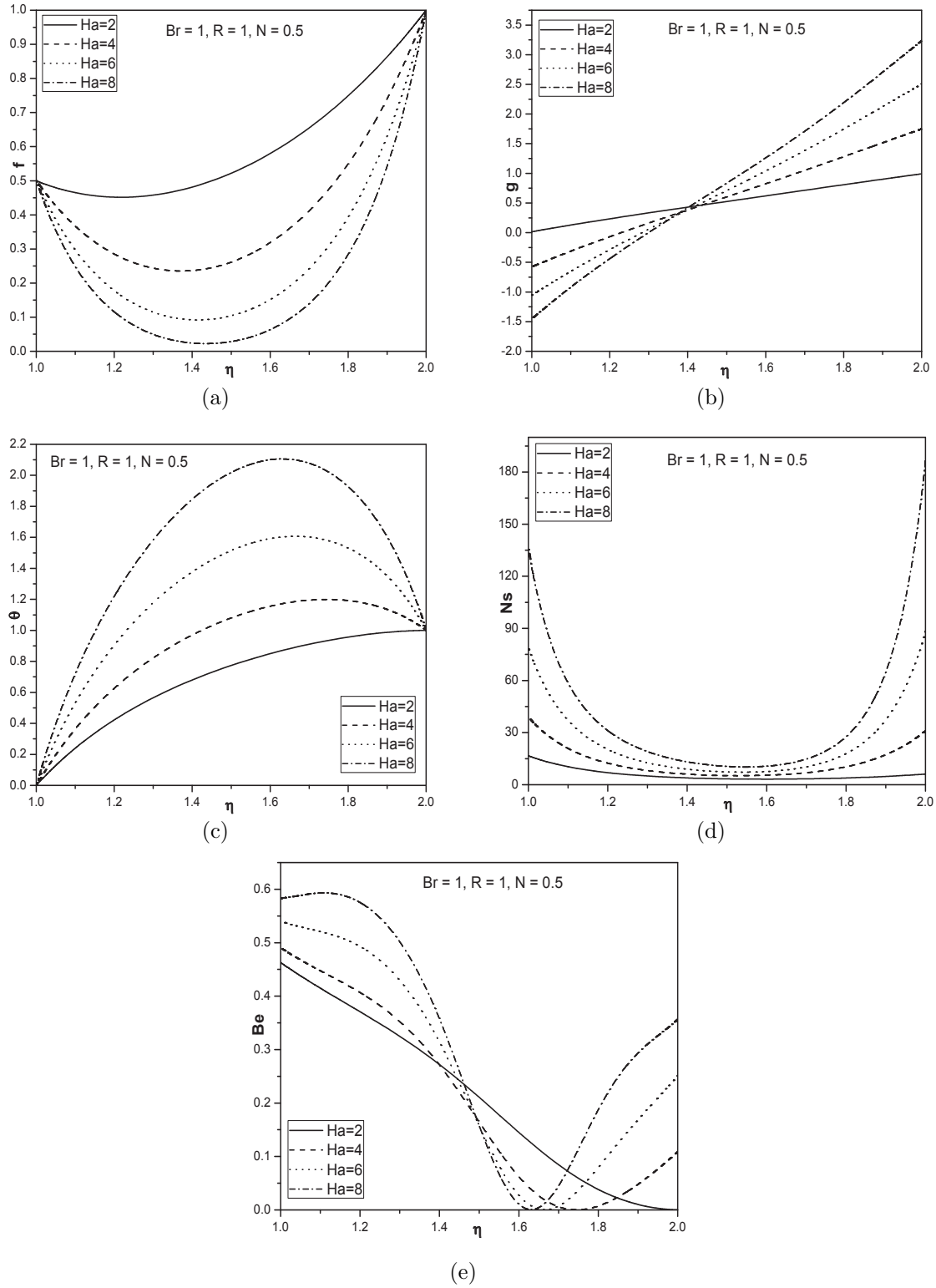

Figure 7.3: Effect of Hartman number on (a)velocity, (b)microrotation, (c)temperature, (d)entropy generation and (e)Bejan number.

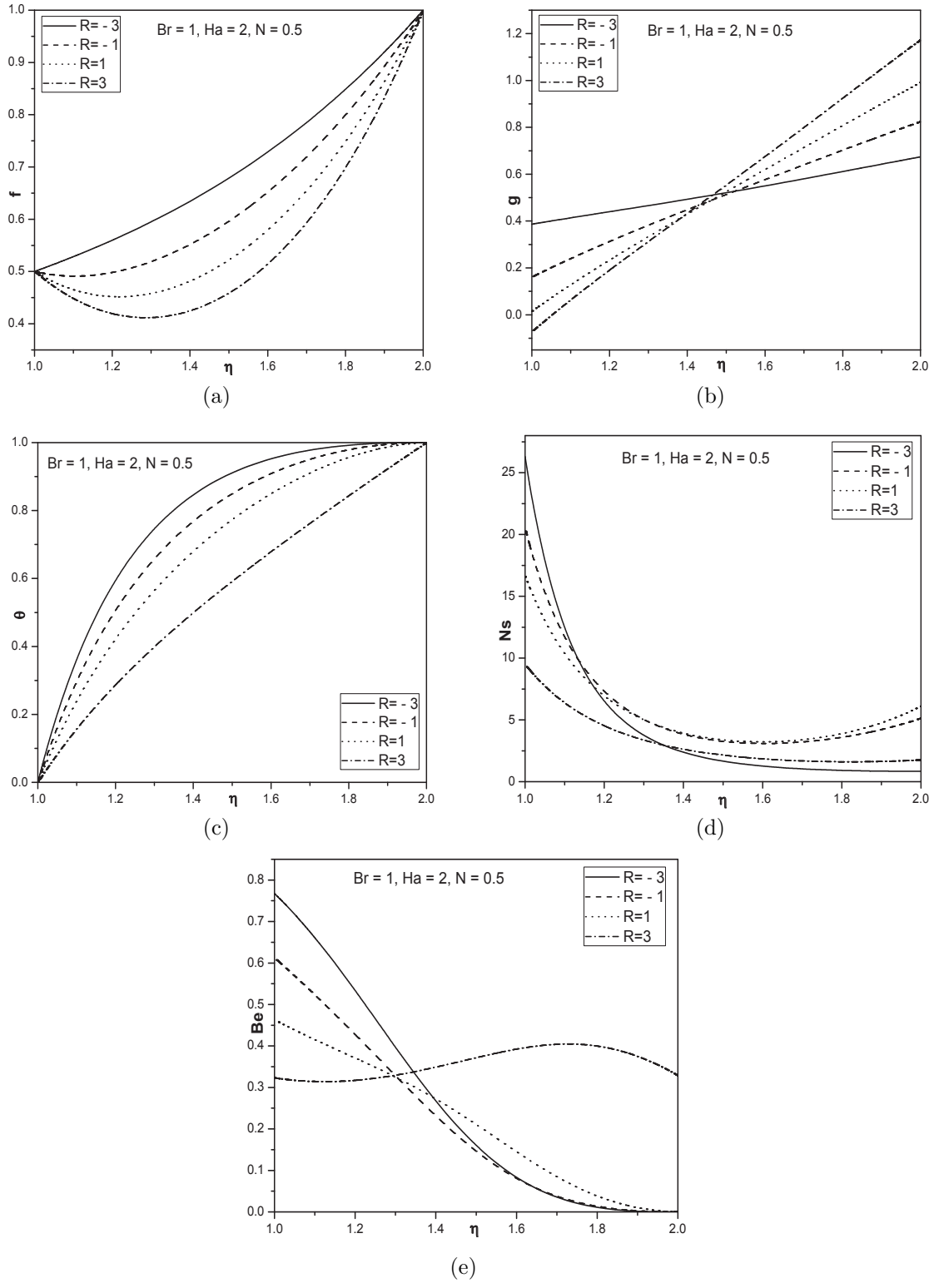

Figure 7.4: Effect of cross flow Reynolds number on (a)velocity, (b)microrotation, (c)temperature, (d)entropy generation and (e)Bejan number.

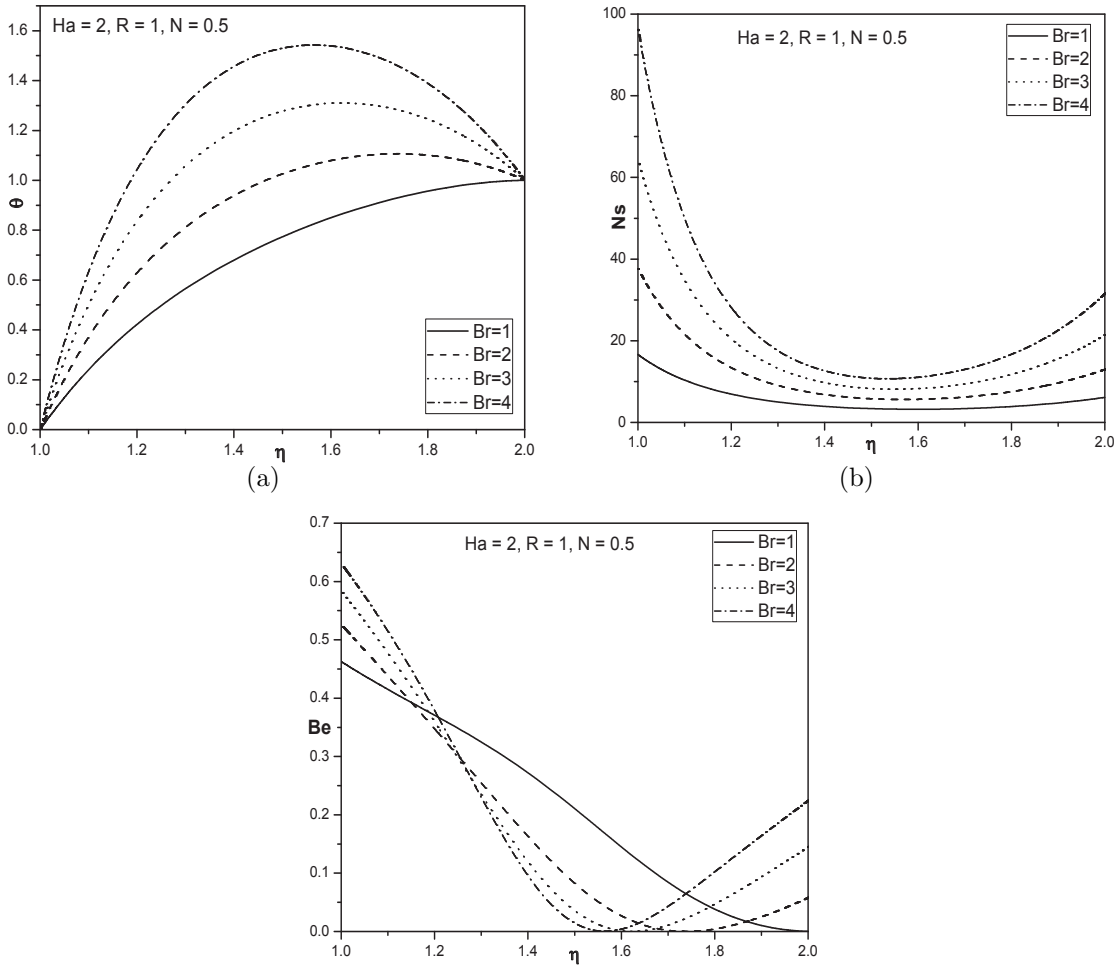

Figure 7.5: Effect of Brinkman number on (a)velocity, (b)microrotation, (c)temperature, (d)entropy generation and (e)Bejan number.

7.2.2 Case(b): Slip and Convective Boundary Conditions

Assume that the fluid slips at the inner and outer cylinders. Let the inner cylinder is heated by convection from a hot fluid with temperature T_2 which provides a heat transfer coefficient h_1 while the outer cylinder losses heat to the ambient with a heat transfer coefficient h_2. Thus, the boundary conditions are

$$\begin{aligned} v &= r_1\Omega_1 + \zeta'\left[\frac{\partial v}{\partial r} - \frac{v}{r}\right], \quad \sigma = \frac{1}{2r}\frac{\partial}{\partial r}(rv), \quad K_f\frac{\partial T}{\partial r} - h_1(T - T_1) = 0 \quad \text{at} \quad r = r_1 \\ v &= r_2\Omega_2 - \zeta'\left[\frac{\partial v}{\partial r} - \frac{v}{r}\right], \quad \sigma = \frac{1}{2r}\frac{\partial}{\partial r}(rv), \quad K_f\frac{\partial T}{\partial r} + h_2(T - T_2) = 0 \quad \text{at} \quad r = r_2 \end{aligned} \tag{7.21}$$

where ζ' slip length of the inner and outer cylinders.

The corresponding dimensionless boundary conditions are:

$$\begin{aligned} f &= P_1 + \zeta\left(f' - \frac{f}{\eta}\right), \quad g = \frac{1}{2}\left(f' + \frac{f}{\eta}\right), \quad \theta' - Bi_1\theta = 0, \quad \text{at} \quad \eta = 1 \\ f &= P_2 - \zeta\left(f' - \frac{f}{\eta}\right), \quad g = \frac{1}{2}\left(f' + \frac{f}{\eta}\right), \quad \theta' + Bi_2\theta = Bi_2, \quad \text{at} \quad \eta = \frac{r_2}{r_1} \end{aligned} \tag{7.22}$$

where $P_1 = \frac{r_1^2\Omega_1}{\nu}$ and $P_2 = \frac{r_1 r_2\Omega_2}{\nu}$ are constants, $\zeta = \frac{\zeta'}{r_1}$ is the slip parameter and $Bi_k = \frac{hr_i}{K_f}$ is the Biot number for each cylinder. Subindexes $k = 1, 2$ refer to the inner and outer cylinders respectively. In general, Biot number is assumed to be same for the inner and outer cylinders. Proceeding as in Case(a), the solution is obtained from the following matrix equation

$$\mathbf{X}_{r+1} = \mathbf{A}_r^{-1}\mathbf{B}_r \tag{7.23}$$

The entropy generation and Bejan number have been calculated for the slip and convective boundary conditions from equations (7.19) and (7.20).

Results and Discussion

The micropolar fluid flow through a horizontal porous concentric cylinders associated with slip and convective boundary conditions are studied in this case. Entropy generation in the flow field due to heat transfer, fluid friction and magnetic field is formulated. The influence of various parameters

on velocity, microrotation, temperature, entropy generation and Bejan number is examined. To study the effects of N, ζ, Ha, R, Bi and Br, computations were carried out by taking $r_1 = 0.5$, $r_2 = 1$, $P_1 = 0.5$, $P_2 = 1$, $m = 2$, $Pr = 1$, $a_j = 0.001$ and $T_p = 1$.

Fig. 7.6, presents the effect of coupling number (N) on non-dimensional velocity, microrotation, temperature, entropy generation and Bejan number. Fig. 7.6(a) shows that the velocity increases as N increases. Fig.7.6(b) depicts that the microrotation component increases with increase in value of N. Fig. 7.6(c) reveals that as N increases temperature increases. The same effect is seen on the entropy generation in Fig. 7.6(d). Fig. 7.6(e) reveals that the Bejan number Be increases at the walls of the cylinders with an increase in the value of coupling number. The Bejan number $Be = 0$ at the interior of annulus indicates that the domination of fluid friction irreversibility due to rotation of the cylinders.

In Fig. 7.7(a) it is observed that an increase in the slip parameter ζ at the cylinders causes a decrease in velocity at injection and suction while a large decrease in the fluid velocity is noticed with a high rate of flow reversal at the suction wall. The decreasing nature of microrotation and temperature is observed to increase in the value of slip parameter as seen in Figs. 7.7(b) and 7.7(c). Fig. 7.7(d) shows that the entropy generation number decreases as ζ increases. Since the effect of slip reduces the velocities and velocity gradients. This results in a decrease in viscous contribution to the entropy generation. Fig. 7.7(e) describes the effect of ζ on Bejan number. It is noticed that the Bejan number at the suction wall of the annulus increases, leads to increasing the influence of heat transfer irreversibility when compared to the fluid friction irreversibility at the outer cylinder.

It is observed from Fig. 7.8(a) that the velocity decreases with an increase in the value of Hartman number Ha. As the imposing magnetic field is normal to the flow direction, it causes the resistive force, thus reducing the fluid movement. Fig. 7.8(b) depicts that, the microrotation component decreases with an increase in the value of Ha. From Fig. 7.8(c), it is observed that the temperature increases as Hartman number increases. As seen from Fig. 7.8(d) an increase in the Hartmann number leads to increase in the entropy generation number. The distribution of the Bejan number Be is shown in Fig. 7.8(e). The Bejan number at injection wall increases while it decreases at the suction wall leading to the increase in the influence of heat transfer irreversibility at the inner cylinder and fluid friction irreversibility at the outer cylinder.

Fig. 7.9, presents the influence of a cross flow Reynolds number of velocity, microrotation,

temperature, entropy generation and Bejan number. It is observed from Fig. 7.9(a) that the velocity decreases with the increase of cross flow Reynolds numbers. It is seen from Fig. 7.9(b) that the microrotation component decreases with an increase in the value of a cross flow Reynolds number. Fig. 7.9(c) shows that as R increases, temperature increases at the suction wall of the annulus. It is noticed from Fig. 7.9(d) that the entropy generation increases as cross flow Reynolds number increases. From Fig. 7.9(e) it is observed that the Bejan number increases near the inner cylinder and decreases near the outer cylinder as R increases.

Fig. 7.10(a) describes the effect of increasing Bi on the temperature. The fluid temperature decreases as increase in Biot number indicates a rise in convective cooling due to heat loss to the ambient surrounding from the annulus walls. It is noticed from Fig. 7.10(b) that the entropy generation Ns increases with an increase in the Biot number. Ns profiles are similar in shape and are almost parallel to one another, for all the parameters, but they vary in magnitude. In Fig. 7.10(c) the dominant influence of heat transfer irreversibility is observed as the parameter values of Bi increases consequently thus the Bejan number increases. Hence, the convective thermal boundary conditions enhance the dominant effects of heat transfer irreversibility on the flow system.

The variation of temperature, entropy generation and Bejan number with Brinkman number is displayed in Fig. 7.11. The parameter Br determines a relative importance of viscous effects and has a significant effect on entropy generation. Fig. 7.11(a) shows an increase in temperature with Brinkman number. It is observed from Fig. 7.11(b) that the entropy generation increases with an increase in the value of Brinkman number. Due to the higher gradient of temperature and velocity, the entropy generation number is high in magnitude near the inner cylinder. The effect of Brinkman number on Bejan number is shown in Fig. 7.11(c). As it can be seen from the figure that the Bejan number increases with increase in Br.

7.3 Conclusions

In this chapter, the problem of entropy generation due to steady, laminar incompressible micropolar fluid flow through horizontal porous concentric cylinders with magnetic effect is investigated. This problem is solved for two types of boundary conditions Case (a) No-slip and isothermal boundary conditions and Case (b) slip and convective boundary conditions. The following conclusions can

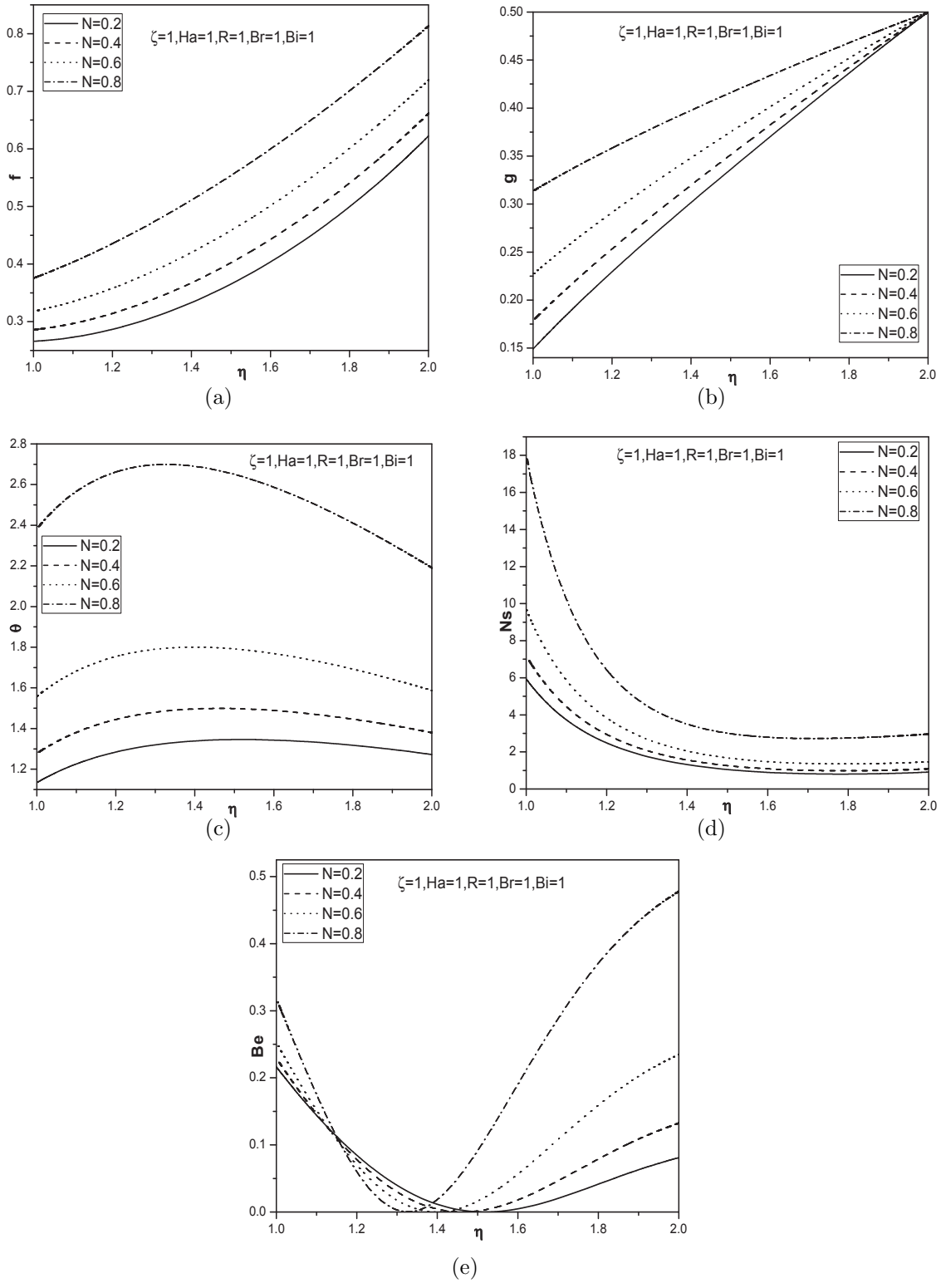

Figure 7.6: Effect of coupling number on (a)velocity, (b)microrotation, (c)temperature, (d)entropy generation and (e)Bejan number.

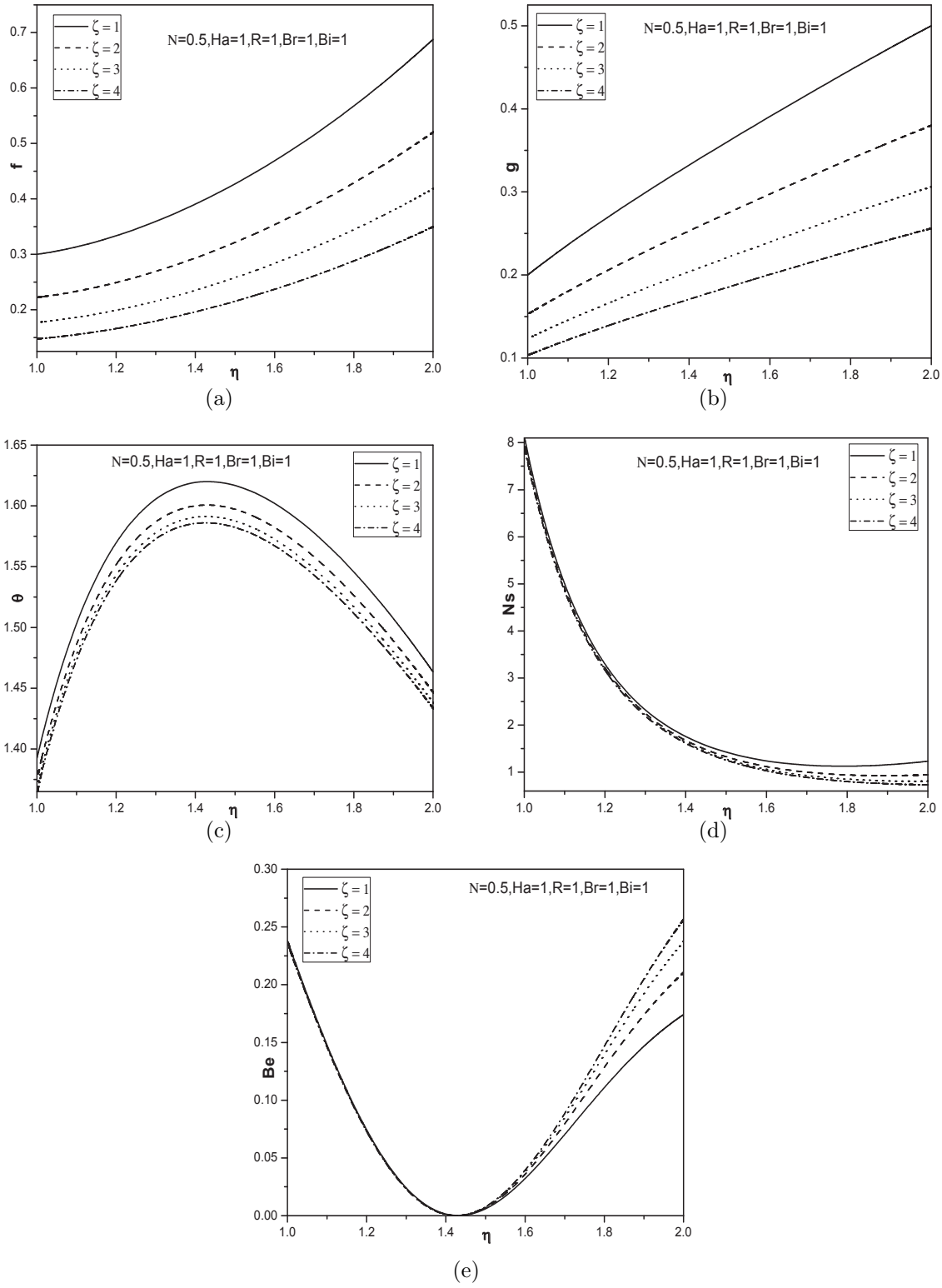

Figure 7.7: Effect of slip parameter on (a)velocity, (b)microrotation, (c)temperature, (d)entropy generation and (e)Bejan number.

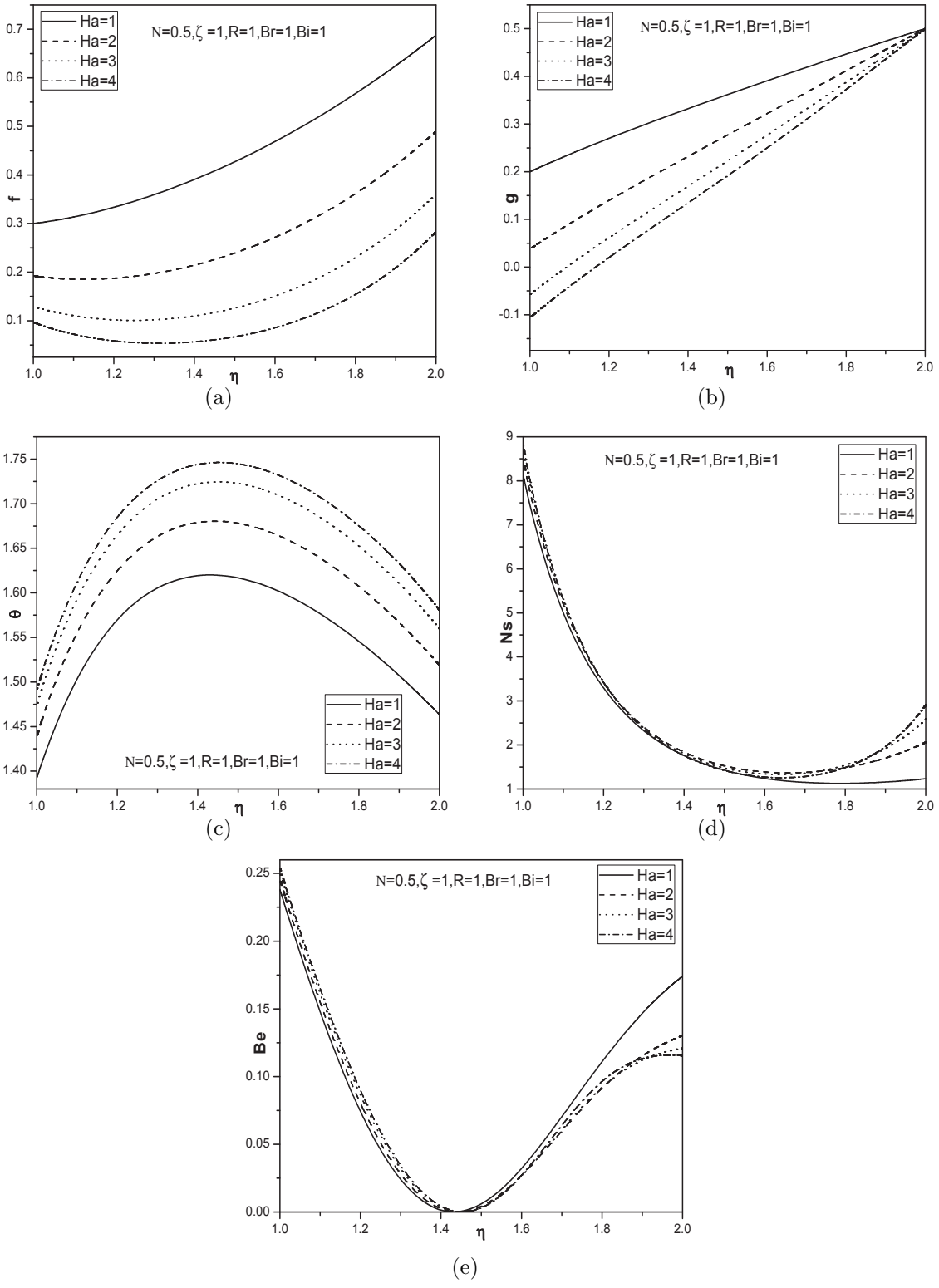

Figure 7.8: Effect of Hartman number on (a)velocity, (b)microrotation, (c)temperature, (d)entropy generation and (e)Bejan number.

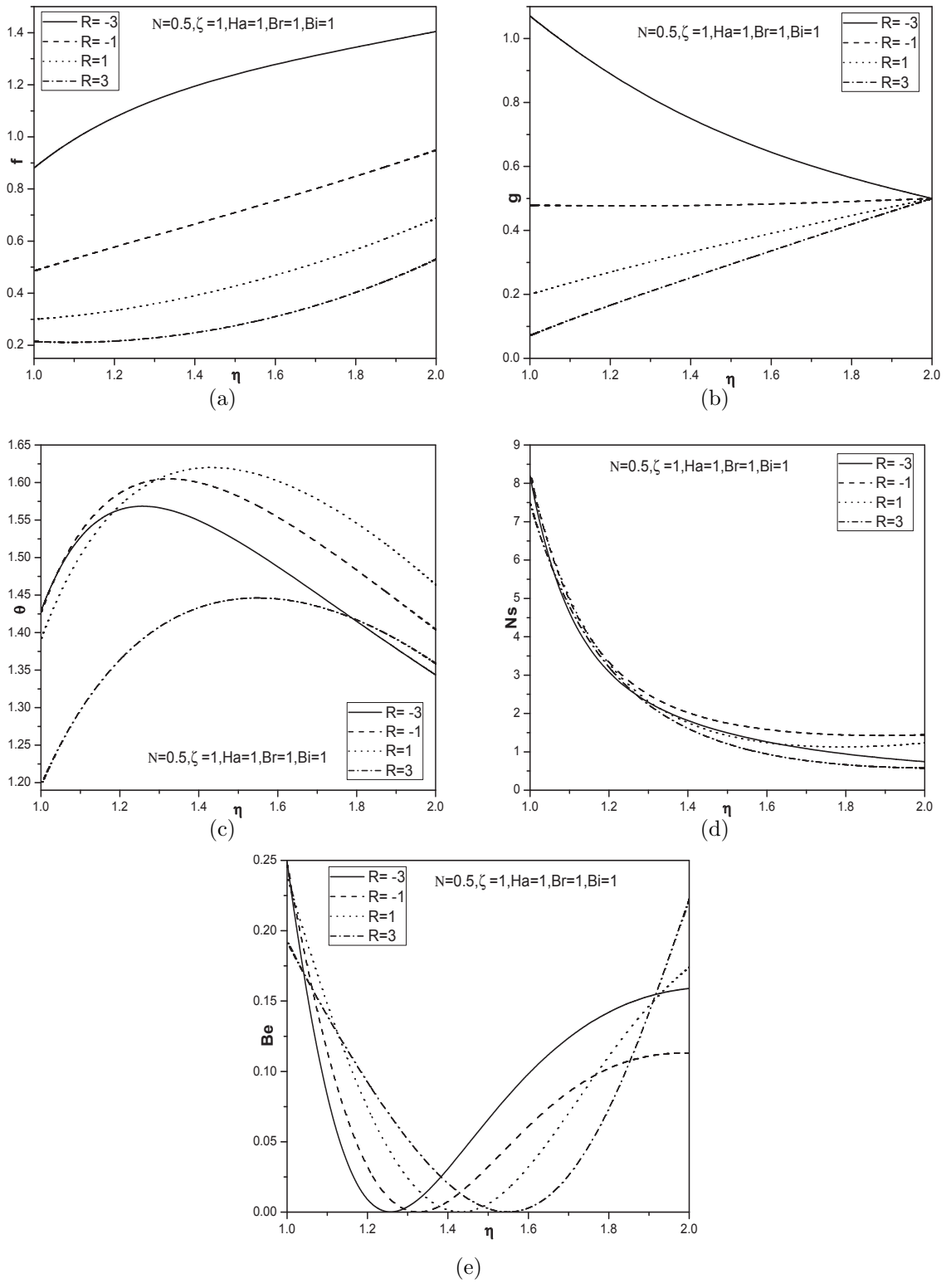

Figure 7.9: Effect of cross flow Reynolds number on (a)velocity, (b)microrotation, (c)temperature, (d)entropy generation and (e)Bejan number profiles.

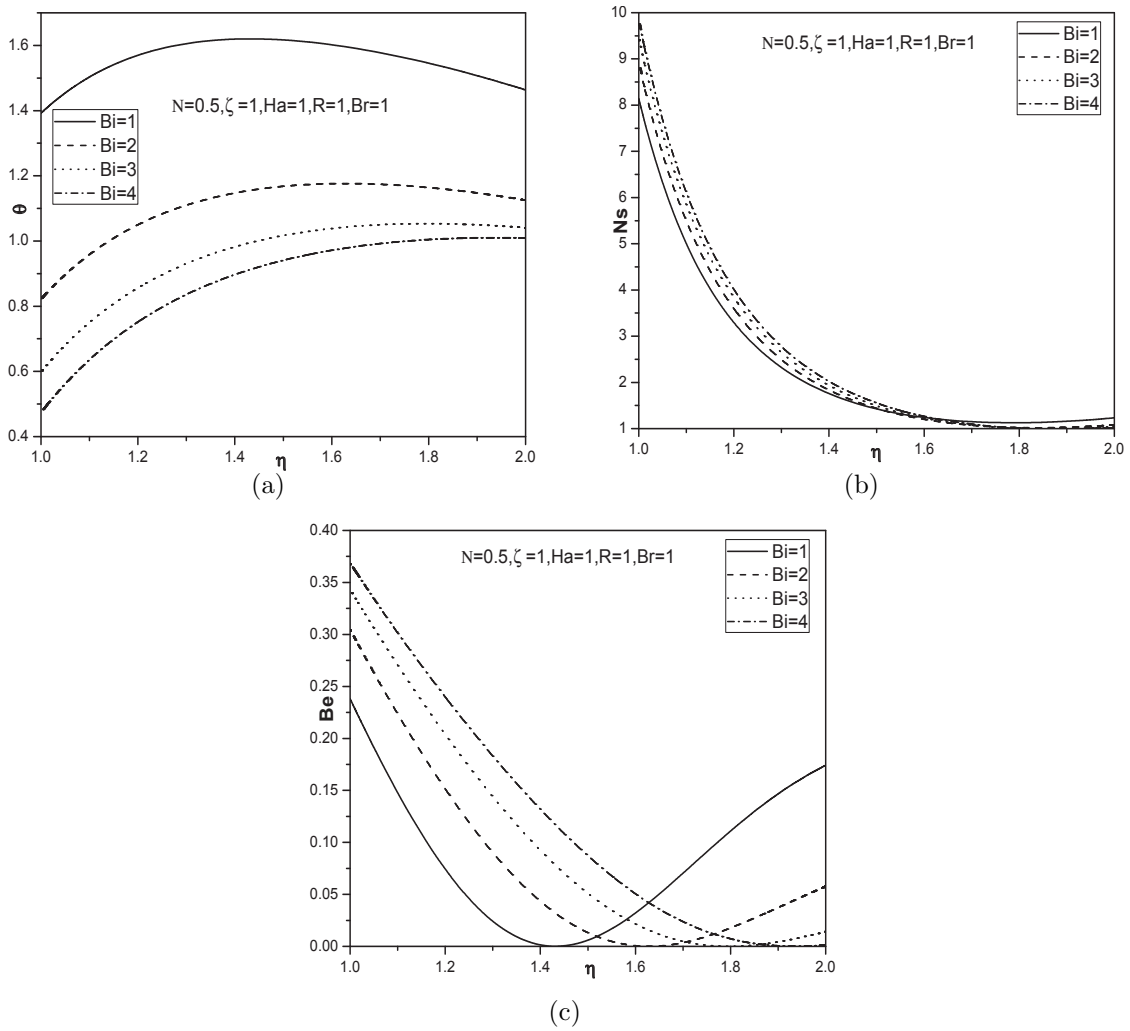

Figure 7.10: Effect of Biot number on (a)velocity, (b)microrotation, (c)temperature, (d)entropy generation and (e)Bejan number.

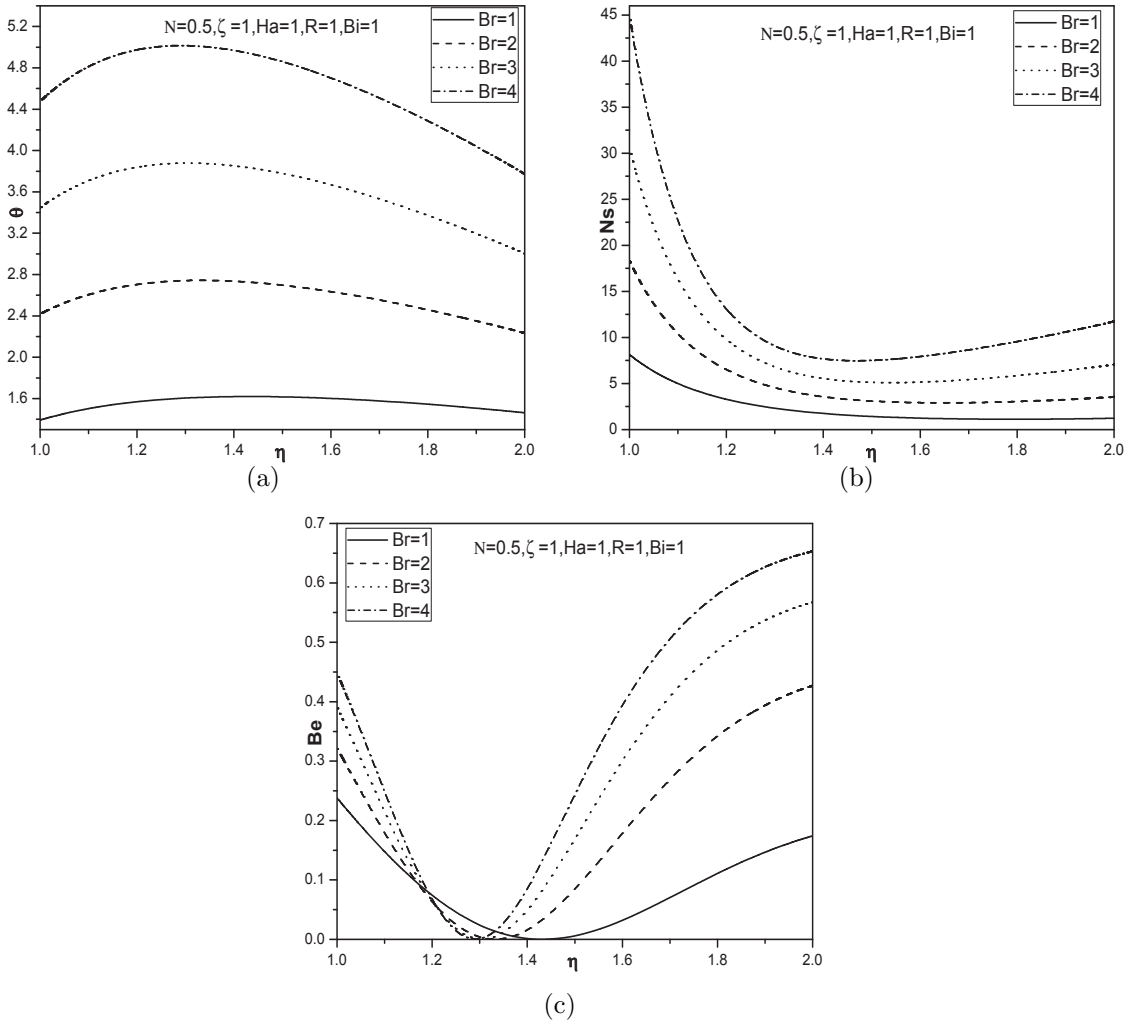

Figure 7.11: Effect of Biot number on (a)velocity, (b)microrotation, (c)temperature, (d)entropy generation and (e)Bejan number.

be drawn for both the cases (a) and (b) from this analysis.

It is observed that the entropy generation number of viscous fluid is less than the corresponding values in micropolar fluid case. The presence of microstructure increases the Bejan number near the inner cylinder as seen in both the cases. The imposing magnetic field is normal to the flow direction, it causes the resistive force, thus enhances the irreversibility. Thus, it can be observed that the entropy generation increases with increase in Hartman number in both the cases. It is observed that as R increases, entropy generation increases in the entire region. The cross flow Reynolds number decreases the Bejan number near the inner cylinder and increases at the outer cylinder in case(a). The reverse trend is observed in case (b). Due to high temperature and velocity gradients, the entropy generation is maximum near the inner cylinder and gradually shows an asymptotic behavior near the outer cylinder in either case. The entropy generation number decreases as ζ increases. As the effect of slip reduces the velocities and velocity gradients. This results in a decrease in viscous contribution to the entropy generation. The dominant influence of heat transfer irreversibility is observed as the parameter values of Bi increases consequently, the Bejan number increases. Hence, the convective thermal boundary conditions enhance the dominant effects of heat transfer irreversibility on the flow system.

Chapter 8

Summary and Conclusions

In this thesis, the steady, laminar flow and entropy generation in channels and pipes due to micropolar fluid flow is considered. Micropolar fluids can model the behavior of lubricants, colloidal suspensions, polymeric fluids, liquid crystals and animal blood etc. Entropy generation is calculated for two types of boundary conditions on different geometries. In view of this, the problems for these two cases are studied jointly.

The considered problems for entropy generation are as follows:

- Entropy generation in a micropolar fluid flow through an inclined channel.
- Second law analysis of micropolar fluid flow through a porous channel.
- Effect of magnetic field on entropy generation due to micropolar fluid flow in a rectangular duct.
- Analysis of entropy generation in a micropolar fluid flow through an inclined circular pipe.
- Entropy generation due to micropolar fluid flow between concentric cylinders.
- Analysis of entropy generation between porous concentric cylinders due to micropolar fluid flow.

Except for the third problem, all are solved by using Spectral quasilinearization method whereas the third one is solved by Finite difference method.

The solutions are obtained for velocity, microrotation and temperature distributions. These distributions are used to compute entropy generation and Bejan number. The main contributions of this thesis are listed below.

- Heat transfer irreversibility dominated at the center of the channel and fluid friction irreversibility dominated at the lower plate of the channel.
- As viscous dissipation parameter i.e., Brinkman number(Br) increases, entropy generation increases irrespective of geometry and boundary conditions.
- As micropolarity increases, entropy generation decreases and Bejan number increases for an inclined channel. This indicates that they can be used as good lubricants.
- The increase in the slip parameter results in decrease the entropy generation for horizontal and vertical concentric cylinders. This analysis helps the designer for the better efficiency calculations and geometrical optimization of rotating systems.
- The dominant influence of heat transfer irreversibility is observed as the parameter values of Bi increases consequently, the Bejan number increases in any geometry. Hence, the convective thermal boundary conditions enhance the dominant effects of heat transfer irreversibility on the flow system.

The work presented in the thesis can be extended to analyze the effect of heat and mass transfer, Joule heating, thermal radiation, chemical reaction etc. In this thesis, we have used micropolar fluid model. These problems can be extended to other fluid models like Jeffery fluid, nanofluid, viscoelastic fluid model etc.

Bibliography

[1] S. O. Adesanya and O. D. Makinde. Entropy generation in couple stress fluid flow through porous channel with fluid slippage. *International Journal of Exergy*, 15:344–362, 2014.

[2] S. O. Adesanya and O. D. Makinde. Effects of couple stresses on entropy generation rate in a porous channel with convective heating. *Computational and Applied Mathematics*, 34:293–307, 2015.

[3] I. T. Al-Zaharnah. Entropy analysis in pipe flow subjected to external heating. *Entropy*, 5:391–403, 2003.

[4] V. Anand. Slip law effects on heat transfer and entropy generation of pressure driven flow of a power law fluid in a microchannel under uniform heat flux boundary condition. *Energy*, 76:716–732, 2014.

[5] M. A. Antar and M. A. El-Shaarawi. The entropy generation for a rotating sphere under uniform heat flux boundary condition in forced-convection flow. *International Journal of Numerical Methods for Heat and Fluid Flow*, 19:396–410, 2009.

[6] T. Ariman and A. S. Cakmak. Some basic viscous flows in micropolar fluids. *Rheologica Acta*, 7:236–242, 1968.

[7] Muhammad Ashraf., M. Anwar Kamal, and K. S. Syed. Numerical study of asymmetric laminar flow of micropolar fluids in a porous channel. *Computers and Fluids*, 38:1895–1902, 2009.

[8] M.E.H. Assad and H.F. Oztop. Parametric study of entropy generation in a fluid with internal heat generation between two rotating cylinders subjected to convective cooling at the surface. *ISRN Chemical Engineering*, 2012:1–9, 2012.

[9] S.O. Atayilmaz. Experimental and numerical study of natural convection heat transfer from horizontal concentric cylinders. *International Journal of Thermal Sciences*, 50:1472–1483, 2011.

[10] T. Basak, K. Ram Satish, and A. R. Balakrishnan. Entropy generation during natural convection in a porous cavity: effect of thermal boundary conditions. *Numerical Heat Transfer*, 62:336–364, 2012.

[11] A. C. Baytas. Entropy generation for natural convection in an inclined porous cavity. *International Journal of Heat and Mass Transfer*, 43:2089–2099, 2000.

[12] A. Bejan. A study of entropy generation in fundamental convective heat transfer. *Journal of Heat Transfer*, 101:718–725, 1979.

[13] A. Bejan. Second law analysis in heat transfer. *Energy*, 5(8):720–732, 1980.

[14] A. Bejan. Second law analysis in heat transfer and thermal design. *Advances in Heat Transfer*, 15:1–58, 1982.

[15] A. Bejan. *Entropy Generation Minimization*. CRC Press, New York, 1996.

[16] R. E. Bellman and R. E. Kalaba. *Quasilinearization and non-linear boundary-value problems*. Elsevier, New York, 1965.

[17] R. Ben-Mansour and A. Z. Sahin. Entropy generation in developing laminar fluid flow through a circular pipe with variable properties. *Heat and Mass Transfer*, 42:1–11, 2005.

[18] M.N. Borjini, C. Mbow, and M. Daguenet. Numerical analysis of combined radiation and unsteady natural convection within a horizontal annular space. *International Journal of Numerical Methods for Heat and Fluid Flow*, 9:742–763, 1999.

[19] N. Bouzid, S. Saouli, and S. Aiboud-Saouli. Entropy generation in ice slurry pipe flow. *International Journal of Refrigeration*, 31:1453–1457, 2008.

[20] Eringen A. C. *Microcontinuum field theories II*. Springer, New York, 2001.

[21] C. Canuto, M. Y. Hussaini, A. Quarteroni, and T. A. Zang. *Spectral Methods in Fluid Dynamics*. Springer, Berlin, Germany, 1988.

[22] C. Canuto, M. Y. Hussaini, A. Quarteroni, and T. A. Zang. *Spectral methods fundamentals in single domains*. Springer, Berlin, 2006.

[23] D. S. Chauhan and V. Kumar. Entropy analysis for third-grade fluid flow with temperature-dependent viscosity in annulus partially filled with porous medium. *Theoretical and Applied Mechanics*, 40:441–464, 2013.

[24] B. S. Chen and C.C. Liu. Heat transfer and entropy generation in fully-developed mixed convection nanofluid flow in vertical channel. *International Journal of Heat and Mass Transfer*, 79:750–758, 2014.

[25] S. Chen, Z. Liu, S. Bao, and C. Zheng. Natural convection and entropy generation in a vertically concentric annular space. *International Journal of Thermal Sciences*, 49:2439–2452, 2010.

[26] T. Chinyoka and O. D. Makinde. Analysis of entropy generation rate in an unsteady porous channel flow with navier slip and convective cooling. *Entropy*, 15:2081–2099, 2013.

[27] D. S. Cimpean and I. Pop. Parametric analysis of entropy generation in a channel filled with a porous medium. *Recent Researches in Applied and Computational Mathematics*, pages 54–59, 2011.

[28] D. S. Cimpean and I. Pop. A study of entropy generation minimization in an inclined channel. *WSEAS TRANSACTIONS on HEAT and MASS TRANSFER*, 6:31–40, 2011.

[29] Y. Damianou and G. C. Georgiou. Viscoplastic poiseuille flow in a rectangular duct with wall slip. *Journal of Non-Newtonian Fluid Mechanics*, 214:88–105, 2014.

[30] S. Das, A. S. Banu, R. N. Jana, and O. D. Makinde. Entropy analysis on mhd pseudo-plastic nanofluid flow through a vertical porous channel with convective heating. *Alexandria Engineering Journal*, 54:325–337, 2015.

[31] S. Das and R. N. Jana. Entropy generation due to mhd flow in a porous channel with navier slip. *Ain Shams Engineering Journal*, 5:575–584, 2014.

[32] S. Das, R. N. Jana, and A. J. Chamkha. Entropy generation in a rotating couette flow with suction/injection. *Communications in Numerical Analysis*, 2015:62–81, 2015.

[33] Cuevas S. De Haro, M. L. and A. Beltrn. Heat transfer and entropy generation in the parallel plate flow of a power-law fluid with asymmetric convective cooling. *Energy*, 66:750–756, 2014.

[34] R.K. Deka and A. Paul. Stability of dean flow between two porous concentric cylinders with radial flow and a constant heat flux at the inner cylinder. *Journal of Fluids Engineering*, 135, 2013.

[35] B. T. L. Devi, B. S. Reddy, G. V. P. N. Srikanth, and G. Srinivas. Finite element analysis of convective micro polar fluid flow through a porous medium in cylindrical annulus. *International Journal Of Modern Engineering Research*, 4:1–7, 2014.

[36] W. S. Don and A. Solomonoff. Accuracy and speed in computing the chebyshev collocation derivative. *SIAM Journal on Scientific Computing*, 16:1253–1268, 1995.

[37] A. S. Eegunjobi and O. Makinde. Entropy generation analysis in transient variable viscosity couette flow between two concentric pipes. *Journal of Thermal Science and Technology*, 9, 2014.

[38] A. S. Eegunjobi and O. D. Makinde. Combined effect of buoyancy force and navier slip on entropy generation in a vertical porous channel. *Entropy*, 14:1028–1044, 2012.

[39] A. S. Eegunjobi and O. D. Makinde. Entropy generation analysis in a variable viscosity mhd channel flow with permeable walls and convective heating. *Mathematical Problems in Engineering*, 2013:1–12, 2013.

[40] L. B. Erbay, M. S. Ercan, B. Sulus, and M. M. Yalcin. Entropy generation during fluid flow between two parallel plates with moving bottom plate. *Entropy*, 5:506–518, 2003.

[41] A. C. Eringen. Theory of micropolar fluids. *Journal of Mathematics and Mechanics*, 16:1–18, 1966.

[42] J. A. Esfahani and P. B. Shahabi. Effect of non-uniform heating on entropy generation for the laminar developing pipe flow of a high prandtl number fluid. *Energy Conversion and Management*, 51:2087–2097, 2010.

[43] D. D. Ganji, H. R. Ashory Nezhad, and A. Hasanpour. Effect of variable viscosity and viscous dissipation on the hagen-poiseuille flow and entropy generation. *Numerical Methods for Partial Differential Equations*, 27:529–540, 2009.

[44] O.M. Haddad, M.K. Alkam, and M.T. Khasawneh. Entropy generation due to laminar forced convection in the entrance region of a concentric annulus. *Energy*, 29:35–55, 2004.

[45] A. Haji-Sheikh. Fully developed heat transfer to fluid flow in rectangular passages filled with porous materials. *Journal of Heat Transfer*, 128:550–556, 2006.

[46] M. Havzali, A. Arikoglu, G. Komurgoz, H. I. Keser, and R. O. Fraser. Analytical numerical analysis of entropy generation for gravity-driven inclined channel flow with initial transition and entrance effects. *Physica Scripta*, 78:045401, 2008.

[47] H. Heidary, M. Pirmohammadi, and M. Davoudi. Control of free convection and entropy generation in inclined porous media. *Heat Transfer Engineering*, 33:565–573, 2012.

[48] M.A. Hessami, G.D. Vaw Davis, and J.A.E. Reizes. Mixed convection in vertical, cylindrical annuli. *International Journal of Heat and Mass Transfer*, 30:151–164, 1987.

[49] K. Hooman. Heat transfer and entropy generation optimization of forced convection in porous-saturated ducts of rectangular cross-section. *International Journal of Heat and Mass Transfer*, 50:2051–2059, 2007.

[50] K. Hooman. Heat transfer and entropy generation for forced convection through a microduct of rectangular cross-section: Effects of velocity slip, temperature jump, and duct geometry. *International Communications in Heat and Mass Transfer*, 35:1065–1068, 2008.

[51] K. Hooman, F. Hooman, and S. R. Mohebpour. Entropy generation for forced convection in a porous channel with isoflux or isothermal walls. *International Journal of Exergy*, 5:78–96, 2008.

[52] G. Ibanez. Entropy generation in mhd porous channel with hydrodynamic slip and convective boundary conditions. *International Journal of Heat and Mass Transfer*, 80:274–280, 2014.

[53] Z. Iman. On the importance of thermal boundary conditions in heat transfer and entropy generation for natural convection inside a porous enclosure. *International Journal of Thermal Sciences*, 47:339–346, 2008.

[54] H. Imtiaz and F. M. Mahfouz. Conjugate heat transfer within a concentric annulus filled with micropolar fluid. *Heat and Mass Transfer*, 50:457–468, 2014.

[55] S. Jarungthammachote. Entropy generation analysis for fully developed laminar convection in hexagonal duct subjected to constant heat flux. *Energy*, 35:5374–5379, 2010.

[56] F. Kamisli and H. F. Oztop. Second law analysis of the 2d laminar flow of two-immiscible, incompressible viscous fluids in a channel. *Heat and Mass Transfer*, 44:751–761, 2008.

[57] T. H. Ko and K. Ting. Entropy generation and optimal analysis for laminar forced convection in curved rectangular ducts: A numerical study. *International Journal of Thermal Sciences*, 45:138–150, 2006.

[58] G. Komurgoz, A. Arikoglu, E. Turker, and I. Ozkol. Second-law analysis for an inclined channel containing porous-clear fluid layers by using the differential transform method. *Numerical Heat Transfer*, 57:603–623, 2010.

[59] H. G. Langeroudi and C. Aghanajafi. Thermodynamics second law analysis for laminar non-newtonian fluid flow. *Journal of Fusion Energy*, 25:165–173, 2006.

[60] K. Y. Leong and H. C. Ong. Entropy generation analysis of nanofluids flow in various shapes of cross section ducts. *International Communications in Heat and Mass Transfer*, 57:72–78, 2014.

[61] C. C. Liu and C. Y. Lo. Numerical analysis of entropy generation in mixed-convection mhd flow in vertical channel. *International Communications in Heat and Mass Transfer*, 39:1354–1359, 2012.

[62] G. Lukaszewicz. *Micropolar fluids: Theory and Applications*. Springer Science and Business Media, Birkhauser, Basel, 1999.

[63] M. Magherbi, H. Abbassi, and A. B. Brahim. Entropy generation at the onset of natural convection. *International Journal of Heat and Mass transfer*, 46:3441–3450, 2003.

[64] M. Magherbi, H. Abbassi, Hidouri, and A. B. Brahim. Second law analysis of convective heat and mass transfer. *Entropy*, 8:1–17, 2006.

[65] M. Mahdavi, M. Saffar-Avval, S. Tiari, and Z. Mansoori. Entropy generation and heat transfer numerical analysis in pipes partially filled with porous medium. *International Journal of Heat and Mass Transfer*, 79:496–506, 2014.

[66] O. Mahian, S. Mahmud, and S. Z. Heris. Analysis of entropy generation between co-rotating cylinders using nanofluids. *Energy*, 44:438–446, 2012.

[67] O. Mahian, S. Mahmud, and S. Wongwises. Entropy generation between two rotating cylinders with magnetohydrodynamic flow using nanofluids. *Journal of Thermophysics and Heat Transfer*, 27:161–169, 2012.

[68] O. Mahian, I. Pop, A. Z. Sahin, H. F. Oztop, and S. Wongwises. Irreversibility analysis of a vertical annulus using tio 2/water nanofluid with mhd flow effects. *International Journal of Heat and Mass Transfer*, 64:671–679, 2013.

[69] A. Mahmud and R.A. Fraser. Flow, thermal and entropy generation characteristics inside aporous channel with viscouss dissipation. *International Journal of Thermal Sciences*, 44:21–32, 2005.

[70] S. Mahmud and R. A. Fraser. Thermodynamic analysis of flow and heat transfer inside channel with two parallel plates. *Exergy*, 2:140–146, 2002.

[71] O. D. Makinde. Entropy-generation analysis for variable-viscosity channel flow with non-uniform wall temperature. *Applied Energy*, 85:384–393, 2008.

[72] O. D. Makinde and A. S. Eegunjobi. Entropy generation in a couple stress fluid flow through a vertical channel filled with saturated porous media. *Entropy*, 15:4589–4606, 2013.

[73] A. Mazgar, F. Ben Nejma, and K. Charrada. Second law analysis of coupled mixed convection and non-grey gas radiation within a cylindrical annulus. *International Journal of Mathematical models and methods in applied sciences*, 7:265–276, 2013.

[74] J. H. Merkin. Natural-convection boundary-layer flow on a vertical surface with newtonian heating. *International Journal of Heat and Fluid Flow*, 15:392–398, 1994.

[75] M. Mirzazadeh, A. Shafaei, and F. Rashidi. Entropy analysis for non-linear viscoelastic fluid in concentric rotating cylinders. *International Journal of Thermal Sciences*, 47:1701–1711, 2008.

[76] M. H. Mkwizu and O. D. Makinde. Entropy generation in a variable viscosity channel flow of nanofluids with convective cooling. *Comptes Rendus Mecanique*, 343:38–56, 2015.

[77] S. S. Motsa, P. G. Dlamini, and M. Khumalo. Spectral relaxation method and spectral quasilinearization method for solving unsteady boundary layer flow problems. *Advances in Mathematical Physics*, 2014:12 pages, 2014.

[78] S.S. Motsa. A new spectral local linearization method for nonlinear boundary layer flow problems. *Journal of Applied Mathematics*, 2013:15 pages, 2013.

[79] S.S. Motsa. A new spectral relaxation method for similarity variable nonlinear boundary layer flow systems. *Chemical Engineering Communications*, 201:241–256, 2014.

[80] S. Nadeem, N. S. Akbar, and M. Y. Malik. Exact and numerical solutions of a micropolar fluid in a vertical annulus. *Numerical Methods for Partial Differential Equations*, 26:1660–1674, 2010.

[81] U. Narusawa. The second-law analysis of mixed convection in rectangular ducts. *Heat and Mass Transfer*, 37:197–203, 2001.

[82] C. L. M. Navier. Memoire sur les lois du mouvement des fluides. *Memoires delAcademie Royale des Sciences*, 6:389–440, 1823.

[83] H. F. Oztop. Effective parameters on second law analysis for semicircular ducts in laminar flow and constant wall heat flux. *International communications in Heat and Mass Transfer*, 32:266–274, 2005.

[84] H. F. Oztop, I. Dagtekin, and A. Z. Sahin. Second law analysis of fully developed laminar flow for rectangular ducts with semicircular ends. *International Communications in Heat and Mass Transfer*, 36:725–730, 2009.

[85] S. Paoletti, F. Rispoli, and E. Sciubba. Calculation of exergetic losses in compact heat exchanger passages. *ASME AES*, 10:21–29, 1989.

[86] D. Ramakrishna, T. Basak, S. Roy, and E. Momoniat. Analysis of thermal efficiency via analysis of heat flow and entropy generation during natural convection within porous trapezoidal cavities. *International Journal of Heat and Mass Transfer*, 77:98–113, 2014.

[87] M. M. Rashid and N. F. Mehr. Effects of velocity slip and temperature jump on the entropy generation in magnetohydrodynamic flow over a porous rotating disk. *Journal of Mechanical Engineering*, 1:4–14, 2005.

[88] A.Z. Sahin. Second law analysis of laminar viscous flow through a duct subjected to constant wall temperature. *Journal of Heat Transfer*, 120:76–83, 1998.

[89] K. D. Sinha and R. C. Chaudhary. Viscous incompressible flow between two coaxial rotating porous cylinders. *Proc. Nat. Inst. Sci.*, 32:81–88, 1966.

[90] S. H. Tasnim, S. Mahmud, and M. A. H. Mamum. Entropy generation in a porous channel with hydromagnetic effect. *Exergy*, 2:300–308, 2002.

[91] S.H. Tasnim and S. Mahmud. Entropy generation in a vertical concentric channel with temperature dependent viscosity. *International Communications in Heat and Mass Transfer*, 39:907–918, 2002.

[92] G.I. Taylor. Distribution of velocity and temperature between concentric rotating cylinders. *Proceedings of the Royal Society of London A: Mathematical, Physical and Engineering Sciences*, 151:494–512, 1935.

[93] R. M. Terril and G. M. Shrestha. Laminar flow through channels with porouswalls and with an applied magnetic field. *Applied Scientific Research*, 11:134–144, 1963.

[94] M. Torabi, K. Zhang, G. Yang, J. Wang, and P. Wu. Heat transfer and entropy generation analyses in a channel partially filled with porous media using local thermal non-equilibrium model. *Energy*, 82:922–938, 2015.

[95] L. N. Trefethen. *Spectral methods in MATLAB*. SIAM.

[96] M. S. Tshehla and O. D. Makinde. Analysis of entropy generation in a variable viscosity fluid flow between two concentric pipes with a convective cooling at the surface. *International Journal of Physical Sciences*, 6:6053–6060, 2011.

[97] M. S. Tshehla, O. D. Makinde, and G. E. Okecha. Heat transfer and entropy generation in a pipe flow with temperature dependent viscosity and convective cooling. *Scientific Research and Essays*, 5:3730–3741, 2010.

[98] H. C. Weng, C. O. Chen, and M. H. Chang. Stability of micropolar fluid flow between concentric rotating cylinders. *Journal of Fluid Mechanics*, 631:343–362, 2009.

[99] G. Yang, J. Y. Wu, and L. Yan. Flow reversal and entropy generation due to buoyancy assisted mixed convection in the entrance region of a three dimensional vertical rectangular duct. *International Journal of Heat and Mass Transfer*, 67:741–751, 2013.

[100] M. Yari. Second-law analysis of flow and heat transfer inside a microannulus. *International Communications in Heat and Mass Transfer*, 36:7887, 2009.

[101] B. S. Yilbas, M. Yurusoy, and M. Pakdemirli. Entropy analysis for non-newtonian fluid flow in annular pipe: constant viscosity case. *Entropy*, 6:304–315, 2004.